Order Number 9417463

# FTIR study of structure and properties of adsorbed monolayers of surfactants at the air/water interface

Gao, Tao, Ph.D.

City University of New York, 1994

U·M·I

300 N. Zeeb Rd.
Ann Arbor, MI 48106

# FTIR Study of Structure and Properties of Adsorbed Monolayers of Surfactants at the Air/Water Interface

by

Tao Gao

A dissertation submitted to the Graduate Faculty in Chemistry in partial fulfillment of the requirements for the degree of Doctor of Philosophy

The City University of New York

1994

This manuscript has been read and accepted for the Graduate Faculty in Chemistry in satisfaction of the dissertation of requirement for the degree of Doctor of Philosophy.

12/15/93
Date

Chair of Examining Committee

12/16/93
Date

Executive Officer

Supervisory Committee

The City University of New York

# Abstract

FTIR Study of Structure and Properties of
Adsorbed Monolayers of Surfactants at the Air/Water Interface
by

Tao Gao

Adviser: Professor Milton J. Rosen

A new technique -- External Reflection-Absorption (RA) FTIR spectroscopy --has been applied to investigate the structure and properties of adsorbed monolayers of individual surfactants: sodium dodecanesulfonate ($C_{12}SNa$), sodium dodecylsulfate ($C_{12}HS$), deuterated sodium dodecylsulfate ($C_{12}DS$), dodecyltrimethylammonium bromide ($C_{12}N$), and their mixtures: $C_{12}HS$ - $C_{12}N$ and $C_{12}DS$ - $C_{12}N$ at the aqueous solution/air interface. A new method has been developed for the simultaneous determination of methylene chain orientation ($\chi$) and surface concentration parameter ($k_{max}$) in adsorbed monolayers. The average chain orientation angle, $\chi$, and the surface concentration parameter, $k_{max}$, of adsorbed monolayers of $C_{12}SNa$ at the air/water interface are found to be: $\chi = 38.4 \pm 3.3°$ (from the normal to the interface) and $k_{max} = 0.53 \pm 0.04$ at saturated adsorption from pure water solution. It is found that the chain orientation angle ($38.4 \pm 3.3°$) at the interface is very close to the chain tilt angle (41°) in crystalline solid. This indicates that the adsorbed monolayer of $C_{12}SNa$ at the air/water interface has a molecular

structure similar to that in the crystalline solid.

The phase transition (from LE to G) concentrations determined from RA spectra are in good agreement with those calculated from surface tension measurements for surfactants $C_{12}SNa$, $C_{12}HS$, and $C_{12}DS$ in pure water and in salt solution. It is observed that saturated adsorbed monolayers of individual surfactants or equimolar cationic-anionic surfactant mixtures at the air/water interface have high-ordered *all- trans* conformation of methylene chains only in pure water solution. Adsorbed monolayers below saturation coverage in pure water or in salt solution and saturated adsorbed monolayers in salt solution have partial *gauche* conformers in their methylene chains.

The experimental data show that $C_{12}DS$ has the same surface properties as $C_{12}HS$. This has provided a good basis by using $C_{12}DS$ instead of $C_{12}HS$ in surfactant mixtures containing $C_{12}HS$ for spectroscopic studies (FTIR, NMR).

The composition of adsorbed mixed monolayers of $C_{12}HS$-$C_{12}N$ and $C_{12}DS$-$C_{12}N$ at the air/water interface with different bulk compositions are determined from RA Intensities, and are in good agreement with those calculated by use of the non-ideal mixing model. The FTIR study has provided new evidence that the surface composition in these mixed monolayers remains at a constant molar ratio of 1:1 at the interface over a large range of molar ratio in the solution phase.

## Dedication

To my wife, Shi-rong Liu, for her love, support, and encouragement throughout my studies.

## ACKNOWLEDGEMENTS

I would like to express my sincere thanks :

to Professor Gary P. Mennitt , member of my thesis committee, for his time and helpful advice.

to Professor Leslie J. Fina, member of my thesis committee, for his guidance, time, and help.

to Dr. Yei-Shin Tung for his cooperative work with me, friendship, and help in using the computer and instruments.

I am, finally, most grateful to Professor Milton J. Rosen, for his intellectual guidance, time, encouragement, friendship, and help throughout this work.

# Contents

# TABLES

# CHAPTER 1
# INTRODUCTION

## 1.1 Surface Monolayers

The characteristic properties of surfactants in solution which render their practical applications such as washing, cleaning, wetting, emulsifying, dispersing, and foaming depend in all cases on the tendency of these compounds to accumulate at interfaces between the solution and the adjacent gas, liquid, or solid phases. It can easily be demonstrated that surfactants are adsorbed at all types of interfaces. The classical work of Langmuir (1) showed that a more or less oriented monolayer of surfactant molecules was adsorbed at the air/water interface. Later contributions have proved that same to hold for the hydrocarbon/water, oil/water as well as the solid/water interfaces (under certain conditions, the surface film may be multilayers).

The principal parameters which characterize the state of a monolayer of a specific compound on aqueous substrate are the temperature (T), the surface pressure ($\pi$), and the area per surfactant molecule (A). $\pi$ is related to $\gamma$ and A to $\Gamma$ as follows:

$$\pi = \gamma_0 - \gamma \qquad (1.1)$$

$$A = 10^{16}/\Gamma N \qquad (1.2)$$

where $\gamma_0$ is the surface tension of pure water or solvent, in mN/m, $\gamma$ is the

surface tension of the surfactant solution investigated, in mN/m, N is Avogadro's number, and $\Gamma$ is the adsorbed surface concentration in mol/cm$^2$, A is the area per molecule, in Å$^2$.

Henri Devaux (2), shortly after 1900, pointed out that molecules in monolayers could exist in different states, more or less analog as to three-dimensional liquids, solids, or gases. It is very clear that various monolayer states represent different diagrams of molecular freedom or order, resulting from the intermolecular forces in the film and between the film and the subphase. It is of great interest to gain information about the interaction between molecules in the monolayer from the surface pressure - area ($\pi$, A) diagrams.

There are two different, but related, types of monolayers at the air/water interface: the spread monolayer for water-insoluble surfactants and the adsorbed monolayer for water-soluble surfactants. In order to study spread monolayers of water-soluble surfactants, Meader and Criddle (3) used a concentrated inorganic salt solution, such as 5M NaCl (92% saturated) solution or 95% saturated $NaNO_3$ solution, as the subphase instead of pure water to investigate properties of polyoxyethylene alkylphenol monolayers. It is difficult to give a general answer to the question of whether spread and adsorbed monolayers of a specific substance are comparable and render identical $\pi$ (surface pressure), A (area per molecule) diagrams. Ter Minassian-Saraga (4-6) concluded that the $\pi$, A diagrams of spread and adsorbed monolayers of lauric acid are identical. But with respect to the effect of dissolved electrolytes in the subphase, no agreement can be observed

between spread and adsorbed monolayers of polyoxyethylene n-dodecanols . For dioxyethylene (or hexaoxyethylene) n-dodecanol spread monolayers, the expansion is increased by addition of electrolytes (at the same $\pi$, the area per molecule in 5M NaCl is larger than in $H_2O$), where as with the adsorbed monolayer, the reverse trend has been reported (7, 8). To explain this discrepancy, one thing should be kept in mind that spread monolayers, in contrast to adsorbed monolayer, are not in equilibrium with the subphase. Kretzchmar and Vollhardt (9) pointed out that equilibrium and non-equilibrium monolayers behave differently, and consequently, there is no equivalency between spread and adsorbed monolayers.

## 1.2 States of Monolayers at The Air/Water Interface

### 1.2.1. Gaseous Monolayers (G)

The monolayer obeys the equation of state of a more or less perfect two-dimensional gas, the area per molecule is large compared to actual molecular areas, and the monolayer may be expanded indefinitely without phase change. Interactions between the molecules in a gaseous monolayer are so weak that these interactions don't prevent free mobility of the molecules along the surface. These $\pi$, A diagrams are mainly characterized by the surface pressure approaching zero asymptotically as area increased (Fig.1.1). The ideal two-dimensional gas equation is :

$$\pi \, NA = kT \qquad (1.3)$$

where $\pi$ is the surface pressure in $10^{-3}$N/m, A is the area per molecule, in $m^2$,

N is Avogadro's number, and k is the Boltzman constant, $1.38X10^{-23}J/K^{\circ}$ mol. Spread monolayers of water-soluble non-ionic surfactants in most cases are of gaseous type.

### 1.2.2. Liquid Expanded Monolayers (LE)

Langmuir (10) proposed the following equation of state for expanded monolayers:

$$(\pi - \pi_0)(A - A_0) = kT \qquad (1.4)$$

where $\pi_0$ corresponds to the spreading coefficient for the hydrocarbon part of the monolayer molecules on water , i.e.

$$\pi_0 = \gamma_{water} - \gamma_{oil} - \gamma_{(water - oil)} \qquad (1.5)$$

$A_0$ is the limiting value of A at zero surface pressure. These liquid expanded monolayers tend to extrapolated to a limiting or zero $\pi$ area of about $50Å^2$. Characteristically, LE monolayers may show a first-order transition to gaseous monolayers at low pressures. On compression, a point of fairly sharp but not abrupt change to a monolayer of much higher compressibility occurs. This high-compressibility region, called "transition" (Adam), is shown in Fig. 1.1 region II.

### 1.2.3.Liquid Condensed Monolayers (LC)

Monolayers in this region are almost close-packed. They have considerably lower compressibility than LE monolayers, and their $\pi$ - A curve undergoes a gradual transition to linearity, reminiscent films. While LC monolayers ultimately extrapolate to some limiting area (22Å$^2$) at zero surface pressures, that area is usually found to be some 20% larger than the cross-sectional area of a hydrocarbon chain taken from X-ray data (20Å$^2$).

### 1.2.4. Solid Films (S).

The general appearance of solid films is that of high density and rigid or plastic phase. This type of films, for example, those of fatty acids and alcohols at low temperature or with sufficiently long chain lengths on water, may show quite linear $\pi$-A plots. It extrapolates to an area at zero pressure of 20.Å$^2$. This area is probably that of close-packed hydrocarbon chains, and is greater than the value of 18.Å$^2$ obtained from the structure of the three-dimensional crystals, but can be accounted for as the preferred surface packing (11). A solid film appears to be quite rigid, but at lower pressure there may be a break to an LC type of film.(Fig. 1.1).

### 1.2.5 Transitions Between Monolayer States

The transition from a gaseous monolayer to all more coherent monolayers (LE or LC), indicated by region I in Figure 1.1, is quite generally present when surface pressure is getting higher and higher. This is in general a first-order transition. As a monolayer is compressed, there is a point at which

intermolecular attractive forces become large enough to pull the film-forming molecules together into a coherent monolayer. Motomura and co-workers (12, 13) studied phase transitions in adsorbed monolayers at the air/water interface. They concluded that the phase transition between the gaseous and the expanded films takes place at the break point on the $\gamma$ vs. m (molality of surfactant solution) curves for sodium dodecylsulfate, dodecyltrimethylammonium chloride, and other surfactant solutions.

A second-well-defined transition region is that between the expanded (LE) and the condensed (LC) state, indicated by the line II in Figure 1.1. As an expanded monolayer is compressed, the transition begins quite sharply with a sudden increase in compressibility. This occurs at an area of about 30 - 40 $Å^2$ per molecule for most straight chain fatty compounds (14). At that point, the $\pi$-A curve may become nearly parallel to the area axis, as though the areas were changing at nearly constant surface pressure (general speaking, there is a slight upward slope). As the area appropriate to the condensed monolayer is approached, the curve turns upward more steeply, and the fully condensed region is reached. In condensed monolayers, the molecules have an almost close packed, well-aligned configuration almost perpendicular to the interface, while in gaseous monolayers at the liquid/air interface they probably lie nearly flat and are widely separated. Apparently, in expanded monolayers, the configuration is in some way intermediate between these extremes. Langmuir (10) introduced the concept that an expanded film could be thought of as a very thin liquid phase. The hydrophobic portions of the molecules in an expanded film are in random, rather than regular, orientation, only the polar

functional groups being constrained to be in contact with the subphase. Therefore, the transition between the condensed liquid and expanded state should be accompanied with changes in orientation, conformation, and packing densities of polymethylene chains of surfactants. These provide good bases for monitoring the phase transition by using spectroscopic methods.

## 1.3. General Properties of Adsorbed Monolayers at The Air/Water Interface

### 1.3.1. The Gibbs Adsorption Equation and The Area Per Surfactant Molecule at The Air/Water Interface

Following Gibbs (15) , the adsorption of dilute (i.e., $<10^{-2}$M) solutions of a nonionic surfactant, or a 1:1 ionic surfactant in the presence of a swamping amount of electrolyte containing a common non-surfactant counter ion, at a liquid/gas (or liquid/liquid) interface is described by :

$$\Gamma_1 = - (1/2.303RT) (d\gamma_1/d\log C_1)_T \qquad (1.6)$$

where $\Gamma_1$ is the surface excess concentration in mol./cm$^2$, R = 8.314 J/mol.K°, and $(d\gamma_1/d\log C_1)_T$ is the slope of the surface tension - log of surfactant solution molar concentration plot at constant temperature, T. For a 1:1 ionic surfactant in the absence of any added electrolyte, (1.6) becomes:

$$\Gamma_1 = - (1/4.606RT) (d\gamma_1/d\log C_1)_T \qquad (1.7)$$

The slope of a typical $\gamma_1$ - $\log C_1$ plot is essentially constant below, but near the critical micelle concentration (cmc). In this region, the surface excess concentration has reached a maximum value (saturated adsorption) and $\Gamma_1$ calculated from (1.6) or (1.7) is labeled $\Gamma_{max}$. A simulated relationship between the surface excess concentration and the bulk concentration of an ionic surfactant solution in pure water is shown in Figure 1.2.

From the maximum surface excess concentration, the minimum area per surfactant molecule at the aqueous solution/air interface in $Å^2$ can be calculated from the relationship:

$$A_{min} = 10^{16}/N\Gamma_{max} \qquad (1.8)$$

where N = Avagadro's number and $\Gamma_{max}$ is in $mol/cm^2$.

### 1.3.2. The Experimental Evidence for Proving the Gibbs Equation

Although Gibbs published his monumental treatise on heterogeneous equilibrium in 1875, his work was not generally appreciated until the turn of the century. It was not until many years later that the field of surface chemistry developed to the point that experimental applications of the Gibbs equation became important. Probably the first successful experimental verification of the Gibbs equation is due to McBain and his co-workers (16) . They adopted the very direct approach of actually skimming off a thin layer of the surface of a solution, using a device called a microtome. A slice about 0.1mm thick could

be taken from about $1 m^2$ of surface, so that a few grams of solution were collected, allowing surface excess determination for aqueous solution of p-toluidine, phenol, and n-hexanoic acid. Tajima et al..(17) used $^3H$ labeling to obtain the adsorption of sodium dodecylsulfate, $C_{12}H_{25}SO_4Na$ ($C_{12}HS$), at the aqueous solution/air interface. The results agreed very well with the Gibbs equation in the form of equation (1.7), but including activity coefficient corrections.

### 1.3.3. Mixed Surfactant Monolayers

Mixed surfactant systems are of scientific and technological interest; in industrial applications, surfactants are almost always used as mixtures. Often, mixtures of surfactants exhibit fundamental and applied properties superior to those of the pure individual surfactant components. The model proposed by Rubingh (18) for non-ideal mixed micellar surfactant systems has had the most use. Rosen and coworkers have extended Rubingh's model to adsorption of binary mixed surfactants at the aqueous solution/air (19), liquid/liquid (20), and liquid/hydrophobic solid interfaces (21). The basic equations for describing adsorption in mixtures of two surfactants at the aqueous solution/air interface (22) are :

$$\frac{(X_1)^2 \ln(\alpha C_{12}/C_1^0 X_1)}{(1-X_1)^2 \ln[(1-\alpha)C_{12}/C_2^0(1-X_1)]} = 1 \qquad (1.9)$$

$$\beta^{\sigma} = \frac{\ln(\alpha C_{12}/X_1 C_1^{0})}{(1-X_1)^2} \qquad (1.10)$$

where $\alpha$ is the mole fraction of surfactant 1 in the total surfactant in the solution phase, i.e. the mole fraction of surfactant 2 equals $1-\alpha$; $X_1$ is the mole fraction of surfactant 1 in total surfactant in the mixed monolayer; $C_1^{0}$, $C_2^{0}$, $C_{12}$ are the molar concentration of surfactant 1, 2, and their mixture in the solution phase, respectively, required to produce a given surface tension value; $\beta^{\sigma}$ is the molecular interaction parameter for mixed monolayer formations at the aqueous solution/air interface.

Equation (1.9) can be solved numerically from experimental data ($\alpha$, $C_1^{0}$, $C_2^{0}$, and $C_{12}$) for $X_1$, and substitution of this in equation (1.10) yields the value of $\beta^{\sigma}$.

### 1.3.4. Interactions in Mixed Monolayers

The molecular interaction parameter, $\beta^{\sigma}$, together with the properties of the individual surfactants are used to predict whether synergism of a particular type will occur when the two surfactants are mixed and, if so, the molar ratio of the two surfactants at which maximum synergism will exists and the relevent

property of the mixture at that point. The interaction parameter $\beta^{\sigma}$ depends upon the nature of the two surfactants and the interface. Since the value of $\beta^{\sigma}$ appears to be related to the free energy of mixing of the two surfactants, a negative value indicates an attractive interaction between the two surfactants;a positive value indicates a repulsive interaction. The larger the value of $\beta^{\sigma}$, the stronger the interaction, either attractive or repulsive, between the two surfactants. A value close to zero indicates little or no interaction, i.e., ideal mixing. Values of $\beta^{\sigma}$, obtained by various investigations, currently range from +2, a weakly repulsive interaction, to over -30, a very strong attractive force between an anionic surfactant, such as $C_{12}H_{25}SO_4Na$, and a cationic surfactant, e.g., $C_{12}H_{25}N(CH_3)_3Br$.

## 1.4. Orientation of Surfactant Molecules at the Aqueous Solution/Air Interface

The idea that unsymmetrical molecules will be oriented at an interface now is well accepted, because surfactant molecules should be oriented so that their mutual interaction energy will have a maximum, and the surface energy will decrease to a minimum. As we know, surfactants have a characteristic molecular structure consisting of a structural group which has very little attraction for the solvent (lyophobic group), together with a group which has strong attraction for the solvent (lyophilic group). This is known as an amphipathic structure. In an aqueous solution of a surfactant, the hydrophobic

group of the surfactant will break down the structure of water (such as H-bonds between water molecules), and increase the free energy of the system. This means that less work is needed to bring a surfactant molecule to the surface than that for a water molecule. The surfactant molecule therefore concentrates at the surface. On the other hand, the presence of the hydrophilic group prevents the surfactant from being expelled completely from the solvent as a separate phase. The amphipathic structure of surfactants eventually causes not only adsorption of the surfactant at the interface and reduction of the surface tension of the water, but also orientation of the molecules at the interface with its hydrophilic group in the aqueous phase and its hydrophobic group oriented away from it.

From molecular models, the cross-sectional area of a polymethylene chain oriented perpendicular to the interface is about 20$Å^2$ (23). The area per molecule of $C_{12}H_{25}SO_3Na$ (sodium dodecane sulfonate, $C_{12}SNa$) at the aqueous solution/air interface, calculated from surface tension measurements and equ. (1.8), is about 57$Å^2$ in absence of NaCl (24). It is apparent that the hydrophobic chains of surfactants adsorbed at the aqueous solution/air interface are generally not in close - packed arrangement at saturation adsorption because of the repulsion forces between the charged head groups. On the other hand, since the cross-sectional area of a methylene chain of $C_{12}SNa$ molecule lying flat in the interface is about 85 $Å^2$ (23), it is clear that the methylene chains of $C_{12}SNa$ molecules are not lying flat in the interface, but with some tilt angle from the normal of the interface.

## 1.5. Determination of Structures and Orientations of Surfactant Monolayers at The Air/Water Interface

Recently, many studies have been conducted on the structures and properties of water-insoluble monolayers (spread monolayers) at the air/water interface. Various optical methods have been used to investigate monolayers in conjunction with surface tension measurements. Kjaer and co-workers (25, 26) studied monolayers of phospholipids and arachidic acid [$CH_3(CH_2)_{18}COOH$] on the surface of pure water and of salt solutions by synchrotron X-ray diffraction and reflection method. They showed that there exists an intermediate phase which is characterized by a long-range orientational order and a short-range positional order for phospholipid monolayers at the air/water interface. They observed that there is an ordered phase existing at pressure of between ca. 1 and 25.6 mN/m. In this phase the methylene chains are uniformly tilted, the tilt angle from the normal decreasing continuously from 33° to 0° with lateral pressure.

Rasing and co-workers (27) have used an optical second-harmonic generation (OSHG) method to measure the molecular orientation of a monolayer of pentadecanoic acid [$CH_3(CH_2)_{13}COOH$] near its LE-LC transition at the air/water interface. The results show that the transition is accompanied by a reorientation of the molecules and that the two phases are separated by an inhomogeneous coexistence region on the isotherms. Rasing et al. (28) have also studied sodium dodecylnaphthalene sulfonate monolayer at the air/water interface. They showed that the orientation of the naphthalene groups varies smoothly from about 43° from the normal at low surface pressure to 30° at higher pressure. The smooth variation in angle was interpreted as the

absence of a phase transition, in agreement with surface pressure isotherms.

Thomas and co-workers (29) have used a neutron specular reflection (NSR) method in conjunction with measurements of surface tension to study structures of decyltrimethylammonium bromide (DTMA) monolayer at the air/water interface. The results show that the structure of the layer consists of three regions: the first, hydrocarbon tail chain region, the second containing a small fraction of chains, the third containing water and a diffuse atmosphere of counterions. But no orientation information was given. Simister et.al. (30, 31) have investigated the structure of tetradecyltrimethylammonium bromide (TTMA) monolayer at the air/water interface. They showed that for the saturated monolayer, the mean center-center distribution of chains and heads was about $7 \pm 0.5$Å, as the same as that between chains and water. They also reported that the mean thickness of the chain region is about $17.5 \pm 1$Å for a uniform layer model which is less than the full-extended chain length.

A particular advantage of the use of vibrational spectroscopic methods to study amphiphilic monolayers is the possibility of obtaining both conformational and orientational information simultaneously. Takenaka and co-workers (32) have used Raman spectroscopy to study structures and orientation of 4'- dicetylamino-azobenzene-4-sulfonic acid sodium (cetyl orange) monolayer at the air/water interface. It is shown that the molecules in the insoluble monolayers show a higher orientation with respect to the vertical axis as compared with these in soluble monolayers adsorbed at the water/carbon tetrachloride interface, and the orientation angle (between the chromophores and the normal of the interface) decreases from 45° to 32° with a decrease in surface area from 56Å$^2$ to 29Å$^2$

Dluhy and co-workers (33-35) are the first group who have used FTIR reflection-absorption spectroscopy to investigate structures and properties of water-insoluble monolayers at the air/water interface. They have described the optics of the reflection-absorption process in isotropic phase monolayers, and subsequently used the frequency shift as the indication of the conformational and phase properties of polymethylene chains in biological monolayers.

Recently, Fina and Tung (36) have developed an optical model to describe the reflection-absorption properties from an anisotropic monolayer at the air/water interface. They have established the relationships between the average orientation angle, the anisotropic optical constants, and the angle of incident light. In this thesis I am going to use this optical model, the related theory, and FTIR reflection-absorption spectroscopy in conjunction with surface tension measurements to investigate the molecular structures, polymethylene chain orientations, chain conformations, and surface concentrations of adsorbed monolayers of water-soluble surfactants (including some surfactant mixtures) at the aqueous solution/air interface in the presence and absence of electrolyte in the water subphase. The comparison of all information obtained from both surface tension and FTIR spectroscopy measurements for ionic and nonionic surfactants (including surfactant mixtures) allows for a comprehensive understanding of molecular structural aspects of surfactants at the aqueous solution/air interface and new insights into the thermodynamic interaction parameter in bicomponent mixtures.

## 1.6. The Critical Micelle Concentration (cmc)

After the maximum surface concentration ($\Gamma_{max}$) is reached, the monomer

concentration in the bulk phases increases with the addition of more surfactant to a point where either any additional monomers added aggregate into clusters called micelles [the concentration of monomers at the point of aggregation formation is called the critical micelle concentration (cmc)], or an insolubility limit is reached (if $T<T_k$, $T_k$ = Krafft point, the temperature at which the solubility of an ionic surfactant becomes equal to the cmc). When micelles form in water, the hydrophobic tail of the surfactant is in the interior of the micelle and the hydrophilic head is on the exterior.

As in adsorption, the reason for micellization is the amphipathic structure of the surfactant molecule and the main driving force, in aqueous solution, is an increase in the entropy of the system upon release of the water molecules from the hydrophobic tails of the surfactant molecules when the tails cluster together in the interior of the micelle. Israelachivili et al. (37) have introduced a theory of self-assembly of surfactant molecules which predicts micelle type, size, and shape, for a given surfactant, and explains the effects of salt, temperature, and solubilized materials on micellization. Many physical methods for the detection of cmcs in aqueous solution exist, since many physical properties change abruptly at this point. Among the physical properties that have been used are: surface tension, interfacial tension, osmotic pressure, light scattering, refractive index, and electrical conductance (for ionic surfactants only). The cmc is taken as the break point in the property - concentration (of surfactant) curve.

# CHAPTER 2
# THEORETICAL BACKGROUND AND OPTICAL MODEL

## 2.1. Theoretical Background

The classical electromagnetic theory used in the formulation of the boundary value problem for a planar, optically isotropic multilayered system has been fully developed (38 - 43). The equations that describe the interaction of plane-polarized radiation with an N-phase system of parallel, optically isotropic layers can be derived from Maxwell's equations by taking into account the continuity requirements of the electric and magnetic field vectors. Shopper (44) has proposed a theoretical model and the relationship between the reflectance and the anisotropic structure for an anisotropic monolayer film. Figure 2.1 is a basic physical description of the anisotropic three-layered sample as an optical model. The parameters of the model are defined as following: (a). The axis system defines z direction as the normal to the plane of the water/air interface, x and y in the plane, and the y coordinate is perpendicular to the plane of incidence. Therefore, radiation with perpendicular polarization (*s*-polarization) has only a vector component of electrical field in y direction, while parallel polarization (*p*-polarization) has both x and z components. (b). The optical properties of the anisotropic monolayer are characterized by the complex refractive indices:

$$\tilde{n}_x = n_x - ik_x \qquad (2.1)$$

$$\tilde{n}_y = n_y - ik_y \qquad (2.2)$$

$$\tilde{n}_z = n_z - ik_z \qquad (2.3)$$

where $n_x$, $n_y$, and $n_z$ are the x, y, and z components of the real refractive index ($\tilde{n}$), respectively, and $k_x$, $k_y$, and $k_z$ are the x, y, and z components of the absorption coefficient ($\tilde{k}$), respectively. (c). The ambient atmosphere and the liquid substrate are assumed to be isotropic: $n_1 = 1.0$, $k_1 = 0.0$,

$$\tilde{n}_2 = n_2 - ik_2 \qquad (2.4)$$

Also defined are the angle of incidence ($\theta_1$), the monolayer thickness (d), *p*-polarized (Ep) and *s*- polarized radiation (Es). The phase constants are written in terms of the anisotropic constants as:

$$a_s^2 - b_s^2 = n_x 2 - k_x 2 - n_1^2 \sin^2\theta_1 \qquad (2.5)$$

$$a_s b_s = n_x k_x \qquad (2.6)$$

$$a_p^2 - b_p^2 = (n_y^2 - k_y^2) A - 2 n_y k_y B \qquad (2.7)$$

$$2 a_p b_p = 2 n_y k_y A + (n_y^2 - k_y^2) B \qquad (2.8)$$

where

$$A = 1 - n_1^2 \sin^2\theta_1 (n_z^2 - k_z^2)/(n_z^2 + k_z^2)^2 \qquad (2.9)$$

and

$$B = 2\, n_1^2 \sin^2\theta_1\, n_z\, k_z/(n_z^2 + k_z^2)^2 \qquad (2.10)$$

Calculation of the Fresnel reflection coefficients for an oriented monolayer on an absorbing isotropic substrate can be performed from the phase constants as:

$$r_{1s} = (n_1\cos\theta_1 - a_s + ib_s)/(n_1\cos\theta_1 + a_s - ib_s) \qquad (2.11)$$

$$r_{1p} = [\tilde{n}_y^2\cos\theta_1 - n_1\,(a_p - ib_p)]/[\tilde{n}_y^2\cos\theta_1 + n_1\,(a_p - ib_p)] \qquad (2.12)$$

$$r_{2s} = (a_s - ib_s - \tilde{n}_2\cos\theta_2)/(a_s - ib_s + \tilde{n}_2\cos\theta_2) \qquad (2.13)$$

$$r_{2p} = [\tilde{n}_2\,(a_p - ib_p) - \tilde{n}_y^2\cos\theta_2]/[\tilde{n}_2\,(a_p - ib_p) + \tilde{n}_y^2\cos\theta_2] \qquad (2.14)$$

The reflected amplitudes are then found from the relationship:

$$r = \{r_1 + r_2\exp[-2i(a-ib)\eta]\}/\{1 + r_1 r_2\exp[-2i(a-ib)\eta]\} \qquad (2.15)$$

where $\eta = 2\pi(d/\lambda)$, with $d = l\cos\chi$ (monolayer thickness), $l$ = all-*trans* chain length, $\chi$ = angle between the chain axis and the surface normal, and $\lambda$ = wavelength. The appropriate subscripts can be inserted into equation (2.15) to determine $r_p$ and $r_s$. Finally, the reflected intensities are found from:

$$R = (r)\,(r^*) \qquad (2.16)$$

where r* is the conjugate complex of r. The reflection-absorption (RA) from an anisotropic monolayer can be calculated from $RA = -\log (R/R_0)$, where R is the reflectance from the three-phase system, and $R_0$ is the reflectance from a pure water (or salt solution) surface. $R_{0s}$ and $R_{0p}$ are found from:

$$r_{0s} = (x_1 - x_2)/(x_1 + x_2) \qquad (2.17)$$

$$r_{0p} = (\tilde{n}_2^2 x_1 - \tilde{n}_1^2 x_2)/ (\tilde{n}_2^2 x_1 + \tilde{n}_1^2 x_2) \qquad (2.18)$$

with $x_i = \tilde{n}_i \cos\theta_i$.

## 2.2. Modeling of Molecular Chain Anisotropy

Figure 2.2 shows the axis used in this optical modeling system. It contains a representative molecular chain, angles that define the chain in axis system ($\alpha$, $\beta$, $\delta$, $\chi$), a representative dipole moment of the chain (M), and an angle between the chain axis and the dipole moment ($\Phi$). In the case of uniaxial symmetry about the Z axis, the angle $\alpha$ and $\beta$ are equal and $\alpha$ can be calculated from $\chi$, the chain orientation angle, by:

$$\alpha = \cos^{-1} (\cos \pi/4 \cos(\pi/2 - \chi)) \qquad (2.19)$$

Both the real (n) and imaginary (k) parts of the refractive index can be defined

in the laboratory frame of reference. The real part in n treated as an axially symmetric ellipsoid with its principal axes coincident with the laboratory frame. The relationship between the anisotropy in n and the chain orientation is:

$$n_x = n_y = n_{max}\cos^2\alpha + n_{min}\cos^2(\pi/2-\alpha) \qquad (2.20)$$

$$n_z = n_{max}\cos^2\chi + n_{min}\cos^2(\pi/2-\chi) \qquad (2.21)$$

where $n_{max}$ and $n_{min}$ are the refractive index components parallel and perpendicular to the axis and $n_{x,y,z}$ are the components along the principal axes of the ellipsoid. In order to find the components of the refractive index, a knowledge of $n_{max}$ and $n_{min}$ is required. This treatment does not consider the effect of the orientation distribution function on the refractive index components. However, the effect on the problem considered here is minor, particularly in the case of a small anisotropy in the refractive index for a system of perfectly aligned chains.

The principal axes components of the absorption coefficient (k) for the oriented monolayer, $k_{x,y,z}$ can be related to the laboratory frame, the chain orientation angle, the dipole moment angle, and the orientation distribution function with the following equations modified from the original (45):

$$k_x = k_y = k_{max}\{[P_2\langle\cos\chi\rangle\sin^2\Phi]/2 + [1 - P_2\langle\cos\chi\rangle]/3\} \qquad (2.22)$$

$$k_z = k_{max}\{ P_2\langle\cos\chi\rangle\cos^2\Phi + [1 - P_2\langle\cos\chi\rangle]/3\} \qquad (2.23)$$

The angle $\chi$ and $\Phi$ are defined in Figure 2.2. $P_2\langle\cos\chi\rangle$ is the second moment of the orientation distribution function and is equal to $(3\langle\cos 2\chi\rangle - 1)/2$. $k_{max}$ is the absorption coefficient for a collection of completely aligned chains and is the parameter that is proportional to the molecular concentration of the monolayer.

Three assumptions are made about the monolayer chain orientation:
a. An uniaxial orientation about the axis that is normal to the air/water interface, and no preferred orientation about the chain axis. Polymethylene chains may rotate freely about the vertical axis (the surface normal).
b. All polymethylene chains have an all-*trans* planar zigzag conformation.
c. An orientation angle distribution function characterized by a delta function, all chains are located at the same angle from the surface normal.

A combination of the various parameters discussed, i.e., the chain orientation dependence of the refractive index (eqns. 2.20 and 2.21), the principal axis components of the absorption coefficient with orientation (eqns. 2.22 and 2.23) and eqns. (2.5) - (2.18) permit quantitative calculations of the polarized reflection-absorption intensities (RAp and RAs).

## 2.3. Modeling Results

A typical example of *s*- and *p*- polarized intensities versus chain orientation angle ($\chi$) is shown in Figure 2.3. The calculations are performed using the following parameters that are the same as in the experiments

presented later. These are: 1). an incident light angle of 30° for both *s*- and *p*-polarized light (angle between the light propagation direction and the surface normal direction), 2) a substrate consisting of pure water with optical constants n = 1.415 and k = 0.0163 at 2920cm$^{-1}$ (47), 3) a dipole moment directed perpendicular to the chain axis ($\Phi = 90°$) with no preferred orientation around the chain, 4) a uniaxially symmetric distribution of chain axes, 5) a $k_{max}$ value of 0.30 where $k_{max} = 3k_{isotropic}$, and 6) a monolayer thickness that depends on the chain orientation. For an all-*trans* polymethylene chain of a sodium dodecanesulfonate molecule ($C_{12}SNa$), the monolayer thickness of 17.8 Å is obtained by using the standard bond lengths and bond angles at $\chi = 0°$. The angle-dependent monolayer thickness (d) is determined by d = 17.8X10$^{-8}$cm cos$\chi$. This assumes that a change in thickness is due to orientation rather conformation. From Figure 2.3, some features are shown for this type of experiment: 1) the intensities are negative throughout the $\chi$ range, 2) the *p*-polarized RA intensity (RAp) is always larger than *s*- polarized RA (RAs), 3) both RAs and RAp decrease as the chain axes lie down toward to the plane of the interface (with increase in $\chi$ angle).

The RA intensities shown in Figure 2.3 also depend on $k_{max}$ which is related to the surface concentration of the surfactant in the monolayer. For water-soluble surfactant solutions, monolayers are formed at the water/air interface by adsorption of surfactant molecules from the bulk solution to the interface, and the surface excess concentration can be calculated from the Gibbs adsorption equation (1.6). Apparently, the chain orientation is affected

by the surface excess concentration of the surfactant molecules. Thus, we are able to change the surface excess concentration by change of the surfactant solution concentration to investigate the chain orientation in the monolayer. Both variables, surface concentration and chain orientation angle of surfactant molecules in the monolayer, need to be determined from RA intensities in order to find either one individually.

## 2.4. Method for Simultaneous Extraction of Variables

In order to determine both surface concentration and orientation simultaneously, two experimental RA intensities are required for a calculation procedure. RAs and RAp from the same infrared peak and sample monolayer are the obvious choices because these intensities are derived from the same $k_{max}$ and chain orientation. The problem can be solved in a variety of ways. A nonlinear least-squares refinement procedure can be used to minimize the difference between calculated and observed intensities when $k_{max}$ and $\chi$ are varied. However, alternative methods have been used based on their simplicity. The methods use the relationship between $k_{max}$, $\chi$ and the *p*- and *s*- polarized RA intensities shown in Figure 2.4 and 2.5, respectively. The curves were calculated using the same parameter values as those used to calculate Figure 2.3. At any given value of $\chi$, an approximately linear relationship exists between $k_{max}$ and the RA intensities for both polarizations. From the linearity, the experimental intensities are used to calculate *s*- and *p*- $k_{max}$ values at all angles $\chi$. The true value of $\chi$ is obtained by minimizing the difference between *s*- and *p*- $k_{max}$ ($\Delta k_{max}$). This also leads to a

determination of kmax, the surface concentration-related variable. The model intensity data shown in Figure 2.3 are used to test the procedure with $k_{max}$ = 0.30 for all $\chi$. Intensities calculated at $\chi$ = 0, 20, 40, 60, and 80° were used as the input experimental intensities in refinement procedure and $\Delta k_{max}$ versus $\chi$ curves generated. The results are shown in Figure 2.6. In each case, the correct orientation angle $\chi$ and $k_{max}$ (=0.30) values are obtained.

An examination of the ratio of polarized intensities (RAp/RAs) is instructive in that no calculations are necessary and qualitative interpretations about the chain orientation are directly available. Figure 2.7 shows plots of the ratio (RAp/RAs) versus **c** for several $k_{max}$ values varying from 0.13 (top) to 0.50 (bottom). The plot clearly shows the influence of changes in surface concentration ($K_{max}$) and chain orientation ($\chi$) on RAp/RAs. The ratio is particularly insensitive to orientation with respect to a fixed $k_{max}$ value in the 0 - 20° angular range and sensitive in the range of 40 - 80°,due to the cosine-squared dependence of intensity on orientation. The figure can be used qualitatively in the following way: Assume a decrease in RAp/RAs is observed experimentally as a result of a decrease in the bulk surfactant concentration. The surface concentration in the monolayer, and therefore $k_{max}$, will either remain constant (surface concentration in saturated adsorption range) or decrease (surface concentration is unsaturated) in the monolayer as a result of the above process. According to Figure 2.7, a decrease in RAp/RAs coupled with a constant or decreasing $k_{max}$ indicates that the orientation angle $\chi$ increases.

An improvement in the sensitivity of the calculations in the 0 - 20° range of

$\chi$ can be implemented by using the intensity ratios $RAp^2/RAs$ or $RAp^3/RAs$ rather than RAp/RAs. In Figure 2.8, one of the curves from Figure 2.7 (RAp/RAs) with a $k_{max}$ value of 0.30 is plotted (top). also shown are $RAp^2/RAs$ and $RAp^3/RAs$. The intensities of the latter two have been normalized to be coincident with the RAp/RAs curve at $\chi = 0°$. The increased sensitivity of the higher order intensity ratios in a $\chi$ prediction is clear from the magnitude of the ratio change and suggests that the simultaneous determination of $k_{max}$ and $\chi$ will benefit from an increase of number of i in $RAp^i/RAs$. A new calculation procedure was designed and is as follows: Using experimentally determined RAs and RAp values and Figures 2.4 and 2.5, *s*- and *p*- $k_{max}$ values are calculated as well as the average $k_{max}$ at every $\chi$. At each average $k_{max}$ ($\chi$), RAs, RAp, and RAp/RAs are calculated. The calculated ratios are compared with the experimental ratios and the difference minimized to find $\chi$. An example of the results of this procedure is shown in Figure 2.9 where the calculations are based on input values of $\chi = 20°$ and $k_{max} = 0.30$. One of the curves from Figure 2.6 is duplicated in Figure 2.9. All four methods correctly predict the $\chi$ and $k_{max}$ values used as input. However, the differential sensitivity in the solution for the higher values of i in $RAp^i/RAs$ is much higher than others. Based on this and other modeling calculations, the remainder of the work presented in this thesis uses $PAp^3/RAs$ for the simultaneous determination of $k_{max}$ and $\chi$.

**Table 2.4 1. Effect of Error in Experimental Intensity Measurement on $\chi$ and $k_{max}$ Prediction**

| Assumed Values | | Calculated Values | | | | | |
|---|---|---|---|---|---|---|---|
| | | +1% change in Rp | | | -1% change in Rp | | |
| $k_{max}$ | $\chi$(°) | $\chi$(°) | $p\text{-}k_{max}$ | $s\text{-}k_{max}$ | $\chi$(°) | $p\text{-}k_{max}$ | $s\text{-}k_{max}$ |
| 0.2 | 80 | 79 | 0.190 | 0.190 | 81 | 0.212 | 0.212 |
| 0.3 | 70 | 69 | 0.288 | 0.288 | 71 | 0.313 | 0.314 |
| 0.4 | 60 | 59 | 0.387 | 0.387 | 61 | 0.415 | 0.415 |
| 0.5 | 50 | 49 | 0.488 | 0.486 | 51 | 0.514 | 0.516 |
| 0.6 | 40 | 38 | 0.575 | 0.574 | 41 | 0.612 | 0.614 |
| 0.7 | 30 | 28 | 0.681 | 0.678 | 32 | 0.723 | 0.725 |
| 0.8 | 20 | 17 | 0.780 | 0.777 | 22 | 0.814 | 0.819 |
| 0.9 | 10 | 3 | 0.884 | 0.879 | 14 | 0.919 | 0.924 |
| 1.0 | 0 | 0 | 1.010 | 1.000 | 9 | 1.016 | 1.021 |

**Table 2.4 2 Results of Error in Experimental Intensity Measurement on $\chi$ and $k_{max}$ Prediction**

| Assumed Values | | Calculated Values | | | | | |
|---|---|---|---|---|---|---|---|
| | | +5% change in Rp | | | -5% change in Rp | | |
| $k_{max}$ | $\chi$(°) | $\chi$(°) | *p*-$k_{max}$ | *s*-$k_{max}$ | $\chi$(°) | *p*-$k_{max}$ | *s*-$k_{max}$ |
| 0.2 | 80 | 76 | 0.167 | 0.167 | 86 | 0.352 | 0.355 |
| 0.3 | 70 | 66 | 0.248 | 0.248 | 76 | 0.406 | 0.407 |
| 0.4 | 60 | 54 | 0.329 | 0.328 | 66 | 0.505 | 0.507 |
| 0.5 | 50 | 43 | 0.418 | 0.414 | 56 | 0.598 | 0.598 |
| 0.6 | 40 | 31 | 0.507 | 0.500 | 47 | 0.708 | 0.718 |
| 0.7 | 30 | 18 | 0.608 | 0.597 | 38 | 0.800 | 0.818 |
| 0.8 | 20 | 0 | 0.739 | 0.718 | 30 | 0.897 | 0.920 |
| 0.9 | 10 | 0 | 0.914 | 0.877 | 24 | 0.997 | 1.024 |
| 1.0 | 0 | 0 | 1.049 | 1.000 | 21 | 1.092 | 1.123 |

The effect of errors in measurement of RA intensity on the calculations of $k_{max}$ and $\chi$ is shown in Tables 2.4.1. and 2.4.2. Errors in intensity measurements occur frequently due to baseline variations. The calculations in Table 2.4.1.and 2.4.2 are based on the assumed values of $k_{max}$ and $\chi$ given in the first two columns. The RA intensities are determined from them and then $\chi$, *s*-, and *p*-$k_{max}$ are calculated with the indicated levels of error imposed on RAp while RAs is held constant. Generally speaking, the predicted values of $\chi$ are more accurate with large $\chi$ and the accuracy of the predicted $k_{max}$ values does not change as the assumed value of $k_{max}$ changes.

## 2.5. Simulation of Reflection - Absorption Spectra

The frequency ( or wavenumber) of infrared absorption of the methylene stretching vibrations has often been used as an indication of conformational content in chain molecules (47-49). A question that arises in the use of the reflection-absorption technique is: do the optics of the experiment result in any peak shifts or band distortions relative to standard transmission spectroscopy? In the past, specular reflection techniques have been shown to produce as much as a 15 $cm^{-1}$ shift in carbonyl stretching peak of poly(methyl methacrylate) as compared to the transmission mode (50). In order to examine for the presence of band distortion or frequency shifts associated with the reflection - absorption experiment, simulated spectra are calculated from the optical constants of sodium dodecanesulfonate. The optical constants are found from the solid surfactant dispersed in a KBr matrix by

using a combination of a Krames-Kronig transform and spectral modeling with Fresnel coefficients. Polarized reflection-absorption spectra of an isotropic monolayer surrounded by air on one side and water on the other side are calculated for a thickness of 10.5Å. The results are shown in Figure 2.10 and compared with the experimental transmission spectrum. The peak positions derived from the spectra (by 3-point quadratic interpolation of resolution = $2cm^{-1}$ data files) are shown in Table 2.5.1. The average magnitude of all shifts is $+0.28cm^{-1}$ and the maximum shift is $+0.7cm^{-1}$. No shifting results from using different polarizations. Figure 2.10 indicates that band distortions as a result of the experimental optics are negligible.

**Table 2.5.1 Peak Position Comparison of Transimission with Simulated Reflection-Absorption Spectra**

| Transimission (in KBr), ($cm^{-1}$) | Simulated RA $RA_p$ ($cm^{-1}$) | Simulated RA $RA_s$($cm^{-1}$) | Assignment |
|---|---|---|---|
| 2957.4 | 2958.1 | 2958.1 | $CH_3$ asymmetric ($\nu_a$) |
| 2919.5 | 2919.9 | 2920.0 | $CH_2$ asymmetric ($\nu_a$) |
| 2872.1 | 2872.0 | 2872.0 | $CH_3$ symmetric ($\nu_s$) |
| 2850.1 | 2850.7 | 2850.7 | $CH_2$ symmetric ($\nu_s$) |

# CHAPTER 3
# EXPERIMENTAL

## 3.1. Materials

Sodium dodecanesulfonate ($C_{12}H_{25}SO_3Na$) and lauryl sodium sulfate ($C_{12}H_{25}SO_4Na$) both of >99% purity were purchased from Research Plus Inc., Bayonne, NJ.

Dodecyltrimethylammonium bromide ($C_{12}H_{25}NC_3H_9Br$), >99% purity was purchased from Sigma Chemical Company, St. Louis, MO.

Dodecyl-$d_{25}$ sodium sulfate ($C_{12}D_{25}SO_4Na$), 98% deuterated was purchased from Cambridge Isotope Laboratories , Woburn, MA.

Sodium chloride, lithium chloride, and sodium bromide for increasing the total ionic strength of surfactant solutions are analytical grade reagents (J.T. Baker Chemical Co., Philisberg, NJ). Each salt was baked in a porcelain casserole for several hours at red heat to remove traces of organic compounds which may affect the surface properties of the studied surfactants.

The water used for preparation of surfactant solutions is first deionized and then distilled twice, the last time from alkaline permanganate solution through a 3-ft-high Vigreaux column with a quartz condenser and receiver (specific conductivity $1.1X10^{-6}$ mho $cm^{-1}$ at 25.0°C).

## 3.2 Surface Tension Measurements

All surface tension measurements were made by the Wilhelmy vertical plate technique, using a sand-blased platinum plate of ca. 5-cm perimeter. Instruments were calibrated against quartz-condensed water each day that

measurements were made. The plate was suspended from a dial-type torsion balance capable of being read to 0.2 mg (ca. 0.04 mN/m). All solution to be tested were immersed in a constant temperature bath at the desired temperature (25.00± 0.02°C), and aged for at least 30 minutes before measurements were made. Set of measurements were taken at 20-minutes intervals until no significant change occurred.

Before being used for surface tension measurements, aqueous solutions of anionic surfactants (sulfonates and sulfates) were further purified by passage four times through minicolumns of octadecylsilanized silica gel (52) to remove any traces of impurities more surface active than the parent compound. The concentration of anionic surfactant in the effluent from these columns was determined by two-phase titration with Hyamine 1622 (53, 54).

### 3.3. Dynamic Surface Tension Measurements

The maximum bubble pressure method was used to measure the dynamic surface tension of surfactant solutions (55). The maximum bubble pressure apparatus consists of a gas-feeding system and a bubble pressure and frequency measuring system. The gas used to produce bubbles is $N_2$. The pressure variation in the capillary during bubble formation is monitored by a pressure transducer. The output from the pressure transducer is fed into an IBM personal computer with a "Notebook" software. Both the bubble frequency and the maximum bubble pressure are measured. Pure water (see chapter 3.1) was used as the standard substance to obtain the calibration factor (voltage to surface tension). The calibration is checked each day . The relative error in the reproducibility of the dynamic surface tension values of the surfactant solutions is about 1%.

### 3.4. Monolayer Preparation

A Teflon trough was immersed in a mixture of $HNO_3$ and $H_2SO_4$ (1:10 ratio) for about 30 minutes for cleaning. The Teflon trough was rinsed in tap water, then quartz-condensed water. The clean Teflon trough was filled with 12.5 ml of a surfactant solution studied at the ambient temperature (25 ± 1°C), and an adsorbed monolayer of the surfactant allowed to form at the air/water interface. A time of 30 minutes of equilibrium was allowed for surfactant molecules to diffuse to the interface before the measurement was carried out.

### 3.5. Spectroscopy

Single external reflection-absorption FTIR spectra of surfactant monolayers at the aqueous solution/air interface were obtained with a Digilab FTS-60A FTIR spectrometer coupled with a monolayer/grazing angle accessory (Specac 19653). The experimental optical arrangement for observing the reflection-absorption spectra of an adsorbed monolayer at the air/water interface is shown in Figure 3.1. The incoming radiation was polarized (*p*- or *s*- polarization) with a Au wire grid polarizer (Perkin-Elmer, Norwalk, CT). The angle of incidence IR beam is 30° from the surface normal. Figure 3.2 and Figure 3.3 show some spectra of the same $C_{12}SNa$ monolayer at different incident angle (θ). It is apparent that increase in the incident angle results in an increase in the intensity of signal and as well as noise. In order to get both strong intensity and good signal-noise ratio simultaneously, 30° incident angle is selected for both *p*- and *s*- polarizations in all experiments. All the spectra are collected by coadding 4096 scans at 8 $cm^{-1}$ resolution with a narrow-band liquid $N_2$ cooled HgCdTe (MCT) detector.

One level of zerofilling yields a data increment of 4 $cm^{-1}$. Final reflection-absorption spectra are generated by dividing a polarized single beam reflectance spectrum of the surfactant monolayer by a same polarized single beam reflectance spectrum of quartz-condensed water (or corresponding salt solution without surfactant) and taking the negative logarithm. All spectra are transferred to a VAX Cluster for spectral manipulation and processing. The computer programs "PLT" and "PLOTTER" written by Dr. Fina (Department of Materials and Engineering, Rutgers University) and standard Digilab software available on the FTS-60A computer were used to obtain band frequencies and spectral plots.

### 3.6. Baseline Determination

The primary source of inaccuracies in the determination of experimental intensities is baseline fluctuations. In the reflection-absorption experiment, baseline fluctuations are minimized by using exactly the same optical path for the sample and the reference (background). The height and the curvature of the surface of the surfactant solution (or the pure water) can dramatically affect the optical path. Figure 3.4 shows the changes in height of the $C_{12}SNa$ ($C = 4.0X10^{-3}$ M) solution and pure water in the Teflon trough during the experiment time at room temperature of $25 \pm 1°C$ and relative humidity of 60%, due to evaporation of water. It is observed that both surfactant and water solution have the same water evaporation rate, and the decrease in the height of solution is directly proportional to the experimental time (about 0.5 mm per hour). An example of the effect of changes in height on the reflection-absorption spectra is shown in Figure 3.5. The spectra are produced using

the negative $\log(I_2/I_1)$ where $I_1$ is a single beam reflectance spectrum of pure water at time $t_0$, and $I_2$ is a single beam reflectance spectrum of the same water at time t (t = 1, 2, 3, 4, 5 hours, respectively). In this case, the change in the height of water surface with the time interval $t\text{-}t_0$ is due to water evaporation. The bottom spectrum with $t - t_0 = 5$ hours has $\Delta RA = 0.006$ in methylene stretching region. Considering the fact that 0.006 is in the same intensity range as typical experimental RA intensities, a procedure should be designed to minimize this effect. Single beam sample spectra are ratioed with all reference (background) spectra. The "correct" ratio is visually determined by the elimination of baseline curvature in the 3050-2800 $cm^{-1}$ region. Figure 3.6 shows a representative RA spectrum of $C_{12}SNa$ monolayer ($C = 4.0X10^{-3}$ M, in pure $H_2O$, *s*-polarized ), the spectrum has a very good signal-noise ratio and a smooth baseline in the C-H stretching region.

### 3.7. Experimental Reproducibility and Errors

Figure 3.7. shows the reproducibility of The RA spectra of the adsorbed monolayers of $C_{12}SNa$ at the aqueous solution/air interface in pure water solution. The spectra are taken for four surfactant solution samples with the same bulk concentration, $C = 4.00X10^{-3}$M, and at different time. All the IR parameters are kept constant. It is observed that all four spectra have a good reproducibility in both the peak intensity and the frequency in the C-H stretching region of methylene groups. The data on peak intensities (heights) and frequencies in this region are listed in Table 3.7.1. It is found that the

**Table 3.7.1.**

**Experimental Reproducibility and Error in RA Intensity and Frequency Measurements**

| sample | $\nu_a$ (C-H) | | | $\nu_s$ (C-H) | | |
|---|---|---|---|---|---|---|
| number | H(mm) | $RA_1(X10^{-3})$ | $Wn_1(cm^{-1})$ | H(mm) | $RA_2(X10^{-3})$ | $Wn_2(cm^{-1})$ |
| 1 | 56.0 | 4.10 | 2917.1 | 40.0 | 2.93 | 2848.8 |
| 2 | 54.0 | 3.96 | 2917.4 | 38.0 | 2.79 | 2849.1 |
| 3 | 53.0 | 3.89 | 2917.5 | 38.0 | 2.79 | 2849.0 |
| 4 | 53.0 | 3.89 | 2917.2 | 38.5 | 2.82 | 2849.2 |

$RA_1 = (3.96 \pm 0.10)X10^{-3}$; $RA_2 = (2.83 \pm 0.07)X10^{-3}$

$Wn_1 = 2917.3 \pm 0.2cm^{-1}$; $Wn_2 = 2849.0 \pm 0.2cm^{-1}$

intensity measurement has a relative percent error of 2.5%, and the frequency measurement only about 0.02% ($\pm$0.2 $cm^{-1}$). It is clear that the accuracy of measuring peak frequencies is much greater than that of measuring RA intensity, thus the small change in peak frequencies is more significant than much larger change in RA intensity.

# CHAPTER 4
# RESULTS AND DISCUSSION

## 4.1. Anionic Surfactant - Sodium Dodecanesulfonate ($C_{12}H_{25}SO_3Na$)

### 4.1.1. Static (Equilibrium) Surface Tension Measurements

Plots of the surface tension, $\gamma$, of aqueous solutions of $C_{12}H_{25}SO_3Na$ ($C_{12}SNa$) vs. log of their solution concentration, in mol/dm$^3$, in pure $H_2O$, 0.1M NaCl, 0.5M NaCl, and 0.1M LiCl solutions at 25.00 $\pm$ 0.02°C are shown in Figure 4.1.1. From this Figure, the surface pressure, $\pi$, in mN/m, the area per molecule (A), in Å$^2$, the surface excess concentration at the interface, $\Gamma$, in mol/cm$^2$, were calculated using equations (1.1), (1.2), (1.6), and (1.7). The data of $\pi$, $\gamma$, and A at various bulk surfactant concentrations in pure $H_2O$, 0.1M NaCl, 0.5M NaCl, and 0.1M LiCl solutions are listed in Table 4.1.1., 4.1.2., 4.1.3., and 4.1.4., respectively. Figure 4.1.2. is a diagram of surface pressure vs. area per molecule for $C_{12}SNa$ in pure $H_2O$, 0.1M NaCl, 0.5M NaCl, and 0.1M LiCl solutions. Comparing these curves with Figure 1.1., we may conclude that the states of all the adsorbed monolayers of $C_{12}SNa$ at the aqueous solution/air interface with various total ionic strengths at the saturated adsorption can be classified as liquid expanded monolayers (LE). From Figure 4.1.2, it is also observed that there exists a phase transition point ($C_t$) for each of the adsorbed monolayers of $C_{12}SNa$ in aqueous solutions between the LE and gaseous (G) states, when the area per molecule abruptly

**Table 4.1.1**

**Data on $\gamma$, $\pi$, and A for $C_{12}H_{25}SO_3Na$ in Pure $H_2O$ Solution (25.0°C)**

| C (M) | logC | $\gamma$ (mN/m) | $\pi$ (mN/m) | A ($Å^2$) |
|---|---|---|---|---|
| $2.69X10^{-2}$ | -1.57 | 39.0 | 33.0 | -* |
| $2.34X10^{-2}$ | -1.63 | 39.0 | 33.0 | -* |
| $1.17X10^{-2}$ | -1.93 | 40.0 | 32.0 | 56.7 |
| $5.89X10^{-3}$ | -2.23 | 47.8 | 24.2 | 56.7 |
| $3.71X10^{-3}$ | -2.43 | 54.0 | 18.0 | 56.7 |
| $3.16X10^{-3}$ | -2.50 | 55.8 | 16.2 | 64.0 |
| $2.40X10^{-3}$ | -2.62 | 59.2 | 12.8 | 72.8 |
| $1.74X10^{-3}$ | -2.76 | 62.4 | 9.6 | 88.0 |
| $1.17X10^{-3}$ | -2.93 | 65.7 | 6.3 | 122.0 |
| $6.31X10^{-4}$ | -3.20 | 68.4 | 3.6 | 182.0 |

* above the cmc.

**Table 4.1.2**

**Data on $\gamma$, $\pi$, and A for $C_{12}H_{25}SO_3Na$ in 0.1M NaCl Solution (25.0°C)**

| C (M) | logC | $\gamma$ (mN/m) | $\pi$ (mN/m) | A ($Å^2$) |
|---|---|---|---|---|
| $2.95X10^{-3}$ | -2.53 | 35.8 | 36.5 | -* |
| $2.40X10^{-3}$ | -2.62 | 35.8 | 36.5 | -* |
| $1.32X10^{-3}$ | -2.88 | 41.4 | 30.9 | 44.0 |
| $7.94X10^{-4}$ | -3.10 | 45.8 | 26.5 | 44.0 |
| $5.25X10^{-4}$ | -3.28 | 50.3 | 22.0 | 44.0 |
| $3.71X10^{-4}$ | -3.43 | 53.3 | 19.0 | 49.0 |
| $2.63X10^{-4}$ | -3.58 | 56.3 | 16.0 | 52.6 |
| $1.07X10^{-4}$ | -3.97 | 62.4 | 9.9 | 64.9 |
| $7.58X10^{-5}$ | -3.28 | 64.7 | 7.6 | 71.2 |

* above the cmc.

**Table 4.1.3**

**Data on $\gamma$, $\pi$, and A for $C_{12}H_{25}SO_3Na$ in 0.5M NaCl Solution (25.0°C)**

| C (M) | logC | $\gamma$ (mN/m) | $\pi$ (mN/m) | A ($Å^2$) |
|---|---|---|---|---|
| $3.98X10^{-4}$ | -3.40 | 38.0 | 35.0 | 41.5 |
| $2.63X10^{-4}$ | -3.58 | 42.2 | 30.8 | 41.5 |
| $1.35X10^{-4}$ | -3.87 | 49.2 | 23.8 | 41.5 |
| $8.91X10^{-5}$ | -4.05 | 52.8 | 20.2 | 42.9 |
| $6.31X10^{-5}$ | -4.20 | 56.3 | 16.7 | 46.9 |
| $4.26X10^{-5}$ | -4.37 | 59.1 | 13.9 | 52.3 |
| $2.69X10^{-5}$ | -4.57 | 62.8 | 10.2 | 60.3 |
| $1.78X10^{-5}$ | -4.75 | 65.3 | 7.7 | 70.7 |

**Table 4.1.4**

**Data on $\gamma$, $\pi$, and A for $C_{12}H_{25}SO_3Na$ in 0.1N LiCl Solution (25.0°C)**

| C (M) | logC | $\gamma$ (mN/m) | $\pi$ (mN/m) | A ($Å^2$) |
|---|---|---|---|---|
| $3.55X10^{-3}$ | -2.45 | 37.2 | 35.1 | 46.8 |
| $3.00X10^{-3}$ | -2.52 | 37.2 | 35.1 | 46.8 |
| $1.48X10^{-3}$ | -2.82 | 42.4 | 29.9 | 46.8 |
| $1.12X10^{-3}$ | -2.95 | 44.9 | 27.4 | 46.8 |
| $5.60X10^{-4}$ | -3.25 | 51.0 | 21.3 | 47.4 |
| $2.80X10^{-4}$ | -3.55 | 57.0 | 15.3 | 50.7 |
| $1.40X10^{-4}$ | -3.85 | 62.3 | 10.0 | 54.6 |

changes from $A_{min}$ to a higher value. It is interesting to note that the phase transition points for all of the four different solutions are at a surface pressure, $\pi$, of about 20mN/m. In fact, values of $C_t$ of all of the four surfactant solutions are very close to their $C_{20}$. Rosen (22) has indicated that when the surface (or interfacial) tension has been reduced by 20mN/m, the surface concentration is 84-99.9% saturated, and $pC_{20}$ is a measure of the standard free energy of adsorption. Thus, the bulk concentration of surfactant required to depress the surface (or interfacial) tension of the solvent by 20mN/m,$C_{20}$, is not only a good measure of the efficiency of adsorption of the surfactant, but also an indication of phase transition between LE and G phases of adsorbed monolayers at the aqueous solution/air interface.

The data of cmc, $\Gamma_{max}$, $A_{min}$, and $C_t$ for $C_{12}SNa$ in pure $H_2O$, 0.1M NaCl, 0.5M NaCl, and 0.1M LiCl are listed in Table 4.1.5. These data are consistent with those reported by Dahanayake (24) and Rosen (22). It is seen that the surface excess concentration increases with increase in the total ionic strength of surfactant solutions, and the area per molecule on the absorbed monolayer at the aqueous solution/air interface consequently decreases. This results in increasing adsorption at the interface because of the decrease in repulsion force between the oriented charged head groups at the interface. It is noteworthy that the value of $\Gamma_{max}$ for $C_{12}SNa$ in 0.1M NaCl solution is larger than that in 0.1M LiCl, even though Li has a smaller atomic radius than Na. It means that $C_{12}SNa$ solution has stronger adsorption at the aqueous solution/air interface in 0.1M NaCl solution than in 0.1M LiCl. This phenomena may be explained by the difference between the hydrated ion

**Table 4.1.5**

**Surface Properties of $C_{12}H_{25}SO_3Na$ Solutions** (25.0°C)

| medium | cmc (M) | $\pi_{cmc}$ (mN/m) | $\Gamma_{max}$ ($X10^{10}$ mol./$cm^2$) | $A_{min}$ ($Å^2$) | $C_t^*$ (M) |
|---|---|---|---|---|---|
| pure $H_2O$ | $1.25X10^{-2}$ | 32.5 | 2.95 | 56.5 | $3.0X10^{-3}$ |
| 0.1M NaCl | 2.50X10-3 | 36.0 | 3.85 | 44.0 | $3.7X10^{-4}$ |
| 0.5M NaCl | - ** | >37.0 | 3.85 | 41.5 | $9.0X10^{-5}$ |
| 0.1M LiCl | $2.69X10^{-3}$ | 35.1 | 3.55 | 46.8 | $4.0X10^{-4}$ |
| [a]pure $H_2O$ | $1.24X10^{-2}$ | 33.0 | 2.93 | 56.7 | - |
| [a]0.1M NaCl | 2.47X10-3 | 36.4 | 3.76 | 44.2 | - |
| [a]0.5M NaCl | - ** | >37.0 | 3.85 | 41.5 | - |

* $C_t$ = phase transition concentration.

** solubility too low to determine cmc.

[a]. data from reference (24)

radii of $Na^+$ and $Li^+$ in aqueous solution. Because $Na^+$ has a smaller charge density in aqueous solution, and consequently a smaller hydrated ion radius than $Li^+$, $Na^+$ is more tightly bounded with surfactant anion ($C_{12}S^-$), and therefore, $C_{12}SNa$ molecules appear to be more effectively adsorbed at the interface than $C_{12}SLi$. Table 4.1.5 also shows that $C_{12}SNa$ solution in 0.1M LiCl has a larger cmc than in 0.1M NaCl due to the same reason.

### 4.1.2. Dynamic Surface Tension and Kinetic Adsorption

Figure 4.1.3 is a plot of dynamic surface tension (maximum bubble pressure method) vs. log of the surface age (bubble lifetime). The data are listed in Table 4.1.6. The static surface tension (Wilhelmy method) of $1.2X\ 10^{-2}M$ $C_{12}SNa$ aqueous solution at different measurement times was also measured. The data are listed in Table 4.1.7, and the plot of surface tension vs. measurement time is shown in Figure 4.1.4.

The generally accepted physical model of adsorption kinetics at the aqueous solution/air interface consists of a two-step process. The first step is the diffusion of surfactant molecules in the bulk phase up to the subphase close to the interface. It is caused by the concentration gradient produced by the adsorption of surfactant molecules at the very beginning of the process. The subphase is not fixed; it is defined as the place from where molecules can be adsorbed without further transport. The second step can be described as the transfer step of molecules from the soluted to the adsorbed state and vice versa. Both steps proceed simultaneously. Depending on the rates of the processes the adsorption is diffusion-controlled if the first step is much

**Table 4.1.6**

**Dynamic Surface Tension Data of $C_{12}H_{25}SO_3Na$ Solution***

| time | dynamic surface tension (mN/m) |
|---|---|
| 0.05 sec. | 56.3 |
| 0.10 sec. | 54.6 |
| 0.16 sec. | 54.0 |
| 0.24 sec. | 53.5 |
| 0.30 sec. | 53.3 |
| 0.50 sec. | 52.9 |
| 1.00 sec. | 52.5 |
| 2.60 sec. | 52.4 |
| 3.30 sec. | 52.2 |
| 6.00 sec. | 51.8 |
| 10.0 sec. | 51.4 |
| 21.4 sec. | 51.0 |
| 50.0 sec. | 50.3 |
| 1.0 hr** | 40.5 |

* maximum bubble pressure method, at 25.0°C, C = $5.0X10^{-3}$M.

** Static surface tension (Wilhelmy method)

**Table 4.1.7**

**Data on Surface Tensions of $C_{12}H_{25}SO_3Na$ Solution***

| time | surface tension (mN/m) |
|---|---|
| 5 min. | 42.6 |
| 20 min. | 40.5 |
| 35 min. | 39.8 |
| 50 min. | 39.5 |
| 65 min. | 39.1 |
| 80 min. | 39.1 |
| 100 min. | 39.1 |

*Wilhelmy method, at 25.0°C, and c = $1.2X10^{-2}$M in pure water.

slower than the second one and kinetically-controlled in the opposite case. If the rates of both steps are of the same order, we speak about a mixed diffusion-kinetic-controlled adsorption process.

Ward and Tordai (56) presented a physical model of such a process, based on the first and second diffusion laws. They derived the following equation for the process:

$$\Gamma = 2\,(D/\Pi)^{1/2}\,[C_0\,t^{1/2} - \int_0^t C(0, t-\tau)\,d(\tau^{1/2})] \qquad (4.1)$$

where $\Gamma$ = surface concentration at the interface, in mol./cm$^2$;

D = diffusion coefficient of surfactant molecule, in cm$^2$/s;

t = time, in seconds.

$C_0$ = surfactant bulk concentration, in mol./cm$^3$.

$\tau$ = variable.

Hansen (57) has discussed the theory of diffusion-controlled adsorption. The general solution, which includes adsorption and desorption, has two limiting cases which can be compared to experiment corresponding to the initial (short time) adsorption and the final (long time) adsorption for systems obeying the Langmuir isotherm. For the short time approximation,

$$(\gamma_0-\gamma)/C_0 = 2RT\,(D/\Pi)^{1/2}\,t^{1/2}; \qquad (4.2)$$

for the long time approximation,

$$\gamma - \gamma_{eq.} = \Gamma^2 RT / [C_0 (\Pi Dt)^{1/2}] \qquad (4.3)$$

where $\gamma_{eq.}$ = equilibrium static surface tension of the surfactant solution investigated, in $10^{-5}$ N/cm;

$\gamma_0$ = surface tension of the solvent, in $10^{-5}$ N/cm;

$\gamma$ = dynamic surface tension of the surfactant solution investigated, in $10^{-5}$ N/cm;

R = gas constant, equal to 831 N.cm/K°mol;

T = absolute temperature, in K°.

Using these equations and experimental data, we can calculate the apparent diffusion coefficient, D. Comparing the calculated D value with the reasonable value (~$10^{-6}$ $cm^2/s$), we are able to determine whether or not the adsorption is diffusion-controlled.

The calculated short time approximation D value for the $C_{12}$SNa solution is about 1.7X $10^{-7}$ $cm^2/s$. This value is much smaller than the regular diffusion value. Therefore, the adsorption of $C_{12}$SNa in pure $H_2O$ solution may not be completely diffusion-controlled.

Figure 4.1.4 shows that it takes about 1 hr. to reach the equilibrium surface tension value for a 1.2X$10^{-2}$M $C_{12}$SNa aqueous solution. Figure 4.1.5 is a plot of reflection-absorption intensity of the adsorbed monolayer of $C_{12}$SNa at the aqueous solution/air interface from various bulk concentrations vs. the measuring time. General speaking, it also takes about

30 minutes to reach a constant RA intensity for all of the $C_{12}SNa$ solutions. Figure 4.1.6 and 7 are plots of peak frequency shifts from the equilibrium frequency vs. the equilibrium time in the asymmetric C-H stretching band ($2920cm^{-1}$) and the symmetric stretching band ($2850cm^{-1}$), respectively. Within experimental error, 30 minutes of equilibrium time is an acceptable period for reaching equilibrium for the adsorbed monolayers of $C_{12}SNa$ at the water/air interface.

### 4.1.3. Orientation of $C_{12}SNa$ Molecules at the Aqueous Solution/Air Interface in Pure $H_2O$ Solution

Figure 4.1.8 is a diagram of a tilted $C_{12}SNa$ molecule at the air/water interface. This diagram explains vibration directions of the symmetric ($\nu_s$) and asymmetric ($\nu_a$) C-H stretching modes in methylene groups ($-CH_2-$) and S-O stretching modes in sulfonate group ($-SO_3^-$) relative to the chain axis . It is noteworthy that both $\nu_s$ and $\nu_a$ of methylene groups are perpendicular to the chain axis and orthogonal to each other.

Figures 4.1.9(a) and (b) are *p*- and *s*-polarized reflection-absorption spectra of $C_{12}SNa$ in pure $H_2O$ in the C-H stretching bands at various bulk concentrations. Spectra are plotted as a function of decreasing surfactant solution concentration from bottom to top. The measured peak intensities from IR spectra are listed in Table 4.1.8. The RA intensity vs. log of the bulk concentration is shown in Figure 4.1.10. From Table 4.1.8 and Figure 4.1.10., it is seen that both intensities of the symmetric and asymmetric bands remain constant to a good approximation as the bulk concentration is above the

phase transition point. The phase transition concentration determined from FTIR spectra is in the range of $2.86X10^{-3}M$. It is in a good agreement with the value of $3.0X10^{-3}M$ from the surface tension measurements (Table 4.1.5).

The average chain orientation angles predicted from the polarized intensities using the higher frequency asymmetric stretching peak ($2920cm^{-1}$) for different bulk concentration of $C_{12}SNa$ aqueous solutions are also listed in Table 4.1.8. At the saturated adsorption, the average orientation angle of methylene chains of $C_{12}SNa$ at the aqueous solution/air interface is $38.4 \pm 3.3°$, and the absorption coefficient of the monolayer, $k_{max} = 0.528 \pm 0.035$.

Table 4.1.9 lists data of orientation angles of methylene chains of some similar compounds (including $C_{12}SNa$) at different interface or in the crystalline solid. It is interesting to find that the chain tilt angle (41.3°) of $C_{12}SNa$ molecules determined by X-ray crystallography (58) in triclinic crystals is almost the same as the orientation angle ($38.4 \pm 3.3°$) at the air/water interface. This result may indicate that the structure of a saturated adsorbed monolayer of $C_{12}SNa$ (with close packing) at the aqueous solution/air interface is very similar to that found in solids of $C_{12}SNa$ crystallized from its supersaturated aqueous solution.

Another important observation is the change in peak frequencies of the C-H stretching bands with bulk concentration. The frequency and width of the $CH_2$ stretching bands are sensitive to the *gauche/trans* conformer ratio and hence, the average amount of disorder in the methylene chains. The increase in wavenumber is partly due to the increase in *gauche* conformers (59), and partly due to the decrease in the density or packing state of the

**Table 4.1.8.**

**Properties of Adsorbed Monolayers of $C_{12}H_{25}SO_3Na$ at The Aqueous Solution/Air Interface in $H_2O$**

| $CX10^3$(M) | $RApX10^3$ | $RAsX10^3$ | RAp/RAs | $\chi$(°) | A($Å^2$) |
|---|---|---|---|---|---|
| 10.0 | 6.45 | 4.05 | 1.61 | 40 | 57 |
| 8.76 | 6.40 | 4.00 | 1.60 | 41 | 57 |
| 5.60 | 6.50 | 4.00 | 1.65 | 30 | 57 |
| 4.48 | 6.30 | 4.00 | 1.58 | 41 | 57 |
| 3.58 | 6.30 | 3.95 | 1.59 | 42 | 57 |
| 2.86 | 3.53 | 2.30 | 1.56 | 48 | 65* |
| 1.87 | 2.67 | 2.00 | 1.34 | - | 96 |
| 1.00 | 2.00 | 1.60 | 1.25 | - | 127 |

| C ($X10^3$M) | $\nu_a$(C-H) ($cm^{-1}$) | $\nu_s$(C-H) ($cm^{-1}$) | $\nu_a$(S-O) ($cm^{-1}$) | $\nu_s$(S-O) ($cm^{-1}$) |
|---|---|---|---|---|
| 10.0 | 2917.2 | 2849.0 | 1167.2 | 1037.6 |
| 8.76 | 2917.3 | 2848.9 | 1167.0 | 1037.6 |
| 5.60 | 2917.2 | 2848.8 | 1167.2 | 1037.5 |
| 4.48 | 2917.3 | 2849.0 | 1166.8 | 1037.6 |
| 3.58 | 2917.3 | 2849.1 | 1167.0 | 1037.4 |
| 2.86 | 2920.0 | 2851.0 | 1166.6 | 1036.8* |
| 1.87 | 2921.0 | 2852.0 | 1164.8 | 1036.3 |

* phase transition concentration region

**Table 4.1.9**

**Data on Orientation Angles of Polymethylene Chains**

| substance | surface | χ(°) | method | ref. |
|---|---|---|---|---|
| $CH_3(CH_2)_{15}SH$ | gold | 40 | IR (reflectance) | 1 |
| $C_{12}H_{25}SO_3Na$ | crystals | 37 | X-ray diffraction | 2 |
| $C_{12}H_{25}SO_3Na$ | ( triclinic crystals) | 41 | X-ray diffraction | 3 |
| $^aC_{12}H_{25}$-$C_{10}H_6SO_3Na$ | water | 43 | OSHG* | 4 |
| $C_{12}H_{25}SO_3Na$ | water | 38.4 ± 3.3° | RA (FTIR)** | 5 |

a. sodium 1-dodecylnaphthalene-4-sulfonate.

*OSHG = optical second harmonic generation.

** RA = reflection-absorption spectroscopy.

**References:**

1. Nuzzo, R.G., *J. Am. Chem. Soci.*, 112, 558(1990).

2. Saito, E. et. al. , *Colloid Interface Sci.*, 3, 771(1972).

3. Lingafelter, E.C. et. al. , *Acta Cryst.*, 3, 257(1950).

4. Rasing, T. et. al. , *Phys. Rev.*, A31, 537(1985).

5. Tung, Y.S., Gao, T. Fina, L.J., and Rosen, M.J. , *Appl. Spectros.*, accepted for publication.

methylene chain (60). Change in frequencies of these bands have been used to characterize the process of micellization as a function of concentration of alkanoates (61), the coagel to micelle transition (critical micellization temperature) (62, 63), and the pressure-induced micelle to coagel transitions of surfactants (64) and phospholipids (65). The data on frequencies of $CH_2$ stretching bands in adsorbed monolayers of $C_{12}SNa$ at the air/water interface with various bulk concentrations are listed in Table 4.1.8. At the saturation adsorption, the bulk concentration is above the phase transition point, both frequencies of the asymmetric and symmetric stretching C-H bands remain at constant values (2917.2$cm^{-1}$ and 2848.9$cm^{-1}$). These values are lower than the corresponding values determined from transmission spectra of $C_{12}SNa$ in a KBr pellet (2919.5$cm^{-1}$ and 2850.1 $cm^{-1}$). One possible reason for the higher values in the KBr pellet of $C_{12}SNa$ is the change in the conformation of methylene chains caused by the mixing and grinding process with KBr powder.

The low frequencies of the $CH_2$ stretching bands in saturated adsorbed monolayers at the aqueous solution/air interface indicate that the methylene chains of $C_{12}SNa$ molecules at the air/water interface are very ordered with all-*trans* conformation. This implies that all carbon atoms of the chain are coplanar. The all-*trans* state is conducive to the closest packing of an assembly of chains due to strong interactions between methylene chains in the monolayer at the interface. The peak frequencies of the C-H stretching bands increase with decrease in bulk concentration when the bulk concentration is below the phase transition point. In this case, the distance

between methylene chains of $C_{12}SNa$ molecules in the monolayer is not close enough (area per molecule increases) to keep methylene chains very ordered, and more and more *gauche* conformers are formed. Theoretically, a bond can rotate from a *trans* angle to one of two *gauche* angles with an energy absorption of about 0.5 kcal/mol (66). After *trans-gauche* rotation, the carbon atoms of a methylene chain are no longer coplanar, the chain is "bent" and takes up a larger monolayer area.

In chapter 2.4, we have already discussed the method for simultaneous extraction of the orientation angle ($\chi$) and absorption coefficient ($k_{max}$) which is related to the surface concentration. The saturated surface excess concentration ($\Gamma_{max}$) of $C_{12}SNa$ monolayer in pure water is determined from the plot of surface tension vs.log C (Fig. 4.1.1.) as $2.93X10^{-10}$ mol./cm$^2$ (Table 4.1.5). This value can be compared with the surface concentration calculated from reflection-absorption data. The conversion of $k_{max}$ to surface concentration is done in the following way: A reference point (one-point standardization method) is needed where both values of bulk $k_{max}$ and concentration of $C_{12}SNa$ are known. Solid $C_{12}SNa$ dispersed in a KBr matrix is used for this purpose. The $k_{max}$ value of the asymmetric methylene stretching band (2919.5cm$^{-1}$)is found by first determining $k_{isotropic}$ using a Kramers-Kronig transform and second, $k_{max} = 3k_{iso}$. An average of three independent trials using finely ground powder yields $k_{iso} = 0.234$, and therefore, $k_{max} = 0.702$ for $C_{12}SNa$ crystal. The bulk concentration of solid $C_{12}SNa$ is calculated from its molecular weight (272.4 g/mol) and the density. The density of $C_{12}SNa$ is measured by a flotation method using mixtures of

1,4-dioxane and carbon tetrachloride. The density of $C_{12}SNa$ is measured as 1.21g/cm$^3$, and the bulk concentration of solid $C_{12}SNa$ is then calculated as 4.44.X10$^{-3}$ mol./cm$^3$. The ratio of the $k_{max}$ values of the adsorbed monolayer and the solid crystals of $C_{12}SNa$ is 0.528/0.702 = 0.752. Since the $k_{max}$ ratio is directly proportional to the concentration ratio, using the one point standardization method, the three-dimensional concentration of the monolayer is $C_0$ = 4.44X10$^{-3}$mol/cm$^3$ X 0.752 = 3.34 X10$^{-3}$ mol/cm$^3$. In order to compare this value with the surface concentration ($\Gamma_{max}$) obtained from surface tension data ($\Gamma_{max}$ = 2.93X10$^{-10}$ mol/cm$^2$), a conversion from the three-dimensional concentration, $C_0$, to the two-dimensional concentration (surface concentration), $C_s$, should be done in the following way:

$C_s = C_0$ (3.34X10$^{-3}$ mol/cm$^3$) X d (thickness of the monolayer, in cm), where d = l X cos $\chi$, l = 17.8X10$^{-8}$cm (molecular length of $C_{12}SNa$, calculated from the standard bond lengths and bond angles), and $\chi$, chain orientation angle, is 38.4°. Therefore, d = 13.9X10$^{-8}$cm, and $C_s$ = 3.34X10$^{-3}$mol/cm$^3$ X 13.9X10$^{-8}$cm = 4.66X10$^{-10}$ mol/cm$^2$. The surface concentration, $C_s$ = 4.66X10$^{-10}$ mol/cm$^2$, predicted by this method is reasonably close to the $\Gamma_{max}$, 2.93X10$^{-10}$ mol/cm$^2$, calculated from the surface tension data, having the same order of magnitude. But, the former one is 1.59 times larger than the latter.

An obvious source of error in the conversion of $k_{max}$ value to surface concentration is the use of $k_{max}$ value from $C_{12}SNa$ in KBr. A considerable amount of grinding and mixing is required to obtain absorption independent of particle size and mixing time. This process undoubtedly destroys the crystal structure of $C_{12}SNa$ and introduces a fraction of gauche conformers into methylene chains. Evidence for the presence of *gauche* conformation in the KBr matrix is seen from changes in frequencies of methylene stretching bands. As compared with the adsorbed saturated monolayer, the asymmetric C-H stretching frequency of $C_{12}SNa$ in KBr is shifted 2.1 $cm^{-1}$ higher, and the symmetric stretching one, 1.1 $cm^{-1}$ higher. The introduction of *gauche* conformers in the $C_{12}SNa$ in KBr reduces the $k_{max}$ of the methylene stretching peaks from the all-*trans* $k_{max}$. This effect at least partly compensates for the higher surface concentration predicted from the infrared data.

Another potential source of error in the determination of orientation and concentration is the assumption that the monolayer thickness varies only as the $\cos\chi$. Although this assumption seems reasonable, there is no direct evidence to prove it. The effect on the problem will, of course, depend on the actual nature of the thickness change. Penfold and his co-workers (67) have studied the structure of aqueous tetramethylammonium dodecylsulphate (TMDS) solutions at the air/water interface using specular reflection of neutrons. They reported a staggered structure of the adsorbed monolayer, the fraction of methylene chains included in the head group region at completion of the monolayer is 0.15 which corresponds to about 2 of 11 $CH_2$

units. Because of the structure similarity of TMDS and $C_{12}SNa$, the adsorbed monolayer of $C_{12}SNa$ at the air/water interface may also have the similar staggered structure, and this will cause a big changes in the thickness of the monolayer and as well as in absorption coefficient of the monolayer.

Thirdly, the distribution function of chain orientation angles may not be a mathematical delta function as assumed in the calculations. Model calculations using orientation distribution functions other than a delta function indicate that the derived chain orientation and $k_{max}$ values are only weakly influenced by increases in the half-width of the distribution function.

The last possible source of error in the determination of surface concentrations is the quantitative method of one point standardization. Beer's law is successful in describing the absorption of dilute solutions. At high concentrations (usually > 0.01M), the average distance between the species responsible for absorption is diminished to the point where each affects the charge distribution of its neighbors. This interaction, in turn can alter their ability to absorb a given wavelength of radiation. Because the extent of this interaction depends upon concentration, the occurrence of this phenomenon causes deviation from the linear relationship between absorbency and concentration. Using a multi-point calibration method (calibration curve) is much better for the purpose of quantitative analysis.

### 4.1.4. Adsorbed Monolayers of $C_{12}SNa$ at The Air/water Interface in 0.1M and 0.5M NaCl Solutions

Because of the limitation of the solubility of $C_{12}SNa$ in NaCl solution (the common ion effect), the bulk concentrations of surfactant studied in NaCl solutions are much lower than those in pure water solution. The spectra of

adsorbed monolayers of $C_{12}SNa$ at the aqueous solution/air interface in 0.1M NaCl solutions are shown in Figure 4.1.11. Changes in RA intensities in the C-H stretching region of the polymethylene chains with changes in surfactant bulk concentrations in 0.1M NaCl solution are shown in Figure 4.1.12. The data of RA intensities of $C_{12}SNa$ monolayers at the interface in both the symmetric and asymmetric C-H stretching regions in 0.1M NaCl aqueous solutions are listed in Table 4.1.10. The same trend of the change in RA intensity with bulk concentration in 0.1M NaCl as in pure water is observed. At saturation adsorption (above the phase transition point), the RA intensity remains basically constant ($3.2X10^{-3}$), and after the phase transition point, the RA intensity decreases with decrease in bulk concentration. The phase transition concentration found from the surface tension measurements is about $3.7X10^{-4}M$ (Table 4.1.2.), in good agreement with that, $4.0X10^{-4}M$ (Table 4.1.10.), determined from the change in RA intensities. Figures 4.1.13(a) and (b) are plots of RA spectra of the adsorbed monolayers of $C_{12}SNa$ at the aqueous solution/air interface in 0.5M NaCl solution. Figure 4.1.14. is a plot of the RA intensity versus log of bulk concentration. Data of RA intensities in the C-H stretching region of methylene groups in 0.5M NaCl solution are listed in Table 4.1.11. The change in RA intensity with bulk concentration for $C_{12}SNa$ monolayers in 0.5M NaCl solution has a slightly different pattern: The RA intensities of both the symmetric and asymmetric stretching modes decrease continuously with decrease in bulk concentration. This may be attributed to the continued change in polymethylene chain conformation in the monolayer with decrease in bulk concentration. We will discuss this later. The phase transition concentration range found from the

**Table 4.1.10.**

**Properties of Adsorbed Monolayers of $C_{12}H_{25}SO_3Na$ at The Aqueous Solution/Air Interface in 0.1M NaCl**

| $CX10^4$(M) | $RApX10^3$ | $RAsX10^3$ | RAp/RAs | $\chi(°)^a$ | $A(Å^2)$ |
|---|---|---|---|---|---|
| 10.0 | 3.20 | 2.00 | 1.60 | 41 | 44 |
| 8.00 | 3.10 | 1.93 | 1.60 | 45 | 44 |
| 6.00 | 3.10 | 1.95 | 1.59 | 45 | 44 |
| 4.00 | 2.30 | 1.47 | 1.56 | 50 | 49* |
| 2.00 | 1.33 | 1.00 | 1.33 | - | 57 |
| 1.00 | 1.00 | 0.80 | 1.25 | - | 4 67 |

| C ($X10^4$M) | $\nu_a$(C-H) ($cm^{-1}$) | $\nu_s$(C-H) ($cm^{-1}$) | $\nu_a$(S-O) ($cm^{-1}$) | $\nu_s$(S-O) ($cm^{-1}$) |
|---|---|---|---|---|
| 10.0 | 2920.5 | 2851.0 | 1169.5 | 1039.5 |
| 8.00 | 2920.6 | 2851.1 | 1169.2 | 1039.3 |
| 6.00 | 2921.0 | 2851.4 | 1169.4 | 1039.3 |
| 4.00 | 2923.9 | 2854.0 | 1169.2 | - |
| 2.00 | 2924.6 | 2855.0 | - | - |
| 1.00 | 2925.5 | 2856.2 | - | - |

* phase transition concentration region

a. see page 64 for the explanation

**Table 4.1.11.**

**Properties of Adsorbed Monolayers of $C_{12}H_{25}SO_3Na$ at The Aqueous Solution/Air Interface in 0.5M NaCl**

| $CX10^4$(M) | $RApX10^3$ | $RAsX10^3$ | RAp/RAs | $\chi(°)^a$ | $A(Å^2)$ |
|---|---|---|---|---|---|
| 2.63 | 2.00 | 1.44 | 1.39 | 53 | 42 |
| 1.77 | 1.87 | 1.38 | 1.36 | 55 | 42 |
| 1.29 | 1.76 | 1.33 | 1.32 | 57 | 42 |
| 0.63 | 1.34 | 1.04 | 1.29 | - | 47* |
| 0.45 | 1.26 | 1.00 | 1.26 | - | 52 |

| C | $\nu_a$(C-H) | $\nu_s$(C-H) | $\nu_a$(S-O) | $\nu_s$(S-O) |
|---|---|---|---|---|
| ($X10^4$M) | ($cm^{-1}$) | ($cm^{-1}$) | ($cm^{-1}$) | ($cm^{-1}$) |
| 2.63 | 2920.2 | 2850.2 | 1173.6 | 1043.0 |
| 1.77 | 2920.3 | 2851.0 | 1172.7 | 1043.0 |
| 1.29 | 2920.8 | 2851.3 | 1173.0 | - |
| 0.63 | 2921.0 | 2851.8 | - | - |
| 0.45 | 2920.5 | 2851.5 | - | - |

* phase transition concentration region

a. see page 64 for the explanation

change in RA intensity (relatively large decrease) is between $1.29X10^{-4}$ and $6.3X10^{-5}$M. It is in good agreement with $8.91X10^{-5}$M determined from the surface tension measurements (Table 4.1.3)

The data on peak frequencies in the C-H stretching region of polymethylene chains in 0.5M NaCl solution are also listed in Table 4.1.11. It is observed that peak frequencies of both the C-H symmetric and asymmetric stretching bands of $C_{12}$SNa monolayers at the interface in 0.5M NaCl solutions continuously increase with decrease in bulk concentration. The continuous change in conformation of methylene chains (more and more *gauche* conformers are formed) results in continuous decreasing in RA intensity (Chapter 4.1.5.will give a detailed explanation).

The frequency ($2920.5cm^{-1}$) of the asymmetric C-H stretching band and the frequency ($2851.0cm^{-1}$) of the symmetric mode of methylene groups of $C_{12}$SNa in the monolayer at the interface in 0.1M NaCl solution are much higher than the corresponding ones ($2917.3cm^{-1}$ and $2848.8cm^{-1}$, respectively) in pure water solution at saturation adsorption, and so are those frequencies in 0.5M NaCl solution. This indicates that at saturated adsorption, a fraction of *gauche* conformers is present in the methylene chains of $C_{12}$SNa in adsorbed monolayers at the aqueous solution/air interface in salt solutions compared with the all-*trans* conformation of methylene chains in pure water solution.

Average chain orientation angles calculated from the previous optical model and assumptions for adsorbed monolayers of $C_{12}$SNa at the aqueous solution/air interface in 0.1M NaCl and in 0.5M NaCl are listed in Tables

4.1.10. and 4.1.11, respectively. One thing should be mentioned here is that all the calculated chain orientation angles are based on three previous important assumptions (Chapter 2.2), and one of these assumption is: all-*trans* conformation of methylene chains in adsorbed monolayers. Unfortunately, this assumption is not valid in these cases ($C_{12}$SNa in salt solutions). Actually, because a relative large amount of *gauche* conformers are involved in the structures of methylene chains in the monolayers at the interface in salt solutions, methylene chains of surfactant are present at a random manner, and the chain orientation angle has no real meaning in these cases.

### 4.1.5. The Effect of Salt Concentration on Structures of Monolayers of $C_{12}$SNa at The Air/Water Interface.

As mentioned above in Chapter 4.1.1., addition of electrolyte (NaCl) to $C_{12}$SNa solution decreases the repulsion force between the charged head groups, by compressing the electrical double layers at the aqueous solution/air interface, and consequently increase adsorption at the interface. This process should result in an increase in RA intensity and decrease in average chain orientation angles.

Figures 4.1.15 shows the differences in RA spectra of the adsorbed monolayers of $6.24X10^{-4}$M $C_{12}$SNa at the interface in pure water and in 0.05M NaCl aqueous solution with *s*-polarization. Figure 4.1.16. shows the differences in RA spectra of monolayers of $1.1X10^{-4}$M $C_{12}$SNa in 0.1M and in 0.5M NaCl aqueous solutions with *s*-polarization. From these Figures, it is apparent that at the same bulk concentration, the RA intensity increases with

an increase in the total ionic strength of surfactant solution, and the peak frequencies of the symmetric and asymmetric C-H stretching bands of methylene groups decrease with an increase in the total ionic strength of solutions. The RAp intensity of the asymmetric C-H stretching mode of the adsorbed monolayer of $1.0X10^{-3}M$ $C_{12}SNa$ in 0.1M NaCl aqueous solution at the saturation adsorption is $3.2X10^{-3}$ (Table 4.1.10.), where as the RAp intensity in pure water is only $2.0X10^{-3}$ (Table 4.1.8.) at unsaturated adsorption. The addition of 0.1M of NaCl to the surfactant solution also decreases the frequency of asymmetric C-H stretching mode in the monolayer at the air/water interface from $2922.5cm^{-1}$ to $2920.5cm^{-1}$. This means that polymethylene chains of $C_{12}SNa$ in the adsorbed monolayer at the interface in 0.1M NaCl solution are more ordered than that in pure water solution with the same bulk concentration (less *gauche* conformers are involved in methylene chains in 0.1M NaCl solution).

Figure 4.1.17 shows the change in methylene chain conformation with bulk concentration in pure water and 0.1M NaCl solutions. It is observed that at the same bulk concentration, the frequencies of both the symmetric and asymmetric C-H stretching modes decreases with increase in the total ionic strength of surfactant solution.

From surface tension measurements (Table 4.1.5.), it is known that the surface excess concentration of $C_{12}SNa$ at the aqueous solution /air interface in 0.1M and 0.5M NaCl solutions are much higher than that in pure water solution at saturation adsorption. When we compare the RA intensity data in Table 4.1.8 (pure water solution) with those in Tables 4.1.10 and

4.1.11 (in salt solutions), a question arises: why are the RA intensities of $C_{12}SNa$ monolayers in salt solutions always smaller than that in pure water solution at saturation adsorption?. From the previous optical model (36), it is established that the RA intensity of adsorbed monolayers at the interface depends on the thickness of the monolayer (as a function of the chain orientation angle $\chi$) and the absorption coefficient ($k_{max}$) of the monolayer, which is related to the surface concentration as well as conformation of methylene chains in the monolayer. In all-*trans* conformation, the thickness of the monolayer can be calculated from the formula: $d=l\cos\chi$, because l, the length of an extended molecule, is fixed, and the $k_{max}$ is proportional to the surface concentration (packing density). When a fraction of *gauche* conformers is introduced into the structure of methylene chains in the monolayer, the situation becomes relatively complicated. Firstly, the thickness of the monolayer is related to both chain orientation angle and chain conformation. Introduction of *gauche* conformers into the polymethylene chains produces "bent" and non-coplanar structures into the methylene chains, and consequently decreases the lengths of molecule chains and the thickness of the monolayer at the interface. Secondly, *gauche* conformation has even more significant effects on the absorption coefficient of the monolayer. Mantsch and his coworkers (63) have studied the temperature-dependence of the methylene chain modes of sodium hexadecyl sulfate (SHS) and sodium dodecyl sulfate (SDS). When the temperature arises from 38°C to 43°C, the peak frequency of the symmetric C-H stretching mode of 0.2M of SHS solution increases from 2850.5$cm^{-1}$ to

2851.5cm$^{-1}$. The peak height of the asymmetric mode decreases drastically from 55.5mm in 38°C to 33.5mm in 43°C. The intensity is decreased about 40%. This indicates that conformationally disordered methylene chains with a high content of *gauche* conformers (such as found in liquid hydrocarbons) have much smaller absorption coefficient , $k_{max}$, than that with all-*trans* conformationally ordered methylene chains.

In conclusion, because *gauche* conformers are present in the structures of methylene chains in the adsorbed monolayer at the aqueous solution/air interface in salt solutions, the absorption coefficient as well as the thickness of the monolayers are decreased considerably. Therefore, the RA intensity of the adsorbed monolayer at the interface is decreased. In fact, the calculated values of average $k_{max}$ of the monolayers in pure water, 0.1M, and 0.5M NaCl solutions are 0.528 $\pm$ 0.04, 0.353 $\pm$ 0.05, and 0.323 $\pm$ 0.02, respectively. This is consistent with our prediction.

Table 4.1.12 summarizes the data on peak frequencies of the C-H stretching bands of methylene groups in the crystalline state, and in the adsorbed monolayers in pure water, 0.1M, and 0.5M NaCl aqueous solutions. In Chapter 4.1.4., it was noted that the frequencies of both the symmetric and asymmetric C-H stretching bands of polymethylene chains of $C_{12}SNa$ monolayers in 0.1M NaCl (or 0.5M NaCl) at saturated adsorption are higher than the corresponding ones in pure water solution, indicating that the structures of adsorbed monolayers in salt solutions are different from that in pure water solution.. Increasing the total ionic strength of surfactant solutions (with the same bulk concentrations) decreases the peak frequencies of C-H stretching bands. This is due to increasing the surface concentration and

decreasing fraction of *gauche* conformers in the structure of methylene chains in adsorbed monolayers at the interface. But from our observation, it seems that the effects of addition of electrolyte to dilute surfactant solution in pure water (up to 0.5M NaCl) are not strong enough to change thoroughly the structure of methylene chains in the adsorbed monolayers at the interface from partially disordered *gauche* conformation to highly ordered all-*trans* conformation. Figure 4.1.18. diagrams suggested structures of the adsorbed monolayers of $C_{12}SNa$ at the aqueous solution/air interface with various bulk concentrations in pure water and in salt solution. It shows that even though high surface concentrations of surfactant at the air/water interface are reached in salt solutions, the polymethylene chains at the interface still have plenty of disordered *gauche* conformers.

### 4.1.6. RA Spectra of Adsorbed $C_{12}SNa$ Monolayers at The Air/Water Interface in the S-O Stretching Region

Figures 4.1.19. and 4.1.20. are the RA spectra of adsorbed monolayers of $C_{12}SNa$ in the S-O stretching region in pure water, and in 0.1M NaCl solution, respectively. Frequencies of the symmetric and asymmetric S-O bands in pure water, 0.1M, and 0.5M NaCl solutions are listed in Table 4.1.8., 4.1.10., and 4.1.11, respectively. Table 4.1.12. also summarizes the data on frequencies of the S-O stretching bands in adsorbed monolayers at saturation adsorption in pure water, 0.1M, and 0.5M NaCl solutions.

From these Tables and Figures, it is observed that peak frequencies of both the symmetric and asymmetric S-O stretching bands in adsorbed monolayers at the air/water interface basically remain constant at saturation adsorption in pure water and salt solutions. The RA intensity in the S-O stretching region looks like

**Table 4.1.12**

**Peak Frequency for the C-H and S-O Stretching Bands of $C_{12}H_{25}SO_3Na$ in Crystalline and Adsorbed Monolayers at the Water/Air Interface**

| Structural group | Stretching mode | Crystalline KBr($cm^{-1}$) | Monolayers ($cm^{-1}$) [$H_2O$ | 0.1M NaCl | 0.5M NaCl] |
|---|---|---|---|---|---|
| $-CH_2-$ | $\nu_a$ | 2919.5 | 2917.3 | 2920.5 | 2920.2 |
| | $\nu_s$ | 2850.1 | 2848.8 | 2851.0 | 2850.2 |
| $-SO_3-$ | $\nu_a$ | 1174.0 | 1167.2 | 1169.5 | 1173.0 |
| | $\nu_s$ | 1045.0 | 1037.5 | 1039.5 | 1043.0 |

showing the same trends as in the C-H stretching region (because of the difficulty to obtain a correct base line, we didn't measure the peak intensity in the S-O region). But the change in peak frequencies of the S-O stretching bands with bulk concentration is in the opposite direction compared with the C-H stretching region. Both frequencies of the symmetric and asymmetric S-O stretching bands decrease with decrease in bulk concentration when the bulk concentration is below the transition point. Mantsch et.al. (63) have indicated that both the frequencies and band shapes in the region of S-O modes differ considerably among the individual alkali hexadecyl sulfates, and the behavior is determined to a large extent by the different electrostatic interaction and counterion binding in these solid surfactants. The greater the interaction between the negatively charged head groups, the higher the peak frequency. When the bulk concentration is below the phase transition point, the surface concentration at the interface decreases with decrease in bulk concentration. Therefore, the repulsive force between the charged head groups at the interface decreases with decrease in bulk concentration, and consequently, the peak frequencies of the S-O stretching modes decrease. In fact, both the symmetric and asymmetric S-O stretching bands have the highest frequencies (1174 and 1045$cm^{-1}$) (68) in crystalline solids.

From Table 4.1.12, it is also observed that both peak frequencies of the symmetric and asymmetric S-O stretching modes increase with an increase in the total ionic strength of surfactant solution. As mentioned before, the addition of electrolyte to ionic surfactant solution decreases the repulsion force between the charged head groups in the adsorbed monolayer, thereby bringing more counterions ($Na^+$) in close contact with the head groups at the interface. For

example, the Debye length, which is proportional to the diffuse layer thickness, decreases from 30Å in the absence of electrolyte to about 10Å in 0.1M NaCl (22). Since the transition moment vector for the symmetric mode points normal to the interface (Fig. 4.1.8) towards the diffuse double layer, the increase in frequency is consistent with an increase in counterion interaction (69, 70).

The change in the asymmetric mode, which are expected to be very sensitive to surfactant - surfactant interactions, is caused by the crowding of the sulfonate head groups. The increased crowding of the sulfonate head groups produces a local site symmetry lowering which leads to increased splitting of the asymmetric modes, i. e. a more solid -like character of the spectra. As the result, the frequency of the asymmetric modes also increases with increase in surface concentration. These results are consistent with those reported by Weers and Scheuing (71) for $C_{12}HS$ micelles.

## 4.2. Cationic Surfactant - Dodecyl Trimethylammonium Bromide, $C_{12}H_{25}N^{+}(CH_3)_3Br^{-}$ ($C_{12}N$)

### 4.2.1. Surface Properties from Surface Tension Measurements

Data on $\gamma$, $\pi$, $\Gamma$, and A of $C_{12}N$ in pure water and in 0.1M NaBr solution at various bulk concentrations are listed in Table 4.2.1. and 4.2.2., respectively. Table 4.2.3. summarizes data on cmc, $\pi_{cmc}$, $\Gamma_{max}$, and $A_{min}$ of $C_{12}N$ in pure water, 0.1M, 0.5M, and 1.0M NaBr solutions. Figure 4.2.1. shows plots of surface tension versus log of bulk concentration of $C_{12}N$ in pure water and 0.1M NaBr solutions. Figure 4.2.2. is plots of surface pressure vs. area per molecule of $C_{12}N$ in pure water and 0.1M NaBr solutions. These data are consistent with those reported by Tanaka (72) and Rosen (22).

**Table 4.2.1**

**Data on $\gamma$, $\pi$, $\Gamma$, and A of $C_{12}H_{25}N(CH_3)_3Br$ in Pure $H_2O$ Solution (25.0°C)**

| C ($X10^3$M) | logC | $\gamma$ (mN/m) | $\pi$ (mN/m) | $\Gamma$ ($X10^{10}$ mol/cm$^2$) | A (Å$^2$) |
|---|---|---|---|---|---|
| 20.0 | -1.70 | 38.0 | 34.0 | - | -* |
| 14.0 | -1.85 | 39.4 | 32.6 | 3.22 | 51.6 |
| 10.0 | -2.00 | 44.4 | 27.6 | 3.05 | 54.5 |
| 7.00 | -2.15 | 49.1 | 22.9 | 2.73 | 60.7 |
| 5.00 | -2.30 | 53.8 | 18.2 | 2.44 | 68.0 |
| 2.50 | -2.60 | 61.0 | 11.0 | 1.84 | 90.2 |
| 1.75 | -2.75 | 63.7 | 8.3 | 1.54 | 108 |

* above the cmc.

**Table 4.2.2**

**Data on $\gamma$, $\pi$, $\Gamma$, and A of $C_{12}H_{25}N(CH_3)_3Br$ in 0.1M NaBr Solution (25.0°C)**

| C ($X10^{3}M$) | logC | $\gamma$ (mN/m) | $\pi$ (mN/m) | $\Gamma$ ($X10^{10}$ mol/cm$^2$) | A (Å$^2$) |
|---|---|---|---|---|---|
| 10.0 | -2.00 | 36.0 | 36.3 | - | - |
| 4.00 | -2.40 | 37.6 | 34.7 | 3.51 | 47.3 |
| 3.16 | -2.50 | 38.4 | 33.9 | 3.42 | 48.5 |
| 2.00 | -2.70 | 43.0 | 29.3 | 3.29 | 50.5 |
| 1.00 | -3.00 | 48.6 | 23.7 | 3.02 | 55.0 |
| 0.56 | -3.25 | 52.8 | 19.5 | 2.74 | 60.5 |

* above the cmc.

**Table 4.2.3**

**Surface Properties of $C_{12}H_{25}N(CH_3)_3Br$ Solutions** (25.0°C)

| Subphase | cmc ($X10^3M$) | $\pi_{cmc}$ (mN/m) | $\Gamma_{max}$ ($X10^{10}$ mol./$cm^2$) | $A_{min}$ ($Å^2$) |
|---|---|---|---|---|
| pure $H_2O$ | 16.0 | 33.6 | 3.19 | 52.0 |
| 0.1M NaBr | 4.25 | 36.5 | 3.45 | 48.0 |
| 0.5M NaBr | 1.50 | 39.0 | 4.00 | 41.5 |
| 1.0M NaBr | 1.00 | 40.0 | 4.05 | 41.0 |
| [a]pure $H_2O$ | 15.5 | 34.0 | 3.22 | 51.6 |
| [a]0.1M NaBr | 4.22 | 36.3 | 3.51 | 47.3 |
| [a]0.5M NaBr | 1.45 | 38.7 | 4.04 | 41.1 |
| [a]1.0M NaBr | 0.91 | 40.4 | 4.05 | 41.0 |

[a]. data from reference (72)

From these data and Figures it is observed that adsorbed monolayers of $C_{12}N$ at the aqueous solution/air interface have some properties in common with monolayers of $C_{12}SNa$: the state of the adsorbed monolayers at saturated adsorption may be classified as liquid expanded monolayers (LE), and the addition of electrolyte (NaBr) decreases the cmc of the solution, increases the surface pressure and adsorption, and consequently, decreases the area per molecule at the interface. But $C_{12}N$ solutions have a slightly different surface property: the curve of surface tension vs. log of bulk concentration does not have a clear linear region. It implies that when the bulk concentration is below the cmc, the adsorption at the interface continuously increases with increase in bulk concentration up to the cmc, the slope of the $\gamma$-logC curve decreases smoothly with decrease in bulk concentration, and therefore, no sharp phase transition point was found.

### 4.2.2. Surface Properties of $C_{12}N$ Monolayers at The Aqueous Solution/Air Interface from RA Spectra

Figure 4.2.3. is a representative spectrum of the adsorbed monolayer of $C_{12}N$ at the aqueous solution/air interface in pure water solution. Comparing this spectrum with Figure 3.6, it is clearly seen that the spectrum of the adsorbed $C_{12}N$ monolayer has relatively stronger absorption in the C-H stretching region of methyl groups, because there are four methyl groups in a $C_{12}N$ molecule, whereas a $C_{12}SNa$ molecule only has one terminal methyl group. The IR band assignments in the C-H stretching region for the methylene chains and methyl groups are listed as follows:

| wavenumber ($cm^{-1}$) | assignment |
|---|---|
| 2957 | $\nu_a$, $CH_3$ |
| 2920 | $\nu_a$, $CH_2$ |
| 2902 | $\nu$, $CH_3$ (?) |
| 2877 | $\nu_s$, $CH_3$ |
| 2850 | $\nu_s$, $CH_2$ |
| 2820 | $\nu$, N-$CH_3$ |

The peak near $2902cm^{-1}$ appears in compounds containing tertiary carbon atoms connected to 3 $CH_3$ groups, such as 2,2,4-trimethylpentane, or N atoms connected to methyl groups, like 2,2-dimethyl ethylamine (73). Figures 4.2.4. and 4.2.5. show plots of RA spectra of the adsorbed monolayers of $C_{12}N$ with various bulk concentrations in pure water solution. Data on RA intensities, peak frequencies (wn) of the symmetric and asymmetric C-H stretching bands of methylene groups as a function of the concentration of $C_{12}N$ are listed in Table 4.2.4.

From Figure 4.2.5. and Table 4.2.4. it is observed that when the bulk concentration is below the cmc, the RA intensity continuously decreases with decrease in bulk concentration. The surfactant solution concentration of $2.0X10^{-2}M$ is above the cmc ($1.5X10^{-2}M$), and this solution has a higher RA intensity than other solutions. Peak frequencies of the C-H stretching modes of methylene chains basically increase with decrease in bulk concentration.

Szulzewsky and his coworkers (74) have studied the crystal structure of

$C_{12}N$ using x-ray crystallography. They have found that the methylene chains in $C_{12}N$ crystals are statistically disordered, and slightly screwed around their chain axes; the area per molecule is 18.7Å$^2$, and the tilt angle of the chain axis with the (100) plane is 67°.

Bursh and his coworkers (75) have studied the relations between the structure in crystalline state and properties of bilayers and monolayers on the basis of systematic structure investigations. They have found that there exist some analogies of the behavior of the three-dimensional crystals of long chain compounds and their two-dimensional mono- or bilayers because of comparable intermolecular interactions within the layer planes, and crystal structure determinations may be used to elucidate the molecular structure and the principles of molecular arrangement of the monolayer.

Simister et al.. (30) have studied the structure of the adsorbed monolayer of tetradecyltrimethylammonium bromide ($C_{14}N$) at the air/water interface by a neutron reflection method. Lee and his coworkers (76) have reported staggered structures of adsorbed monolayers of tetradecyltrimethylammonium bromide ($C_{14}N$) and decyltrimethylammonium bromide ($C_{10}N$) at the air/water interface. They have reported that in order to fit a saturated monolayer model, the thickness of the chain region is 17.5 ± 1Å for $C_{14}N$, which is less than the fully extended chain length, and the thickness of the head region 7 ± 3Å. When the bulk concentration is above the cmc, the surfactant ($C_{14}N$) is more closely packed at the interface and the thickness of the head-group distribution increases to 12 ± 3Å. They attributed this phenomena to a "roughening" of the head group part of the layer (staggered monolayers). The similarity of the molecular structures of $C_{12}N$ and $C_{14}N$ (or $C_{10}N$) makes it not unrealistic to

**Table 4.2.4**

**Properties of Adsorbed Monolayers of $C_{12}H_{25}N(CH_3)_3Br$ at The Aqueous Solution /Air Interface**

| C | subphase | $\nu_a$ | | $\nu_s$ | | A |
|---|---|---|---|---|---|---|
| ($X10^3M$) | | $RA_s(X10^3)$ | $Wn(cm^{-1})$ | $RA_s(X10^3)$ | $Wn(cm^{-1})$ | ($Å^2$) |
| 20.0 | $H_2O$ | 1.20 | 2921.0 | 0.85 | 2851.6 | - |
| 14.0 | $H_2O$ | 1.12 | 2921.4 | 0.82 | 2851.5 | 51.6 |
| 10.0 | $H_2O$ | 1.04 | 2921.5 | 0.77 | 2851.4 | 54.5 |
| 7.00 | $H_2O$ | 0.97 | 2922.8 | 0.62 | 2852.0 | 60.7 |
| 5.00 | $H_2O$ | 0.85 | 2922.7 | 0.55 | 2852.0 | 68.0 |
| 2.50 | $H_2O$ | 0.80 | 2923.7 | 0.40 | 2854.0 | 90.2 |
| 1.75 | $H_2O$ | .0.72 | 2923.6 | 0.40 | 2855.0 | 108 |
| 10.0 | 0.1M NaBr | 1.24 | 2923.7 | 0.80 | 2853.6 | - |
| 4.00 | 0.1M NaBr | 1.18 | 2924.6 | 0.80 | 2854.7 | 47.3 |
| 2.00 | 0.1M NaBr | 0.80 | 2924.7 | 0.56 | 2854.8 | 50.5 |
| 1.00 | 0.1M NaBr | 0.70 | 2924.8 | 0.46 | 2855.2 | 55.0 |

expect that the staggered structure of adsorbed monolayers also occurs in $C_{12}N$ solutions. Figure 4.2.10. is a diagram to explain the structure and distribution of water and $C_{12}N$ molecules at the aqueous solution/air interface. When the bulk surfactant concentration is relatively low, the adsorbed monolayer is unsaturated, the distances between methylene chains and between head groups within the monolayer are relatively large, and the monolayer is uniform. When the bulk concentration is getting higher and higher (close to or above the cmc), the adsorbed monolayers in pure water solution have more and more staggered structures (the thickness of the head-group distribution also increases).

Continuous changes in RA intensity and peak frequencies of RA spectra with decrease in bulk concentration may be caused by this type of staggered structure of the monolayer. If the adsorbed monolayer has a staggered structure, the surface concentration (chain packing density) at the interface will continuously increase with increase in bulk concentration up to the cmc, and so does the head group distribution region. Therefore the interactions between methylene chains and between methylene chain and adjacent head groups in the monolayer also increase with the increase in bulk concentration. Since RA intensity increases with increasing surface concentration and the peak frequency in the C-H stretching bands decreases with increasing interaction between methylene chains (Van Der Waals force) in the monolayer at the interface, then RA intensity should increase continuously with increasing bulk concentration, and the peak frequency should decrease continuously with increasing bulk concentration.

Because there are no abrupt turning points in the plots of RA intensity, peak frequencies, and surface tension versus log of bulk concentrations, it appears

that the transition between LE and G phases is smooth; no sharp transition point was found.

The lowest frequency (2851.6cm$^{-1}$) of the symmetric C-H stretching band in adsorbed monolayer of $C_{12}N$ at the interface is close to that (2851.0cm$^{-1}$) reported for $C_{16}N$ in the coagel phase by Scheuing and Weers (77). But frequencies of both the symmetric (2851.6cm$^{-1}$) and the asymmetric (2921.0cm$^{-1}$) C-H stretching bands of methylene groups in saturated $C_{12}N$ monolayers (bulk concentration just below its cmc) are much higher than the corresponding ones (2848.8cm$^{-1}$ and 2917.3cm$^{-1}$, respectively) in $C_{12}SNa$ monolayers. One possible reason for this is the difference in their head group structures. A $C_{12}SNa$ molecule has a negatively charged, $-SO_3^-$, head group, whereas $C_{12}N$ has a positively charged, $-N^+(CH_3)_3$, head group. They have totally different inductive effects on their methylene chains. The absolute frequency of the C-H stretching bands of methylene chains are affected by the types of head groups on the methylene groups, due to through-band inductive effects (78). Secondly, the frequency difference between $C_{12}N$ and $C_{12}SNa$ monolayers may be partially attributed to the disordered and screwed chains of $C_{12}N$ in the adsorbed monolayer, which are found in the crystalline state (75).

### 4.2.3. RA Spectra of Adsorbed Monolayers of $C_{12}N$ at the Interface in 0.1M NaBr Solution

Figures 4.2.6.(a) and (b) are plots of RA spectra of the adsorbed

monolayers of $C_{12}N$ at the aqueous solution/air interface in 0.1M NaBr solution with various bulk concentrations at *p*- and *s*--polarization, respectively. Data on RA intensities and peak frequencies of the C-H stretching bands of methylene groups are listed in Table 4.2.4.

It is observed that when the bulk concentration ($1.0X10^{-2}M$) is above its cmc ($4.22X10^{-3}M$), the adsorbed monolayer at the interface has a larger RA intensity and lower peak frequencies than others; when the bulk concentrations below the cmc, RA intensity decreases with decrease in bulk concentration and peak frequencies remain almost constant. It is also observed that peak frequencies of both symmetric and asymmetric C-H stretching bands of methylene chains of $C_{12}N$ monolayers at the interface in salt solutions are higher than the corresponding frequencies ($2852.5cm^{-1}$ and $2921.4cm^{-1}$) in pure water solution whether the bulk concentration is above, close, or below its cmc.

Figure 4.2.7 shows the effects of salt on the RA spectra of $C_{12}N$ monolayers at the interface. Figure 4.2.8 and 4.2.9 are plots of RA intensity and peak frequency shift (compared with the frequency value at the saturated adsorption, the bulk concentration just below the cmc) in the C-H stretching region of methylene groups versus log of bulk concentration in pure water and in 0.1M NaBr solution, respectively.

It can be seen that RA intensity and peak frequency (both the symmetric and asymmetric C-H stretching modes) increase with increase in the total ionic strength of surfactant solutions at the same bulk concentration. At saturated adsorption (the bulk concentration just below the cmc), the RA intensities of the

asymmetric and symmetric C-H stretching bands in adsorbed $C_{12}N$ monolayer are $1.18X10^{-3}$ and $8.0X10^{-4}$, respectively, in 0.1M NaBr. The corresponding intensities are $1.12x10^{-3}$ and $8.2X10^{-4}$ in pure water. Within the experimental error, These intensities are essentially the same. From Table 4.2.3. we know that the surface concentration ratio is 1.09 at the saturated adsorption. The intensity ratio is less than the surface concentration ratio. From the previous optical model (36) it is established that the RA intensity depends on the chain packing density in the adsorbed monolayer (surface concentration), the average chain orientation angle (the thickness of the monolayer),and conformation of methylene chains in the monolayer. Because of a great change in conformation of polymethylene chains from pure water to salt solutions (peak frequency from $2921.4cm^{-1}$ and $2851.5cm^{-1}$ to $2924.6cm^{-1}$ and $2854.7cm^{-1}$, respectively), there are more *gauche* conformers formed in structures of methylene chains in salt solutions, and the absorption coefficient ($k_{max}$) became much smaller. As a result, the intensity ratio is smaller than the surface concentration ratio.

Why are methylene chains in monolayers with the subphase of salt solution more disordered than that with the subphase of pure water? So far we have not yet found a satisfactory interpretation. This may be caused by the "roughening" structures of the adsorbed monolayers of $C_{12}N$ at the interface. The high frequencies of the C-H stretching bands of methylene groups in salt solutions indicate that this type of staggered structure consists of a great amount of *gauche* conformers.

## 4.3. Sodium Dodecylsulfate, $C_{12}H_{25}SO_4Na$ ($C_{12}HS$), and Deuterated Sodium Dodecylsulfate, $C_{12}D_{25}SO_4Na$ ($C_{12}DS$) Monolayers

### 4.3.1. Surface Properties from Surface Tension Measurements

Since peak frequencies of the symmetric and asymmetric C-D bands of deuterated polymethylene chains are completely different from the corresponding ones of the C-H bands, it is convenient to distinguish methylene chains from deuterated polymethylene chains in surfactant mixtures containing the same methylene chains as $C_{12}HS$ to investigate structures and compositions of mixed monolayers at the aqueous solution/air interface. It is therefore important to determine whether the surface properties of the two isotopic compounds $C_{12}HS$ and $C_{12}DS$) are the same.

Data on $\gamma$, $\pi$, $\Gamma$, and A of $C_{12}HS$ in pure water and in 0.1M NaBr solutions with various bulk concentrations are listed in Table 4.3.1. and 4.3.2., respectively. Data on $\gamma$, $\pi$, $\Gamma$, and A of $C_{12}DS$ in pure water solution with different bulk concentrations are listed in Table 4.3.3. Plots of surface tension versus log of bulk concentration of $C_{12}HS$ and $C_{12}DS$ in pure water solutions are shown in Figure 4.3.1. Plots of surface pressure ($\pi$) vs. area per molecule (A) of $C_{12}HS$ and $C_{12}DS$ in pure water and 0.1M NaBr solutions are shown in Figure 4.3.2. Table 4.3.4. lists surface properties (cmc, $\pi_{cmc}$, $\Gamma_{max}$, and $A_{min}$) of $C_{12}HS$ in pure water and 0.1M NaBr solution, and $C_{12}DS$ in water solution. Our experimental data on surface properties of $C_{12}HS$ in pure $H_2O$ are consistent with those reported by Dahanayake (24). From these data and Figures, it is seen that $C_{12}HS$ and $C_{12}DS$ have the same maximum surface

**Table 4.3.1**

**Data on $\gamma$, $\pi$, $\Gamma$, and A of $C_{12}H_{25}SO_4Na$ in Pure $H_2O$ Solution (25.0°C)**

| C ($X10^3M$) | logC | $\gamma$ (mN/m) | $\pi$ (mN/m) | $\Gamma$ ($X10^{10}$ mol/cm$^2$) | A (Å$^2$) |
|---|---|---|---|---|---|
| 10.0 | -2.00 | 39.5 | 32.5 | - | -* |
| 7.00 | -2.15 | 41.0 | 31.0 | 3.13 | 53.0 |
| 5.00 | -2.30 | 46.4 | 25.6 | 3.13 | 53.0 |
| 3.50 | -2.45 | 52.0 | 20.0 | 2.86 | 58.0 |
| 2.50 | -2.60 | 57.0 | 15.0 | 2.48 | 67.0 |
| 1.75 | -2.75 | 63.7 | 8.3 | 2.09 | 79.5 |

* above the cmc.

**Table 4.3.2**

**Data on $\gamma$, $\pi$, $\Gamma$, and A of $C_{12}H_{25}SO_4Na$**

**in 0.1M NaBr Solution (25.0°C)**

| C ($X10^4$M) | logC | $\gamma$ (mN/m) | $\pi$ (mN/m) | $\Gamma$ ($X10^{10}$ mol/cm$^2$) | A (Å$^2$) |
|---|---|---|---|---|---|
| 15.8 | -2.80 | 33.6 | 38.7 | - | -* |
| 10.0 | -3.00 | 37.2 | 35.1 | 4.15 | 40.0 |
| 5.00 | -3.30 | 44.3 | 28.0 | 4.15 | 40.0 |
| 2.50 | -3.60 | 51.2 | 21.1 | 3.70 | 44.9 |
| 1.58 | -3.80 | 55.8 | 16.5 | 3.37 | 49.3 |
| 0.89 | -4.05 | 59.6 | 12.7 | 2.96 | 56.0 |

* above the cmc.

**Table 4.3.3**

**Data on $\gamma$, $\pi$, $\Gamma$, and A of $C_{12}D_{25}SO_4Na$ in Pure $H_2O$ Solution (25.0°C)**

| C ($X10^3M$) | logC | $\gamma$ (mN/m) | $\pi$ (mN/m) | $\Gamma$ ($X10^{10}$ mol/cm$^2$) | A (Å$^2$) |
|---|---|---|---|---|---|
| 10.0 | -2.00 | 39.0 | 33.0 | - | -* |
| 7.00 | -2.15 | 40.0 | 32.0 | 3.13 | 53.0 |
| 3.50 | -2.45 | 50.8 | 21.2 | 3.13 | 53.0 |
| 2.00 | -2.70 | 58.4 | 13.6 | 2.07 | 80.0 |
| 1.00 | -3.00 | 64.0 | 8.0 | 1.38 | 120 |

* above the cmc.

**Table 4.3.4**

**Surface Properties of $C_{12}H_{25}SO_4Na$ ($C_{12}HS$) and $C_{12}D_{25}SO_4Na$ ($C_{12}DS$) Solutions** (25.0°C)

| Surfactant | cmc ($X10^3M$) | $\pi_{cmc}$ (mN/m) | $\Gamma_{max}$ ($X10^{10}$ mol./$cm^2$) | $A_{min}$ ($Å^2$) |
|---|---|---|---|---|
| $C_{12}HS$ (in $H_2O$) | 8.00 | 32.0 | 3.10 | 53.5 |
| $C_{12}DS$ (in $H_2O$) | 7.59 | 33.0 | 3.13 | 53.0 |
| $C_{12}HS$ (in 0.1M NaBr)) | 1.40 | 38.7 | 4.15 | 40.0 |
| [a]$C_{12}HS$ (in $H_2O$) | 7.94 | 32.5 | 3.16 | 52.5 |

a. data from reference (24)

concentration ($\Gamma_{max}$)and the same area per molecule (A) at the saturated adsorption at the aqueous solution/air interface, and their cmc and $\pi_{cmc}$ values are very close to each other. Therefore It is concluded that within experimental error, $C_{12}$DS has the same surface properties as $C_{12}$HS, and consequently, replacement of $C_{12}$HS by $C_{12}$DS in mixtures with a cationic surfactant (such as $C_{12}$N) will not have significant effect on the surface properties of the mixed monolayer at the air/solution interface.

### 4.3.2. RA Spectra of Adsorbed Monolayers of $C_{12}$HS at The Aqueous Solution/Air Interface in Pure Water Solution

*The C-H stretching region of polymethylene chain*

RA spectra of the adsorbed monolayers of $C_{12}$HS at the aqueous solution/air interface in the C-H stretching region of methylene groups in water solution with various bulk concentrations are shown in Figure 4.3.3(a). Data on RA intensities and peak frequencies in this region are listed in Table 4.3.5. Plots of RA intensity and peak frequency shift versus log of bulk concentration are shown in Figure 4.3.5. and 4.3.6., respectively. It is observed that the adsorbed monolayers of $C_{12}$HS at the interface have the similar trends as the monolayers of $C_{12}$SNa: the intensity and peak frequency remain basically constant at saturated adsorption; after the phase transition point, the intensity decreases and peak frequency increases with decrease in bulk concentration. The phase transition point, $3.50X10^{-3}$M, determined from surface tension measurements (Table 4.3.1.) is the same as the one calculated from the abrupt change in RA intensity (Table 4.3.5.).

It is also found that when the bulk concentration continuously increases

**Table 4.3.5**

**Properties of Adsorbed Monolayers of $C_{12}H_{25}SO_4Na$ at The Aqueous Solution /Air Interface in Pure $H_2O$ (The C-H Stretching Region)**

| C | $\nu_a$ | | $\nu_s$ | | A |
|---|---|---|---|---|---|
| ($X10^3M$) | $RA_s(X10^3)$ | $Wn(cm^{-1})$ | $RA_s(X10^3)$ | $Wn(cm^{-1})$ | ($Å^2$) |
| 10.0 | 1.73 | 2920.8 | 1.27 | 2850.5 | - |
| 7.00 | 1.70 | 2921.1 | 1.22 | 2850.8 | 53.0 |
| 5.00 | 1.60 | 2921.4 | 1.10 | 2851.0 | 53.0 |
| 3.50 | 1.60 | 2922.0 | 1.10 | 2851.1 | 58.0* |
| 2.50 | 1.57 | 2922.4 | 1.02 | 2851.1 | 67.0 |
| 1.75 | 1.47 | 2922.4 | 1.00 | 2851.0 | 79.5 |

* phase transition concentration region.

from below to above its cmc, the RA intensity also increases slightly, and peak frequencies of C-H stretching bands of methylene groups decrease. This means that when the bulk concentration is above its cmc, $7.94X10^{-3}M$, the methylene chains in the adsorbed monolayers at the interface are more closely packed and more ordered than that in solutions whose bulk concentrations are below the cmc.

Sundell and his coworkers (79) have studied the crystal structure of $C_{12}HS$ using X-ray crystallography. They have reported that $C_{12}HS$ crystals have a monoclinic structure, with full extended hydrocarbon chains, chain tilt angle of 79° to the layer plane, and the average area per molecule is $20.9Å^2$. They have also found that the sulfate groups of adjacent molecules are alternately displaced (perpendicular to the layer plane) by about 2Å in order to have favorable electrostatic interactions. This slightly staggered structure in crystals also possibly occurs in monolayers (as mentioned before for $C_{12}N$ monolayers), and cause the continuous change in RA intensity with increase in bulk concentration up to the cmc.

It is interesting to note that $C_{12}SNa$ and $C_{12}HS$ molecules have the same methylene chains and similarly charged head groups, but the RA intensity and peak frequencies of their adsorbed monolayers at the aqueous solution/air interface are different. This difference is probably due to the different structure of their head groups. A $C_{12}SNa$ molecule has a $-SO_3^-$ head group, and a C-S bond linkage between its methylene chain and head group, while $C_{12}HS$ has a $-SO_4^-$ and C-O bond linkage. It is well-known that oxygen atom is more electronegative than sulfur (electronegativity of O is 3.5, and 2.5 for S), the C-O

bond is more polar than C-S, and therefore, $-SO_4^-$ head group has a stronger inductive effect on its methylene chain in $C_{12}HS$ molecules than $-SO_3^-$ in $C_{12}SNa$. From this point of view, It is expected that the frequencies of the symmetric and the asymmetric C-H stretching modes of methylene chains of $C_{12}HS$ in monolayers should be slightly higher than those of $C_{12}SNa$ at saturated adsorption. Experimental data have proved this argument: 2921.1 and 2850.8$cm^{-1}$ for $C_{12}HS$ monolayer and 2917.3 and 2848.8 $cm^{-1}$ for $C_{12}SNa$. The difference in structures of their head groups also produces a big change in absorption coefficients ($k_{max}$) of their adsorbed monolayers. The RA intensity of the asymmetric C-H stretching band (with *s*-polarization) in the saturated adsorbed monolayer of $C_{12}SNa$ at the interface is about $4.0X10^{-3}$, while the corresponding RA intensity of $C_{12}HS$ is only $1.7X10^{-3}$, less than half that of $C_{12}SNa$. From surface tension measurements , it is observed that the adsorbed monolayers of $C_{12}SNa$ and $C_{12}HS$ have almost the same maximum surface concentration (2.93 and 3.13 $X10^{-10}$ $mol/cm^2$, for $C_{12}SNa$ and $C_{12}HS$, respectively) at the interface in pure water solutions. From the structure similarity between the crystalline state and the adsorbed monolayer, it is expected that the chain orientation of $C_{12}HS$ in the monolayer at the interface is not far from the chain tilt angle, 11°, in crystals (81). Thus the big decrease in RA intensity in $C_{12}HS$ monolayers is attributed to the decrease in the absorption coefficient ($k_{max}$) of the monolayer.

*the S-O stretching region of head group*

Figure 4.3.3(b). shows plots of RA spectra of adsorbed monolayers of $C_{12}HS$ at the interface in the S-O stretching region in pure water solution. The broad peak near 1203cm$^{-1}$ is assigned to the asymmetric S-O stretching band, and the small peak near 1060cm$^{-1}$ the symmetric band. Mantsch et al.. (63) have reported 1270 and 1207 cm-1 as the asymmetric S-O stretching band and 1070cm$^{-1}$ as the symmetric mode for sodium hexadecyl sulfate micelle at the temperature below the CMT (Critical Micellization Temperature, 43°C).

Because the bands haps and the signal/noise ratio of both symmetric and asymmetric S-O stretching bands are not good enough to determine the peak frequencies, information about the frequency change is not available.

### 4.3.3. RA Spectra of Adsorbed Monolayers of $C_{12}DS$ at The Aqueous Solution/Air Interface.

*the C-D stretching region of polymethylene chain*

Figure 4.3.4(a) shows plots of RA spectra of adsorbed monolayers of $C_{12}DS$ in the C-D stretching region at the aqueous solution/air interface in pure water solution with various bulk concentrations. The peaks near 2195 and 2091cm-1 are assigned to the asymmetric and symmetric C-D stretching bands of deuterated methylene groups, respectively. Data on RA intensities and peak frequencies are listed in Table 4.3.6. Changes in RA intensity and peak frequency in the C-D stretching region with bulk concentration are plotted in Figure 4.3.7. and 4.3.8, respectively.

The same trends of changes in RA intensity and peak frequency are found in the C-D stretching region of $C_{12}DS$ monolayers as in the C-H stretching

**Table 4.3.6**

**Properties of Adsorbed Monolayers of $C_{12}D_{25}SO_4Na$ at The Aqueous Solution/Air Interface in Pure $H_2O$**

| C | subphase | $\nu_a$ | | $\nu_s$ | | A |
|---|---|---|---|---|---|---|
| ($X10^3M$) | | $RA_s(X10^4)$ | $Wn(cm^{-1})$ | $RA_s(X10^4)$ | $Wn(cm^{-1})$ | ($Å^2$) |
| 10.0 | $H_2O$ | 8.80 | 2194.8 | 6.00 | 2091.0 | - |
| 7.00 | $H_2O$ | 8.80 | 2195.2 | 6.00 | 2091.0 | 53 |
| 3.50 | $H_2O$ | 8.80 | 2195.2 | 5.70 | 2091.1 | 53* |
| 2.00 | $H_2O$ | 6.70 | 2196.2 | 4.30 | 2094.3 | 80 |
| 1.00 | $H_2O$ | 4.50 | 2199.0 | 2.90 | 2095.2 | 120 |

*phase transition concentration region

region of $C_{12}HS$ monolayers: at saturated adsorption both intensity and the peak frequency remain constant, after the phase transition point the intensity decreases and the peak frequency increases with decreasing bulk concentration. The phase transition point (from LE to G), $3.50X10^{-3}M$, determined from the surface tension measurements (Table 4.3.3.) is equal to the one found from IR spectra (Table 4.3.7.). It is observed that RA intensities (*s*-polarization, $8.80X10^{-4}$ and $6..00X10^{-4}$) of the C-D stretching bands of saturated $C_{12}DS$ monolayers are much lower than those ($1.70X10^{-3}$ and $1.30X10^{-3}$) of the corresponding C-H bands of saturated $C_{12}HS$ monolayers. This is due to the great difference in atomic mass between D and H atoms. The smaller RA intensity indicates that the absorption coefficient ($k_{max}$) of the C-D stretching vibration is much smaller than that of the corresponding C-H modes.

*the S-O stretching region of head group*

Figure 4.3.4(b) is RA spectra of adsorbed monolayers of $C_{12}DS$in the S-O stretching region at the interface in pure water solution. The peaks near 1205 and $1032cm^{-1}$ are assigned as the asymmetric and the symmetric S-O stretching band of $-SO_4^-$ group, respectively. The intensity and peak frequencies in this region qualitatively have the same changing trends as that in the $C_{12}HS$ monolayers.

## 4.4. Mixed Monolayers of $C_{12}N$ and $C_{12}HS$ (or $C_{12}DS$) at The Aqueous Solution/Air Interface.

### 4.4.1. Surface Properties from Surface Tension Measurements

Data on $\gamma$, $\pi$, $\Gamma$, and A of equimolar mixtures $C_{12}HS$-$C_{12}N$, $C_{12}DS$-$C_{12}N$ in pure water, and $C_{12}DS$-$C_{12}N$ in 0.1M NaBr are listed in Table 4.4.1., 4.4.2., and 4.4.3., respectively. The determined values of cmc, $\pi_{cmc}$, $\Gamma_{max}$, and $A_{min}$ from surface tension measurements for these systems are listed in Table 4.4.4. Our experimental data on mixture $C_{12}HS$-$C_{12}N$ in pure water are consistent with those reported by Lucassen-Reynders (80).

Plots of the surface tension vs. log of the bulk concentration for $C_{12}HS$, $C_{12}DS$, $C_{12}N$, and their equimolar mixtures ($C_{12}HS$-$C_{12}N$ and $C_{12}DS$-$C_{12}N$) in pure water are shown in Figure 4.4.1(a). Plots of the surface tension vs. log of the bulk concentration for $C_{12}DS$, $C_{12}N$, and their equimolar mixture ($C_{12}DS$-$C_{12}N$) in 0.1M NaBr are shown in Figure 4.4.1(b). Plots of the surface pressure vs. the area per molecule for these mixed systems are shown in Figure 4.4.2. It is observed that all of these mixed monolayers at saturation adsorption at the interface are LE type monolayers, and there exists a phase transition point between the LE and G phase for each of these adsorbed mixed monolayers. Figures 4.4.1(a) and (b) also show strong interactions between these anionic and cationic surfactants at the interface as well as in formation of micelles. Synergism in both surface tension reduction efficiency and surface tension reduction effectiveness is observed. Gu and Rosen (81) have investigated interactions in cationic-anionic mixed monolayers at various interfaces. Using the equations derived by them, which include a correction for changes in area per surfactant molecule at the interface resulting from intermolecular interaction in the mixed monolayer, we have calculated the

**Table 4.4.1**

**Data on $\gamma$, $\pi$, $\Gamma$, and A for Equimolar $C_{12}H_{25}SO_4Na$-$C_{12}H_{25}N(CH_3)_3Br$ Mixed Solution in Pure $H_2O$ (25.0°C)**

| $C^a$ ($X10^5M$) | logC | $\gamma$ (mN/m) | $\pi$ (mN/m) | $\Gamma$ ($X10^{10}$ mol/cm$^2$) | A (Å$^2$) |
|---|---|---|---|---|---|
| 5.00 | -4.30 | 29.0 | 43.0 | - | -* |
| 4.00 | -4.40 | 32.0 | 40.0 | 2.89 | 57.5 |
| 2.00 | -4.70 | 42.3 | 29.7 | 2.89 | 57.5 |
| 1.00 | -5.00 | 51.6 | 21.4 | 2.61 | 63.6 |
| 0.50 | -5.30 | 60.5 | 11.5 | 2.29 | 72.5 |
| 0.25 | -5.60 | 67.0 | 5.0 | 1.98 | 84.0 |

* above the cmc.

a. the bulk concentration of either surfactant component.

**Table 4.4.2**

**Data on $\gamma$, $\pi$, $\Gamma$, and A for Equimolar $C_{12}D_{25}SO_4Na$-$C_{12}H_{25}N(CH_3)_3Br$ Mixed Solution in Pure $H_2O$ (25.0°C)**

| $C^a$ ($X10^5$M) | logC | $\gamma$ (mN/m) | $\pi$ (mN/m) | $\Gamma$ ($X10^{10}$ mol/cm$^2$) | A (Å$^2$) |
|---|---|---|---|---|---|
| 5.00 | -4.30 | 29.6 | 42.4 | - | -* |
| 4.00 | -4.40 | 32.5 | 39.5 | 2.73 | 60.8 |
| 2.00 | -4.70 | 45.0 | 27.0 | 2.73 | 60.8 |
| 1.00 | -5.00 | 52.0 | 20.0 | 2.50 | 66.5 |
| 0.50 | -5.30 | 58.5 | 13.5 | 2.08 | 80.0 |

* above the cmc.

a. the bulk concentration of either surfactant component.

**Table 4.4.3**

**Data on $\gamma$, $\pi$, $\Gamma$, and A for Equimolar $C_{12}D_{25}SO_4Na$-$C_{12}H_{25}N(CH_3)_3Br$ Mixed Solutions in 0.1M NaBr (25.0°C)**

| $C^a$ ($X10^5M$) | logC | $\gamma$ (mN/m) | $\pi$ (mN/m) | $\Gamma$ ($X10^{10}$ mol/cm$^2$) | A ($Å^2$) |
|---|---|---|---|---|---|
| 5.00 | -4.30 | 27.3 | 45.0 | - | -* |
| 2.50 | -4.60 | 29.4 | 42.9 | 2.81 | 59.0 |
| 1.75 | -4.75 | 34.2 | 38.1 | 2.81 | 59.0 |
| 1.25 | -4.90 | 38.8 | 33.5 | 2.81 | 59.0 |
| 0.875 | -5.05 | 43.8 | 28.5 | 2.73 | 60.8 |
| 0.625 | -5.20 | 48.5 | 23.8 | 2.55 | 65.0 |
| 0.44 | -5.35 | 53.0 | 19.3 | 2.41 | 69.0 |
| 0.31 | -5.50 | 57.0 | 15.3 | 2.25 | 73.6 |

* above the cmc.

a. the bulk concentration of either surfactant component.

**Table 4.4.4**

**Surface Properties of Equimolar $C_{12}HS$-$C_{12}N$ and $C_{12}DS$-$C_{12}N$ Solutions in Pure $H_2O$ (25.0°C)**

| Mixture | cmc[a] ($X10^5$M) | $\pi_{cmc}$ (mN/m) | $\Gamma_{max}$ ($X10^{10}$ mol./cm$^2$) | $A_{min}$ (Å$^2$) |
|---|---|---|---|---|
| $C_{12}HS$-$C_{12}N$ (in $H_2O$) | 4.10 | 43.0 | 2.89 | 57.5 |
| $C_{12}DS$-$C_{12}N$ (in $H_2O$) | 4.05 | 42.4 | 2.73 | 60.8 |
| $C_{12}DS$-$C_{12}N$ (in 0.1M NaBr) | 2.95 | 45.0 | 2.81 | 59.0 |

| Mixture | $\beta^\sigma$ | $\beta^m$ | $X_1^s$ | $X_1^m$ |
|---|---|---|---|---|
| $C_{12}HS$-$C_{12}N$ (in $H_2O$) | -32.8 | -29.0 | 0.51 | 0.51 |
| $C_{12}DS$-$C_{12}N$ (in $H_2O$) | -32.6 | -28.6 | 0.51 | 0.51 |
| $C_{12}DS$-$C_{12}N$ (in 0.1M NaBr) | -16.8 | -15.7 | 0.55 | 0.53 |

a. bulk concentration of either surfactant component.

interaction parameters $\beta^{\sigma}$ (in formation of mixed monolayers), $\beta^{m}$ (in formation of mixed micelles), $X_1$ (the molar fraction of component 1 in the mixed monolayer), and $X_1^{m}$ (the molar fraction of component 1 in the mixed micelle). The data are also listed in Table 4.4.4. These data are in good agreements with those reported by Rosen (22). Figure 4.4.1(a) also shows that the mixed monolayer of $C_{12}$DS-$C_{12}$N basically has the same surface properties as the mixed monolayer of $C_{12}$HS-$C_{12}$N at the interface in pure water. This has provided good basis by using $C_{12}$DS instead of $C_{12}$HS in surfactant mixtures containing the same polymethylene chains as $C_{12}$HS for spectroscopic studies (FTIR, NMR). From Table 4.4.4., it is also found that the salt concentration has no significant effect on the properties of the mixed monolayer of $C_{12}$DS-$C_{12}$N, because the complex compound $C_{12}$DS-$C_{12}$N has surface properties similar to that of a non-ionic surfactant. On the other hand, the interaction between the anionic surfactant and the cationic surfactant, as measured by the values of $\beta^{\sigma}$ and $\beta^{m}$, is reduced in the presence of added electrolyte, because of compression of the electrical double layer surrounding their respective head groups.

### 4.4.2. RA Spectra of Mixed Monolayers of Equimolar mixtures $C_{12}$HS-$C_{12}$N and $C_{12}$DS-$C_{12}$N at the Aqueous Solution/Air Interface.

Plots of RA spectra in the C-H stretching region of the adsorbed mixed monolayers of $C_{12}$HS-$C_{12}$N at the interface in pure water are shown in Figure

4.4.3. The peak intensities and frequencies of the symmetric and asymmetric C-H stretching bands are listed in Table 4.4.5. The plots of RA intensity and peak frequency shift vs. log of the bulk concentration are shown in Figure 4.4.4. and 4.4.5., respectively. It is observed that when the bulk concentration is below the cmc, the peak intensities of both the symmetric and asymmetric C-H stretching bands decrease continuously with decrease in bulk concentration, and peak frequencies increase continuously with decrease in bulk concentration. Figure 4.4.3. also shows the same trends for the change in frequency of the asymmetric stretching C-H band (near 2960$cm^{-1}$) of methyl groups. As we have discussed in Chapter 4.2 and 4.3, both adsorbed monolayers of $C_{12}N$ and $C_{12}HS$ at saturated adsorption at the interface are more or less staggered. It is reasonable to expect that their adsorbed mixed monolayers ($C_{12}HS$-$C_{12}N$) at the interface may also have the similar staggered structure. Therefore, this staggered structure generates the continuous changes in both peak intensity and frequency in mixed monolayers at the interface.

Figures 4.4.6(a), (b), and (c) are plots of RA spectra of adsorbed mixed monolayers of $C_{12}DS$-$C_{12}N$ at the aqueous solution/air interface in the C-H, in the C-D, and in the S-O stretching regions, respectively, with various bulk concentrations (equimolar mixture) in pure water. The data on RA intensities and peak frequencies of the symmetric and the asymmetric C-H, C-D and S-O stretching bands are listed in Table 4.4.6., 4.4.7., respectively. Figures 4.4.8. and 4.4.9. show RA intensity and peak frequency shift in the C-H and C-D stretching regions as a function of log of the bulk concentration, respectively. It is observed that the changes in RA intensity and peak frequency in the C-H and

**Table 4.4.5**

**Properties of Adsorbed Mixed Monolayers of Equimolar $C_{12}H_{25}SO_4Na$ -$C_{12}H_{25}N(CH_3)_3Br$ at The Aqueous Solution /Air Interface in Pure $H_2O$**

| C[a] | $\nu_a$ | | $\nu_s$ | | A |
|---|---|---|---|---|---|
| ($X10^5M$) | $RA_s(X10^3)$ | $Wn(cm^{-1})$ | $RA_s(X10^3)$ | $Wn(cm^{-1})$ | ($Å^2$) |
| 5.00 | 2.10 | 2920.2 | 1.20 | 2850.7 | - |
| 4.00 | 2.30 | 2920.1 | 1.36 | 2850.4 | 57.5 |
| 2.00 | 2.10 | 2920.6 | 1.20 | 2850.9 | 57.5 |
| 1.00 | 1.90 | 2921.3 | 1.10 | 2851.3 | 63.6 |
| 0.50 | 1.70 | 2921.5 | 0.90 | 2851.6 | 72.5 |
| 0.25 | 1.25 | 2922.9 | 0.64 | 2852.1 | 84.0 |

a. the bulk concentration of either surfactant component.

C-D stretching regions for mixed monolayer of $C_{12}DS$-$C_{12}N$ at the interface have the same trends as those in the C-H stretching region for the mixed monolayer of $C_{12}HS$-$C_{12}N$. It implies that the adsorbed mixed monolayers of $C_{12}DS$-$C_{12}N$ at the interface may also have the staggered structures. Because of the continuous change in RA intensity, the phase transition point from the RA spectra was not determined.

### 4.4.3. Calculation of Surface Composition at The Air/Water Interface from RA Spectra of Mixed Monolayers

In Chapters 4.2.and 4.3. we have already measured the RA intensities of the adsorbed monolayers of the individual surfactants, $C_{12}N$, $C_{12}HS$, and $C_{12}DS$ (Tables 4.2.5, 4.3.5) at saturation adsorption at the interface. We have also determined the maximum surface concentration ($\Gamma_{max}$) at the interface for the individual surfactants of $C_{12}N$, $C_{12}HS$, and $C_{12}DS$ (in Tables 4.2.3. and 4.3.4.). Table 4.4.4. lists $\Gamma_{max}$ data for the mixed monolayers of $C_{12}HS$-$C_{12}N$ and $C_{12}DS$-$C_{12}N$ in pure water. Tables 4.4.5., 4.4.6., and 4.4.7. list RA intensities of the mixed monolayers of $C_{12}HS$-$C_{12}N$ and $C_{12}DS$-$C_{12}N$ in the C-H, and C-D stretching regions. Now using these data, we are able to calculate the composition in the mixed monolayer at the interface.

From the previous optical model (36), it is known that the RA intensity of the adsorbed monolayers at the interface depends on the thickness of the monolayer, the surface concentration, and the chain orientation of surfactant molecules in the monolayer. Assuming that the chain orientations and conformation of each component in the mixed monolayer are the same as those in their individual adsorbed monolayers (It also means that the thickness of the

**Table 4.4.6**

**Properties of Adsorbed Mixed Monolayers of Equimolar $C_{12}D_{25}SO_4Na$ -$C_{12}H_{25}N(CH_3)_3Br$ at The Aqueous Solution /Air Interface in Pure $H_2O$ (the C-H Stretching Bands)**

| C[a] | | $\nu_a$(C-H) | | $\nu_s$(C-H) | A |
|---|---|---|---|---|---|
| ($X10^5$M) | $RA_s(X10^3$ | Wn($cm^{-1}$) | $RA_s(X10^3)$ | Wn($cm^{-1}$) | ($Å^2$) |
| 5.00 | 1.20 | 2918.4 | 0.90 | 2848.6 | - |
| 4.00 | 1.10 | 2919.1 | 0.82 | 2849.1 | 60.8 |
| 2.00 | 1.06 | 2920.4 | 0.74 | 2850.8 | 60.8 |
| 1.00 | 1.00 | 2921.5 | 0.56 | 2851.6 | 66.5 |
| 0.50 | 0.90 | 2922.6 | 0.50 | 2853.0 | 80.0 |
| 0.25 | 0.72 | 2923.4 | 0.40 | 2853.3 | 95.0 |

a. the bulk concentration of either surfactant component.

**Table 4.4.7**

**Properties of Adsorbed Mixed Monolayers of Equimolar $C_{12}D_{25}SO_4Na$ -$C_{12}H_{25}N(CH_3)_3Br$ at The Aqueous Solution /Air Interface (the C-D and S-O Stretching Bands)**

| C | $\nu_a$(C-D) | | $\nu_s$(C-D) | | $\nu_a$(S-O) | $\nu_s$(S-O) |
|---|---|---|---|---|---|---|
| ($X10^5$M) | $RA_s(X10^4)$ | $Wn(cm^{-1})$ | $RA_s(X10^4)$ | $Wn(cm^{-1})$ | $(cm^{-1})$ | $(cm^{-1})$ |
| 5.00 | 8.00 | 2191.6 | 5.60 | 2087.0 | 1216.9 | 1040.7 |
| 4.00 | 8.00 | 2191.6 | 5.30 | 2087.5 | 1216.6 | 1040.3 |
| 2.00 | 6.40 | 2194.0 | 5.00 | 2088.6 | 1215.9 | 1037.2 |
| 1.00 | 5.60 | 2196.9 | 4.50 | 2090.0 | 1215.0 | 1037.2 |
| 0.50 | 5.00 | 2197.5 | 4.00 | 2090.7 | 1215.2 | 1037.3 |

mixed monolayer is equal to those of individual monolayers), then the RA intensity of the mixed monolayer only depends on the composition (surface concentration) of each component in the monolayer, and it can be calculated by using the RA intensity and the surface concentration of individual surfactants in the following ways:

$$I_{2920}(C_{12}HS\text{-}C_{12}N) = \frac{I_{2920}(C_{12}HS) \cdot \Gamma_{max}(C_{12}HS\text{-}C_{12}N) \cdot X_1}{\Gamma_{max}(C_{12}HS)} + \frac{I_{2920}(C_{12}N) \cdot \Gamma_{max}(C_{12}HS\text{-}C_{12}N) \cdot (1\text{-}X_1)}{\Gamma_{max}(C_{12}N)} \quad (4.6)$$

where $I_{2920}(C_{12}N)$, $I_{2920}(C_{12}HS)$, and $I_{2920}(C_{12}HS\text{-}C_{12}N)$ are the RA intensities of the asymmetric C-H stretching bands of methylene groups in adsorbed monolayers of $C_{12}N$, $C_{12}HS$, and their mixed monolayer of $C_{12}HS\text{-}C_{12}N$, respectively, in pure water. $X_1$ is the molar fraction of the component 1 ($C_{12}HS$) in the mixed monolayer at the interface.

Table 4.4.8. lists experimental data on RA intensities and $\Gamma_{max}$ for the individual and mixed monolayers. Solving the equation (4.6), we have $X_1 = 0.45$. This value, 0.45, predicted from IR spectra is in good agreement with $X^{\sigma}=0.51$, calculated from a non-ideal mixing solution model (Table 4.4.4.).

Because the RA intensities in the C-H stretching region in the $C_{12}DS$-$C_{12}N$ mixed monolayers at the interface is only contributed by the methylene chains of the $C_{12}N$ component, and the RA intensities in C-D stretching region by the deuterated methylene chains of $C_{12}DS$, the difference between the RA intensities of mixed $C_{12}HS$-$C_{12}N$ and $C_{12}DS$-$C_{12}N$ in the C-H stretching region are contributed only by the $C_{12}HS$ components. Comparing this value with the RA intensity and $\Gamma_{max}$ for the individual $C_{12}HS$ monolayer, we can also calculate the surface concentration of the $C_{12}HS$ component in the mixed monolayer at the interface in the following way:

$$I_{2920}(C_{12}HS^{*}) = I_{2920}(C_{12}HS\text{-}C_{12}N) - I_{2920}(C_{12}DS\text{-}C_{12}N)$$

$$= 2.40\times10^{-3} - 1.10\times10^{-3} = 1.30\times10^{-3}$$

$$X_1 = \frac{I_{2920}(C_{12}HS^{*}) \cdot \Gamma_{max}(C_{12}HS)}{I_{2920}(C_{12}HS) \cdot \Gamma_{max}(C_{12}HS\text{-}C_{12}N)} \qquad (4.7)$$

$$= 1.30\times10^{-3} \cdot 3.16\times10^{-10}/1.70\times10^{-3} \cdot 5.54\times10^{-10} = 0.44$$

where $I_{2920}(C_{12}HS^{*})$ is the intensity of the asymmetric C-H stretching band in the mixed monolayer of $C_{12}HS$-$C_{12}N$. This value is also in good agreement with $X^{\sigma}$. These good agreements between $X_1$ and $X^{\sigma}$ values may indicate that

**Table 4.4.8**

**Data on Maximum Surface Concentration ($\Gamma_{max}$) and Peak Intensity for Adsorbed Monolayers**

| Monolayer | $\Gamma_{max}$ | C-H | | C-D | |
|---|---|---|---|---|---|
| | | $I_{2920}$ | $I_{2850}$ | $I_{2195}$ | $I_{2091}$ |
| | ($X10^{-10}$ mol/cm$^2$) | ($X10^{-3}$) | ($X10^{-3}$) | ($X10^{-4}$) | ($X10^{-4}$) |
| $C_{12}N$ | 3.22 | 1.12 | 0.82 | - | - |
| $C_{12}HS$ | 3.16 | 1.70 | 1.22 | - | - |
| $C_{12}DS$ | 3.12 | - | - | 8.80 | 6.00 |
| *$C_{12}HS$-$C_{12}N$ | 5.54 | 2.40 | 1.36 | - | - |
| *$C_{12}DS$-$C_{12}N$ | 5.46 | 1.10 | 0.82 | 8.00 | 5.30 |

* equimolar solution.

the previous assumptions (the orientations and conformation of surfactant molecules in the individual adsorbed monolayers are the same as in their mixed monolayers) are basically correct.

### 4.4.4. Peak Frequencies of Mixed Monolayers of $C_{12}HS$- $C_{12}N$ and $C_{12}DS$-$C_{12}N$ at The Aqueous Solution/Air Interface

Data on peak frequencies in the C-H, C-D, and S-O stretching regions of methylene, deuterated methylene, methyl, and sulfate groups for the individual surfactant monolayers of $C_{12}N$, $C_{12}HS$, $C_{12}DS$ and their mixed monolayers of $C_{12}HS$- $C_{12}N$ and $C_{12}DS$- $C_{12}N$ are listed in Table 4.4.9. When the total surfactant concentration ($C_T = 1.2X10^{-4}M$) of the mixed equimolar surfactant $C_{12}DS$-$C_{12}N$ solution is higher than the cmc ($8.10X10^{-5}M$), some fine crystalline solids were formed at the air/water interface as well as in the mixed solution. These fine solids are eye-visible, and also detectable by the decrease in the transmittance of visible light compared with the transparent mixed surfactant solution. Figures 4.4.7.(a), (b), and (c) are RA spectra of the $C_{12}DS$- $C_{12}N$ crystalline particles at the aqueous solution/air interface in the C-H, in the C-D, and in the S-O stretching regions, respectively. It is seen that the fine crystalline particles formed from the equimolar mixture $C_{12}DS$-$C_{12}N$ at the interface generate RA spectra with a very good signal-noise ratio and strong absorption in all three regions. These unnormal high intensities of the RA spectra in all three regions indicate the presence of multilayers or solid particles at the interface. Data on these peak frequencies are listed in the bottom line of Table 4.4.9. for comparison.

*C-H and C-D stretching regions of polymethylene chains*

**Table 4.4.9**

**Peak Frequencies in Adsorbed Monolayers**

| system | C-H ($CH_2$) | | C-D ($CD_2$) | | S-O ($SO_4$) | C-H ($CH_3$) |
|---|---|---|---|---|---|---|
| | $\nu_a$ | $\nu_s$ | $\nu_a$ | $\nu_s$ | $\nu_a$ | $\nu_a$ |
| | ($cm^{-1}$) | ($cm^{-1}$) | ($cm^{-1}$) | ($cm^{-1}$) | ($cm^{-1}$) | ($cm^{-1}$) |
| $C_{12}N$ | 2921.4 | 2851.5 | - | - | - | 2957.8 |
| $C_{12}HS$ | 2921.1 | 2850.8 | - | - | 1204.5 | 2957.4 |
| $C_{12}DS$ | - | - | 2195.2 | 2091.0 | 1205.7 | - |
| $^aC_{12}HS$ | | | | | | |
| $-C_{12}N$ | 2920.1 | 2850.4 | - | - | 1215.0 | 2956.0 |
| $^aC_{12}DS$ | | | | | | |
| $-C_{12}N$ | 2919.1 | 2849.1 | 2191.8 | 2087.5 | 1216.6 | 2955.8 |
| $^aC_{12}DS$ | | | | | | |
| $-C_{12}N^*$ | 2918.0 | 2848.0 | 2191.1 | 2086.5 | 1217.4 | 2954.3 |

* The crystalline solid at the interface.

a. equimolar solution.

It is found that the frequencies in the C-H and C-D stretching regions of methylene and deuterated methylene chains of the crystalline precipitates at the interface have the lowest values among all of the individual and mixed monolayers. This indicates that the polymethylene and deuterated methylene chains in this equimolar mixture (crystalline solids) are very high-ordered, all-*trans* conformational. It is also noted that the frequencies of the C-H and C-D stretching bands in the mixed monolayer at the interface at saturation adsorption are always lower than the corresponding ones in their individual surfactant monolayers. Even though the polymethylene and deuterated methylene chains in the mixed monolayer conformationally are the same (all-*trans*) as in their individual adsorbed monolayers at saturated adsorption, the methylene chains are more closely packed (the area per metnylene chain is smaller). The lower peak frequencies in the C-H stretching region are probably caused by the strong interactions between the methylene chains in the mixed monolayer.

Scheuing and Weers (82) have studied the mixed micelles of dodecyltrimethylammonium chloride (DTAC) and $C_{12}HS$ by FTIR. They have reported that the frequencies of the symmetric and asymmetric C-H stretching bands of polymethylene chains in a precipitate formed from the equimolar mixture of DTAC and $C_{12}HS$ are 2851.0 and 2919.4$cm^{-1}$, respectively. These frequencies are close to ours in $C_{12}HS$-$C_{12}N$ mixed monolayers (2850.4 and 2920.1$cm^{-1}$), but higher than the corresponding ones in the $C_{12}DS$-$C_{12}N$ crystalline solids (2848.0 and 2918.0$cm^{-1}$). This frequency difference may be caused by different processes of formation of precipitates, or different structures

between $C_{12}$DS-$C_{12}$N and $C_{12}$HS-DTAC. The former is slowly formed from the adsorbed monolayer at the interface and has both methylene and deuterated methylene chains , while the latter is formed from the mixed micelles in solution and has only methylene chains. It is expected that the former has more ordered methylene chain structures.

It is observed that the peak frequencies in the C-H stretching region for our adsorbed monolayers are much lower than those reported for the pure and mixed micelles of $C_{12}$HS (82) These relative low frequencies indicate that the methylene chains in the adsorbed monolayers at the interface is more ordered (less *gauche* conformers) than those in the pure or mixed micelles in surfactant solutions. Weeres and Scheuing (71) have also reported that accommodating the greater aggregation numbers from spherical micelle to non-spherical micelles (like rod-like and lamellar) the methylene chains of the surfactant must adopt a slightly higher ordering, i.e., a lower *gauche/trans* conformer ratio. Generally speaking, molecular ordering increases in the following order: monomers (in solution) < spherical micelles < rod-like micelles < lamellar micelles < liquid crystals < adsorbed monolayer < solid crystals.

*S-O stretching region*

Scheuing and Weers (82) have reported a broad doublet asymmetric S-O stretching band near 1214$cm^{-1}$ and a single symmetric S-O stretching band near 1060$cm^{-1}$ for the pure SDS ($C_{12}$HS) and its non-equimolar mixed (with DTAC) micelles of $C_{12}$HS-DTAC. It is interesting to compare the RA spectra in the S-O stretching regions of the individual surfactant monolayers of $C_{12}$HS [Fig. 4.3.3(b)], $C_{12}$DS [Fig. 4.3.4(b)], and the mixed monolayer of $C_{12}$DS-$C_{12}$N

[Fig. 4.4.4.(b)], and also to compare ours with those reported by other investigators. The RA spectra of the adsorbed monolayers of $C_{12}HS$ are slightly different from those reported for the pure $C_{12}HS$ micelle (82). Spectra of the $C_{12}HS$ monolayer have a strong broad asymmetric S-O stretching band near 1205$cm^{-1}$ with a very small high frequency (1260$cm^{-1}$) shoulder and a weak symmetric S-O stretching band at 1060$cm^{-1}$. The differences in band shapes and frequencies in this region between spectra of the adsorbed $C_{12}HS$ monolayer at the interface and the micelles in surfactant solutions can be attributed to the different molecular structure and arrangement. The former (monolayers) have a relatively high ordered conformation (basically, all-*trans* conformation), while the latter (micelles) have a more disordered conformation (0.77 double-*gauche* and 0.68 kink states per molecule of $C_{12}HS$) (83)

Colthup et.al.. (73) have reported two strong bands around 1270 and 1207$cm^{-1}$ for the asymmetric S-O stretching modes and one strong band at 1170$cm^{-1}$ for the symmetric mode for solid $C_{12}HS$. The changes in the band shape and frequency in the asymmetric S-O stretching mode for different $C_{12}HS$ sample states and structures may be summarized as follows: two strong doublet peaks (1207 and 1270$cm^{-1}$), for crystal solids; one strong broad peak near 1205$cm^{-1}$ with a small higher frequency shoulder, for adsorbed monolayers; broad doublet, with major peak near 1214$cm^{-1}$, and a large higher frequency shoulder, for pure or mixed micelles.

The RA spectra of the adsorbed monolayers of $C_{12}DS$ are slightly different from that of $C_{12}HS$ monolayers in the symmetric S-O stretching band. The

former ($C_{12}DS$) has the peak near 1040cm$^{-1}$, and the latter near 1060cm$^{-1}$. The difference in this peak frequency can be attributed to the different structures in the chains (methylene and deuterated methylene) attached to the same head groups. In the asymmetric S-O stretching regions, both $C_{12}HS$ and $C_{12}DS$ monolayers have similar band shapes and peak frequencies. This indicates that relative to the symmetric S-O band, the asymmetric S-O stretching band is less sensitive to the structure of the attached chains.

The RA spectra of the mixed monolayer of $C_{12}DS$-$C_{12}N$ at the interface have a strong asymmetric S-O stretching band near 1214cm$^{-1}$ with a small higher frequency shoulder (near 1250cm$^{-1}$) and a relatively weak symmetric band around 1040cm$^{-1}$. The increase in the low frequency component of the asymmetric S-O stretching mode from 1205cm$^{-1}$ in the individual monolayer of $C_{12}DS$ to 1214cm$^{-1}$ in the mixed $C_{12}DS$-$C_{12}N$ monolayer is probably caused by the electrostatic interactions of the $C_{12}DS$ and $C_{12}N$ head groups at the interface. These interactions cause a shifting and a splitting of the asymmetric S-O stretching modes, due to a "local site" symmetric lowering of the asymmetric modes (82). From Table 4.4.9. it is seen that the asymmetric S-O stretching band in the crystalline solids formed at the interface has the highest frequency due to the strong interaction between the head groups and highly ordered structure in this equimolar anionic-cationic mixture.

*asymmetric C-H stretching band of methyl groups*

The head group,-$N^+(CH_3)_3$, of the $C_{12}N$ molecule contains three methyl groups. In the mixed monolayer of $C_{12}HS$-$C_{12}N$ or $C_{12}DS$-$C_{12}N$, this head

group undergoes a large change in its electrostatic environment. These changes should result in altering the band shapes and frequencies in the deforming modes of the methyl group in the $-N^{+}(CH_3)_3$ head group of the $C_{12}N$. Scheuing and Weers (82) have reported these changes in mixed micelles of $C_{12}HS$-DTAC with different micelle compositions. Unfortunately, the RA spectra in this region (1300-1500$cm^{-1}$) could not be resolved due to the very strong absorption of water vapor at the aqueous solution/air interface.

### 4.4.5. The Effects of The Bulk Surfactant Composition on Surface Properties of Mixed Monolayers of $C_{12}DS$-$C_{12}N$ at The Aqueous Solution/Air Interface

*surface tension measurements*

We have measured the surface tensions of mixed $C_{12}DS$-$C_{12}N$ aqueous solutions with various compositions ($\alpha$=0.1, 0.2, 0.4, 0.5, 0.6, 0.8, and 0.9). The plots of surface tension vs. log of the total bulk concentration with different $\alpha$ values are shown in Figure 4.4.10. The determined values of cmc, $A_{min}$, $\Gamma_{max}$ with different $\alpha$ values are listed in Table 4.4.10. Using equations including the correction of changes in area per surfactant molecule (81), we have calculated the interaction parameters, $\beta^{\sigma}$, $\beta^{m}$ and the mole fractions $X_1^{\sigma}$, and $X_1^{m}$. Data are listed in Table 4.4.10.

It is observed that the area per polymethylene chain at the interface slightly decreases with increase in $\alpha$, and reaches a minimum value at $\alpha$ = 0.5

(equimolar mixture), then increases with increase in $\alpha$. This means that the composition in bulk surfactant solution has a small effect on the packing density in the monolayer at the interface In the non-equimolar cationic-anionic surfactant solution, the complex compound $C_{12}DS$-$C_{12}N$ at the interface is electrically neutral, but after interactions between cationic and anionic surfactant molecules, either the cationic or the anionic surfactant molecules are in excess in bulk solution. Because of the concentration gradient between the bulk solution and the interface, these excess cationic (or anionic) surfactant molecules still have a chance (although very small) to diffuse to the interface. Therefore, it is expected that a small amount of individual cationic (or anionic) surfactant molecules are present in the monolayer at the interface (in kinetic equilibrium). As a result, these positively (or negatively) charged molecules should slightly expand the monolayer (because of the repulsion between the charged head groups), and consequently increase the are per polymethylene chain at the interface. When $\alpha$ is getting further and further from 0.5, the concentration gradient is larger and larger, and the chance for the individual surfactant molecules to adsorb at the monolayer becomes greater and greater. As a result, the area per methylene chain at the interface is getting bigger and bigger.

From Table 4.4.10. it is seen that the calculated interaction parameters $\beta^{\sigma}$ and $\beta^{m}$ are very close to each other for different $\alpha$ values. This indicates that in a wide range of bulk compositions ($\alpha$ = 0.1 - 0.9), the interactions between the cationic and anionic surfactants in the adsorbed mixed monolayers as well as in mixed micelles basically remain at the same levels. It is also found that the

**Table 4.4.10.**

**Effects of $\alpha$ on Interaction Parameters of $\beta^{\sigma}$, $\beta^{m}$, Mole Fractions of $X^{\sigma}$ and $X^{m}$, $A_{min}$, $\Gamma_{max}$, and cmc in Mixed $C_{12}DS$-$C_{12}N$ Solutions**

| $\alpha$ | $\beta^{\sigma}$ | $X_1^{\sigma}$ | $\beta^{m}$ | $X_1^{m}$ | $X_1^{*}$ |
|---|---|---|---|---|---|
| 0.1 | -32.1 | 0.48 | -27.8 | 0.47 | 0.46 |
| 0.2 | -31.6 | 0.49 | -26.9 | 0.48 | 0.55 |
| 0.4 | -31.0 | 0.50 | -27.9 | 0.50 | 0.54 |
| 0.5 | -32.6 | 0.51 | -28.6 | 0.51 | 0.52 |
| 0.6 | -30.5 | 0.52 | -27.0 | 0.52 | 0.54 |
| 0.8 | -32.5 | 0.53 | -29.0 | 0.53 | 0.52 |
| 0.9 | -33.0 | 0.54 | -29.2 | 0.55 | 0.52 |

| $\alpha$ | $A_{min}$ ($Å^2$/per chain) | $\Gamma_{max}$ ($X10^{-10}$mole/$cm^2$) | cmc ($X10^{-5}$M) |
|---|---|---|---|
| 0.1 | 34.0 | 4.93 | 10.0 |
| 0.2 | 33.0 | 5.08 | 9.50 |
| 0.4 | 31.6 | 5.30 | 8.58 |
| 0.5 | 30.7 | 5.46 | 8.10 |
| 0.6 | 31.9 | 5.25 | 8.45 |
| 0.8 | 32.8 | 5.11 | 9.12 |
| 0.9 | 33.8 | 4.96 | 9.56 |

$X_1^{*}$ - the caclulated mole fraction of component $C_{12}DS$ in the mixed monolayer at the interface from RA spectra

mole fractions of component $C_{12}DS$ in both the mixed monolayer ($X_1^{\sigma}$) and in the mixed micelle ($X_1^{m}$) continuously, and very slowly increase with increase in $\alpha$, but both values of $X_1^{\sigma}$ and $X_1^{m}$ are very close to 0.5. This shows that for the mixed cationic-anionic surfactant system, in a wide range ($\alpha$ = 0.1-0.9), the composition in the bulk solution has no significant effect on the compositions in the mixed monolayer at the interface as well as in the mixed micelle in solution.

Rosen has indicated that at the point of maximum synergism, the mole fraction, $\alpha^*$, of surfactant 1 in the total surfactant used in the solution phase is equal to the value of $X^*$, the mole fraction of surfactant 1 in the total surfactant in the mixed monolayer at the interface, and can be calculated by the expression:

$$X^* = \alpha^* = \frac{\ln(C_1^0/C_2^0) + \beta^{\sigma}}{2\beta^{\sigma}} \qquad (4.8)$$

where $C_1^0$, $C_2^0$, and $\beta^{\sigma}$ are defined in equations (1.9) and (1.10). Because of the strong interaction between the cationic and anionic surfactants, the $\beta^{\sigma}$ value, -32, is much larger than $\ln(C_1^0/C_2^0)$, -0.64. Then $X^* = \alpha^*$ =0.51 and

equimolar amounts give maximum synergism, irrespective of the ($C_1^0/C_2^0$) ratio.

From Table 4.4.10., it is observed that the the cmc values continuously decrease with increase in $\alpha$, and reach a minimum value at $\alpha = 0.5$, then increase with increase in $\alpha$. In an equimolar mixture, the complex compound, $C_{12}DS\text{-}C_{12}N$, has the maximum concentration in the solution. This complex with two long hydrocarbon chains is the most surface active and has the the lowest cmc value compared to the individual ionic surfactants in the mixed surfactant solutions. When $\alpha$ is getting further and further from 0.5, the bulk surfactant solutions contain more and more individual ionic surfactant component (either cationic or anionic, depending on $\alpha$ is less or more than 0.5), and the cmc values of the mixed surfactant solutions become larger and larger.

*RA spectra of mixed monolayers of $C_{12}DS\text{-}C_{12}N$ with various $\alpha$ values*

Figures 4.4.11.(a) and (b) are plots of RA spectra of the mixed monolayers of $C_{12}DS\text{-}C_{12}N$ at the same total bulk concentration ($8.0X10^{-5}M$) with different $\alpha$ values in the C-H and in the C-D stretching regions, respectively. The data on the peak intensities and frequencies in the C-H and in the C-D stretching regions are listed in Tables 4.4.11. and 4.4.12., respectively. Plots of RA intensity and the frequency shift in the C-H and C-D stretching regions vs. $\alpha$ values are shown in Figure 4.4.12. and in Figure 4.4.13., respectively.

It is found that the RA intensities in both the C-H and C-D stretching regions basically remain constant, and the bulk compositions ($\alpha$ values) have no

significant effects on the RA intensities of the mixed monolayers at the interface.

The RA intensity of the mixed monolayer of $C_{12}DS$-$C_{12}N$ in the C-H stretching region is contributed only by the component $C_{12}N$, and the RA intensity in the C-D stretching region only by $C_{12}DS$. Using all the assumptions in Chapter 4.4.3., we are able to use the RA intensities of the asymmetric C-D stretching bands (higher intensity) of the mixed monolayer to calculate the composition in the mixed monolayers in the following way:

$$X_1^*(C_{12}DS) = \frac{I_{2195}(C_{12}DS\text{-}C_{12}N) \cdot \Gamma_{max}(C_{12}DS)}{I_{2195}(C_{12}DS) \cdot \Gamma_{max}(C_{12}DS\text{-}C_{12}N)} \qquad (4.9)$$

where $X_1^*$ is the mole fraction of $C_{12}DS$ in the mixed monolayer at the interface. The calculated $X_1^*$ values for different $\alpha$ values are listed in Table 4.4.10. Comparing values of $X_1^*$ with $X_1^\sigma$, determined from surface tension measurements, we have found good agreements between these values, and all the values are close to 0.5. This has provided new evidence that the $\alpha$ value has no significant effect on the surface composition in the mixed monolayer at the interface, and in a relative large range ($\alpha$ = 0.1-0.9), the cationic and anionic surfactants at the interface remain at almost constant 1:1 ratio.

From Tables 4.4.11. and 4.4.12. it is interesting to note that even the RA intensities in both C-H and C-D stretching regions keep almost constant at the

**Table 4.4.11**

**The Effects of α on Properties of Adsorbed Mixed Monolayers of $C_{12}DS$-$C_{12}N$ at The Aqueous Solution /Air Interface in Pure $H_2O$ ($C_T$ = 8.0X10$^{-5}$M, the C-H Stretching Region)**

| α | $\nu_a$(C-H) | | $\nu_s$(C-H) | |
|---|---|---|---|---|
| | $RA_s$(X10$^3$) | Wn(cm$^{-1}$) | $RA_s$(X10$^4$) | Wn(cm$^{-1}$) |
| 0.00 | 1.12 | 2921.4 | 8.20 | 2851.5 |
| 0.10 | 1.10 | 2923.0 | 7.80 | 2851.5 |
| 0.20 | 1.08 | 2923.0 | 7.00 | 2851.2 |
| 0.40 | 1.20 | 2922.6 | 6.80 | 2850.8 |
| 0.50 | 1.20 | 2919.1 | 8.20 | 2849.1 |
| 0.60 | 1.10 | 2920.0 | 6.80 | 2849.5 |
| 0.80 | 1.08 | 2920.7 | 7.20 | 2849.9 |
| 0.90 | 1.06 | 2921.3 | 6.80 | 2850.2 |

*α = the mole fraction of $C_{12}D_{25}SO_4Na$ in the mixture of $C_{12}D_{25}SO_4Na$ - $C_{12}H_{25}N(CH_3)_3Br$ in pure $H_2O$.

**Table 4.4.12**

**The Effects of α on Properties of Adsorbed Mixed Monolayers of $C_{12}DS$-$C_{12}N$ at The Aqueous Solution /Air Interface in Pure $H_2O$**

**($C_T$ = 8.0X10$^{-5}$M, the C-D Stretching Region)**

| α | $\nu_a$(C-D) | | $\nu_s$(C-D) | |
|---|---|---|---|---|
| | $RA_s$(X10$^4$) | Wn(cm$^{-1}$) | $RA_s$(X10$^4$) | Wn(cm$^{-1}$) |
| 0.10 | 6.40 | 2197.3 | 4.80 | 2095.0 |
| 0.20 | 7.90 | 2197.2 | 5.10 | 2094.6 |
| 0.40 | 8.00 | 2196.0 | 4.80 | 2093.5 |
| 0.50 | 8.10 | 2191.8 | 5.30 | 2087.5 |
| 0.60 | 8.00 | 2194.4 | 5.10 | 2090.7 |
| 0.80 | 8.10 | 2196.7 | 5.00 | 2092.7 |
| 0.90 | 8.10 | 2197.0 | 5.10 | 2093.1 |
| 1.00 | 8.80 | 2195.2 | 6.00 | 2091.0 |

*α = the mole fraction of $C_{12}D_{25}SO_4Na$ in the mixture of $C_{12}D_{25}SO_4Na$ - $C_{12}H_{25}N(CH_3)_3Br$ in pure $H_2O$.

same total bulk concentration in different α values, but the peak frequencies in these regions have relatively large changes. The peak frequencies in both C-H and C-D stretching regions decrease with α values, and reach minimum values at α=0.5, then increase with increase in α. This trend is the same as that observed for the area per methylene chain at the interface. Scheuing and Weers (82) have reported the same trends for the mixed $C_{12}$DS-DTAC micelles: the frequencies for both bands (C-H and C-D) show a decrease as the mixed micelle composition becomes equimolar. They have attributed this increase to the changes in the absolute frequencies of C-H and C-D bands due to the electrostatic effects in the non-equimolar mixed micelles. Comparing the data in Tables 4.4.11. 4.4.12. with those in Table 4.4.9., we have found that both the symmetric and asymmetric C-D stretching band frequencies in most of the non-equimolar mixed monolayers (except α=0.6) are actually higher than those (2195.2 and 2091.0$cm^{-1}$) in the adsorbed monolayer of pure $C_{12}$DS solution, and the asymmetric C-H stretching band frequencies in the mixed monolayers of the $C_{12}$N-rich mixed solutions are higher than that (2921.4$cm^{-1}$) in the saturated adsorbed monolayer of individual $C_{12}$N solution. This increase in frequency may be related to several factors. The first one is the packing density of the methylene chains at the interface. As discussed in Chapter 4.4.5., when α value is getting far from 0.5, the area per polymethylene chain at the interface increases , and the interactions between methylene chains at the interface decrease. This results in increasing frequencies for both the C-H and C-D stretching bands. The second factor may be the extent to which the total

surfactant concentration in mixed solutions deviates from its cmc. As mentioned before, the cmc of mixed surfactant solutions has a minimum value at $\alpha = 0.5$, and increases with increase in the extent at which the $\alpha$ value deviates from 0.5. At the same total surfactant concentration, $C_T=8.0X10^{-5}M$, which is below the minimum cmc value, when $\alpha$ is getting further and further from 0.5, the $C_T$ is less and less than its cmc, since the cmc is increasing when $\alpha$ deviates more and more from 0.5. As we discussed in Chapter 4.4.4., the peak frequencies in both C-H and C-D stretching regions continuously increase with decrease in bulk concentration due to the possible staggered structures of the mixed $C_{12}DS$-$C_{12}N$ monolayers at the interface. Therefore, when the $C_T$ is getting less and less than its cmc, the peak frequencies in these two regions are higher and higher. The third factor may be the different environments surrounding the head groups at the interface. As the composition of the mixed surfactant solutions is changed from $C_{12}N$-rich to $C_{12}DS$-rich, the interactions between head groups at the interface are also changed, and these changes may affect the absolute frequencies of the C-H and C-D stretching bands somewhat.

## Figure Legends

Fig. 1.1. Surface pressure - area per molecule ($\pi$-A) diagrams of different types of monolayers. Schematic; not in scale.

Fig. 1.2. Simulated relationship between the surface excess concentration and the bulk concentration for a monolayer absorbed at the air/water interface.

Fig. 2.1. Optical model of an anisotropic monolayer on an isotropic liquid substrate.

Fig. 2.2. Laboratory axis system with a representative chain (long arrow), a representative dipole moment (M), and the definition of angles.

Fig. 2.3. Calculated value of the reflection-absorption intensity vs. chain orientation angle for *s*- and *p*-polarized incident light at constant surface concentration.

Fig. 2.4 .Relationship between reflection-absorption intensity and $k_{max}$ at different chain orientation angles (30°, *p*-pol.).

Fig. 2.5 .Relationship between reflection-absorption intensity and $k_{max}$ at different chain orientation angles (30°, *s*-pol.).

Fig. 2.6. Results of refinement procedure which minimize $\Delta k_{max}$ to calculate the chain orientation angle $\chi$ and $k_{max}$.

Fig. 2.7. Polarized reflection-adsorption intensity ratios (RAp/RAs) vs. chain orientation angle at various values of $k_{max}$.

Fig. 2.8. $RAp^{i}/RAs$ ratios vs. chain orientation angle at different i values, $k_{max}$ is constant (0.30).

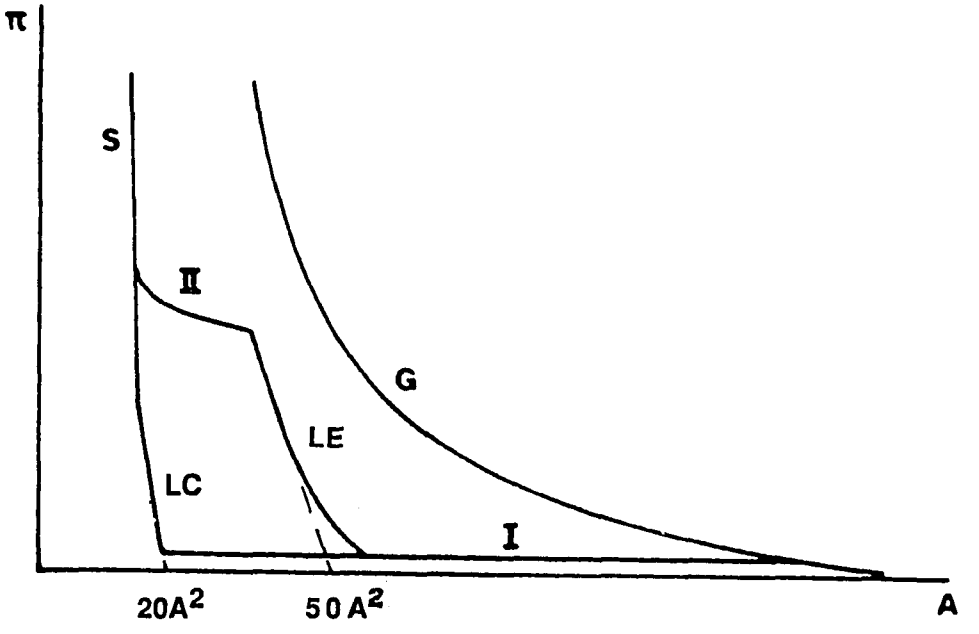


**Fig. 1.1. Surface pressure - area per molecule ($\pi$-A) diagrams of different types of monolayers. Schematic; not in scale.**

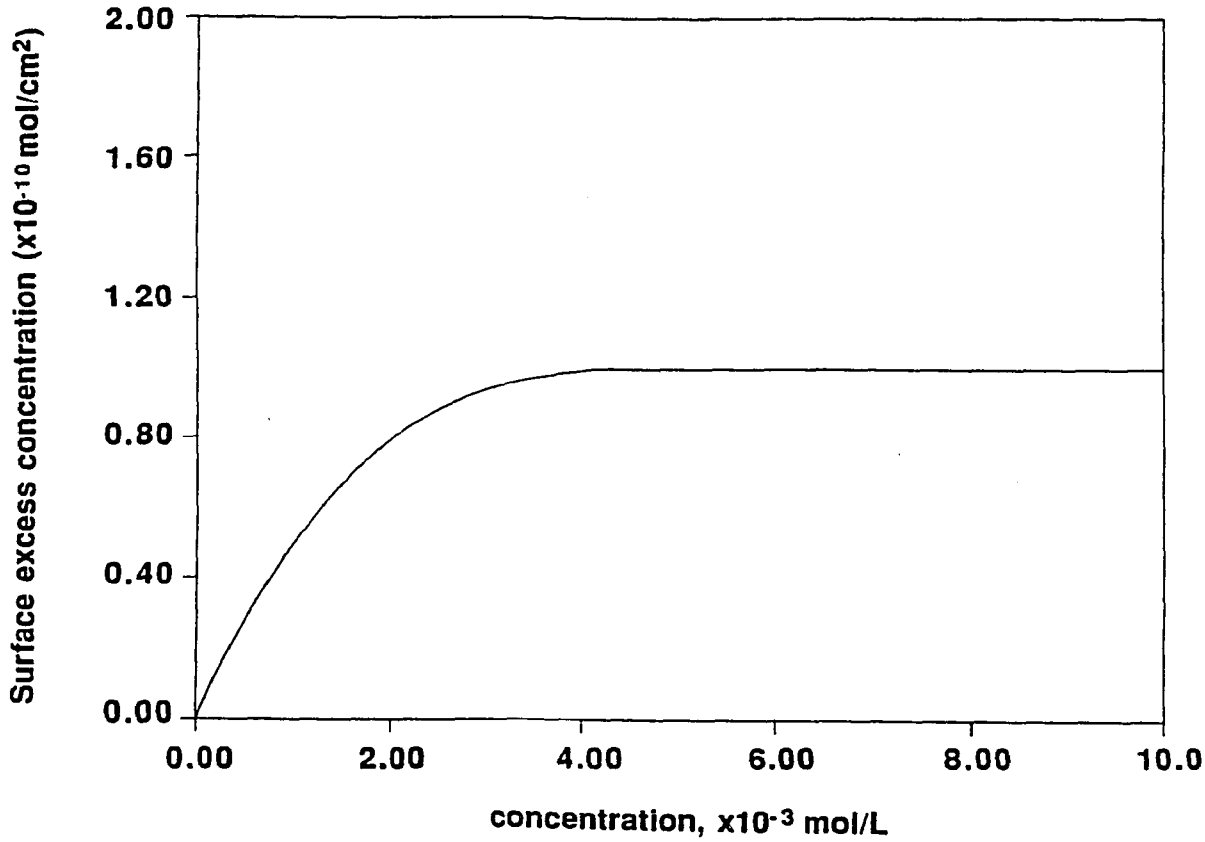


**Fig. 1.2. Simulated relationship between the surface excess concentration and the bulk concentration for a monolayer absorbed at the air/water interface.**

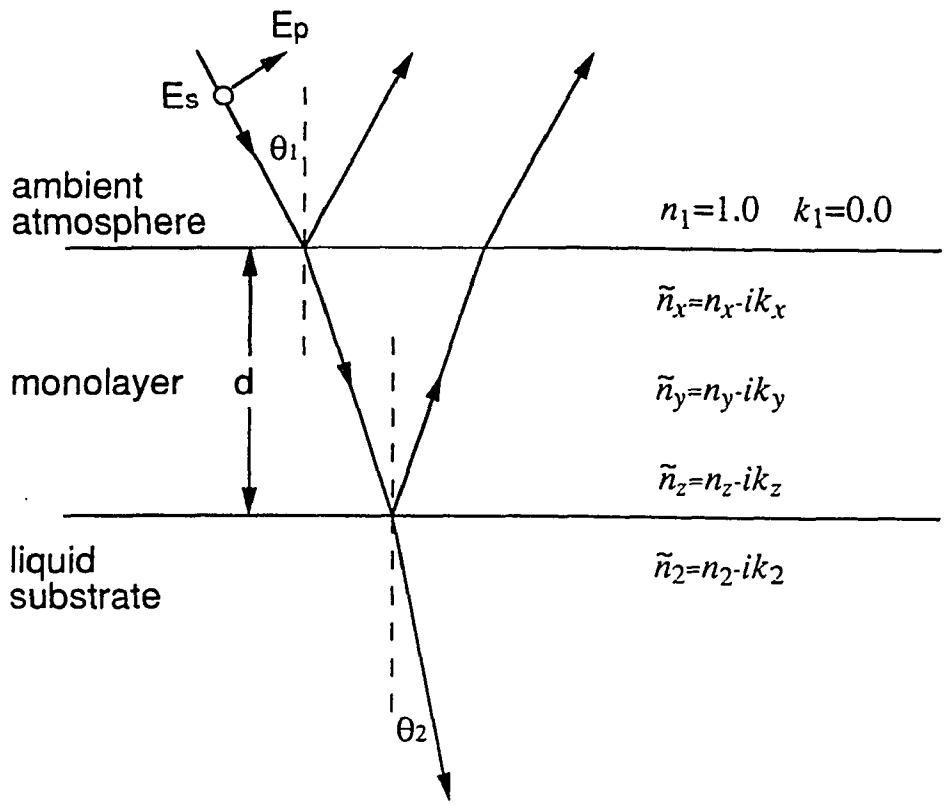


**Fig. 2.1. Optical model of an anisotropic monolayer on an isotropic liquid substrate.**

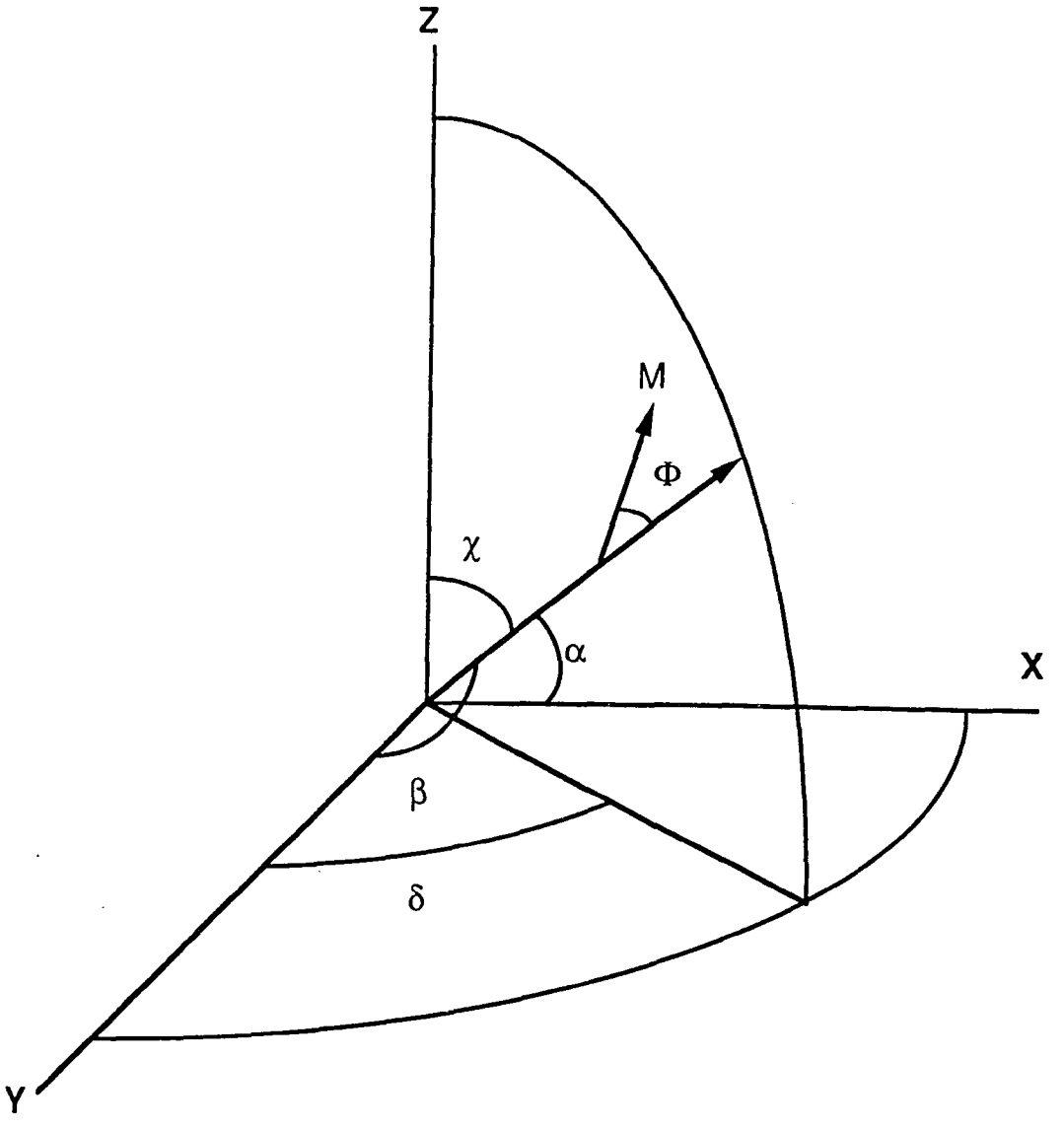


**Fig. 2.2. Laboratory axis system with a representative chain (long arrow), a representative dipole moment (M), and the definition of angles.**

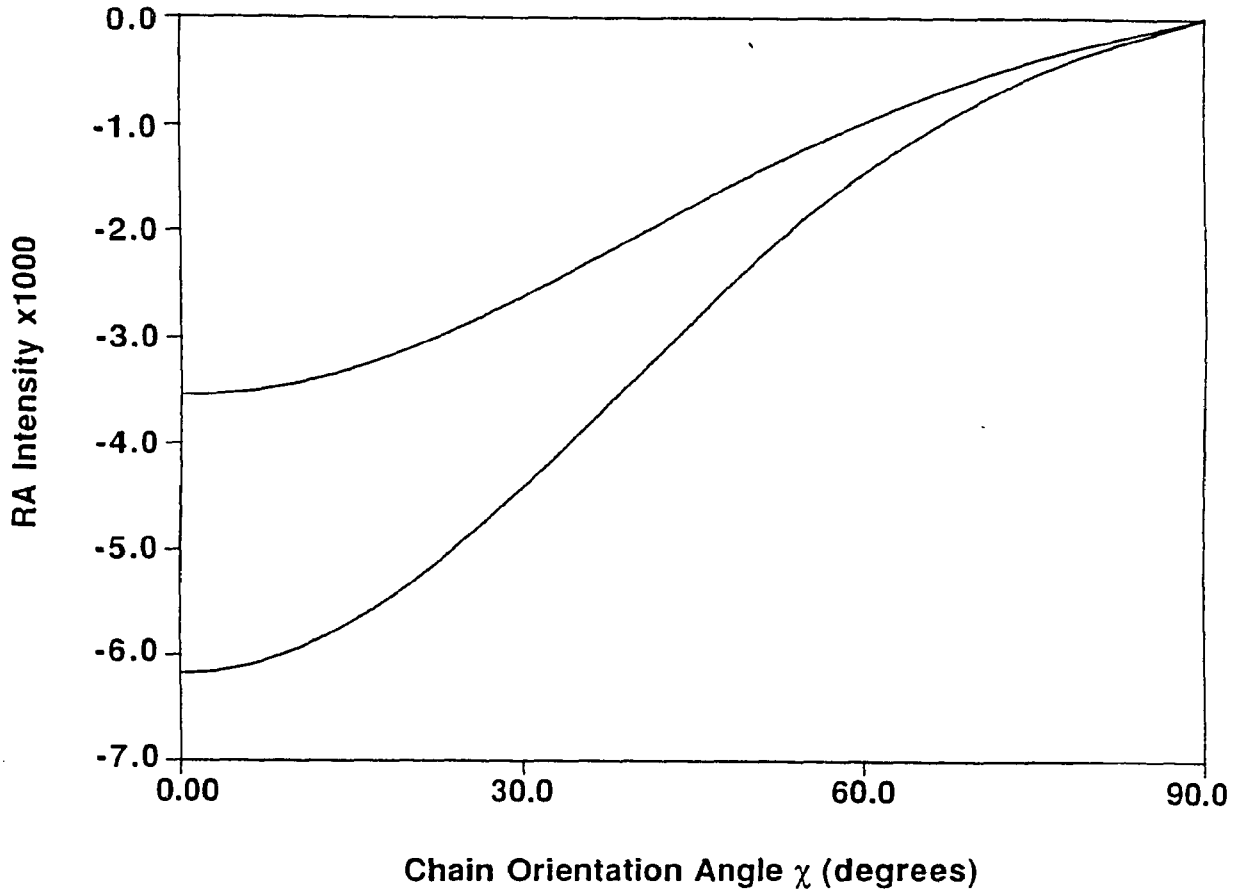


**Fig. 2.3. Calculated value of the reflection-absorption intensity vs. chain orientation angle for *s*- (the top line) and *p*-polarized (the bottom one) incident light at constant surface concentration.**

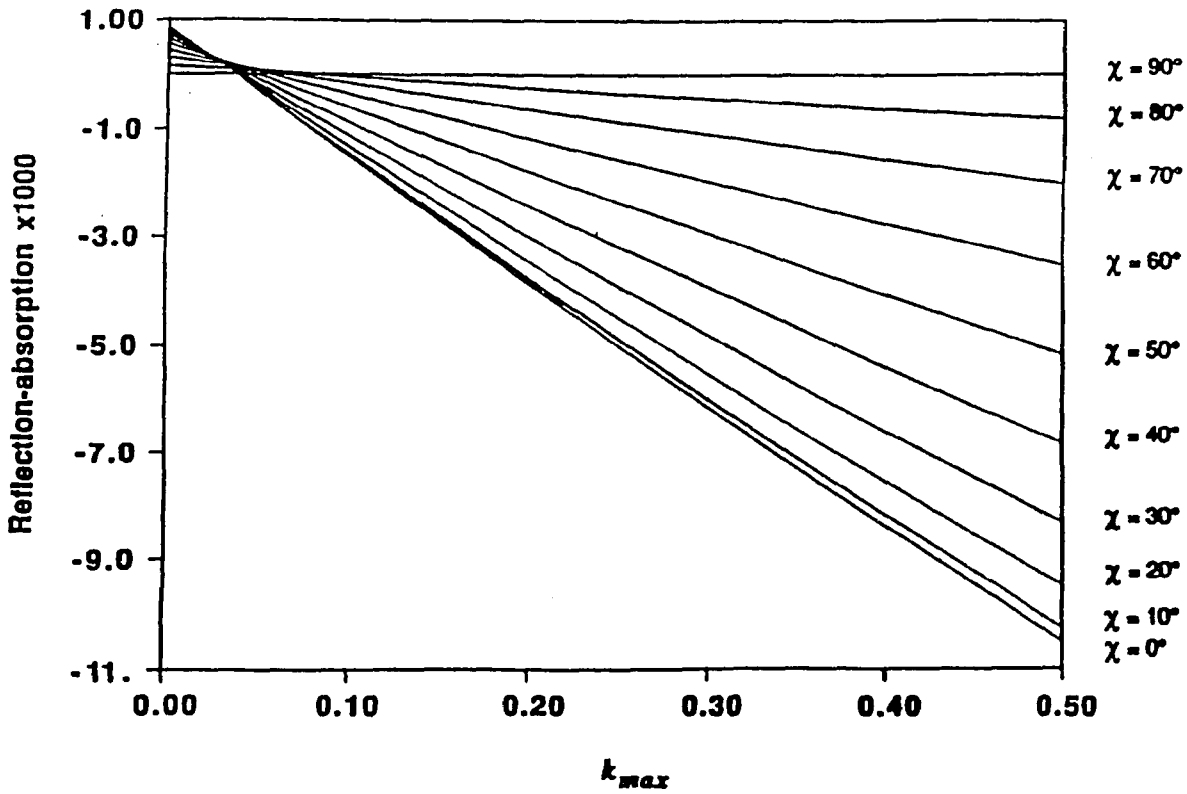


**Fig. 2.4. Relationship between RA intensity and $K_{max}$ at different chain otientation angles. (30°, *p*-pol.).**

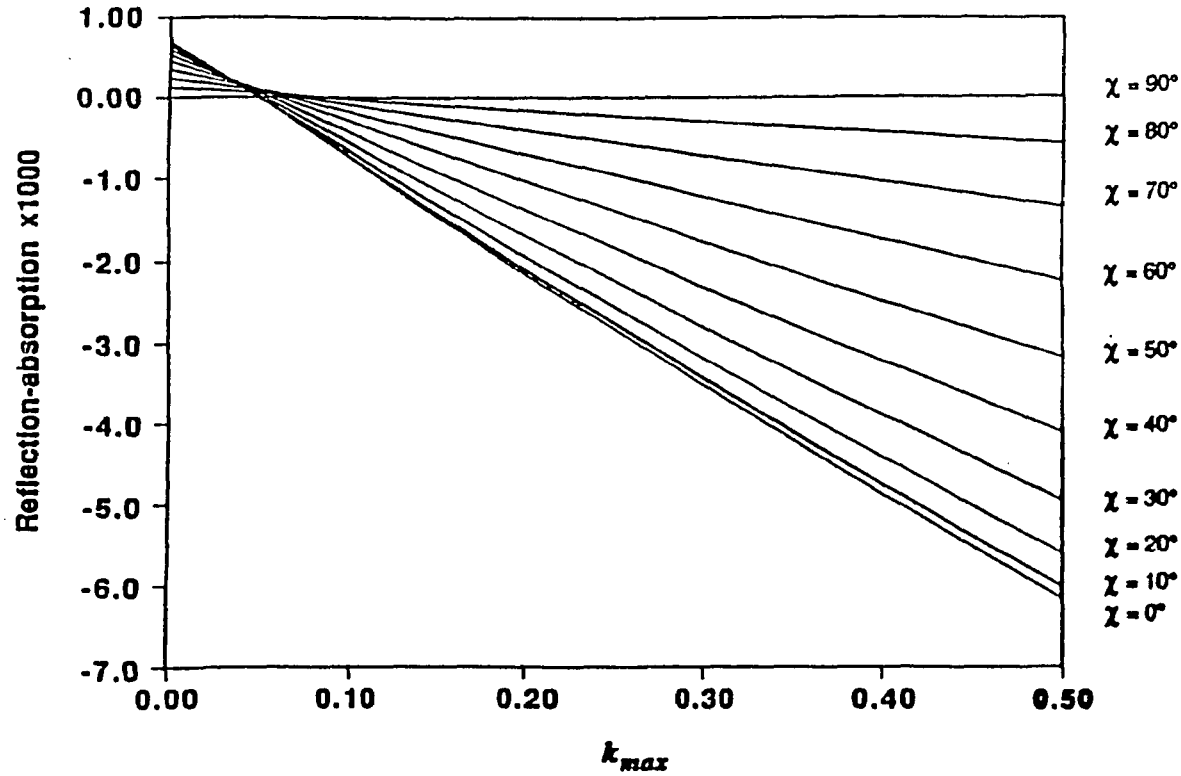


**Fig. 2.5. Relationship between RA intensity and $K_{max}$ at different chain otientation angles. (30°, *s*-pol.)**

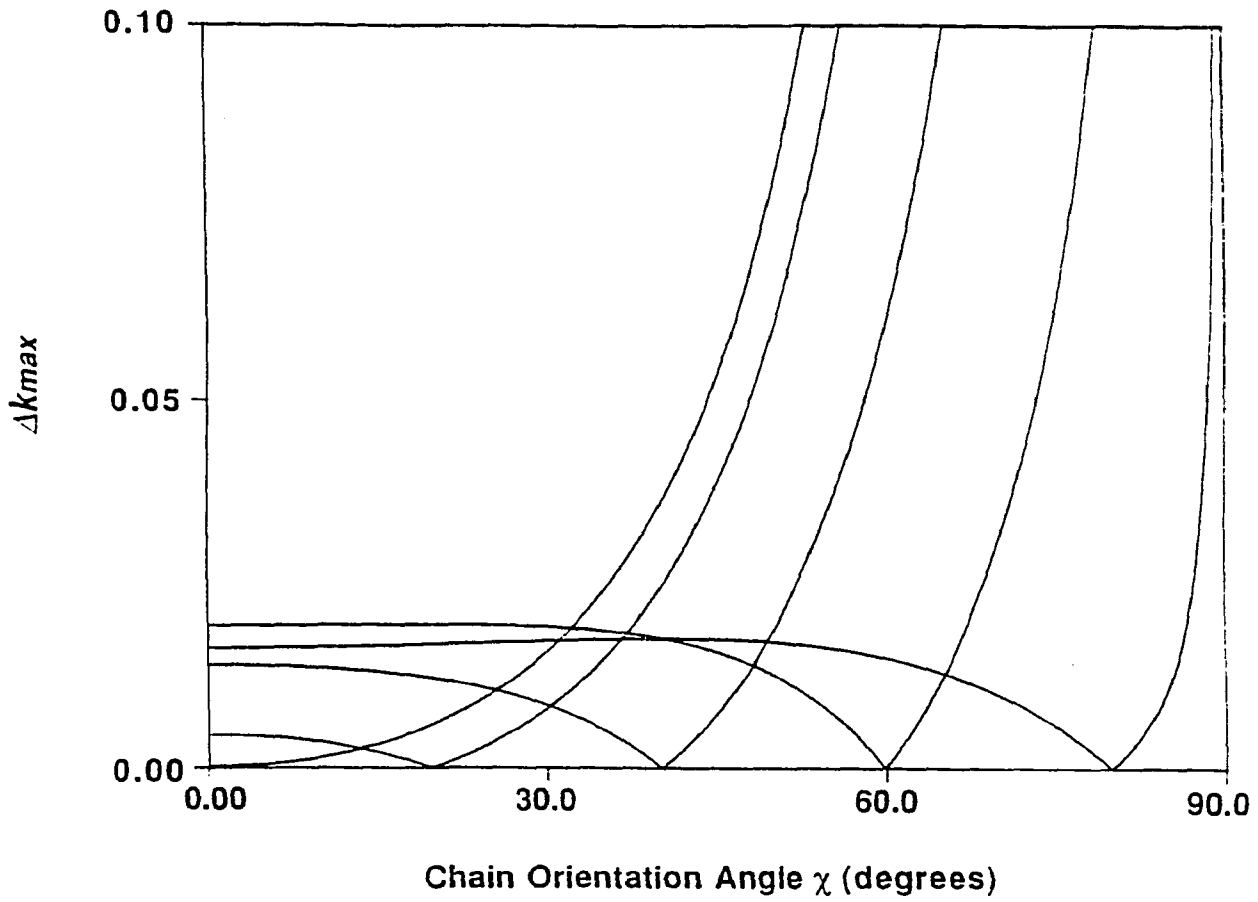


**Fig. 2.6. Results of refinement procedure which minimize $\Delta k_{max}$ to calculate the chain orientation angle $\chi$ and $k_{max}$.**
**From left to right: $\chi$ = 0°, 20°, 40°, 60°, and 80°, respectively.**

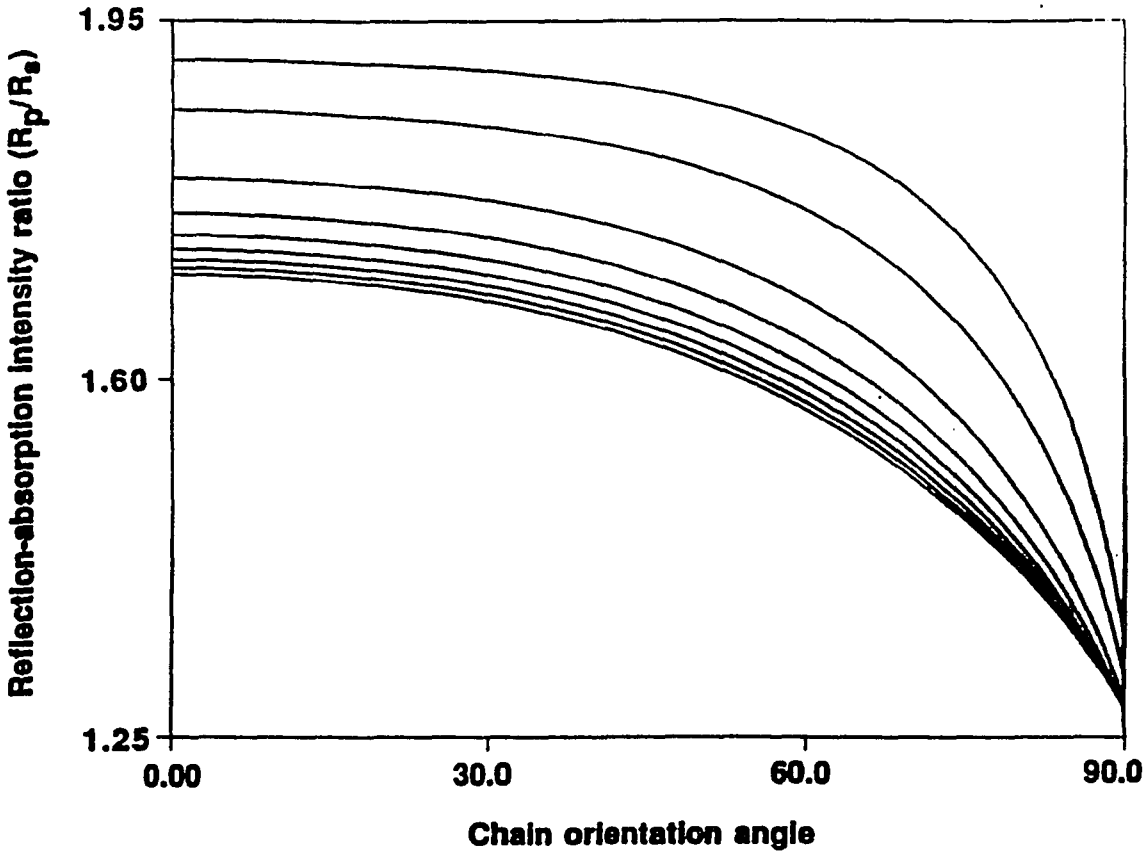


**Fig. 2.7. Polarized reflection-adsorption intensity ratios (RAp/RAs) vs. chain orientation angle at various values of $k_{max}$. From top to bottom : $k_{max}$ = 0.13, 0.15, 0.20, 0.35, 0.30, 0.35, 0.40, 0.45, and 0.50, respectively.**

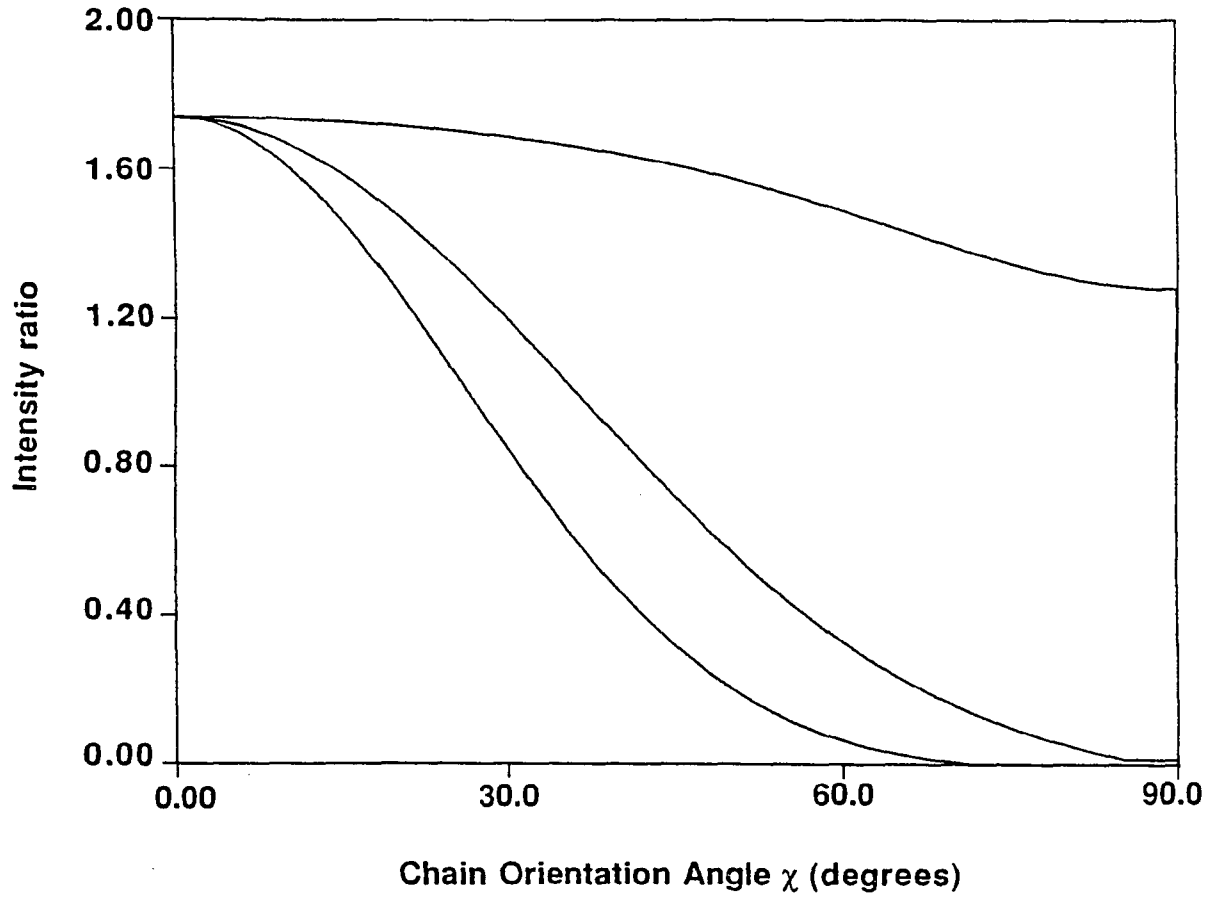


**Fig. 2.8. $RAp^i/RAs$ ratios vs. chain orientation angle at different i values, $k_{max}$ constant (=0.30). From top to bottom: RAp/RAs, $RAp^2/RAs$, and $RAp^3/RAs$, respectively.**

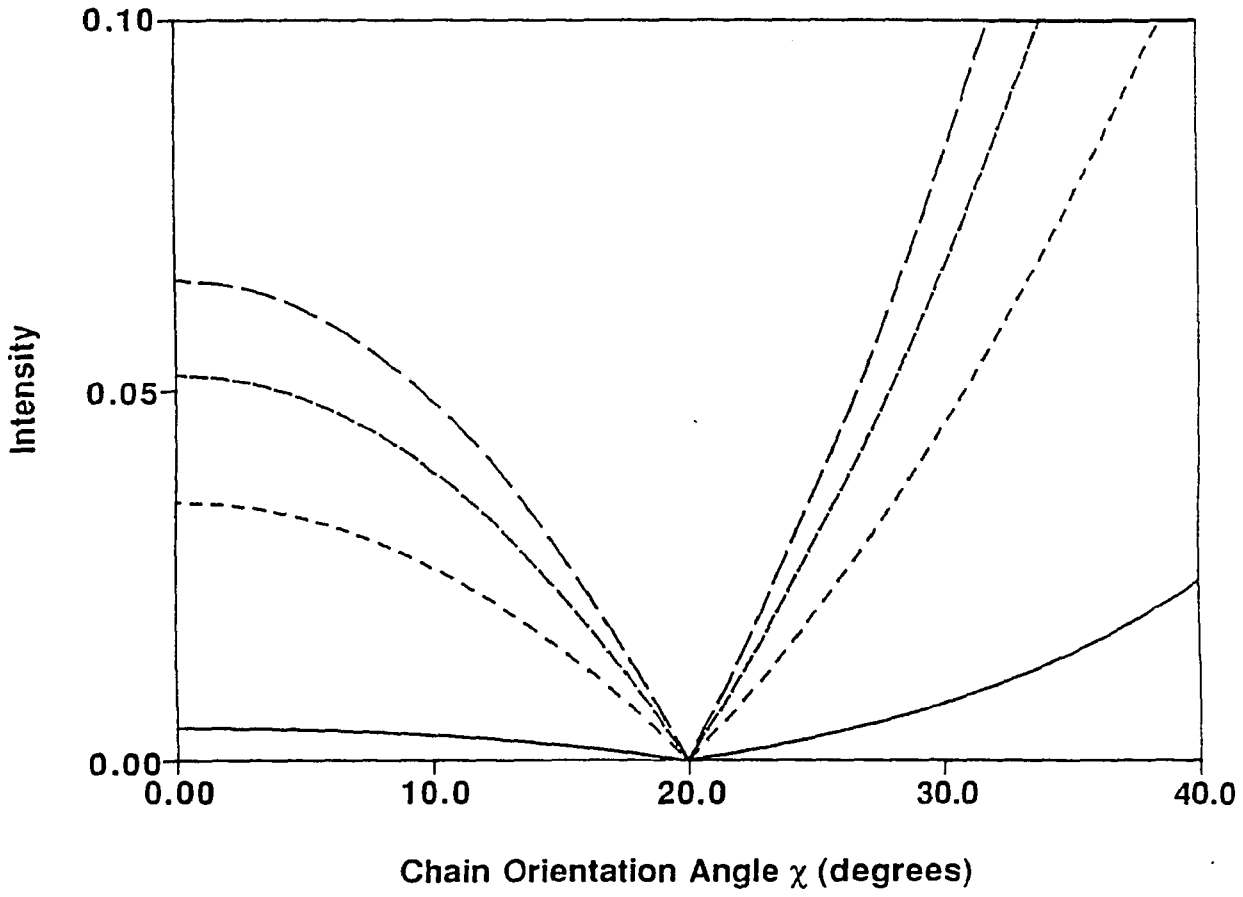


**Fig. 2.9. Determination of orientation angle using various methods of minimization. From top to bottom:**
**$\Delta(RAp^3/RAs)$, $\Delta(RAp^2/RAs)$, $\Delta(RAp/RAs)$, respectively.**

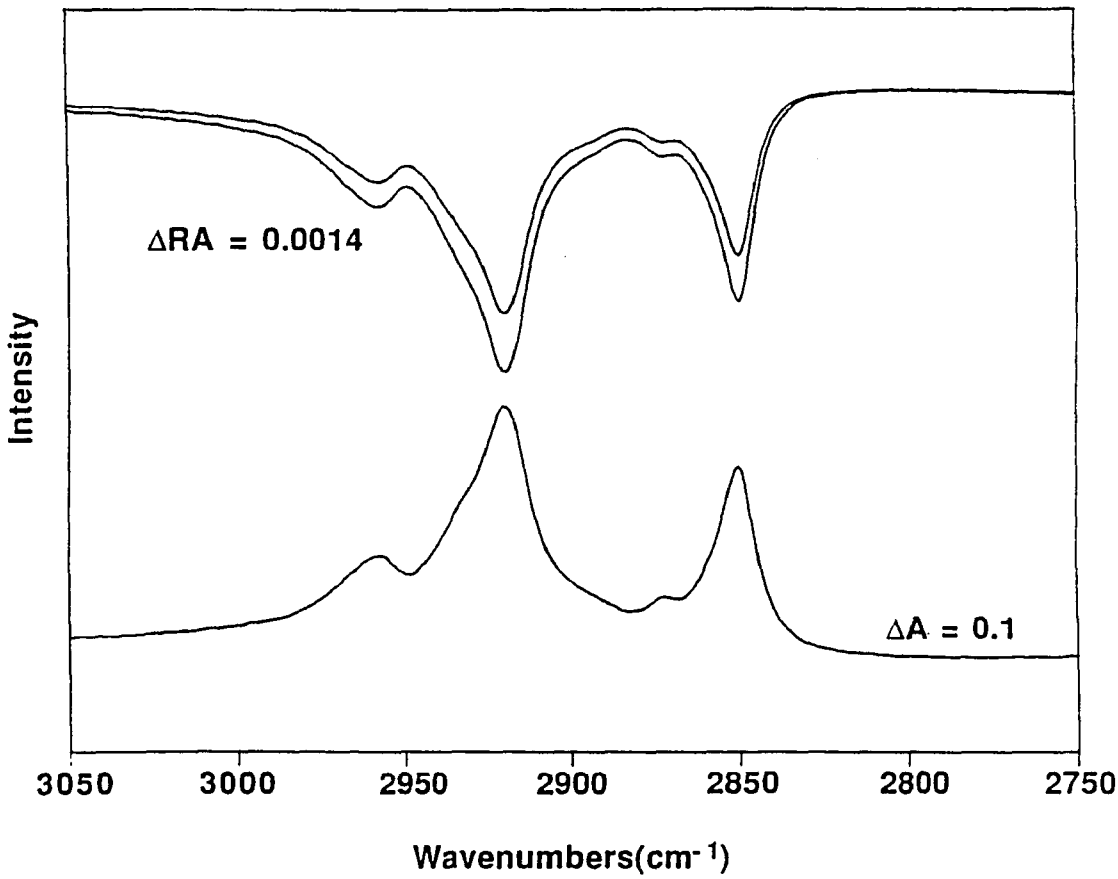


**Fig. 2.10. Comparison of an experimental transmission spectrum with simulated RA spectra for the adsorbed monolayer of $C_{12}H_{25}SO_3Na$ ($C_{12}SNa$) at the air/water interface. From top to bottom: simulated RAs, RAp, and experimental spectrum of $C_{12}SNa$ dispersed in a KBr matrix.**

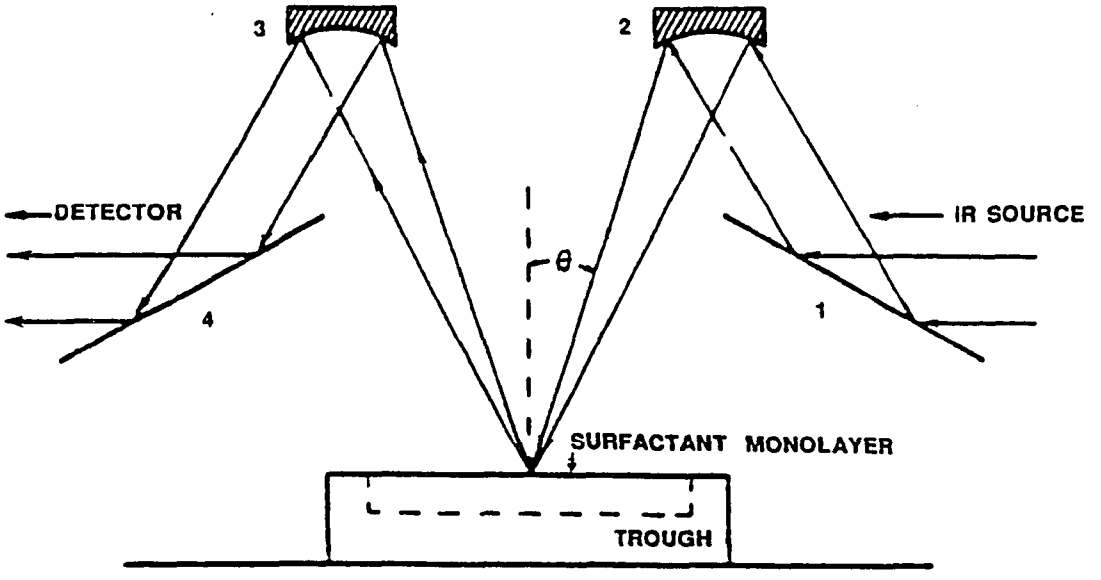


**Fig. 3.1. Schematic diagram of the optical arrangement used for obtaining RA spectra of adsorbed monolayers at the air/water interface.**

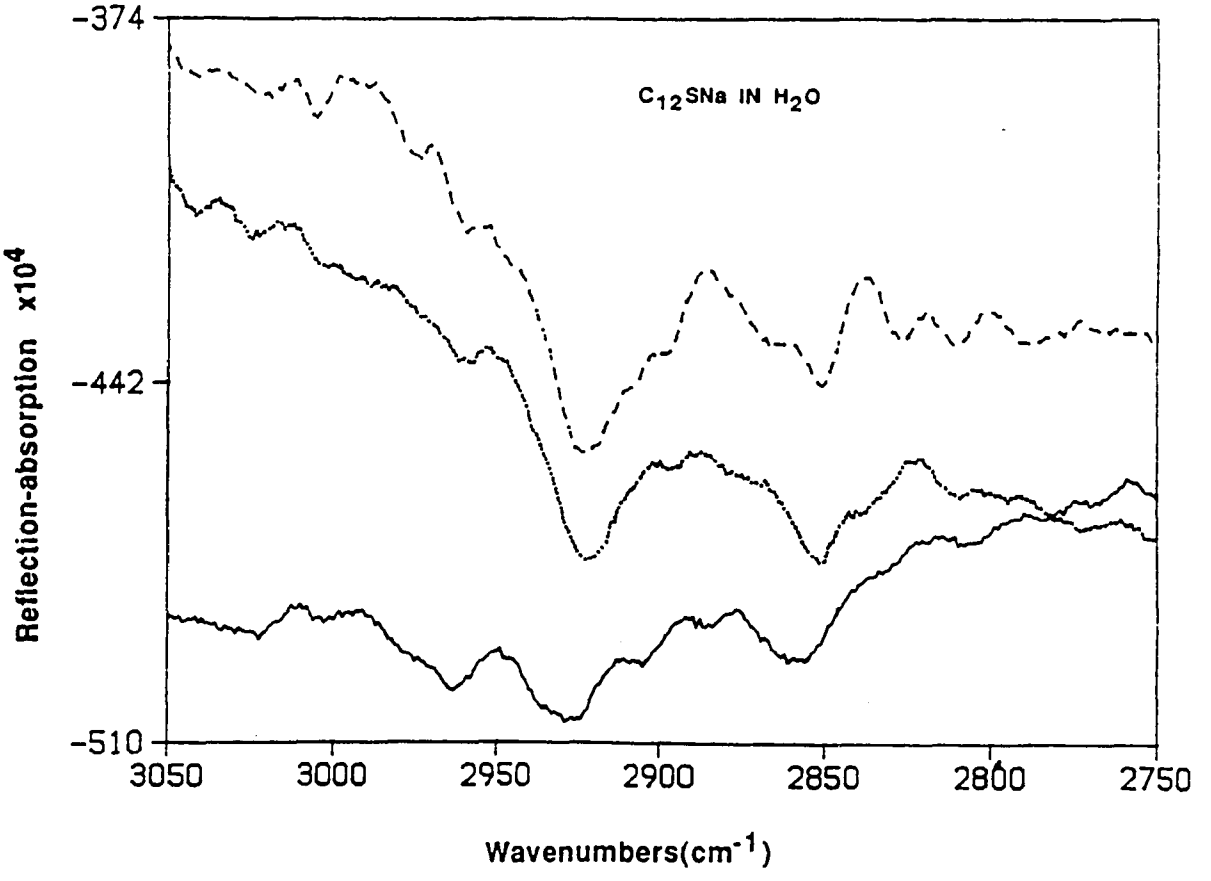


**Fig. 3.2. RA spectra (*p*-polarization) of the adsorbed $C_{12}SNa$ monolayers at the air/water interface with different angles of incident light, but the same bulk concentration.**
**From top to bottom: $\theta$ = 44°, 30°, and 16°, respectively.**

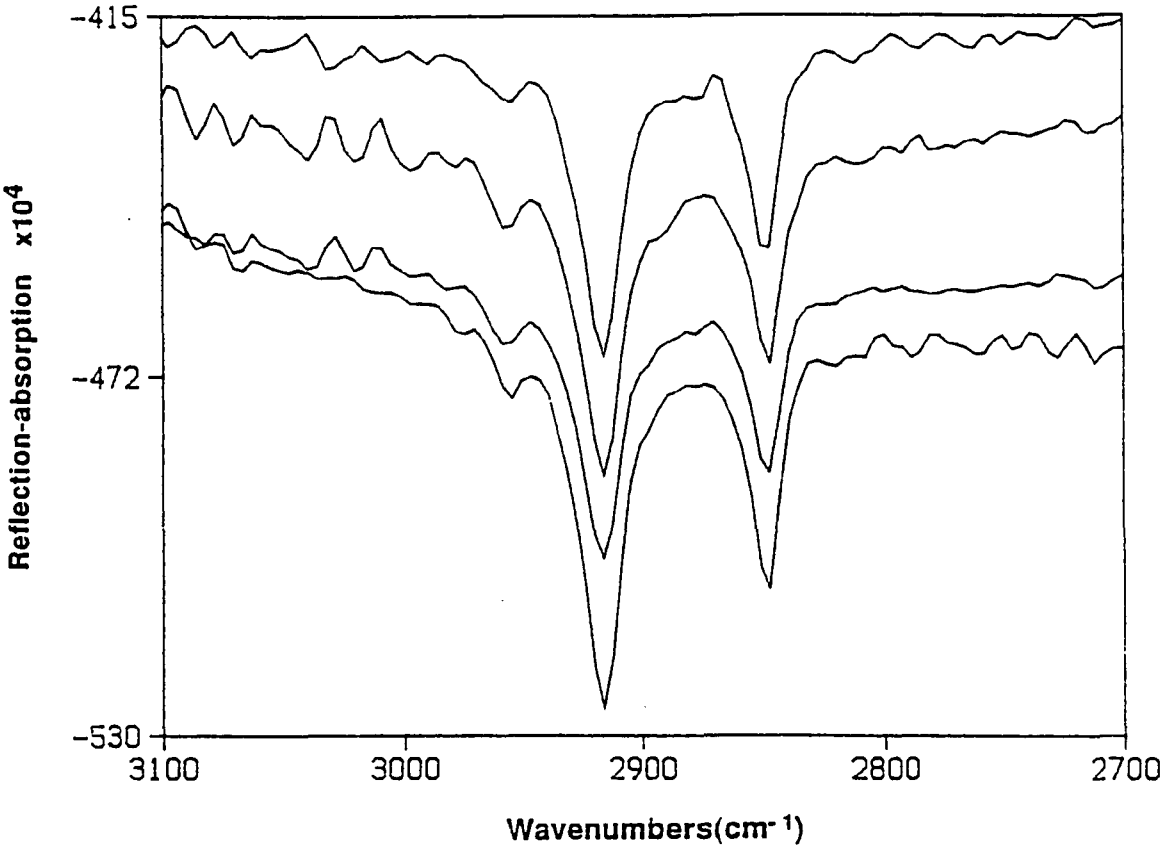


**Fig. 3.3. RA spectra of the adsorbed $C_{12}$SNa monolayers at the air/water interface with different polarizations and angles of incident light, but the same bulk concentration.**
**From top to bottom: *s*-polarized, θ=10°; *p*-polarized, θ=10°; *s*-polarized, θ=30°, and *p*-polarized, θ=30°, respectively.**

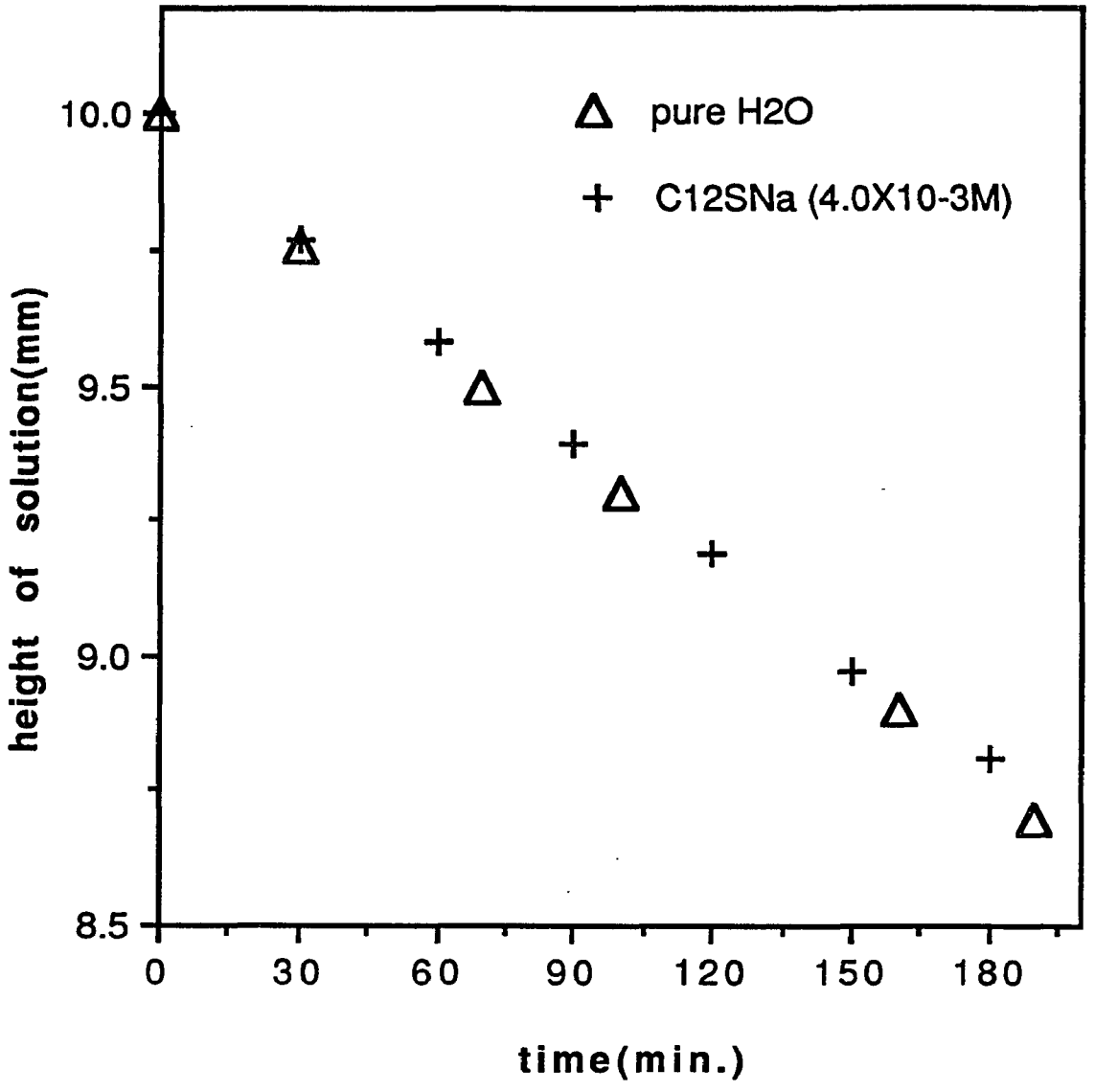


**Fig. 3.4. The height of the solution vs. the experimental period time.**

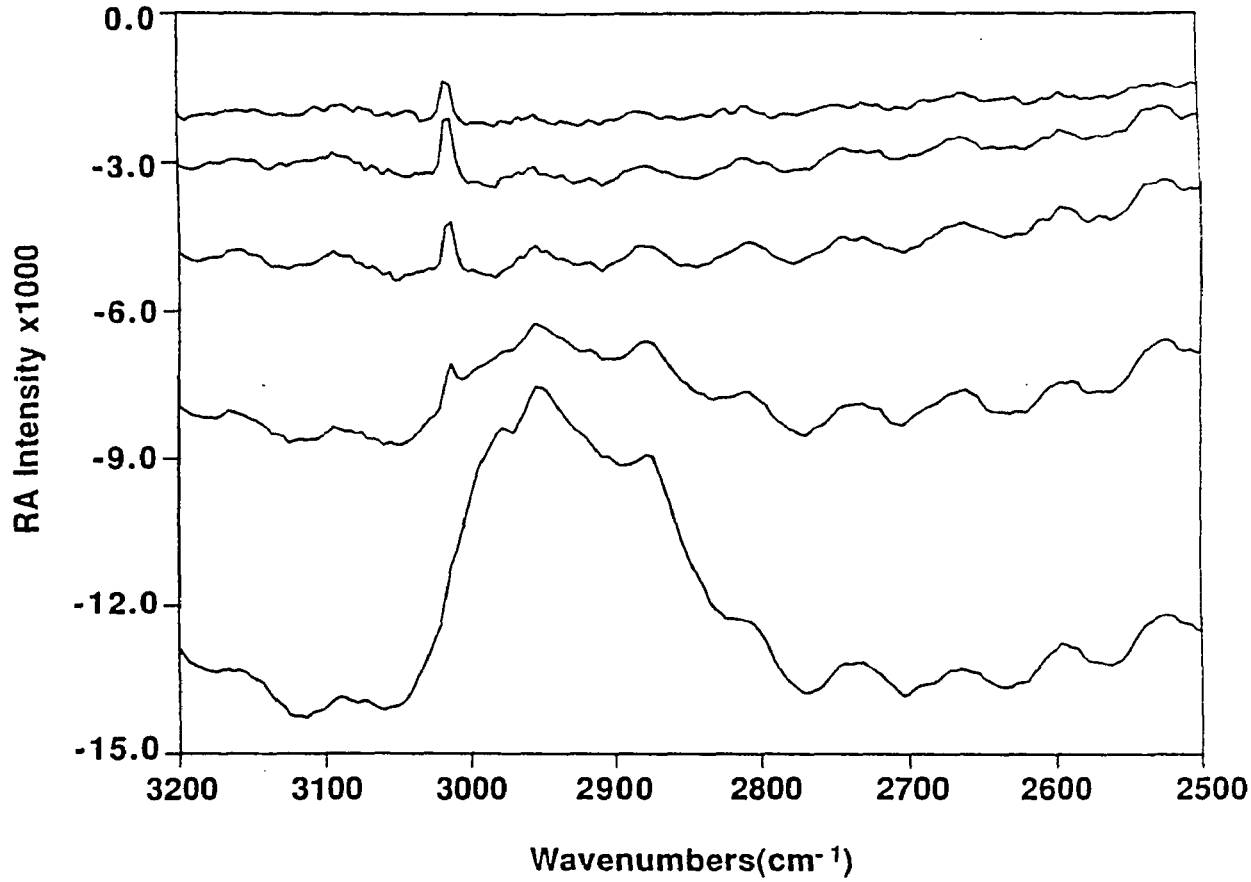


**Fig. 3.5. Ratios of a single beam *s*-polarized reflectance spectrum of a water surface against the same water surface $-\log(R_t/R_0)$, but at different height of the water. The height of the water changes with the time of evaporation (t).**
**From top to bottom: t=1, 2, 3, 4, and 5 hours, respectively.**

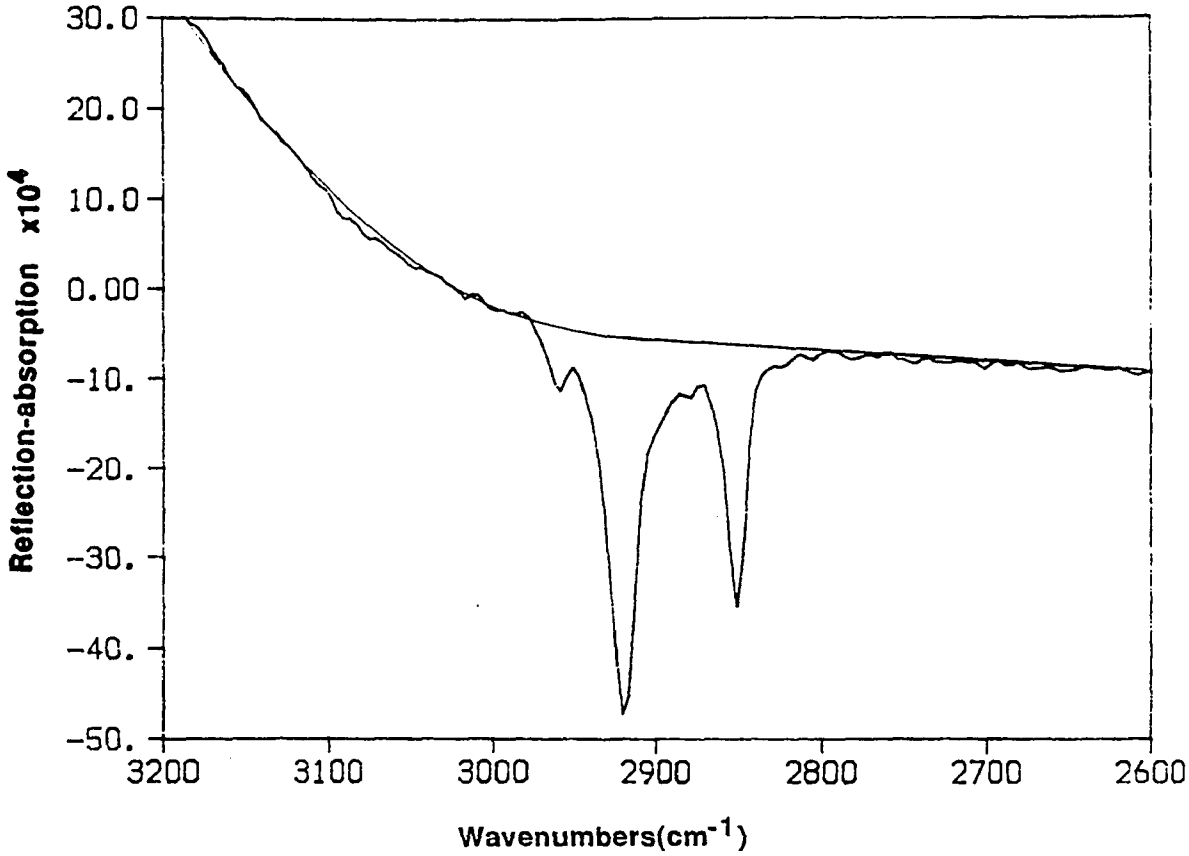


**Fig. 3.6. A representative RA spectrum of the adsorbed $C_{12}SNa$ monolayer at the air/water interface, at 30° incident angle and *s*-polarization; surfactant concentration, C= $4.80X10^{-3}M$.**

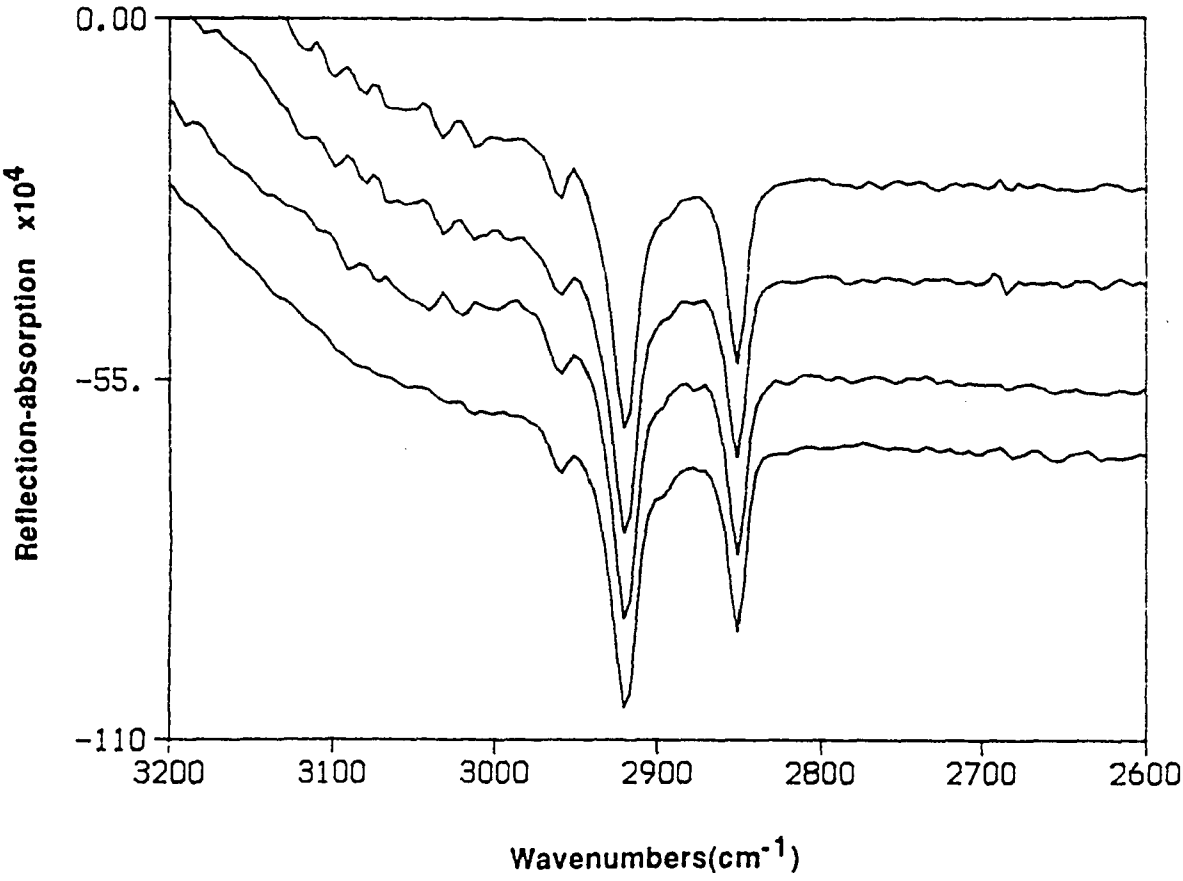


**Fig. 3.7. Reproducibility of RA spectra of the adsorbed monolayers of $C_{12}SNa$ at the air/water interface, C= $4.0X10^{-3}M$, *s*-polarization**

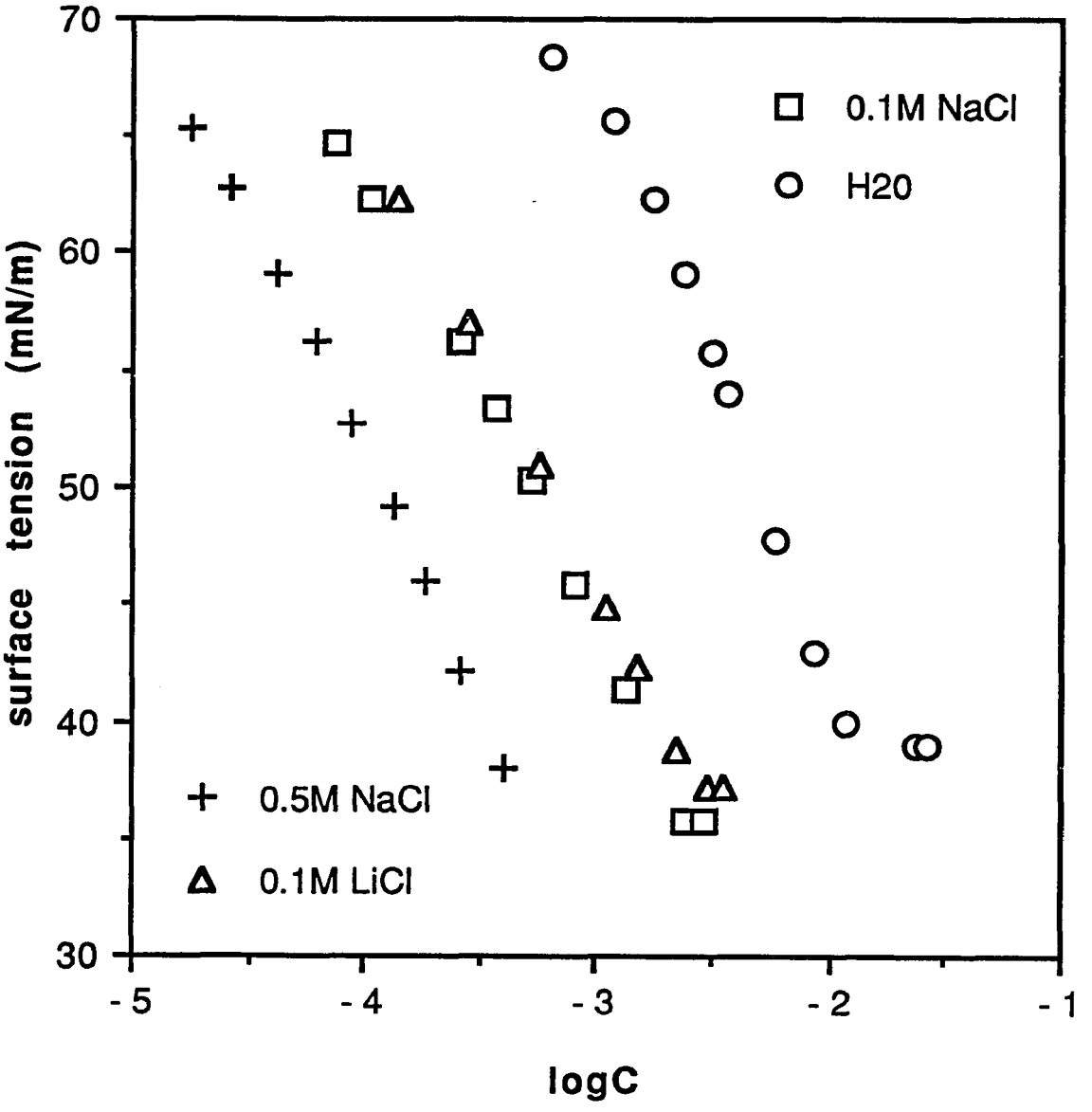


**Fig. 4.1.1. Surface tension vs. log of the molar concentration of $C_{12}SO_3Na$ in aqueous solutions of $H_20$, 0.1M NaCl, 0.5M NaCl, and 0.1M LiCl at 25.0°C.**

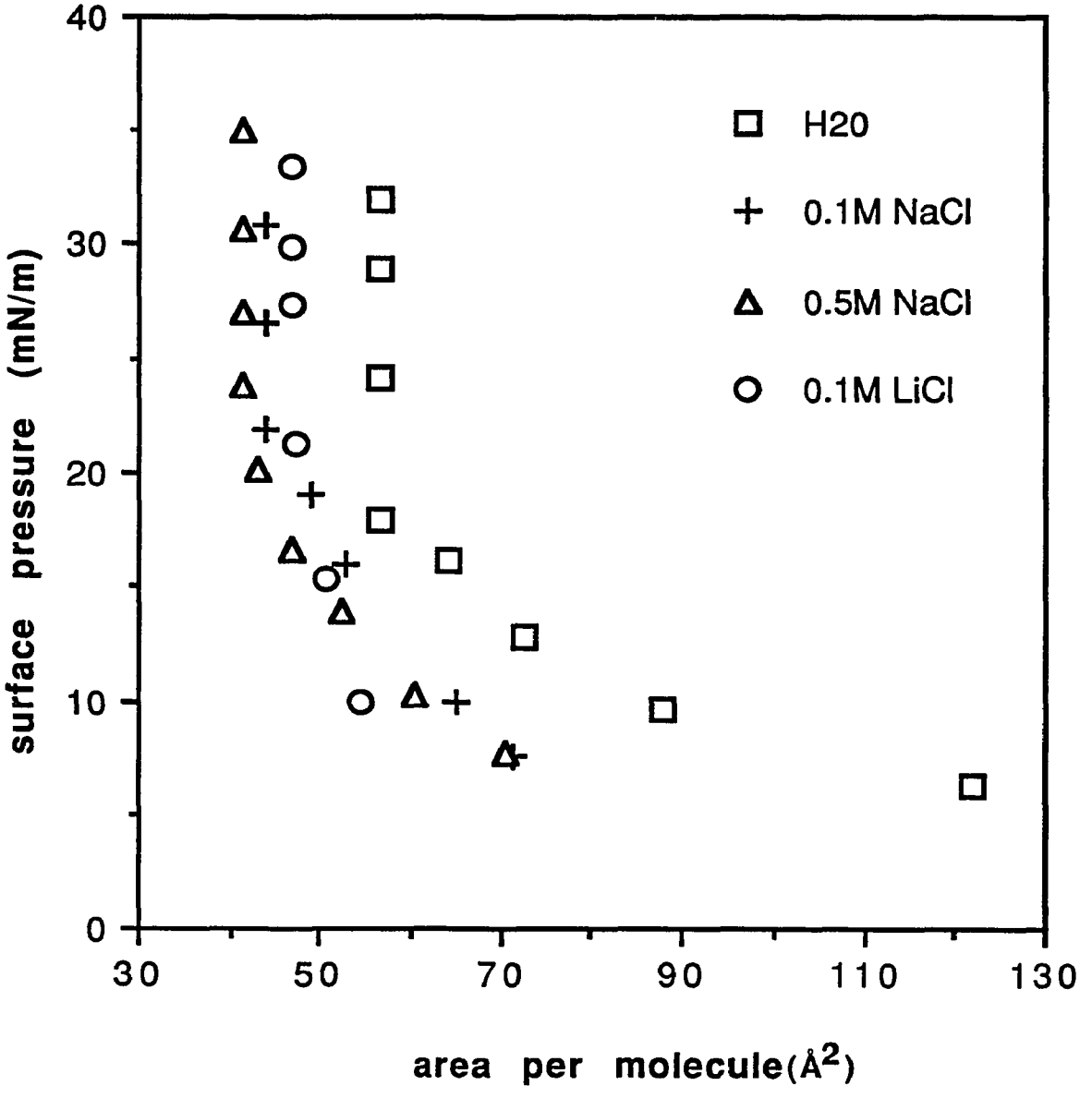


**Fig. 4.1.2. Surface pressure vs. area per molecule (A) of $C_{12}SO_3Na$ in aqueous solutions of $H_20$, 0.1M NaCl, 0.5M NaCl, and 0.1M LiCl at 25.0°C.**

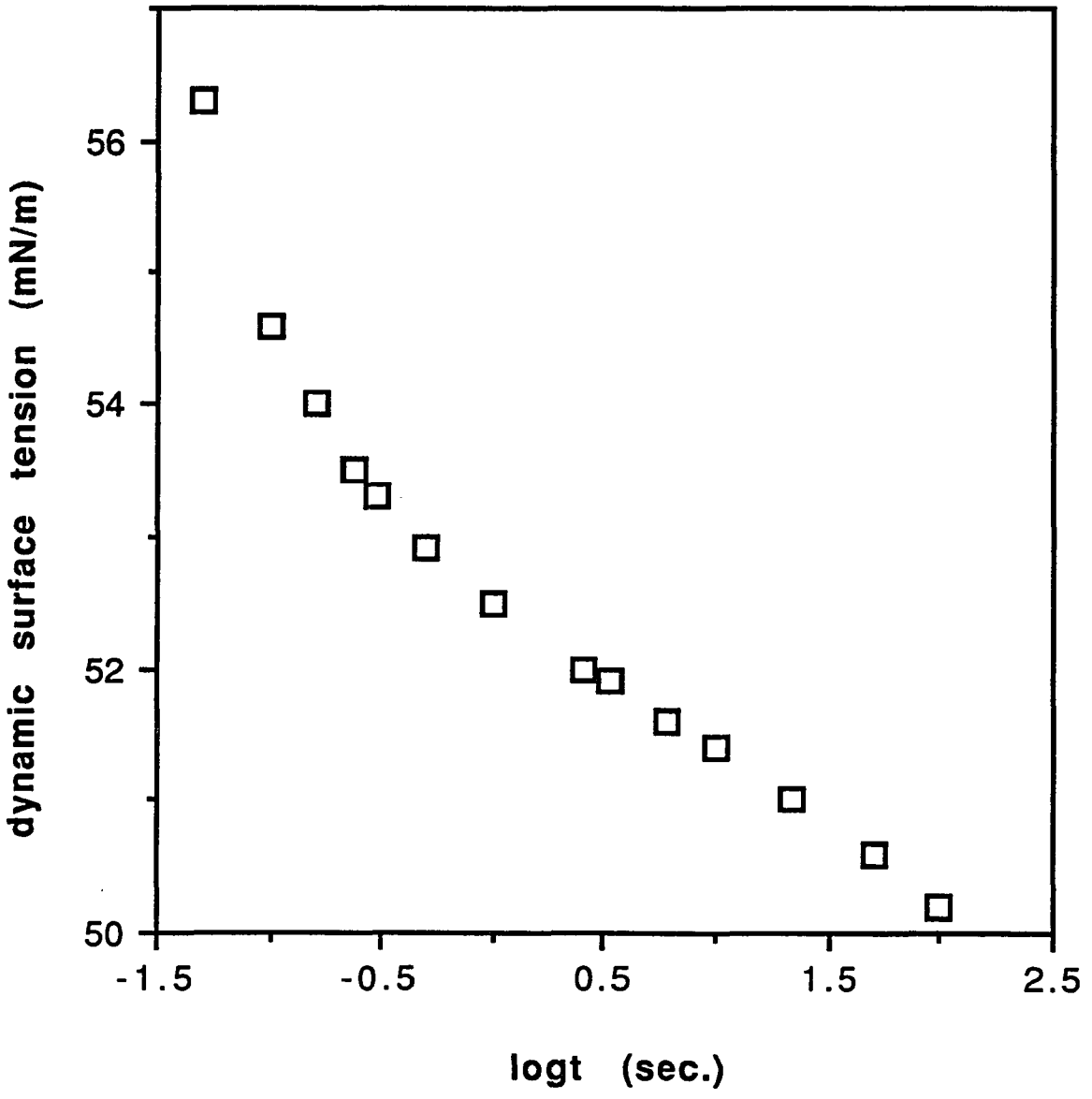


**Fig. 4.1.3. Dynamic surface tension vs. log of the surface age time of $5.0X10^{-3}$ M $C_{12}SO_3Na$ in pure $H_20$ at 25.0°C (maximum bubble pressure method).**

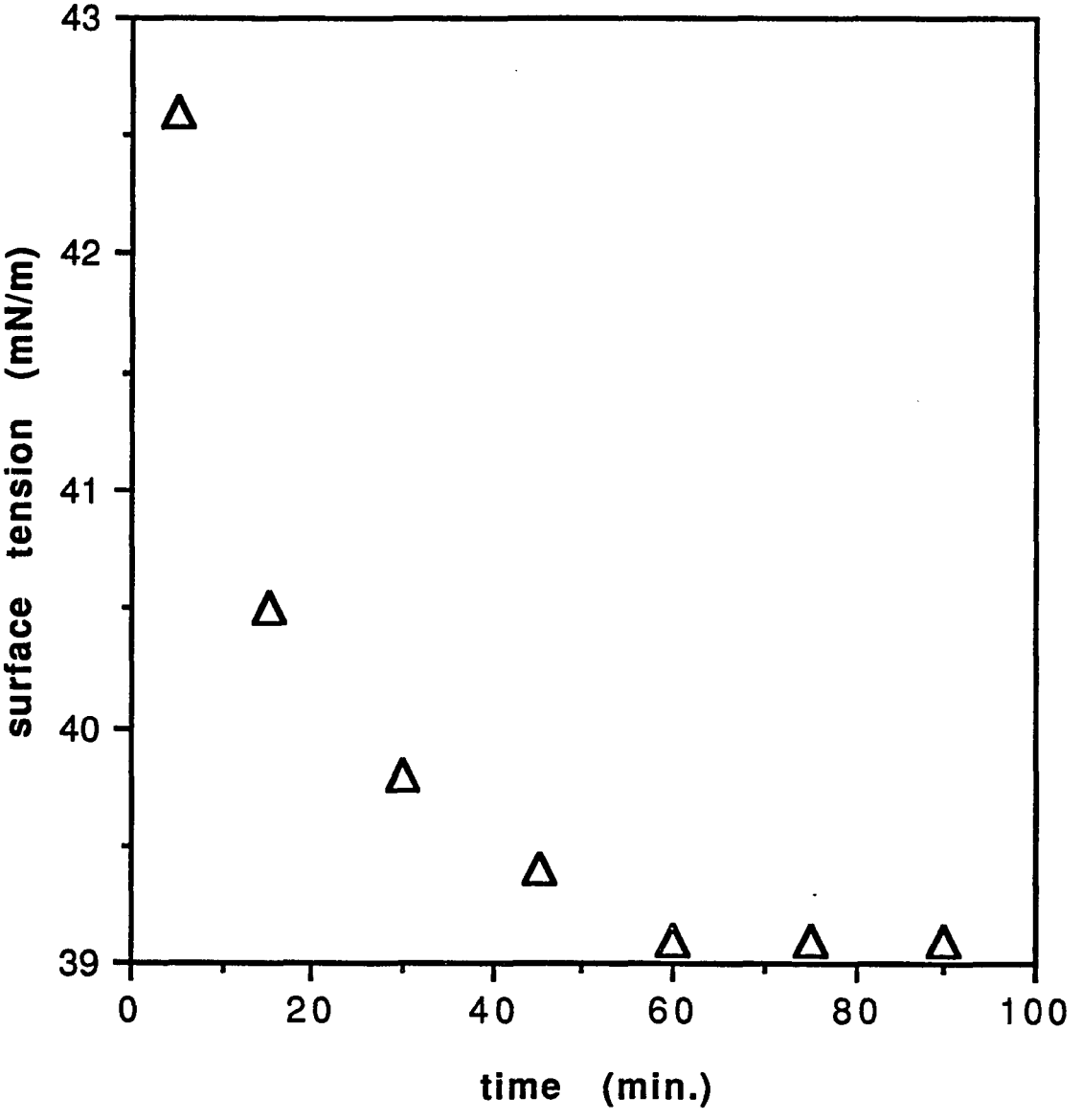


**Fig. 4.1.4. Surface tension vs. measuring time for $1.2X10^{-2}$ M $C_{12}SO_3Na$ in pure $H_2O$ at 25.0°C (Wilhelmy method).**

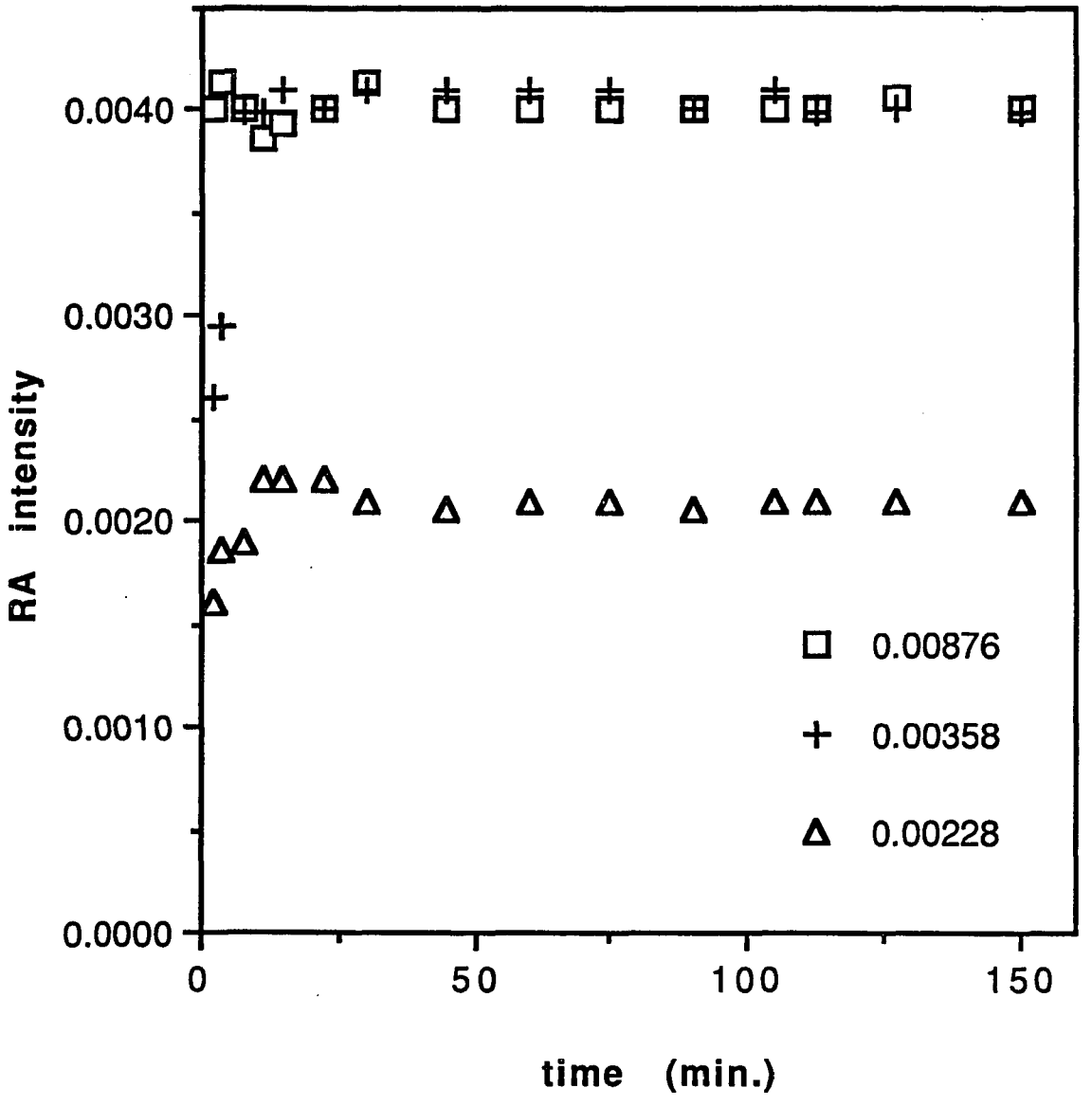


**Fig. 4.1.5. RA intensity vs. measuring time of $C_{12}SO_3Na$ monolayers at the air/water interface from different bulk concentrations.**

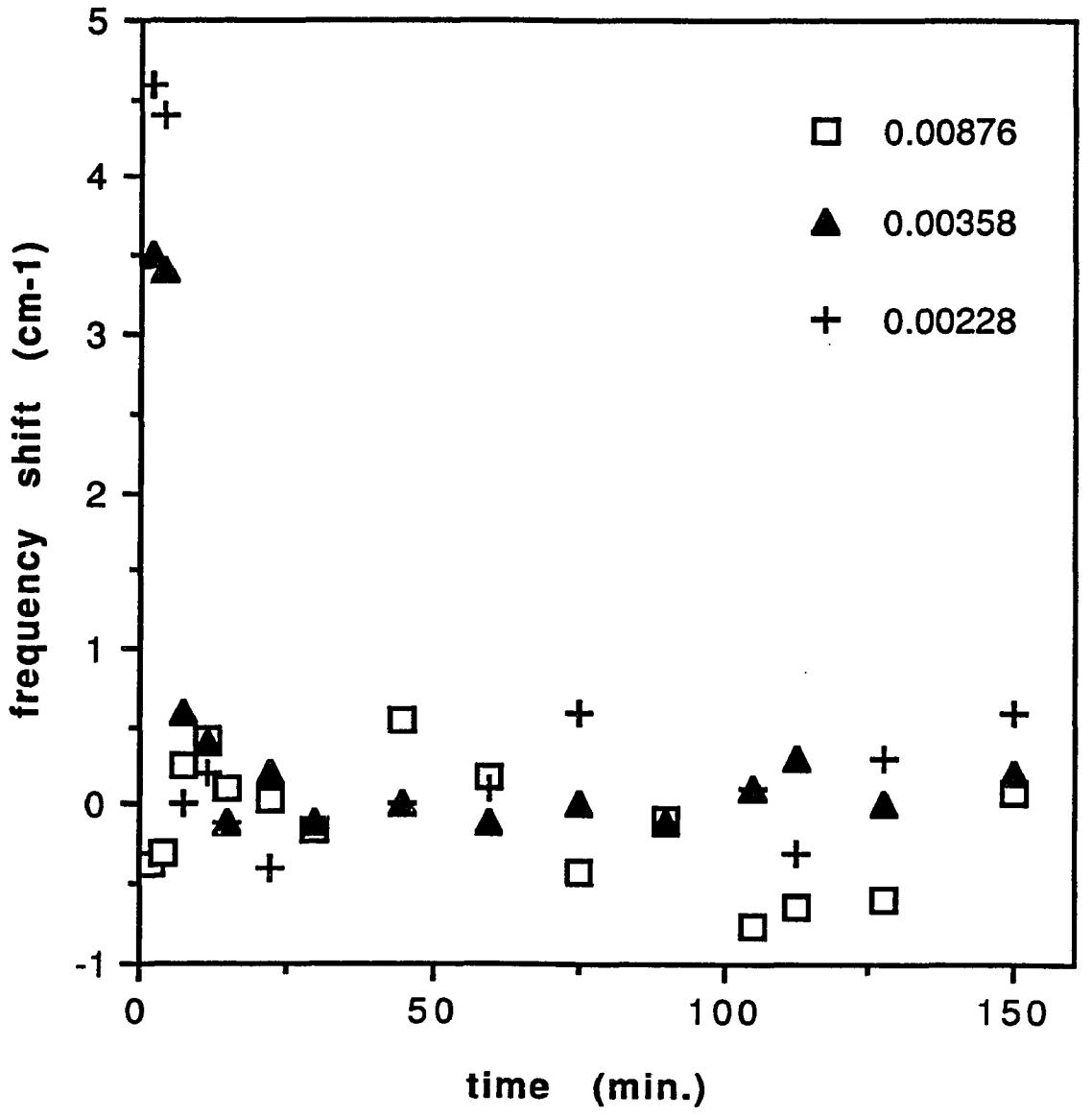


**Fig. 4.1.6. Peak frequency shift of the asymmetric C-H stretching vibration vs. measuring time of $C_{12}SO_3Na$ monolayers at the air/water interface with different bulk concentrations.**

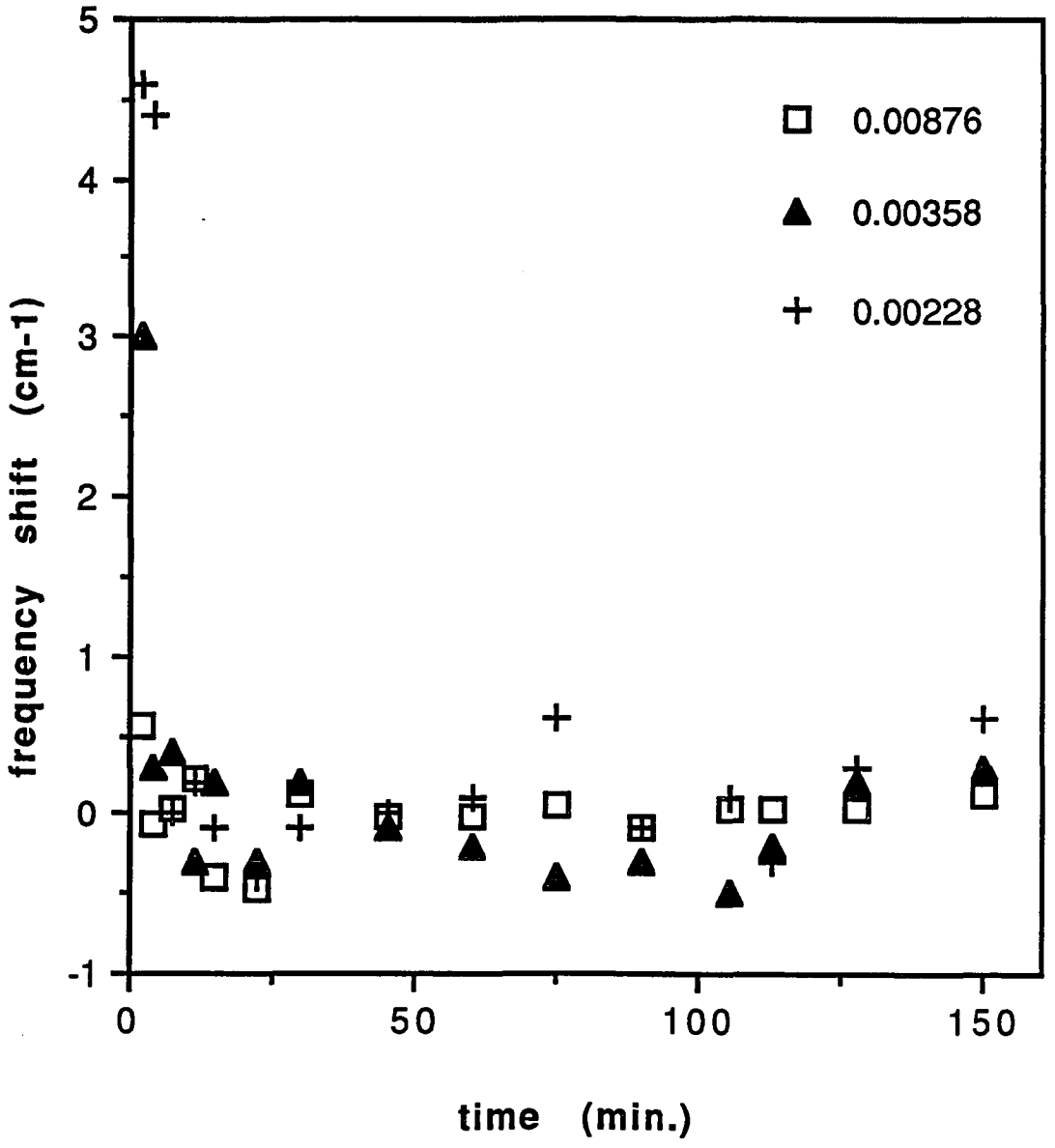


**Fig. 4.1.7. Peak frequency shift of the symmetric C-H stretching vibration vs. measuring time of $C_{12}SO_3Na$ monolayers at the air/water interface from different bulk concentrations.**

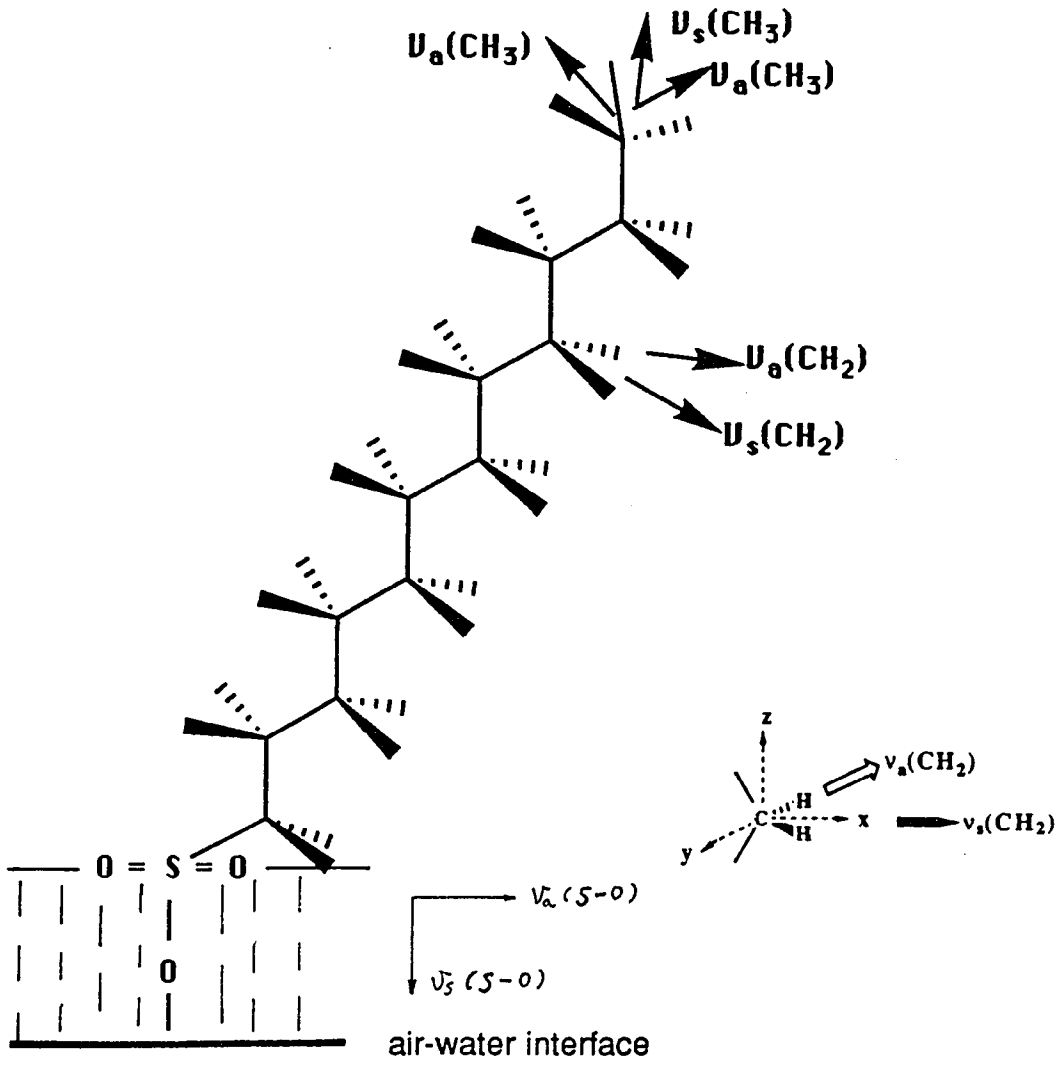


**Fig. 4.1.8. A diagram of a $C_{12}SO_3Na$ molecule at the air/water interface.**

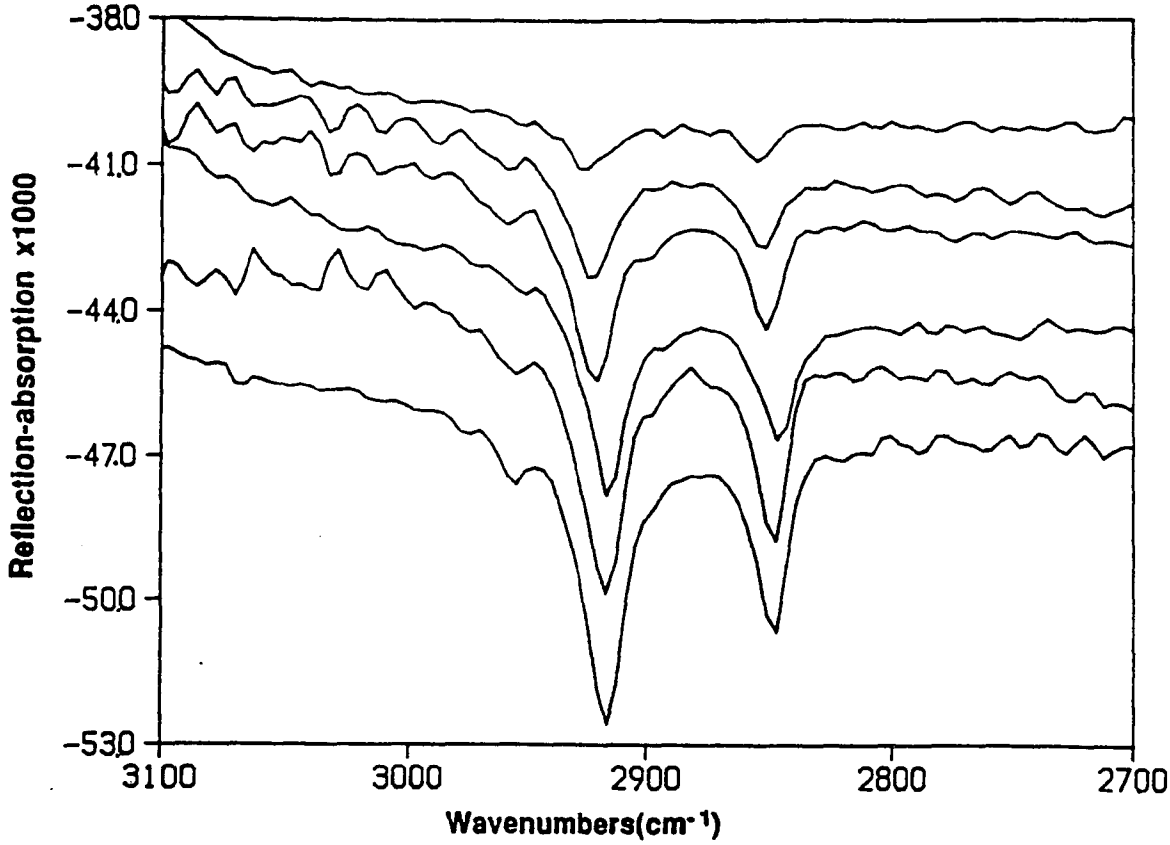


**Fig. 4.1.9(a-1). RA spectra of the adsorbed monolayers of $C_{12}SO_3Na$ at the aqueous solution/air interface in pure water at 30° incidence angle and *p*-polarization.**
**From top to bottom:**

| surfactant concentration | logC |
|---|---|
| $6.24X10^{-4}$ M | -3.20 |
| $9.90X10^{-4}$ M | -3.00 |
| $1.98X10^{-3}$ M | -2.70 |
| $3.12X10^{-3}$ M | -2.51 |
| $4.00X10^{-3}$ M | -2.40 |
| $4.80X10^{-3}$ M | -2.32 |

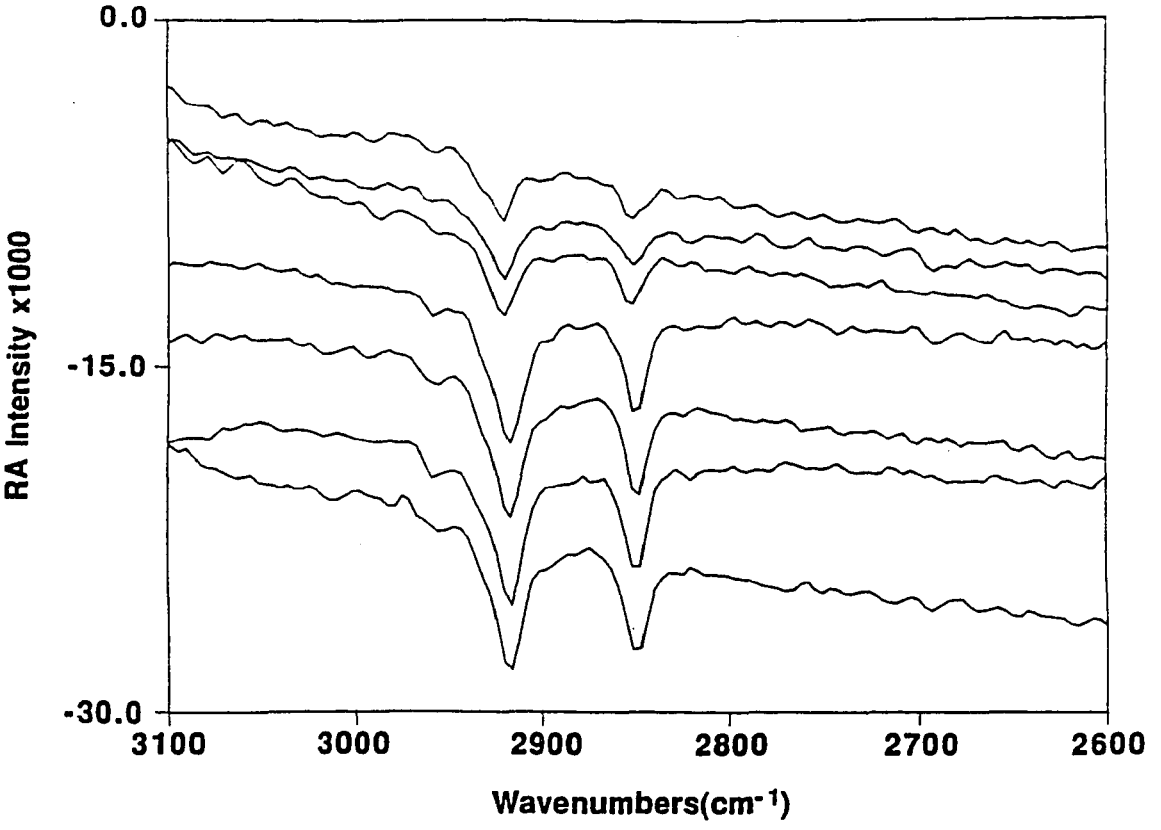


**Fig. 4.1.9(a-2). RA spectra of the adsorbed monolayers of $C_{12}SO_3Na$ at the aqueous solution/air interface in pure water at 30° incidence angle and *p*-polarization.**
**From top to bottom:**

| surfactant concentration | logC |
|---|---|
| $1.87X10^{-3}$ M | -2.73 |
| $2.28X10^{-3}$ M | -2.64 |
| $2.86X10^{-3}$ M | -2.54 |
| $3.58X10^{-3}$ M | -2.45 |
| $4.48X10^{-3}$ M | -2.35 |
| $5.60X10^{-3}$ M | -2.25 |
| $8.76X10^{-3}$ M | -2.06 |

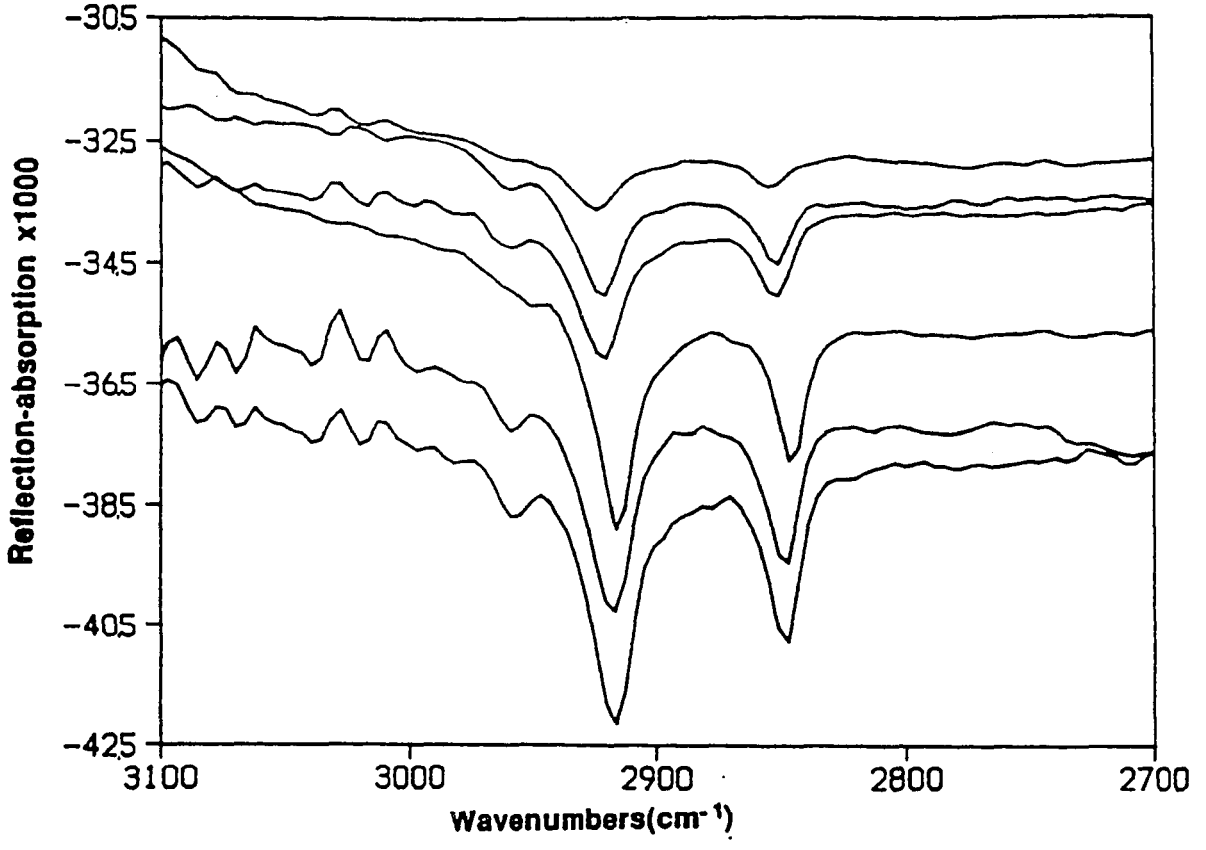


**Fig. 4.1.9(b-1). RA spectra of the adsorbed monolayers of $C_{12}SO_3Na$ at the aqueous solution/air interface in pure water at 30° incidence angle and *s*-polarization.**
**From top to bottom:**

| surfactant concentration | logC |
|---|---|
| $6.24X10^{-4}$ M | -3.20 |
| $9.90X10^{-4}$ M | -3.00 |
| $1.98X10^{-3}$ M | -2.70 |
| $3.12X10^{-3}$ M | -2.51 |
| $4.00X10^{-3}$ M | -2.40 |
| $4.80X10^{-3}$ M | -2.32 |

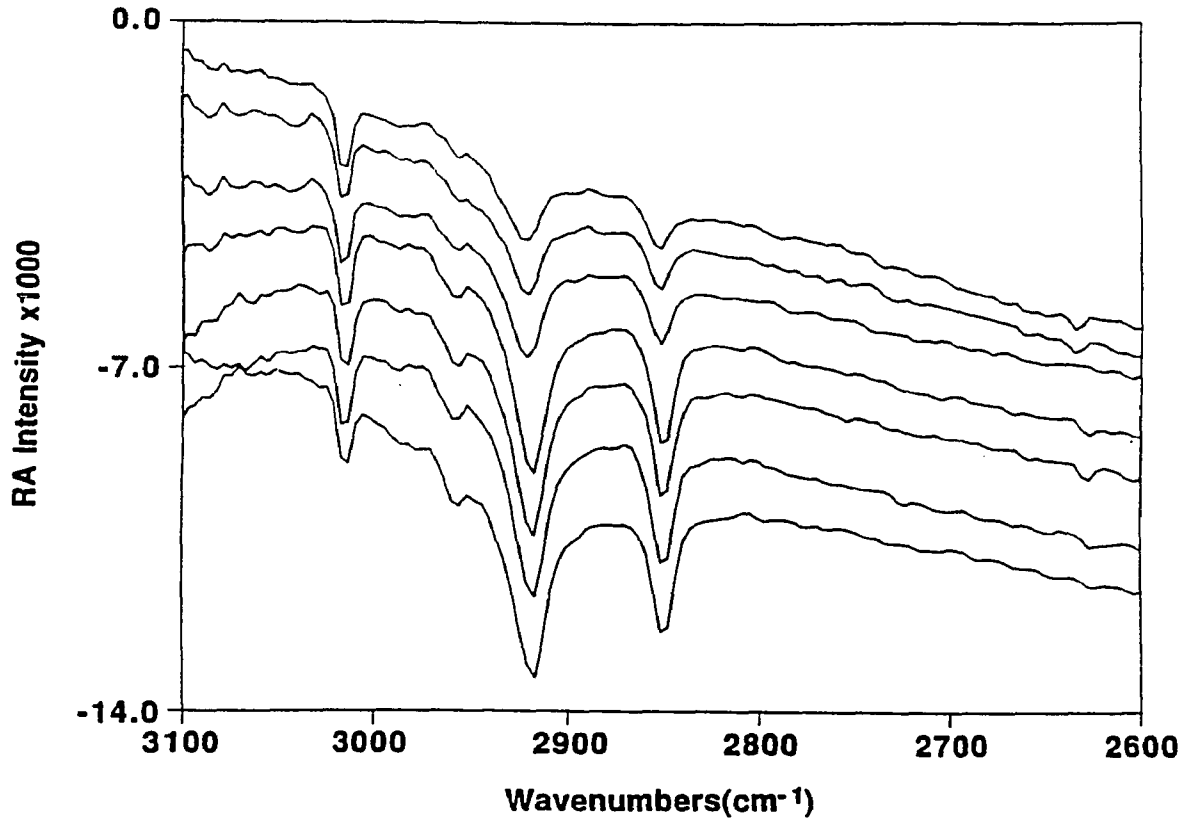


**Fig. 4.1.9(b-2). RA spectra of the adsorbed monolayers of $C_{12}SO_3Na$ at the aqueous solution/air interface in pure water at 30° incidence angle and *s*-polarization.**
**From top to bottom:**

| surfactant concentration | logC |
|---|---|
| $1.87X10^{-3}$ M | -2.73 |
| $2.28X10^{-3}$ M | -2.64 |
| $2.86X10^{-3}$ M | -2.54 |
| $3.58X10^{-3}$ M | -2.45 |
| $4.48X10^{-3}$ M | -2.35 |
| $5.60X10^{-3}$ M | -2.25 |
| $8.76X10^{-3}$ M | -2.06 |

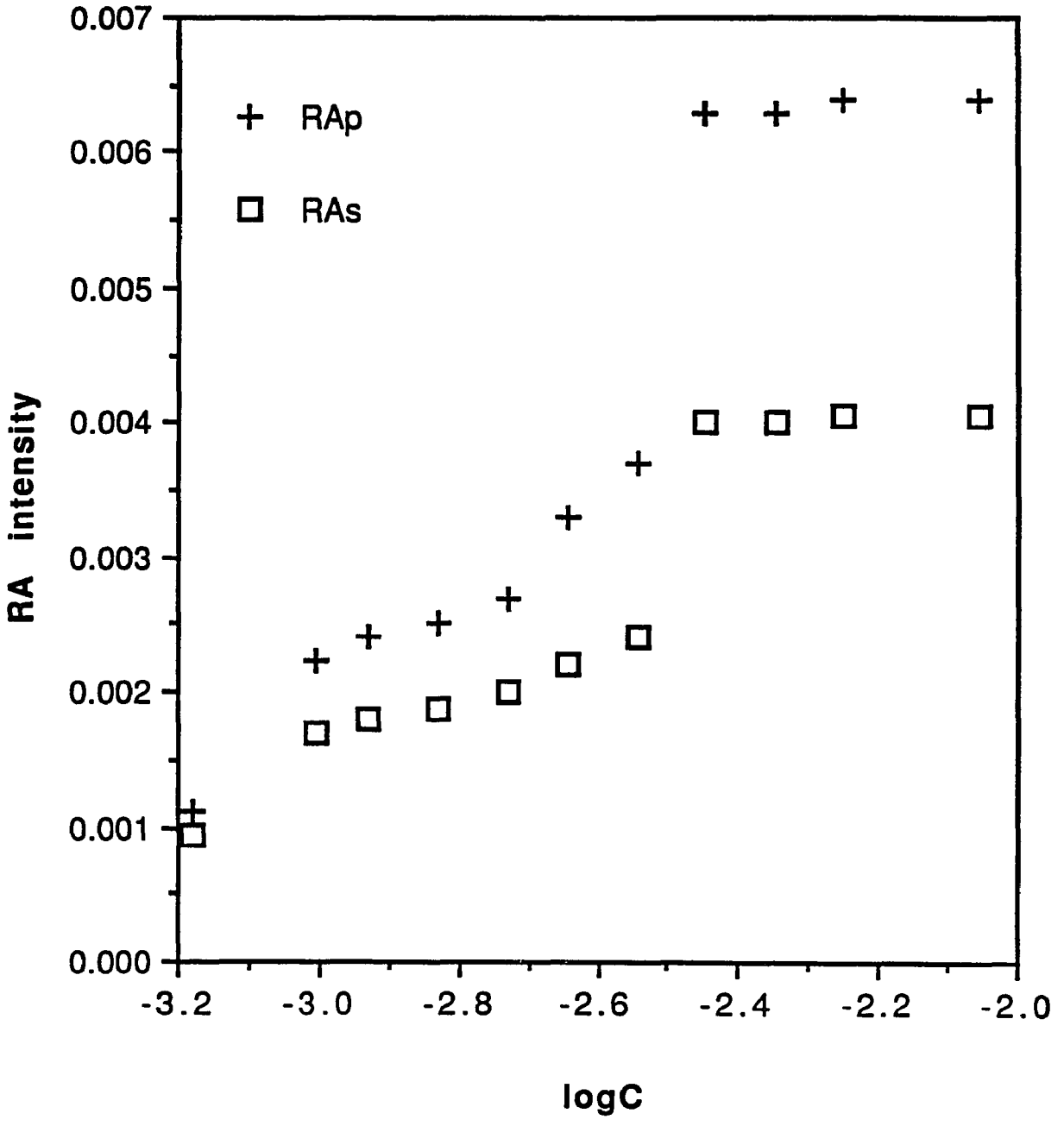


**Fig. 4.1.10. Changes in RA intensity of the adsorbed monolayers of $C_{12}SO_3Na$ at the air/water interface with different bulk concentrations in water solution.**

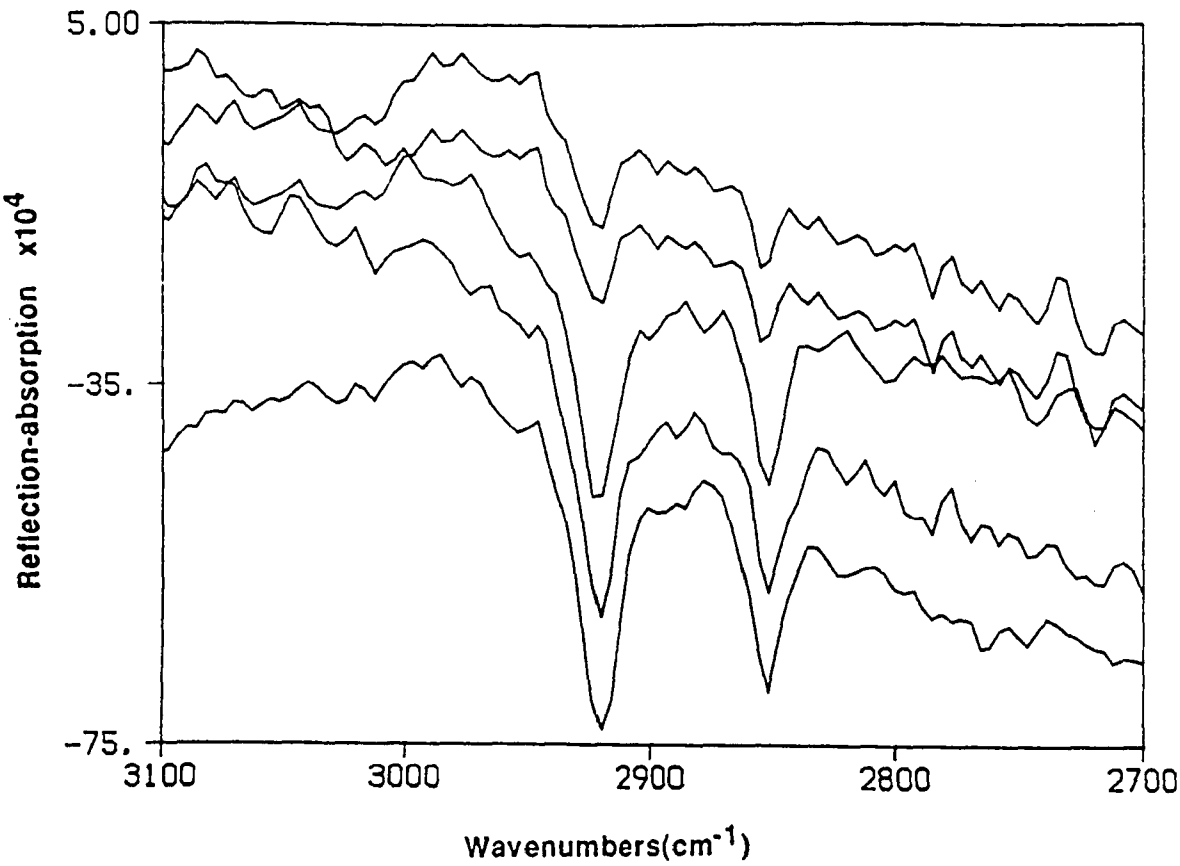


**Fig. 4.1.11(a). RA spectra of the adsorbed monolayers of $C_{12}SO_3Na$ at the aqueous solution/air interface in 0.1M NaCl at 30° incidence angle and *p*-polarization.**
**From top to bottom:**

| surfactant concentration | logC |
|---|---|
| $1.00X10^{-4}$ M | -4.00 |
| $2.00X10^{-4}$ M | -3.70 |
| $4.00X10^{-4}$ M | -3.40 |
| $8.00X10^{-4}$ M | -3.10 |
| $1.00X10^{-3}$ M | -3.00 |

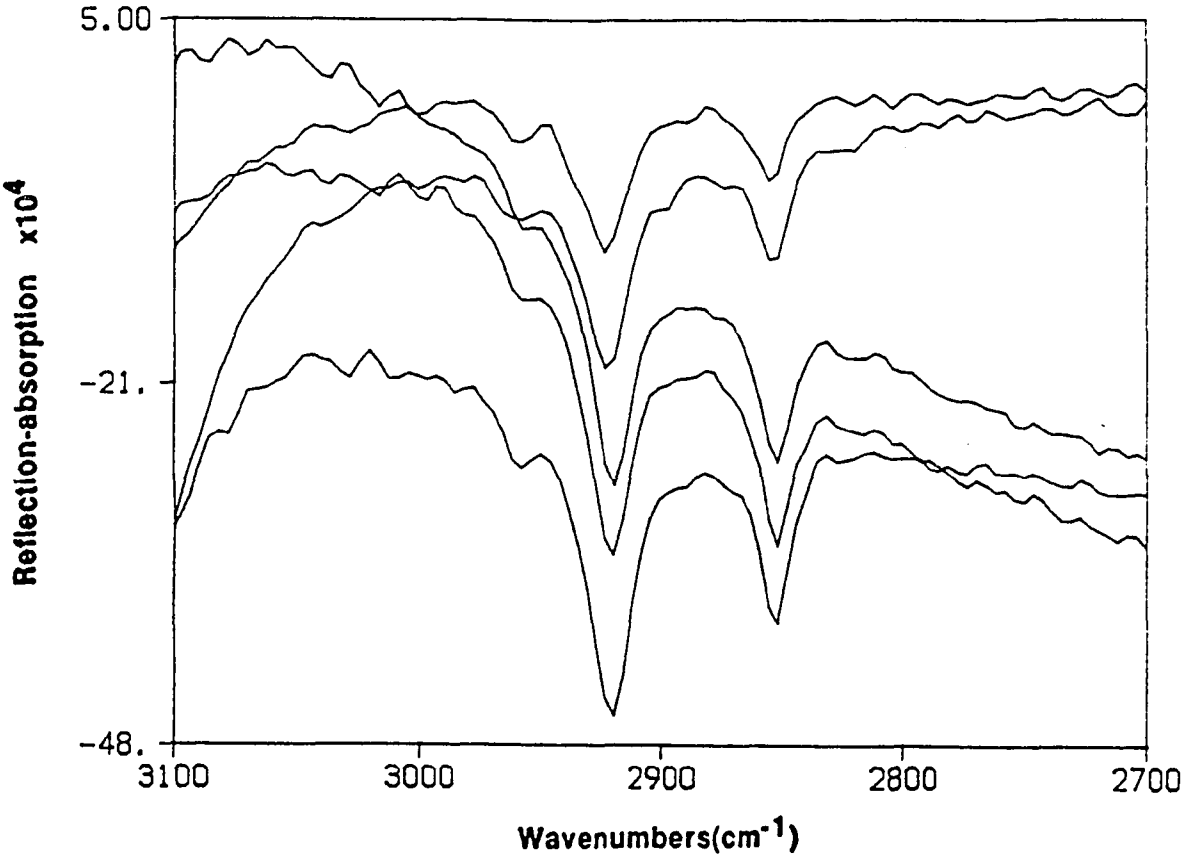


**Fig. 4.1.11(b). RA spectra of the adsorbed monolayers of $C_{12}SO_3Na$ at the aqueous solution/air interface in 0.1M NaCl at 30° incidence angle and *s*-polarization.**
**From top to bottom:**

| surfactant concentration | logC |
|---|---|
| $1.00X10^{-4}$ M | -4.00 |
| $2.00X10^{-4}$ M | -3.70 |
| $4.00X10^{-4}$ M | -3.40 |
| $8.00X10^{-4}$ M | -3.10 |
| $1.00X10^{-3}$ M | -3.00 |

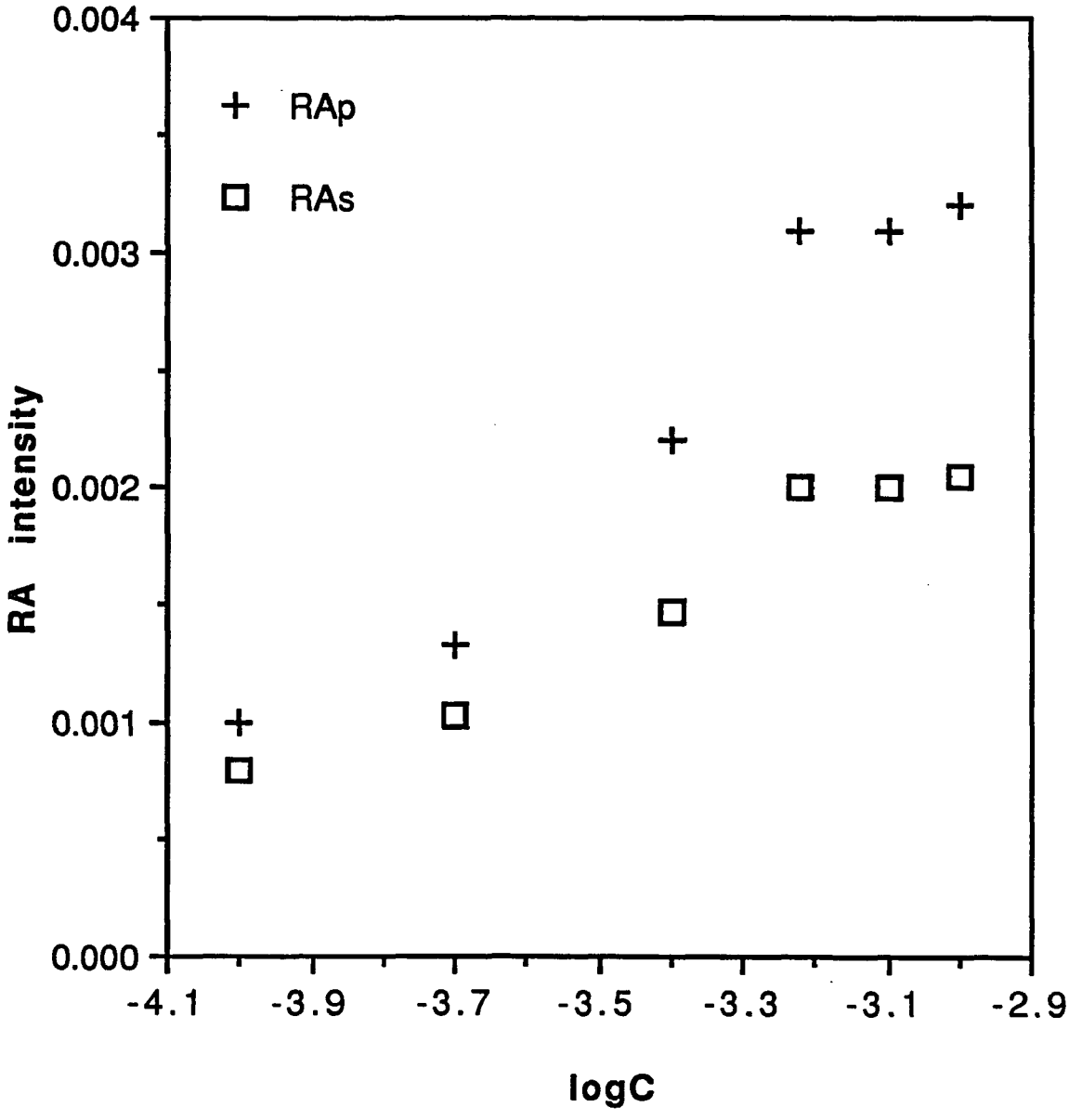


**Fig. 4.1.12. Changes in RA intensity of the adsorbed monolayers of $C_{12}SO_3Na$ at the air/water interface with different bulk concentrations in 0.1M NaCl solution.**

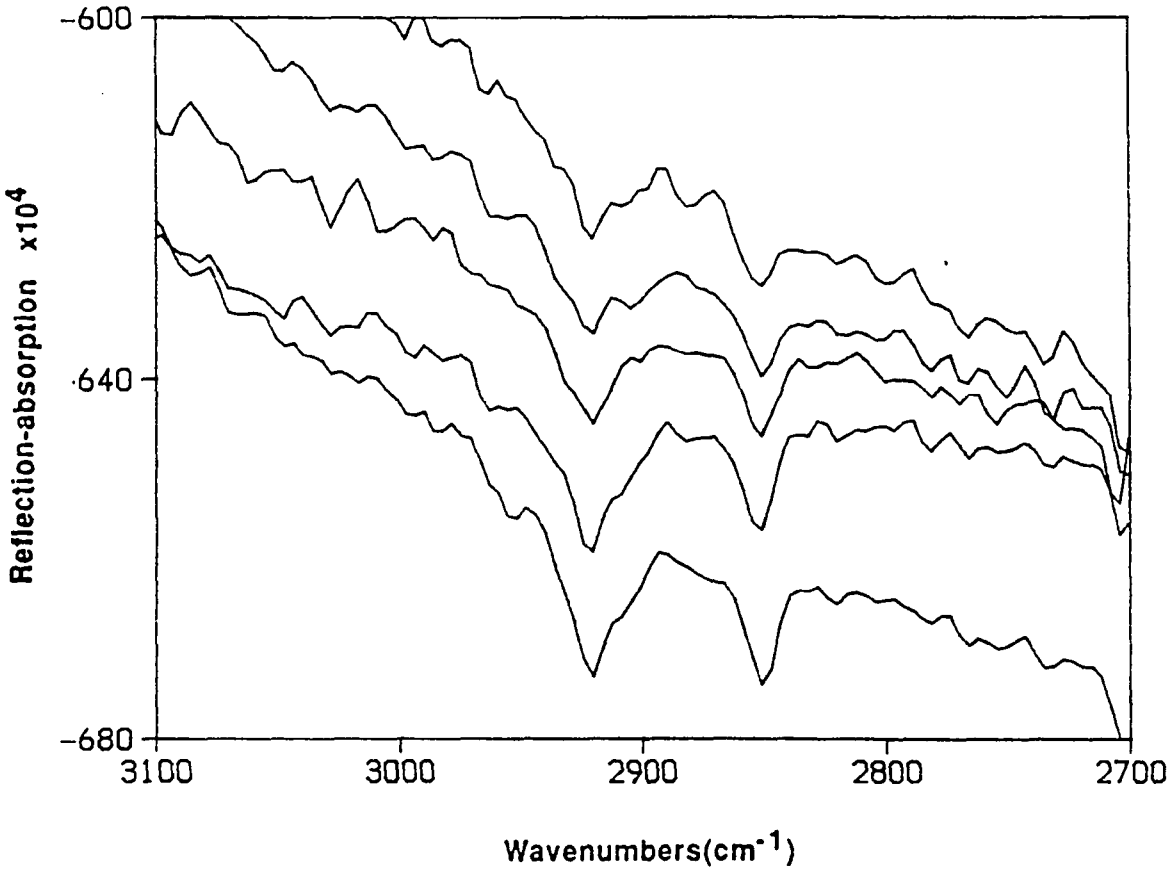


**Fig. 4.1.13(a). RA spectra of the adsorbed monolayers of $C_{12}SO_3Na$ at the aqueous solution/air interface in 0.5M NaCl at 30° incidence angle and *p*-polarization**
**From top to bottom:**

| surfactant concentration | logC |
|---|---|
| $4.47X10^{-5}$ M | -4.35 |
| $6.31X10^{-5}$ M | -4.20 |
| $1.29X10^{-4}$ M | -3.89 |
| $1.77X10^{-4}$ M | -3.75 |
| $2.63X10^{-4}$ M | -3.58 |

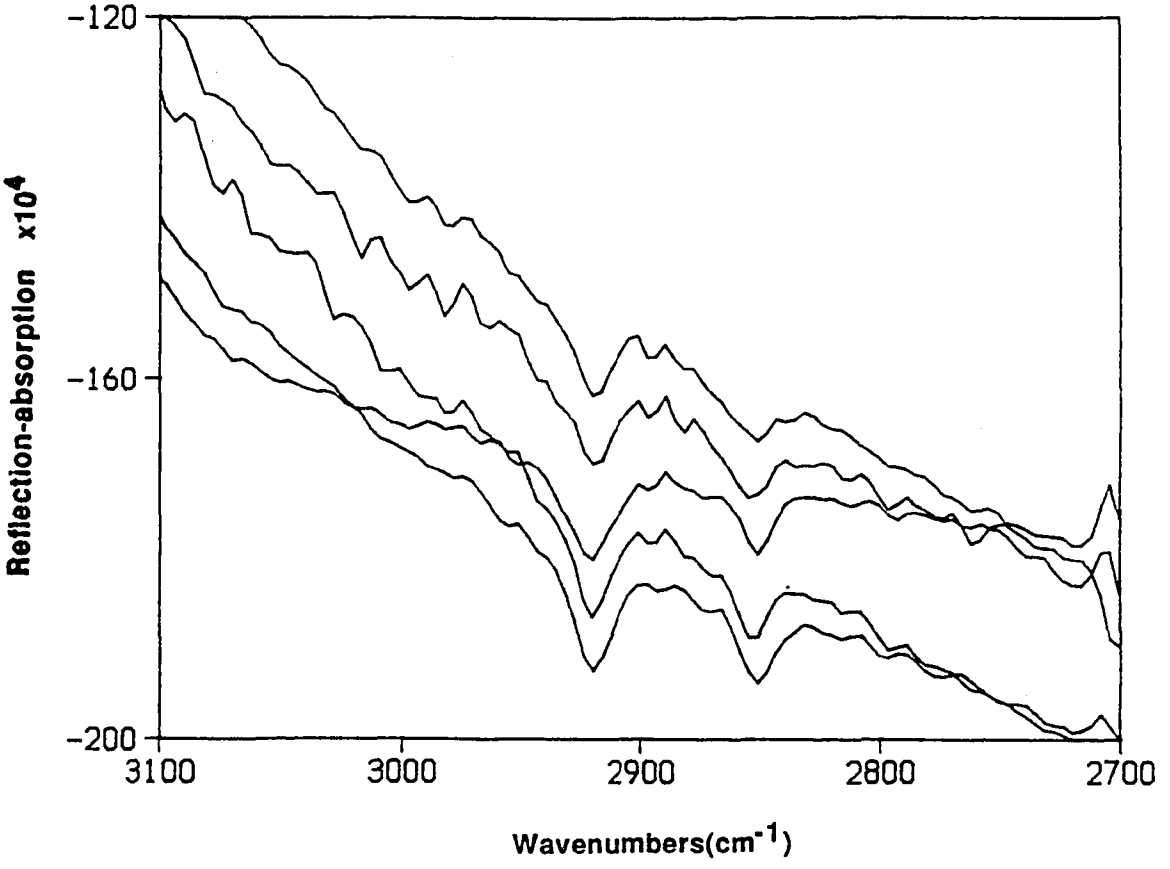


**Fig. 4.1.13(b). RA spectra of the adsorbed monolayers of $C_{12}SO_3Na$ at the aqueous solution/air interface in 0.5M NaCl at 30° incidence angle and *s*-polarization**

**From top to bottom:**

| surfactant concentration | logC |
|---|---|
| $4.47X10^{-5}$ M | -4.35 |
| $6.31X10^{-5}$ M | -4.20 |
| $1.29X10^{-4}$ M | -3.89 |
| $1.77X10^{-4}$ M | -3.75 |
| $2.63X10^{-4}$ M | -3.58 |

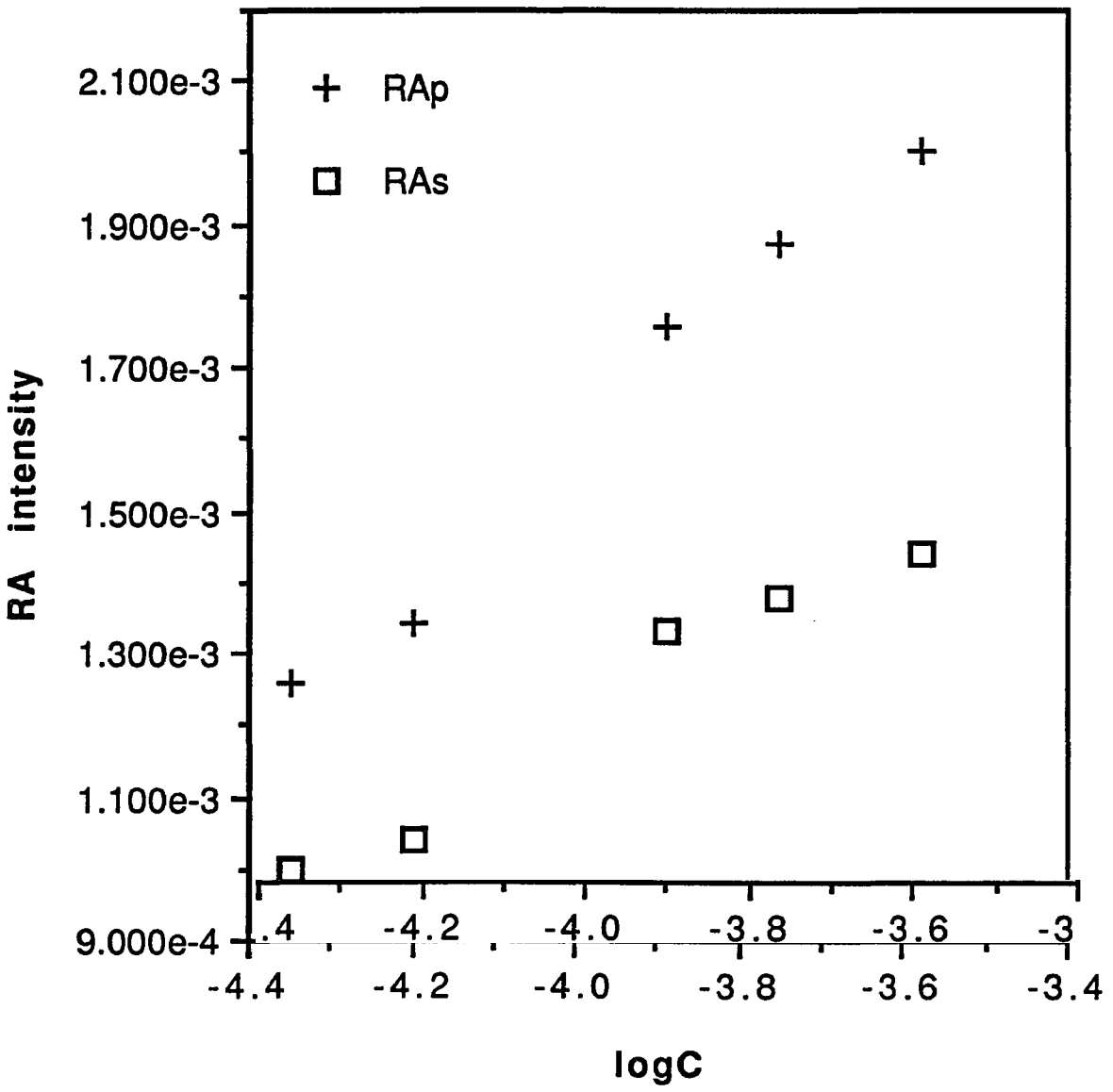


**Fig. 4.1.14. Changes in RA intensity of the adsorbed monolayers of $C_{12}SO_3Na$ at the air/water interface with different bulk concentrations in 0.5 M NaCl solution.**

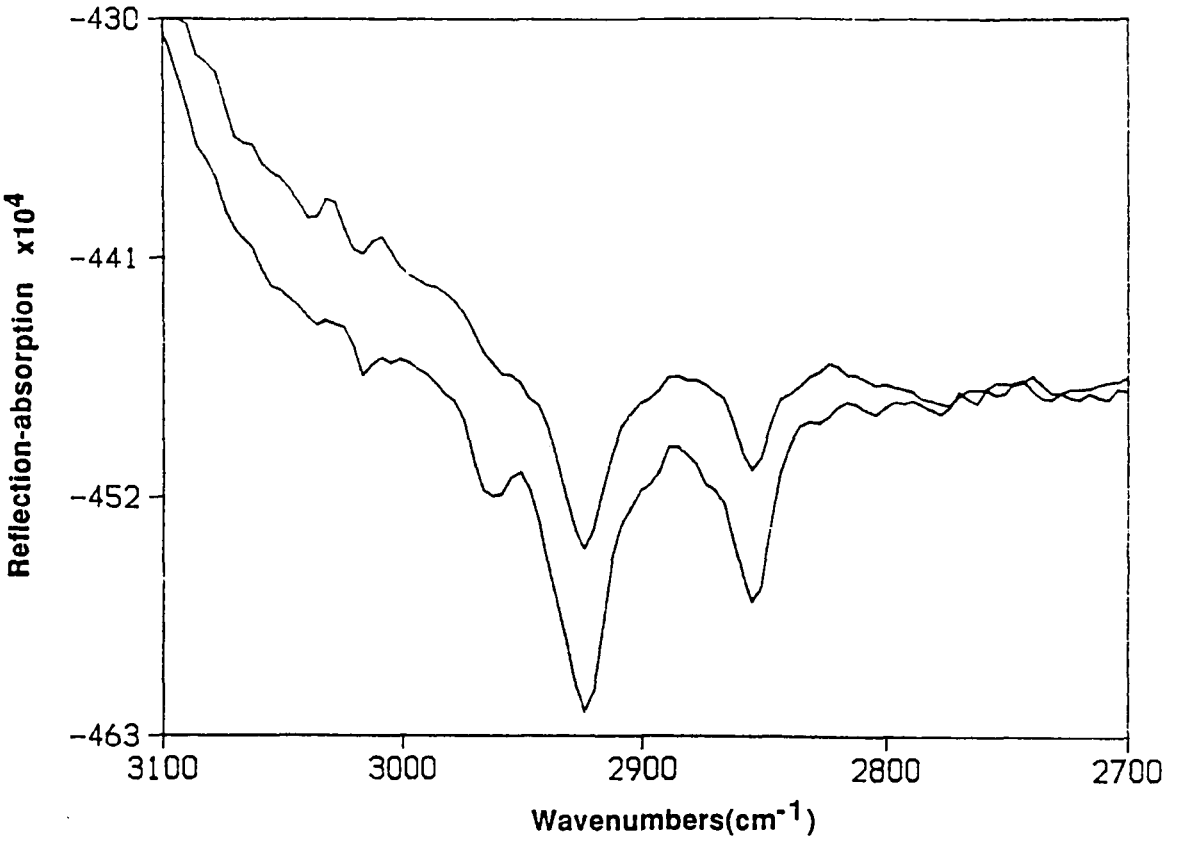


**Fig. 4.1.15. Effects of NaCl concentration on RA spectra of the adsorbed monolayers of $C_{12}SO_3Na$ at the air/water interface at *s*-polarization.**
**From top to bottom:**

| surfactant concentration | NaCl concentration |
|---|---|
| $6.24X10^{-4}$ M | 0 |
| $6.24X10^{-4}$ M | 0.05M |

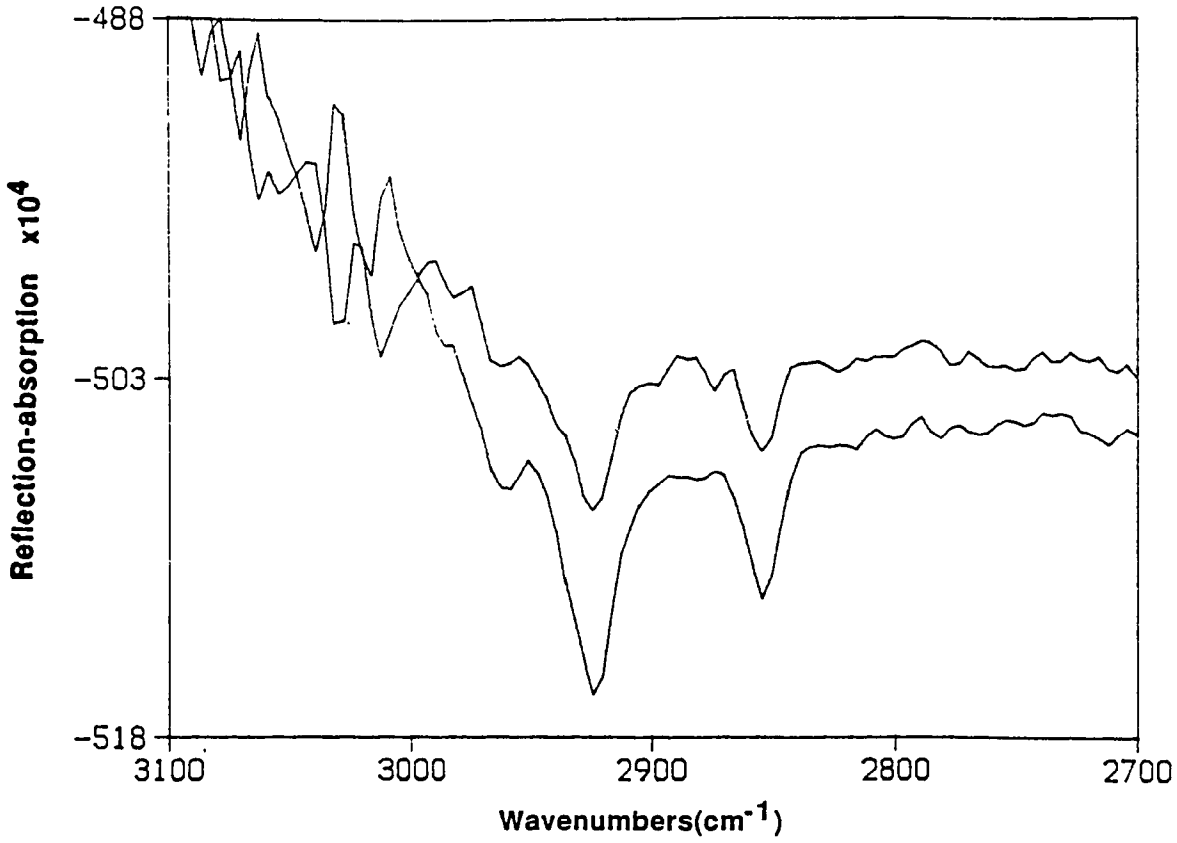


**Fig. 4.1.16. Effects of NaCl concentration on RA spetra of the adsorbed monolayers of $C_{12}SO_3Na$ at the air/water interface at *s*-polarization.**
**From top to bottom:**

| surfactant concentration | NaCl concentration |
|---|---|
| $1.10X10^{-4}$ M | 0.1M |
| $1.10X10^{-4}$ M | 0.5M |

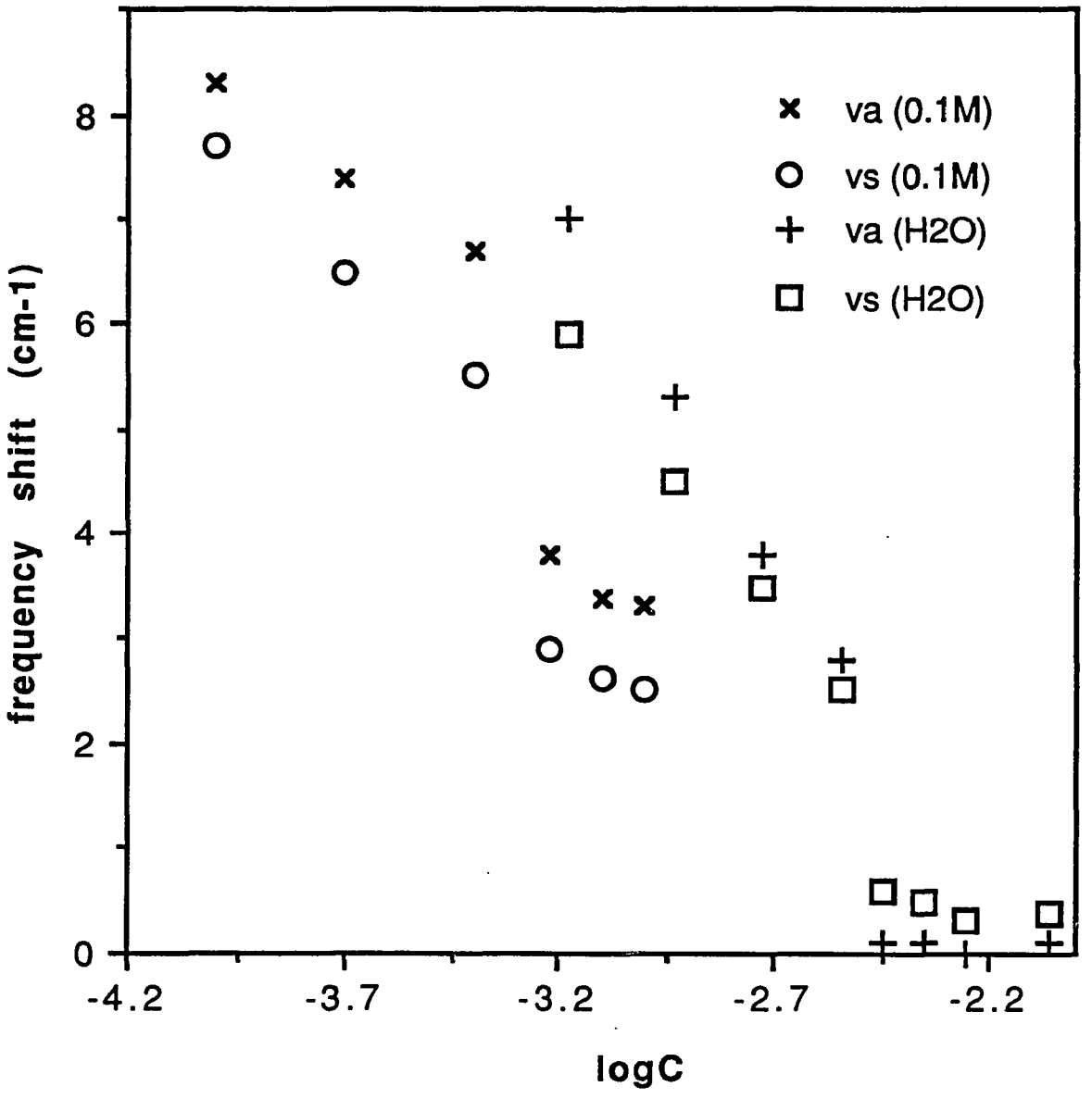


**Fig. 4.1.17. Frequency shifts in the C-H stretching bands vs. log of bulk concentration in pure water and 0.1M NaCl solution.**

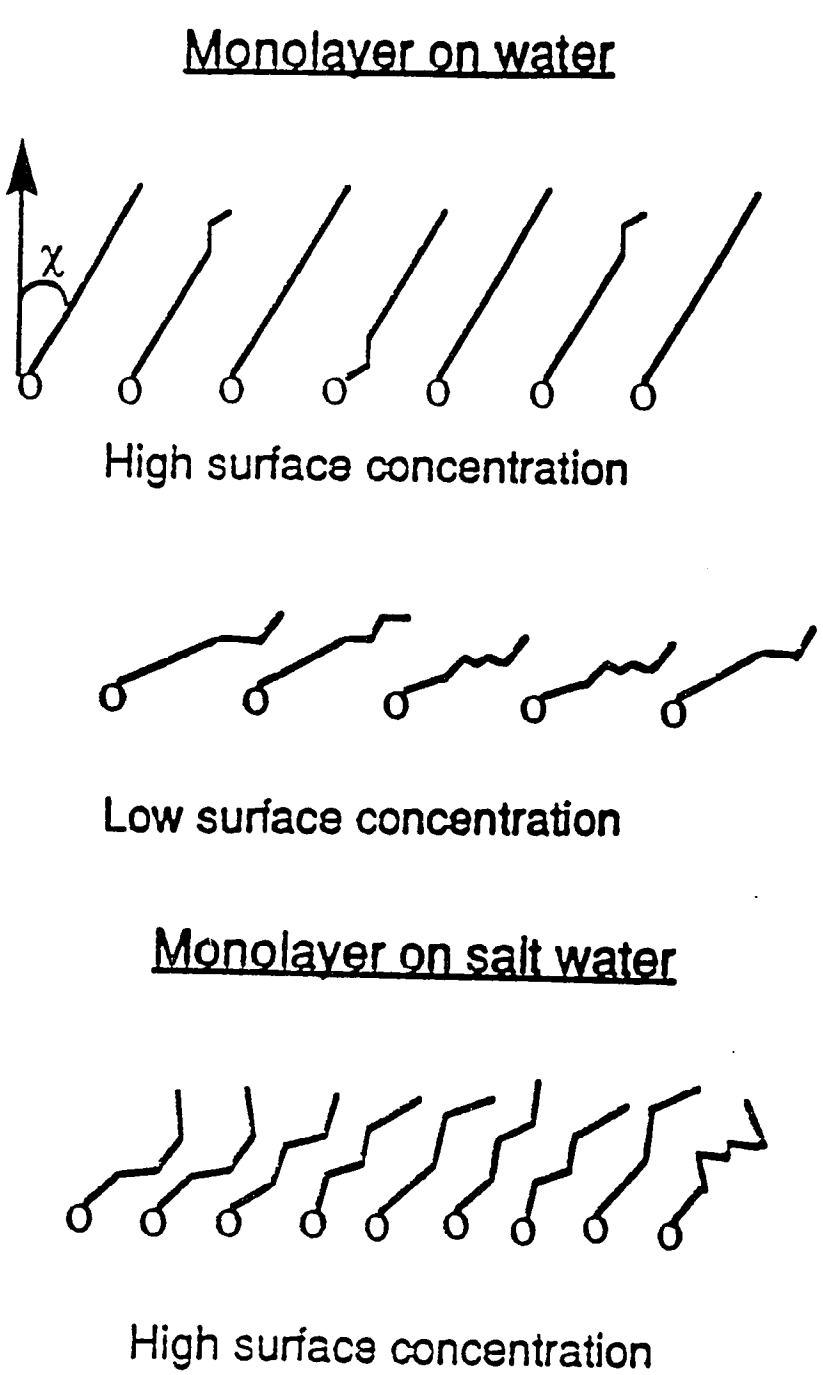


**Fig. 4.1.18. A diagram explanation of the structures of the adsorbed $C_{12}SO_3Na$ monolayer at the air/water interface.**

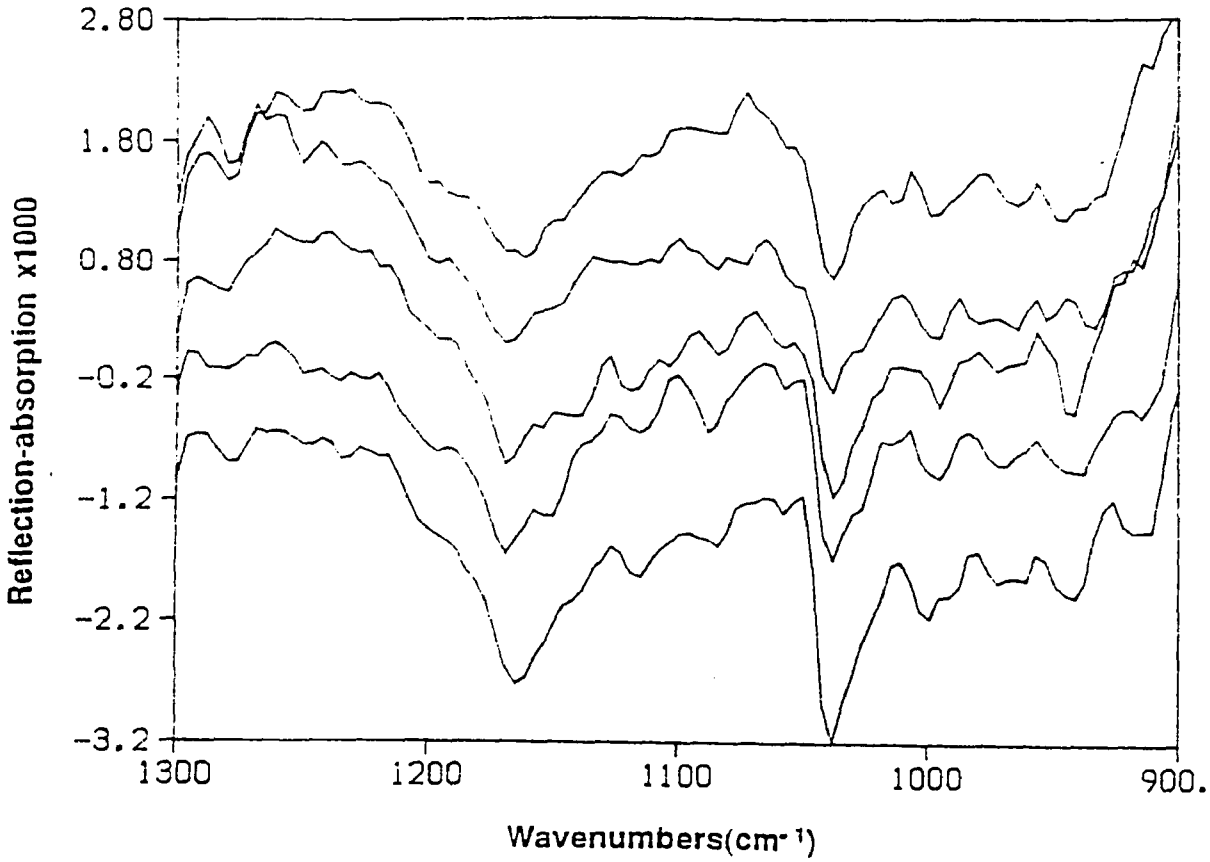


**Fig. 4.1.19. RA spectra of the adsorbed monolayers of $C_{12}SO_3Na$ at the aqueous solution/air interface in pure water at 30° incidence angle and *s*-polarization in the S-O stretching region.**
**From top to bottom:**

| surfactant concentration | logC |
|---|---|
| $2.28X10^{-3}$ M | -2.64 |
| $2.86X10^{-3}$ M | -2.54 |
| $3.58X10^{-3}$ M | -2.45 |
| $4.48X10^{-3}$ M | -2.35 |
| $5.00X10^{-3}$ M | -2.30 |

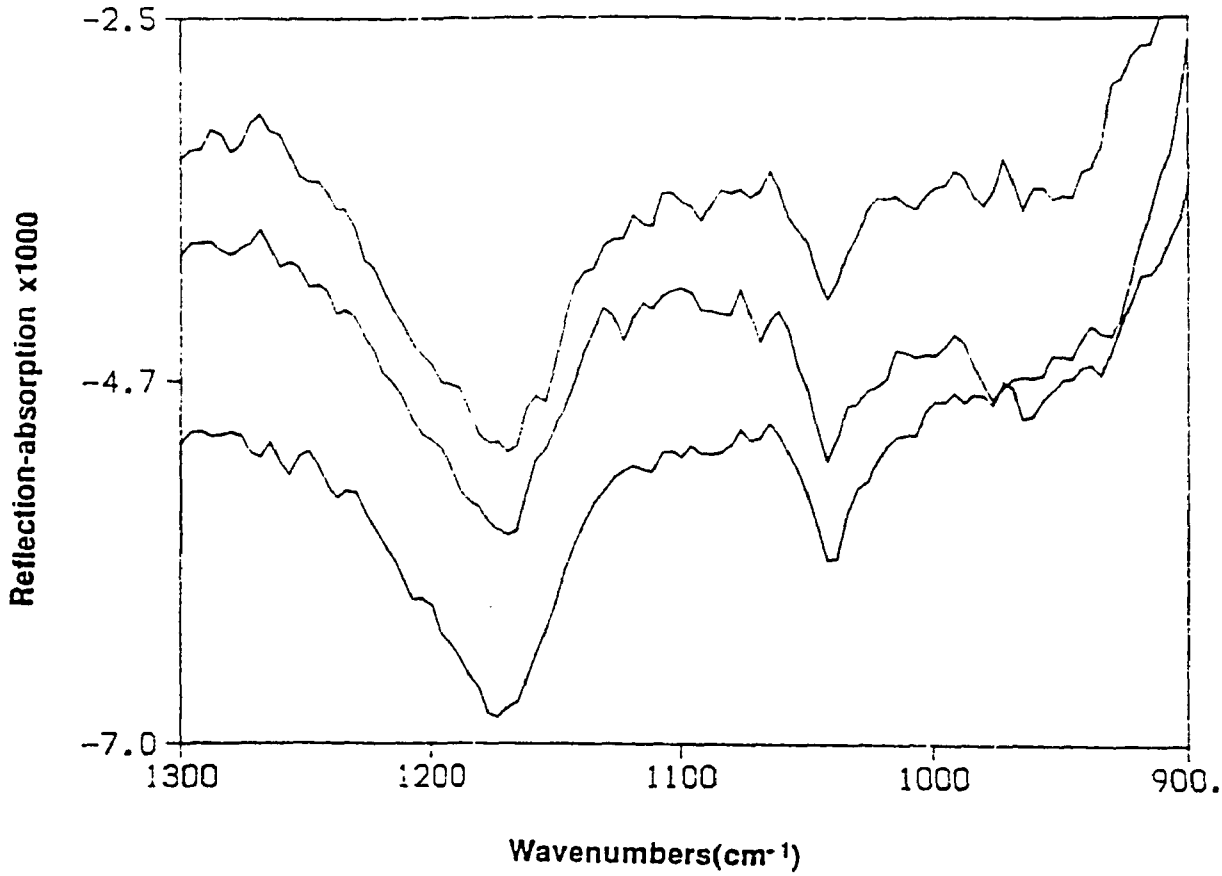


**Fig. 4.1.20. RA spectra of the adsorbed monolayers of $C_{12}SO_3Na$ at the aqueous solution/air interface in 0.1M NaCl at 30° incidence angle and *s*-polarization in the S-O stretching region.**
**From top to bottom:**

| surfactant concentration | logC |
|---|---|
| $6.00X10^{-4}$ M | -3.22 |
| $8.00X10^{-4}$ M | -3.10 |
| $1.00X10^{-3}$ M | -3.00 |

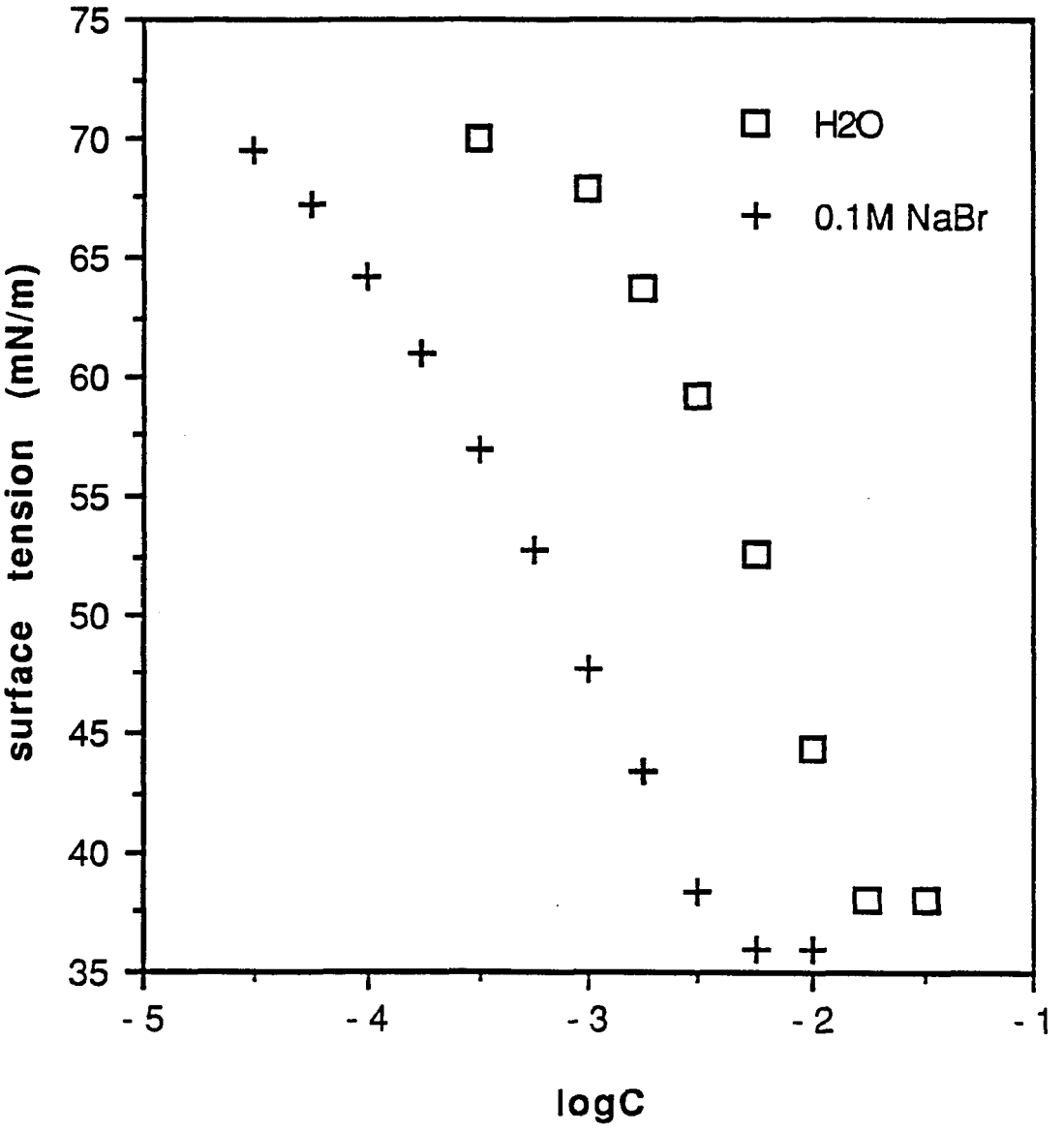


**Fig. 4.2.1. Surface tension vs. log of the concentration of $C_{12}N(CH_3)_3Br$ ($C_{12}N$) in pure $H_20$ and 0.1M NaBr solution at 25.0°C.**

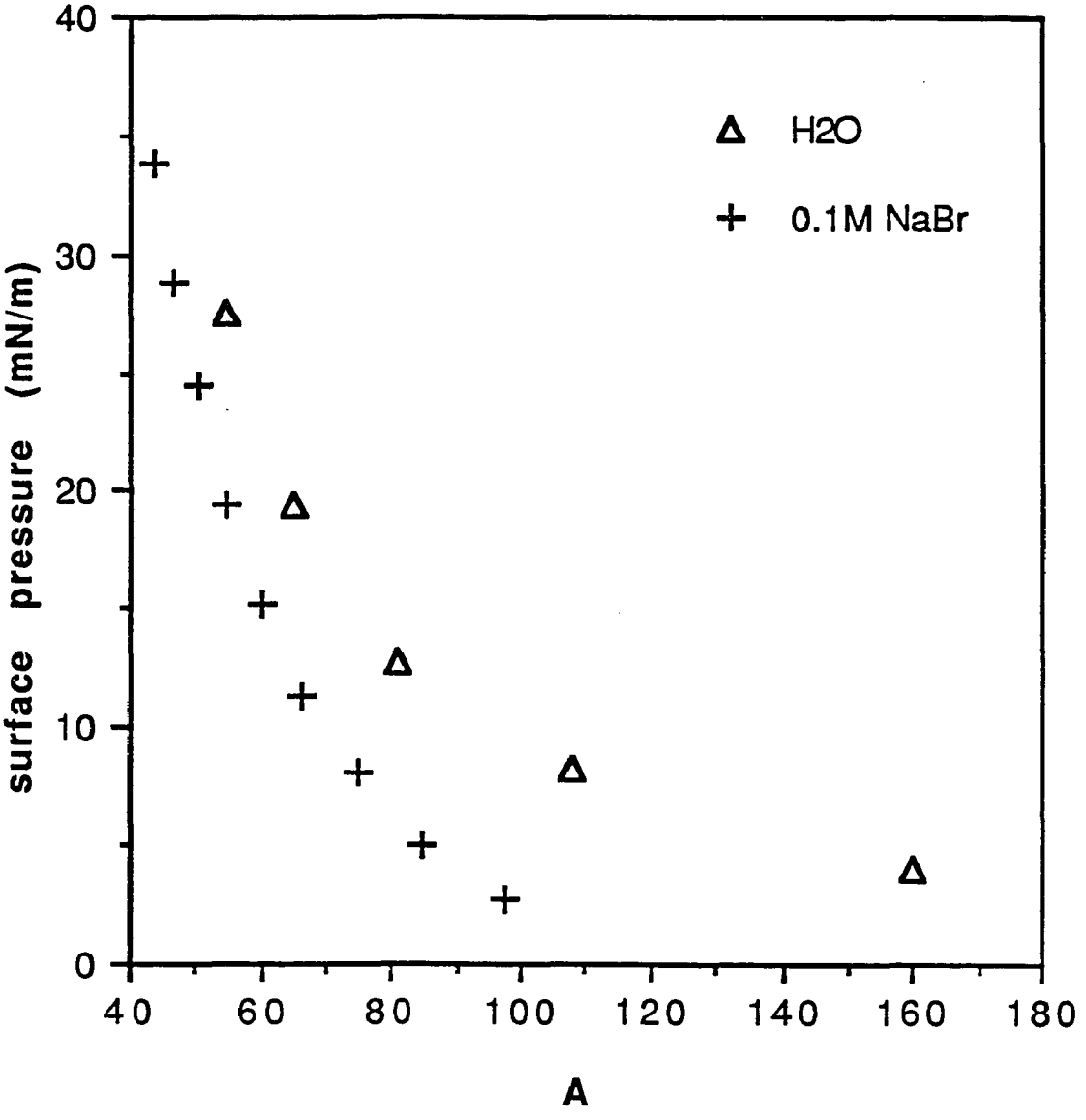


**Fig. 4.2.2. Surface pressure vs. area per molecule (A) of $C_{12}N$ in pure $H_20$ and 0.1M NaBr solution at 25.0°C.**

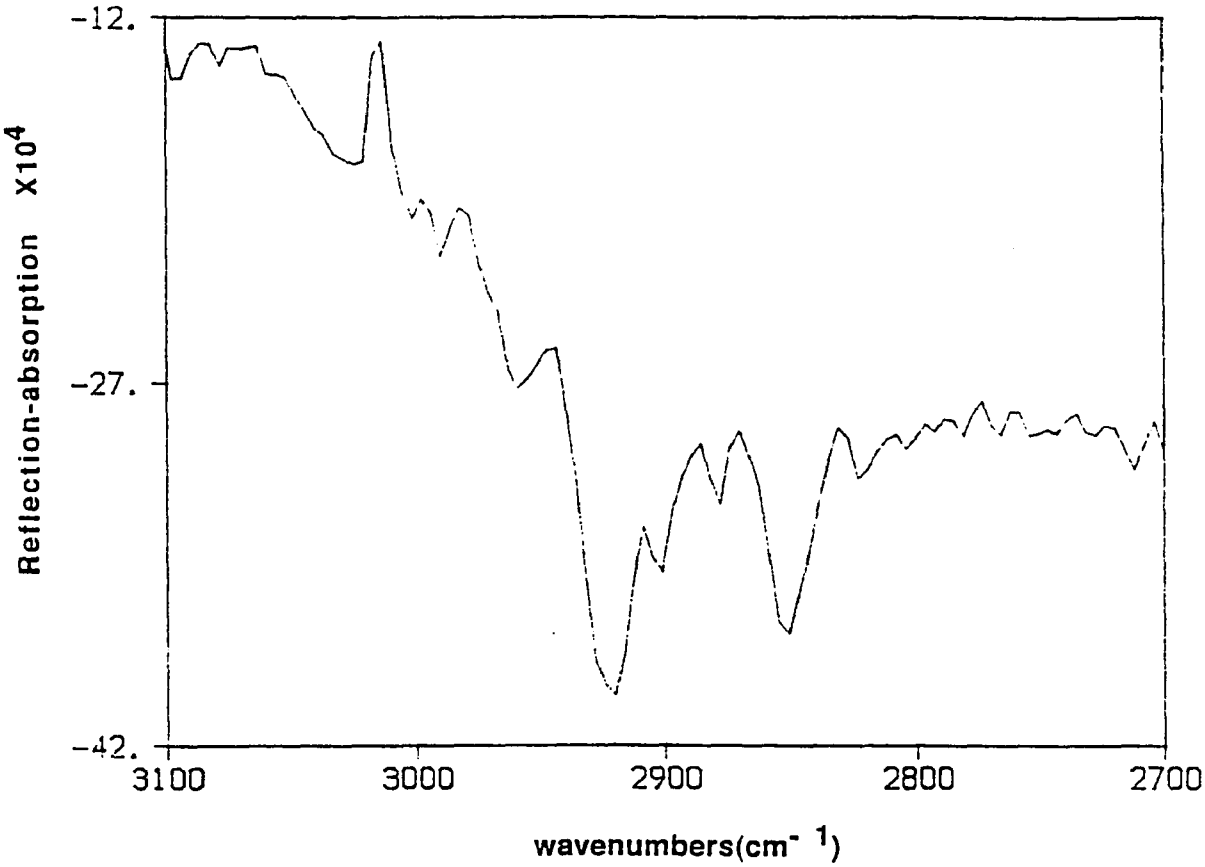


**Fig. 4.2.3. A representative RA spectrum of the adsorbed monolayer of $C_{12}N$ (C = 1.4X10$^{-2}$M) at the aqueous solution/air interface in pure $H_2O$ at 30° incidence angle and s-polarization.**

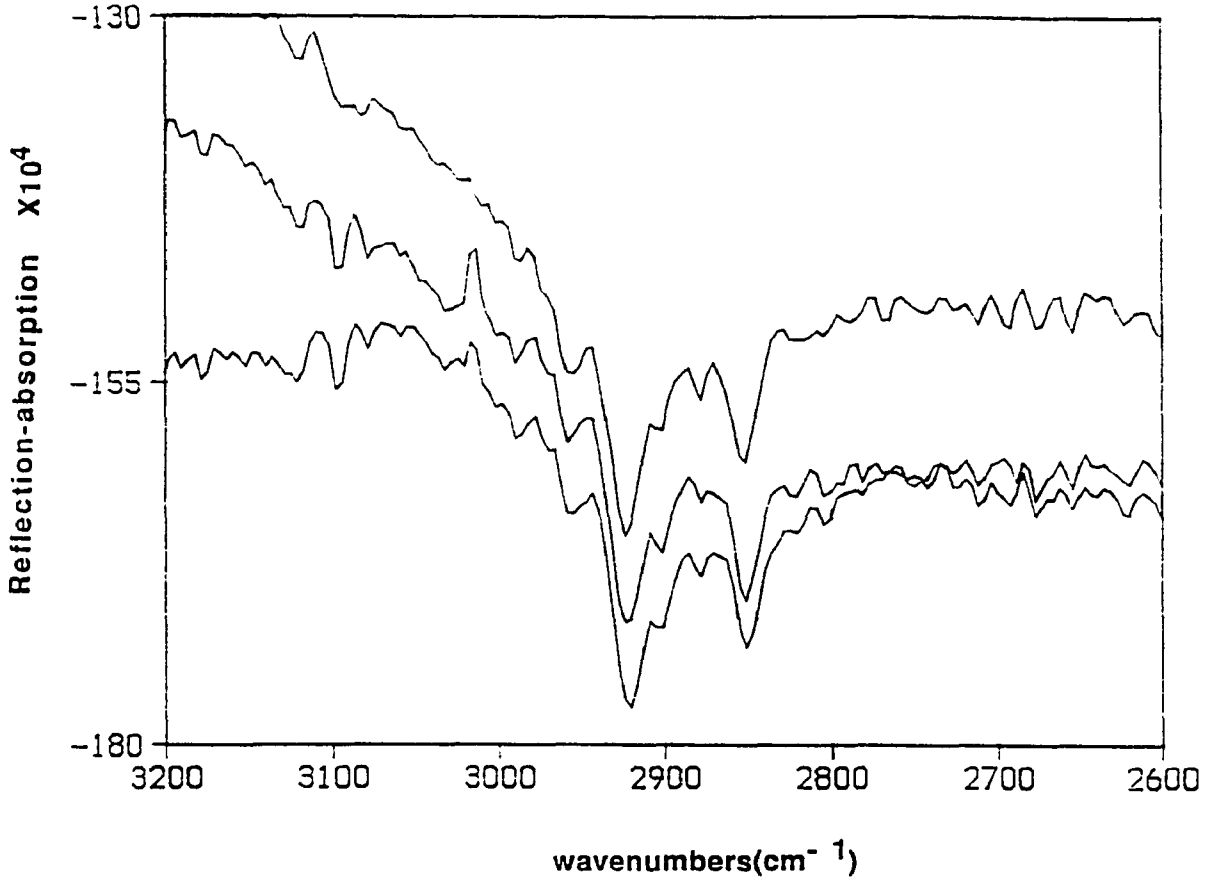


**Fig. 4.2.4. RA spectra of the adsorbed monolayers of $C_{12}N$ at the air/water interface in pure $H_2O$ at 30° incidence angle and *s*-polarization**
**From top to bottom:**

| | |
|---|---|
| **$1.00X10^{-2}$ M** | **-2.00** |
| **$1.40X10^{-2}$ M** | **-1.85** |
| **$2.00X10^{-2}$ M** | **-1.70** |

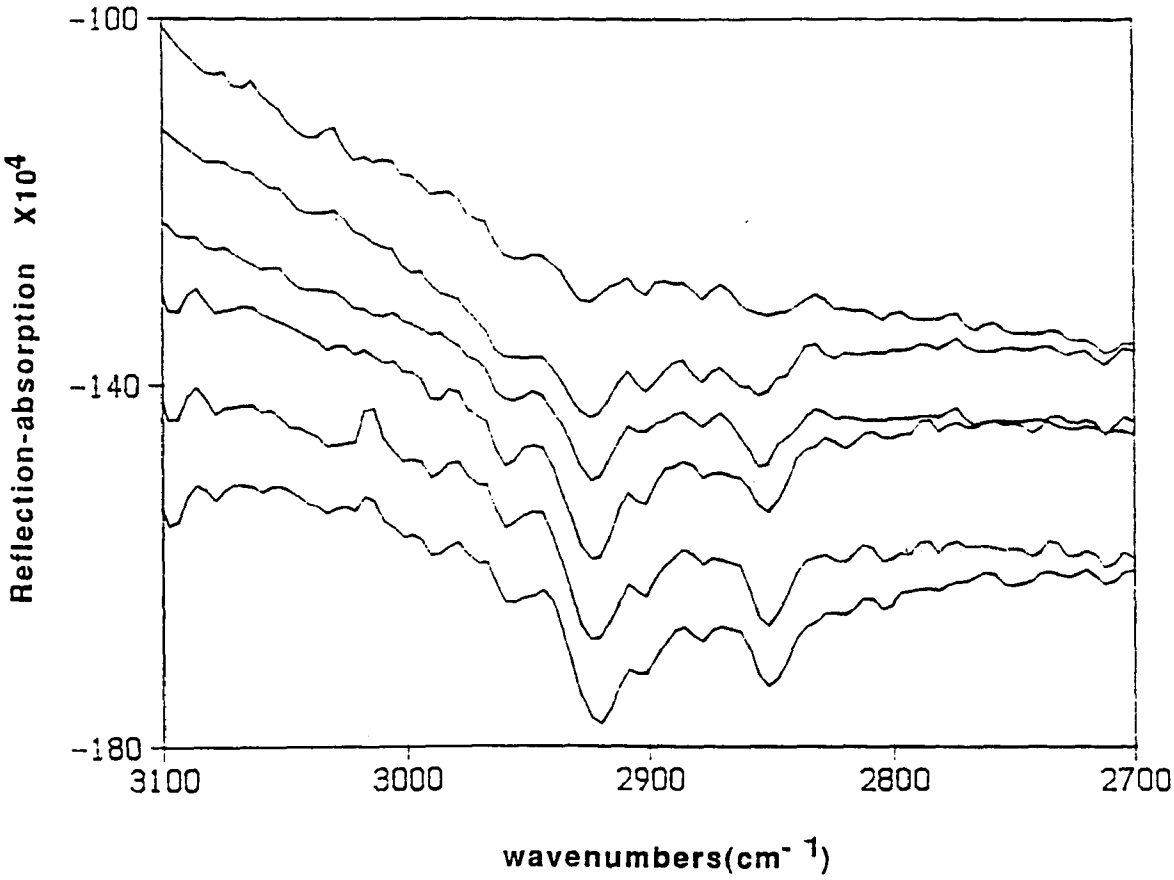


**Fig. 4.2.5. RA spectra of the adsorbed monolayers of $C_{12}N$ solutions at the air/water interface in pure $H_2O$ at 30° incidence angle and *s*-polarization**

**From top to bottom:**

| surfactant concentration | logC |
|---|---|
| $1.75X10^{-3}$ M | -2.75 |
| $2.50X10^{-3}$ M | -2.60 |
| $5.00X10^{-3}$ M | -2.30 |
| $1.00X10^{-2}$ M | -2.00 |
| $1.40X10^{-2}$ M | -1.85 |
| $2.00X10^{-2}$ M | -1.70 |

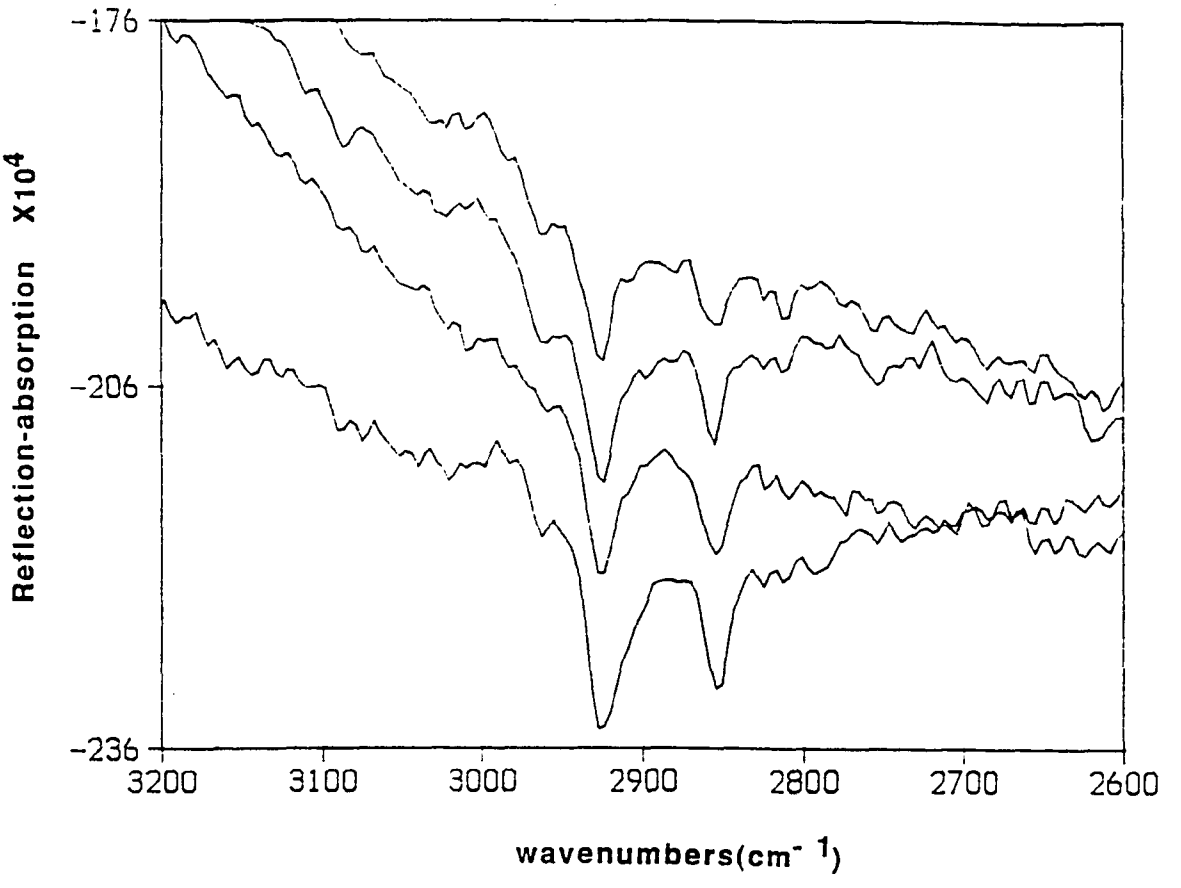


**Fig. 4.2.6 (a). RA spectra of the adsorbed monolayers of $C_{12}N$ at the air/water interface in 0.1M NaBr at 30° incidence angle and *p*-polarization**
**From top to bottom:**

| surfactant concentration | logC |
|---|---|
| $1.00X10^{-3}$ M | -3.00 |
| $2.00X10^{-3}$ M | -2.70 |
| $4.00X10^{-3}$ M | -2.40 |
| $1.00X10^{-2}$ M | -2.00 |

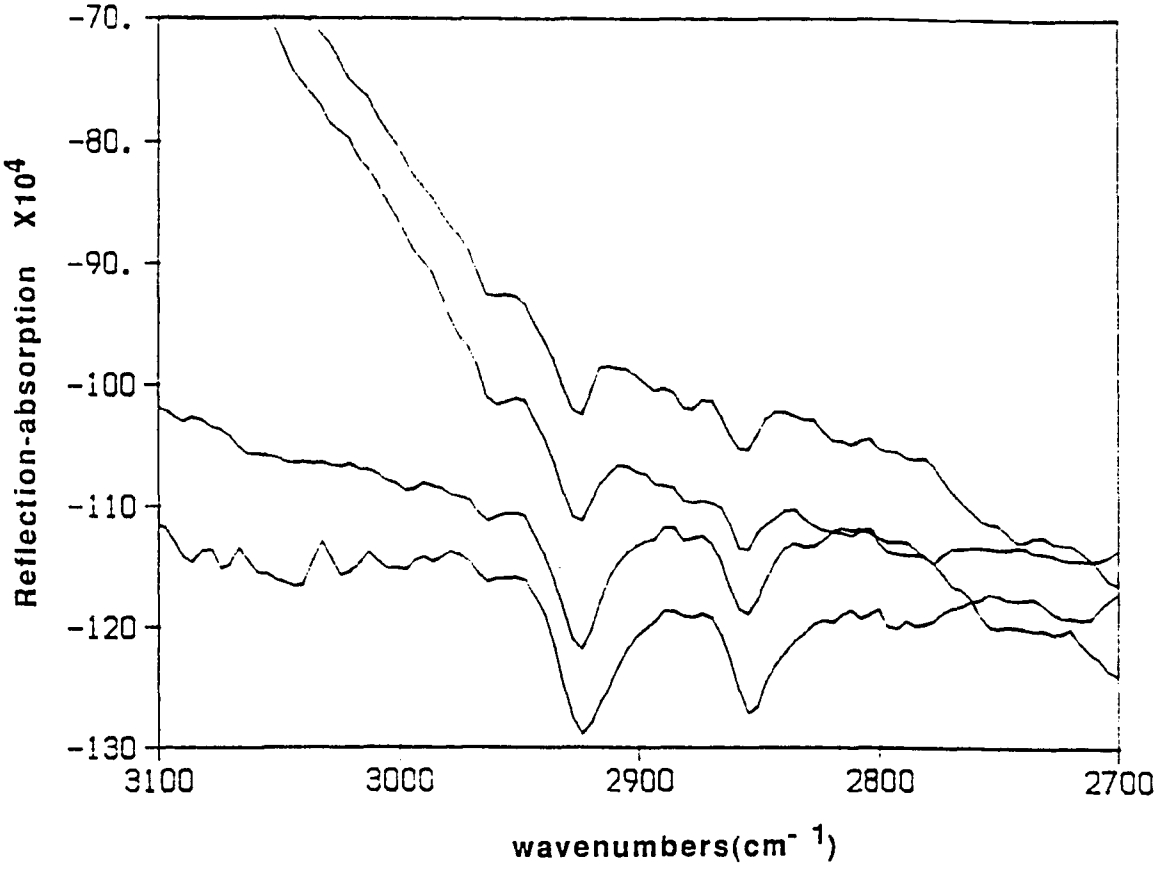


**Fig. 4.2.6 (b). RA spectra of the adsorbed monolayers of $C_{12}N$ at the air/water interface in 0.1M NaBr at 30° incidence angle and *s*-polarization**
**From top to bottom:**

| surfactant concentration | logC |
|---|---|
| $1.00X10^{-3}$ M | -3.00 |
| $2.00X10^{-3}$ M | -2.70 |
| $4.00X10^{-3}$ M | -2.40 |
| $1.00X10^{-2}$ M | -2.00 |


**Fig. 4.2.7. Effects of NaBr concentration on RAs of $C_{12}N$ monolayers at the air/water interface at 30° incidence angle and *s*-polarization**

**From top to bottom:**

| surfactant concentration | subphase |
|---|---|
| $1.40X10^{-2}$ M | pure $H_2O$ |
| $4.00X10^{-3}$ M | 0.1M NaBr |

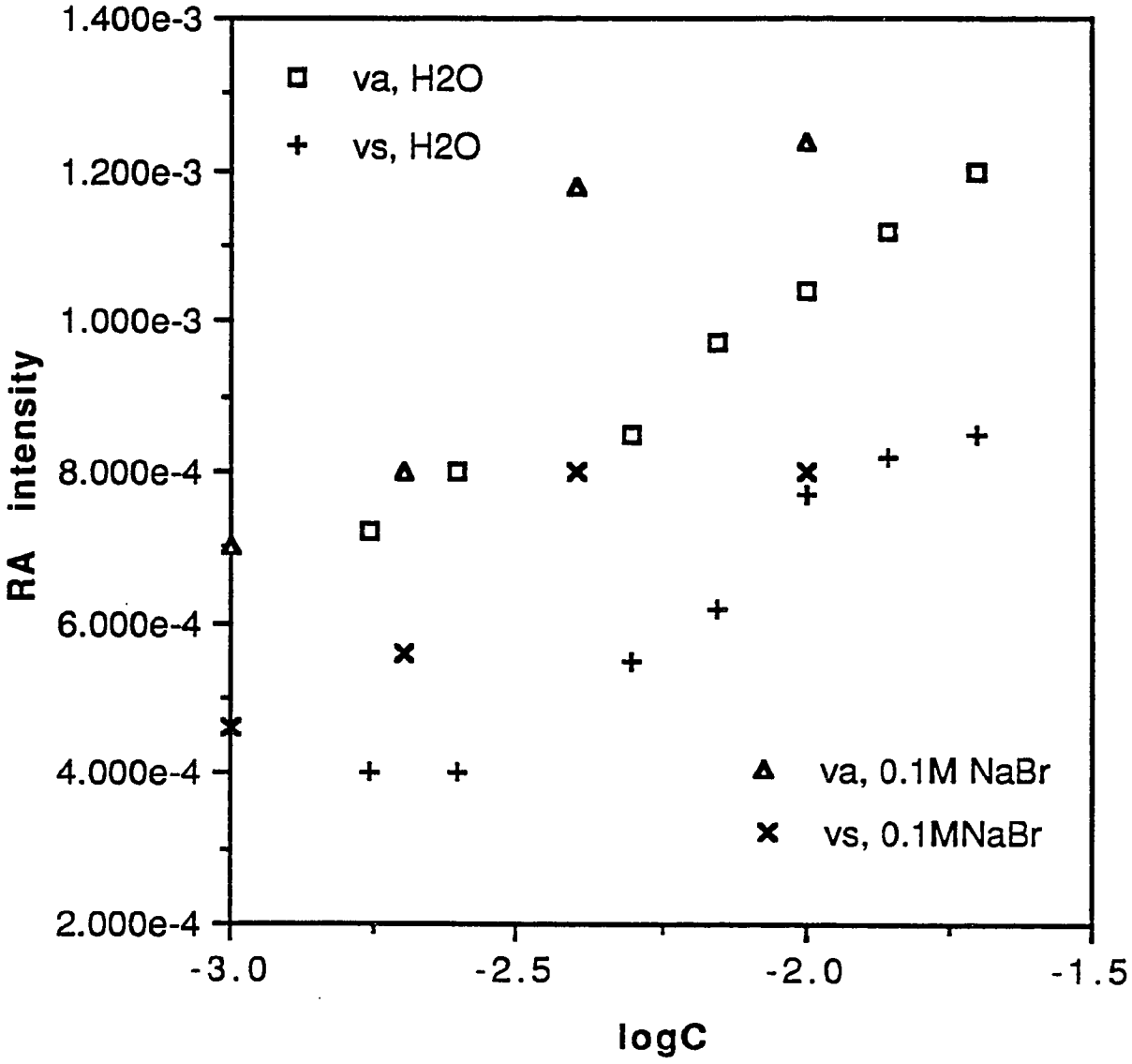


**Fig. 4.2.8. Changes in RA intensity of the adsorbed monolayers of $C_{12}N$ at the air/water interface with different surfactant bulk concentrations in pure $H_2O$ and 0.1M NaBr solution (in the C-H stretching region).**

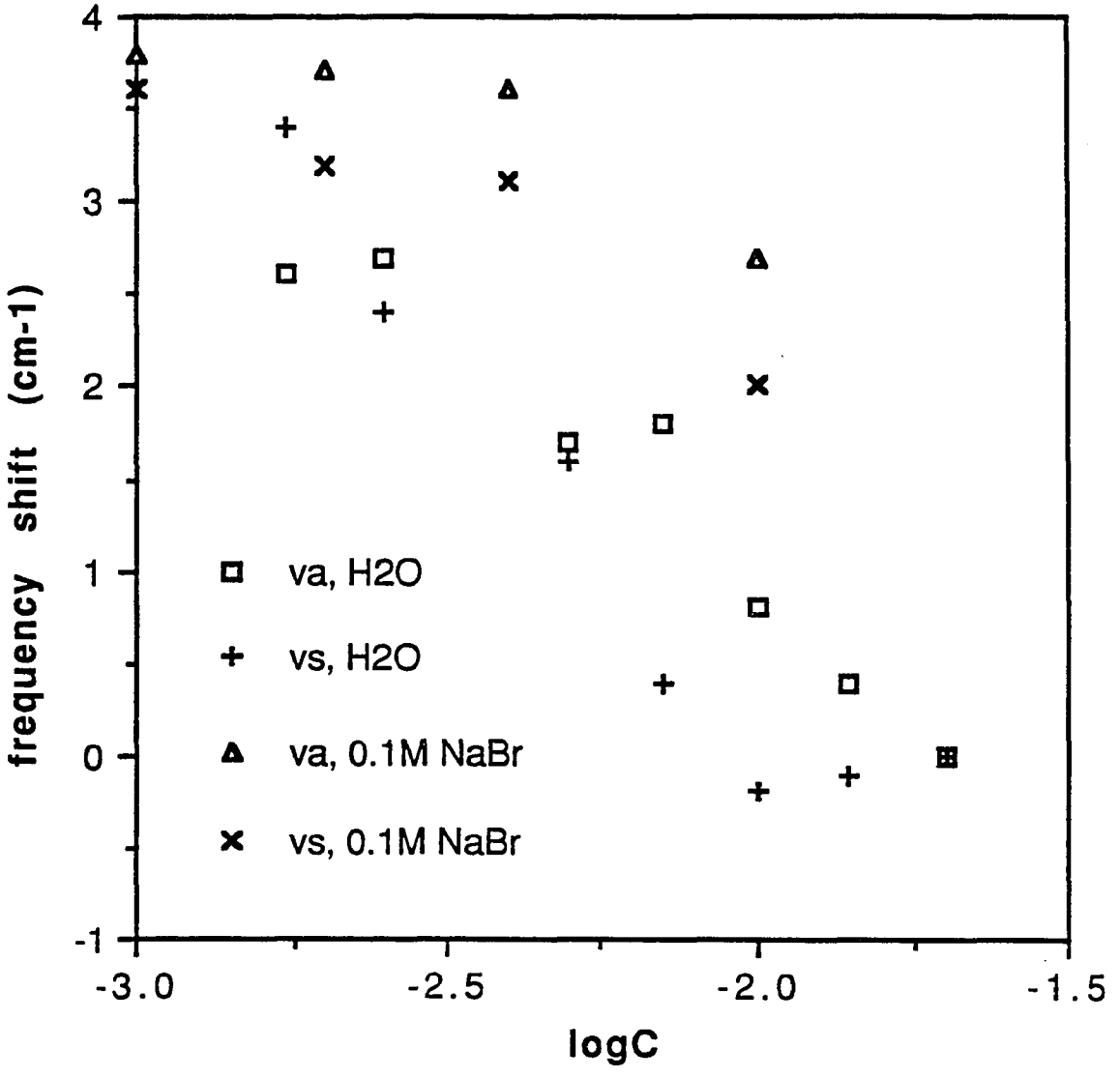


**Fig. 4.2.9. Changes in peak frequency of the adsorbed monolayers of $C_{12}N$ at the air/water interface with different surfactant concentrations in pure water and 0.1M NaBr solution (in the C-H stretching region).**

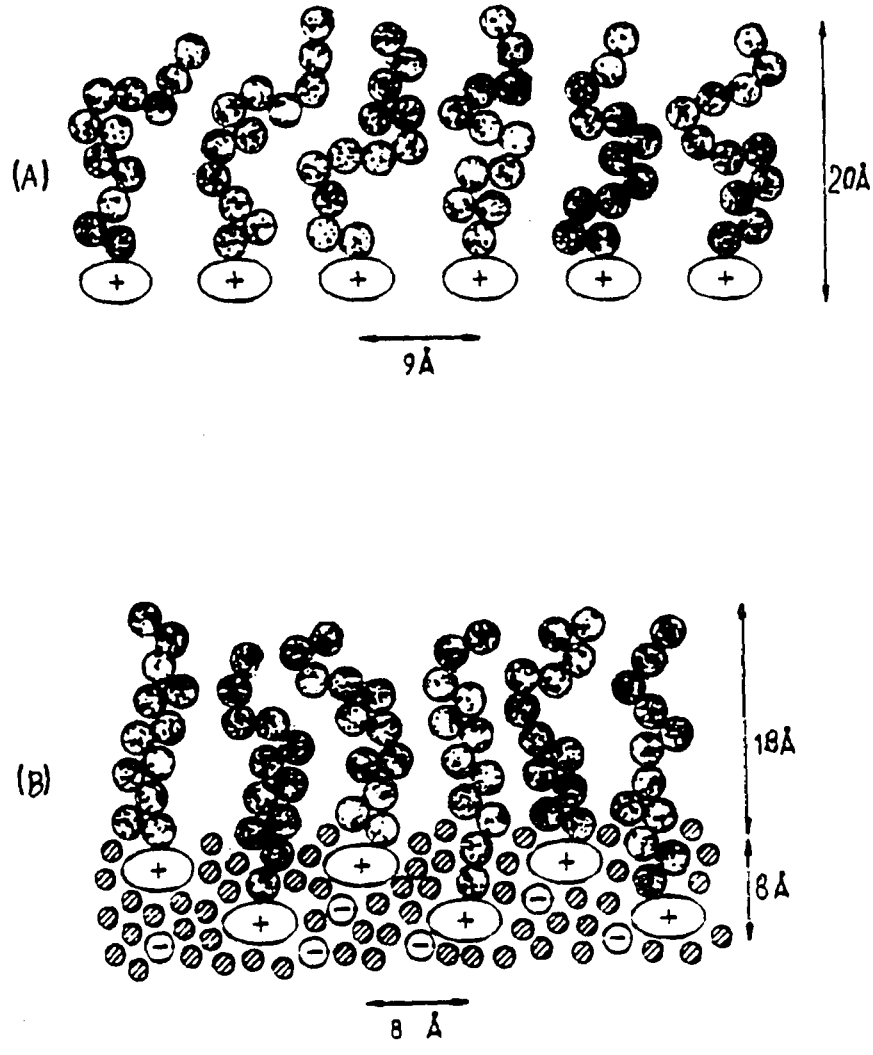


**Fig. 4.2.10. Structure and distribution of water and $C_{12}N$ molecules in adsorbed monolayers at the air/water interface*.**
**(A). A uniform layer at dilute surface concentration.**
**(B). A staggered layer at concentrated surface concentration.**
*** reference (29)**

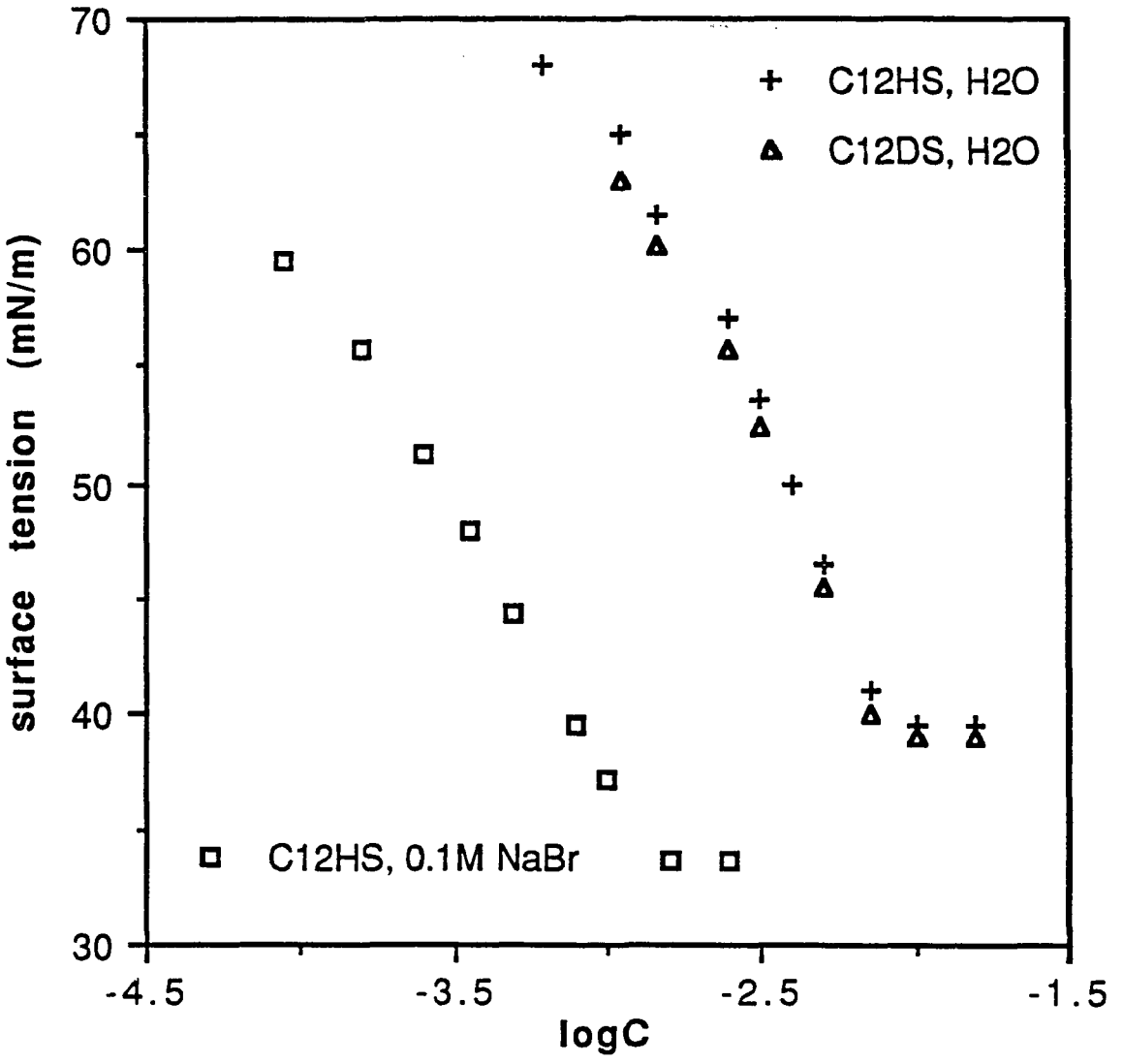


**Fig. 4.3.1. Surface tension vs. log of the concentration of $C_{12}H_{25}SO_4Na$ ($C_{12}HS$) and $C_{12}D_{25}SO_4Na$ ($C_{12}DS$) in pure $H_20$ and 0.1M NaBr solution at 25.0°C.**

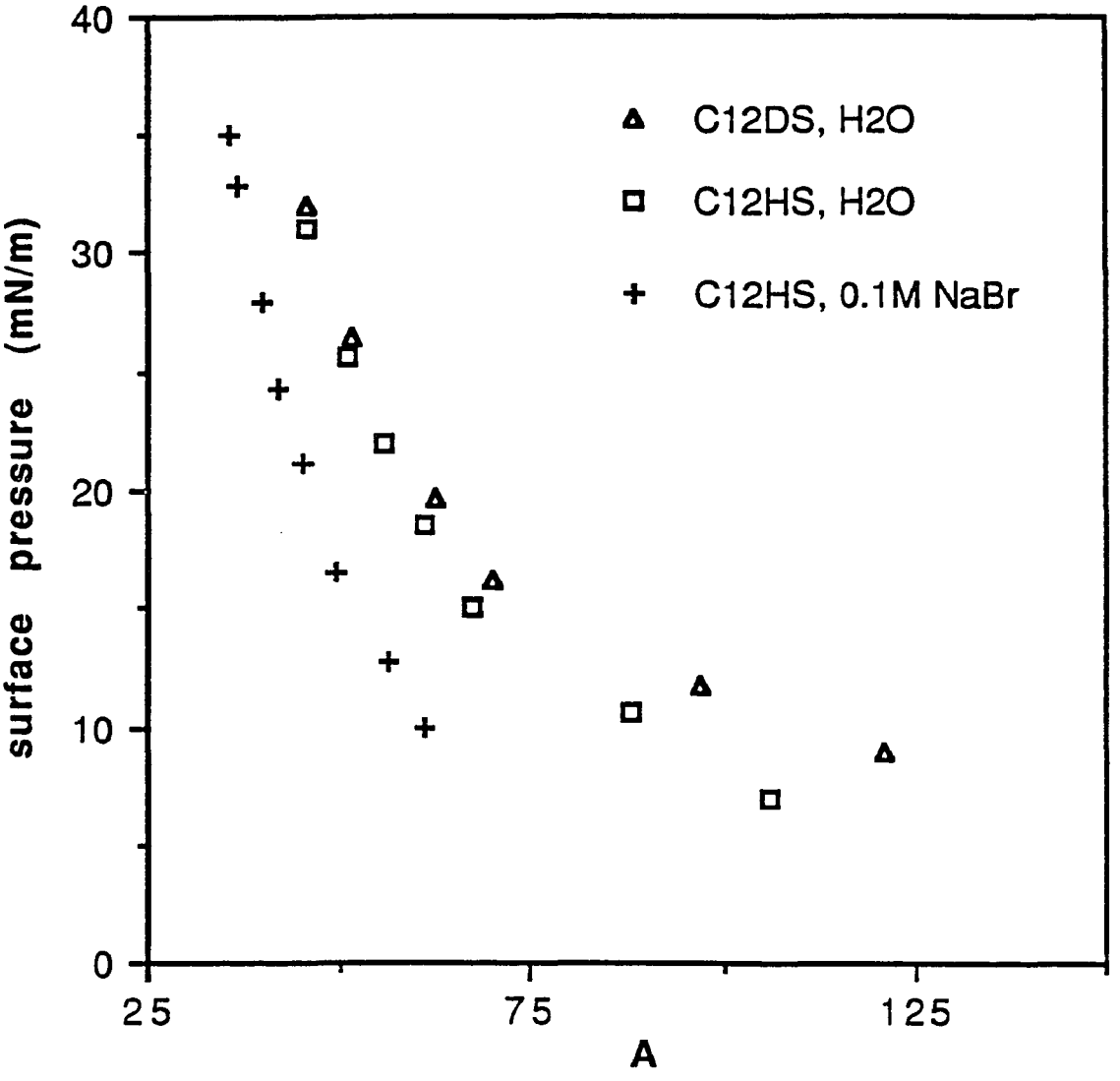


**Fig. 4.3.2. Surface pressure vs. area per molecule (A) of $C_{12}HS$ and $C_{12}DS$ in pure $H_20$ and 0.1M NaBr solution at 25.0°C.**

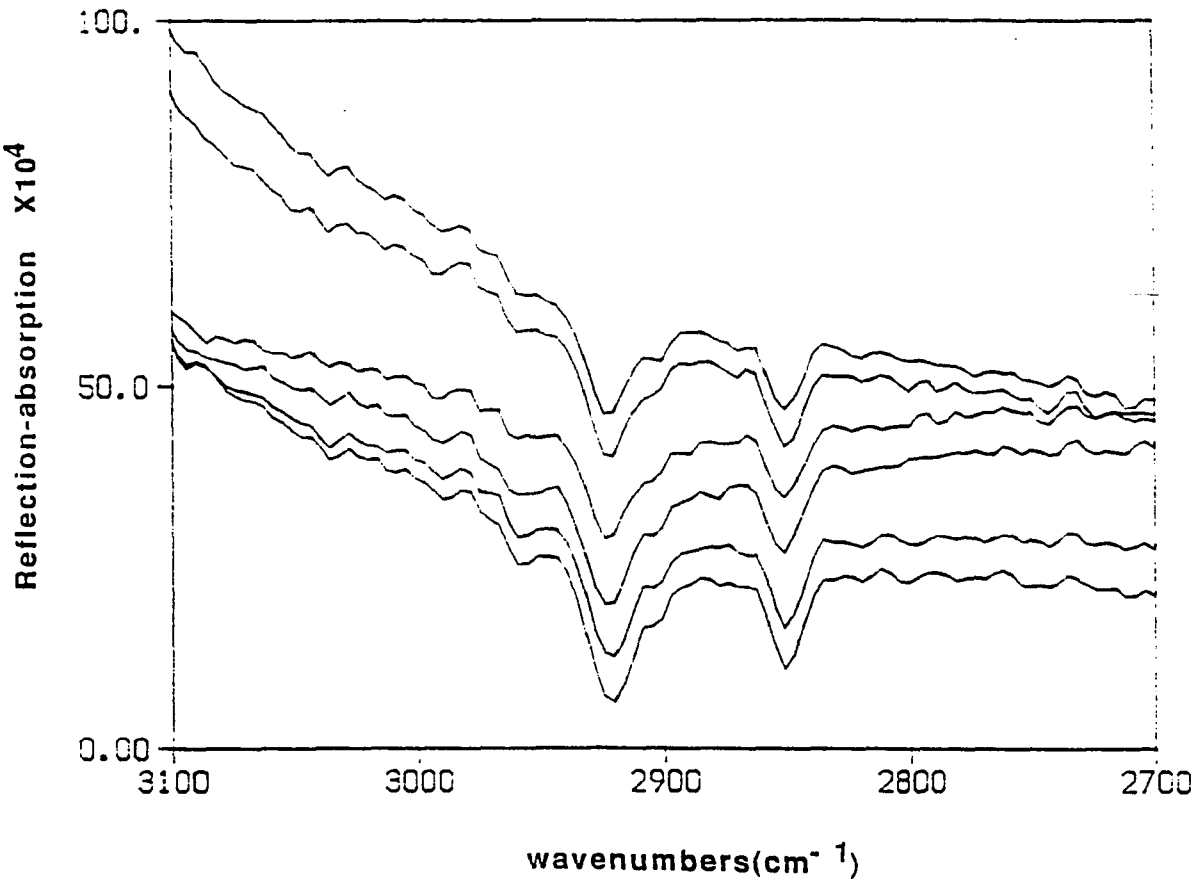


**Fig. 4.3.3 (a). RA spectra of the adsorbed monolayers of $C_{12}HS$ at the air/water interface in pure $H_2O$ at 30° incidence angle and *s*-polarization (the C-H stretching region)**
**From top to bottom:**

| surfactant concentration | logC |
|---|---|
| $1.75X10^{-3}$ M | -2.75 |
| $2.50X10^{-3}$ M | -2.60 |
| $3.50X10^{-3}$ M | -2.45 |
| $5.00X10^{-3}$ M | -2.30 |
| $7.00X10^{-3}$ M | -2.15 |
| $1.00X10^{-2}$ M | -2.00 |

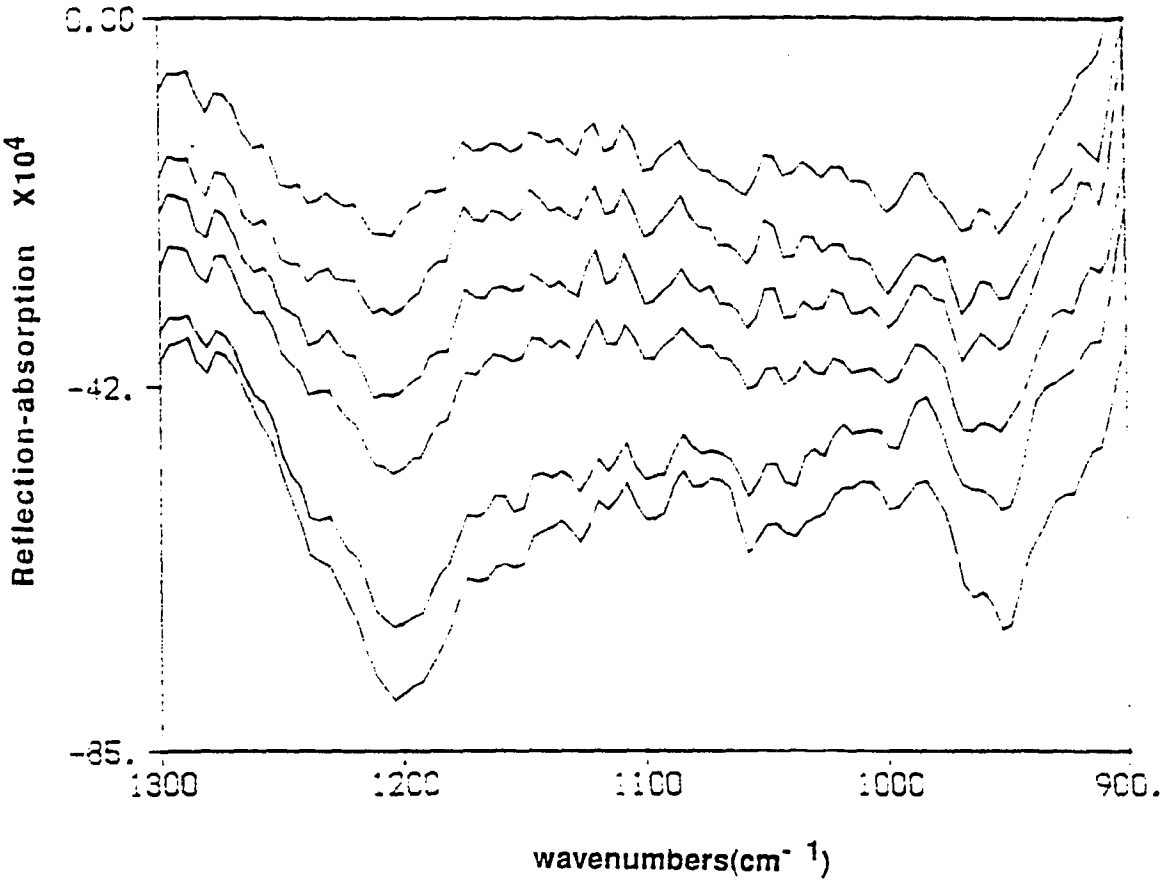


**Fig. 4.3.3 (b). RA spectra of the adsorbed monolayers of $C_{12}HS$ at the air /water interface in pure $H_2O$ at 30° incidence angle and *s*-polarization (the S-O stretching region)**
**From top to bottom:**

| surfactant concentration | logC |
|---|---|
| $1.75X10^{-3}$ M | -2.75 |
| $2.50X10^{-3}$ M | -2.60 |
| $3.50X10^{-3}$ M | -2.45 |
| $5.00X10^{-3}$ M | -2.30 |
| $7.00X10^{-3}$ M | -2.15 |
| $1.00X10^{-2}$ M | -2.00 |

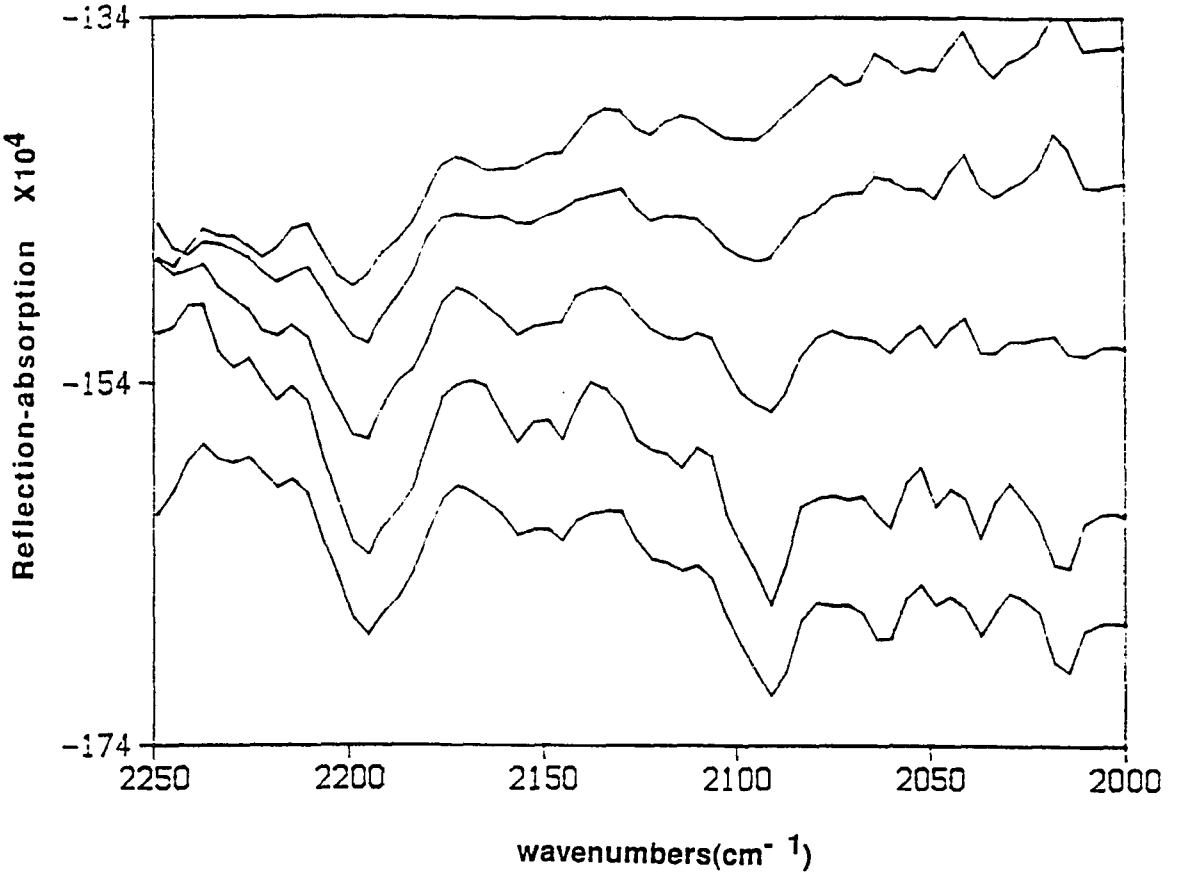


**Fig. 4.3.4 (a). RA spectra of the adsorbed monolayers of $C_{12}DS$ at the air/water interface in pure $H_2O$ at 30° incidence angle and *s*-polarization (the C-D stretching region)**
**From top to bottom:**

| surfactant concentration | logC |
|---|---|
| $1.00X10^{-3}$ M | -3.00 |
| $2.00X10^{-3}$ M | -2.70 |
| $4.00X10^{-3}$ M | -2.40 |
| $8.00X10^{-3}$ M | -2.10 |
| $1.00X10^{-2}$ M | -2.00 |

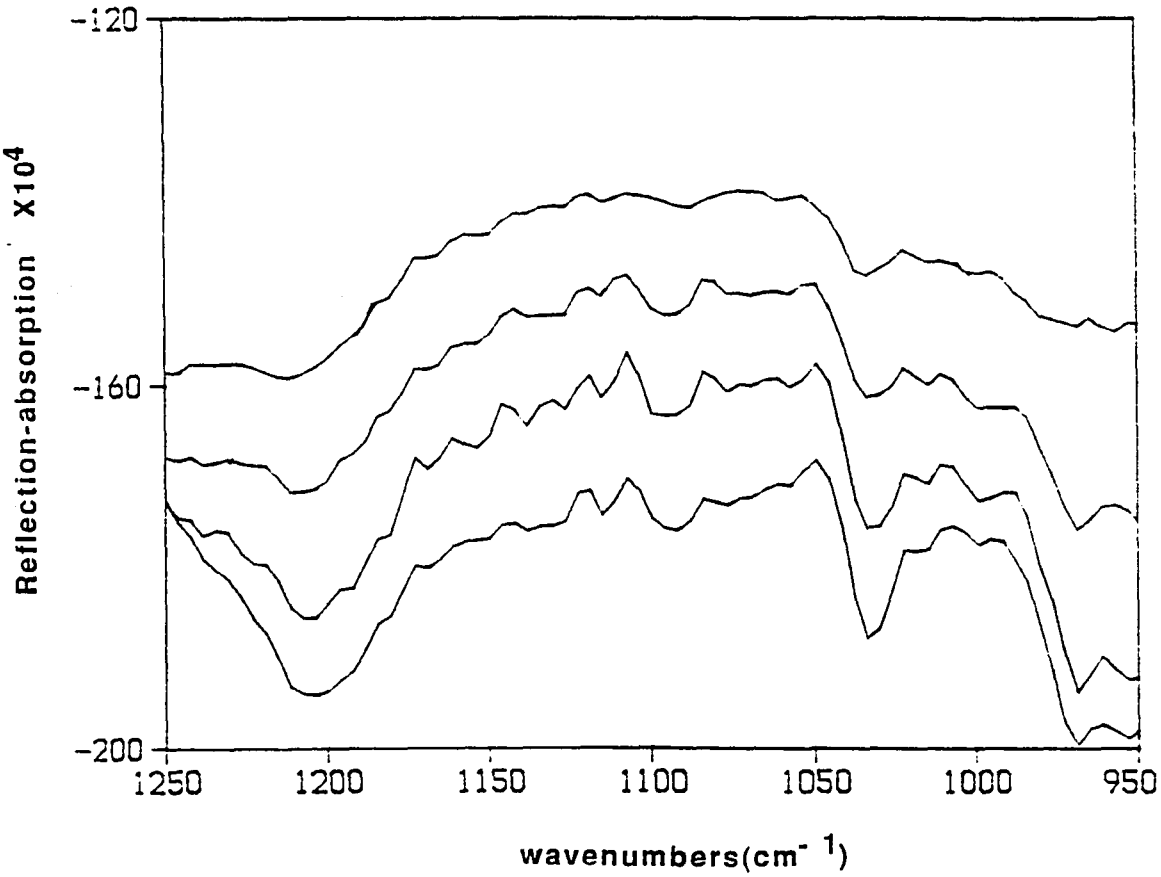


**Fig. 4.3.4 (b). RA spectra of the adsorbed monolayers of $C_{12}DS$ at the air/water interface in pure $H_2O$ at 30° incidence angle and *s*-polarization (the S-O stretching region)**
**From top to bottom:**

| surfactant concentration | logC |
|---|---|
| $2.00X10^{-3}$ M | -2.70 |
| $4.00X10^{-3}$ M | -2.40 |
| $8.00X10^{-3}$ M | -2.10 |
| $1.00X10^{-2}$ M | -2.00 |

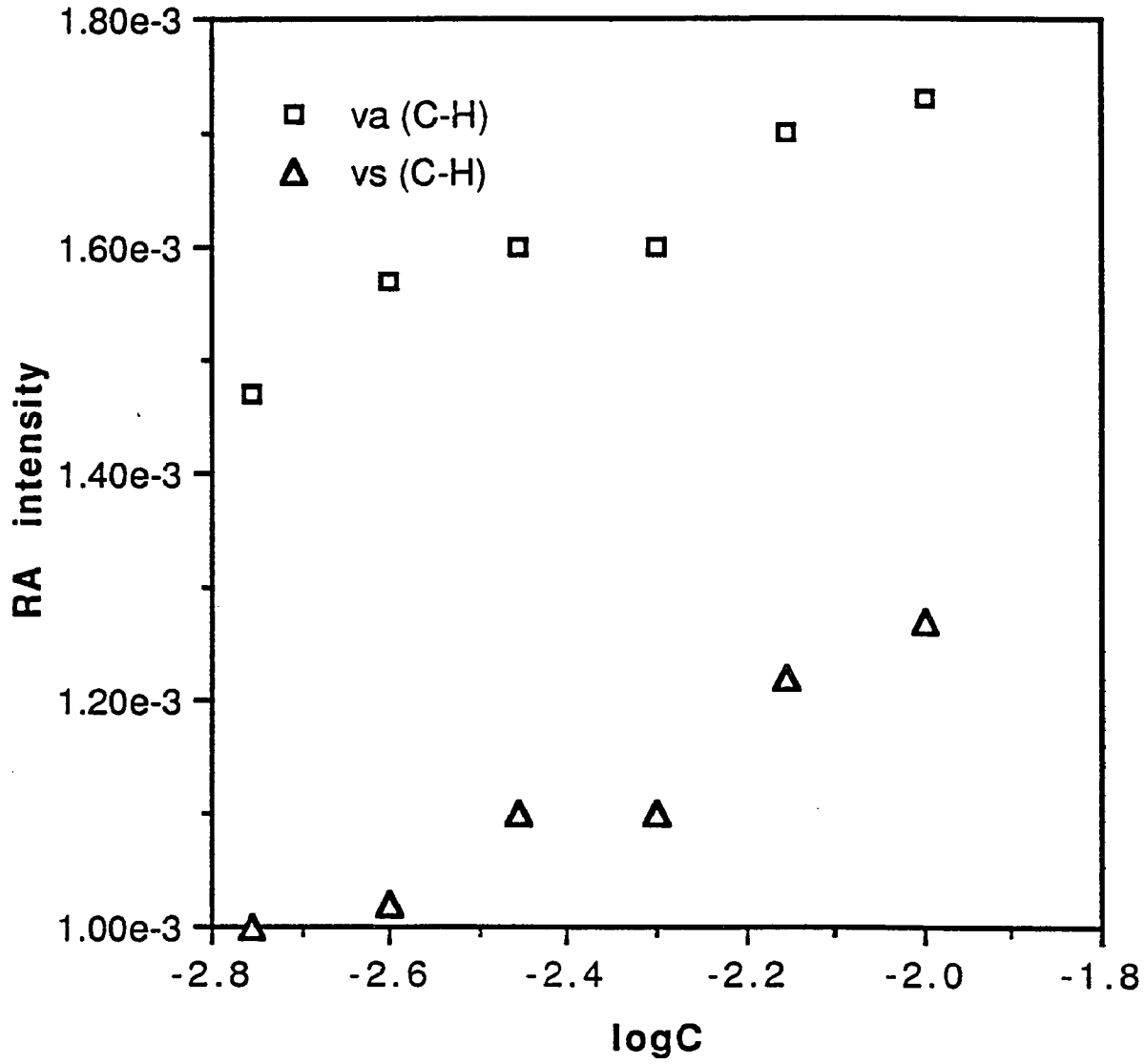


**Fig. 4.3.5. Changes in RA intensity of the adsorbed monolayers of $C_{12}HS$ at the air/water interface with different bulk concentrations in pure $H_2O$ (in the C-H stretching region).**

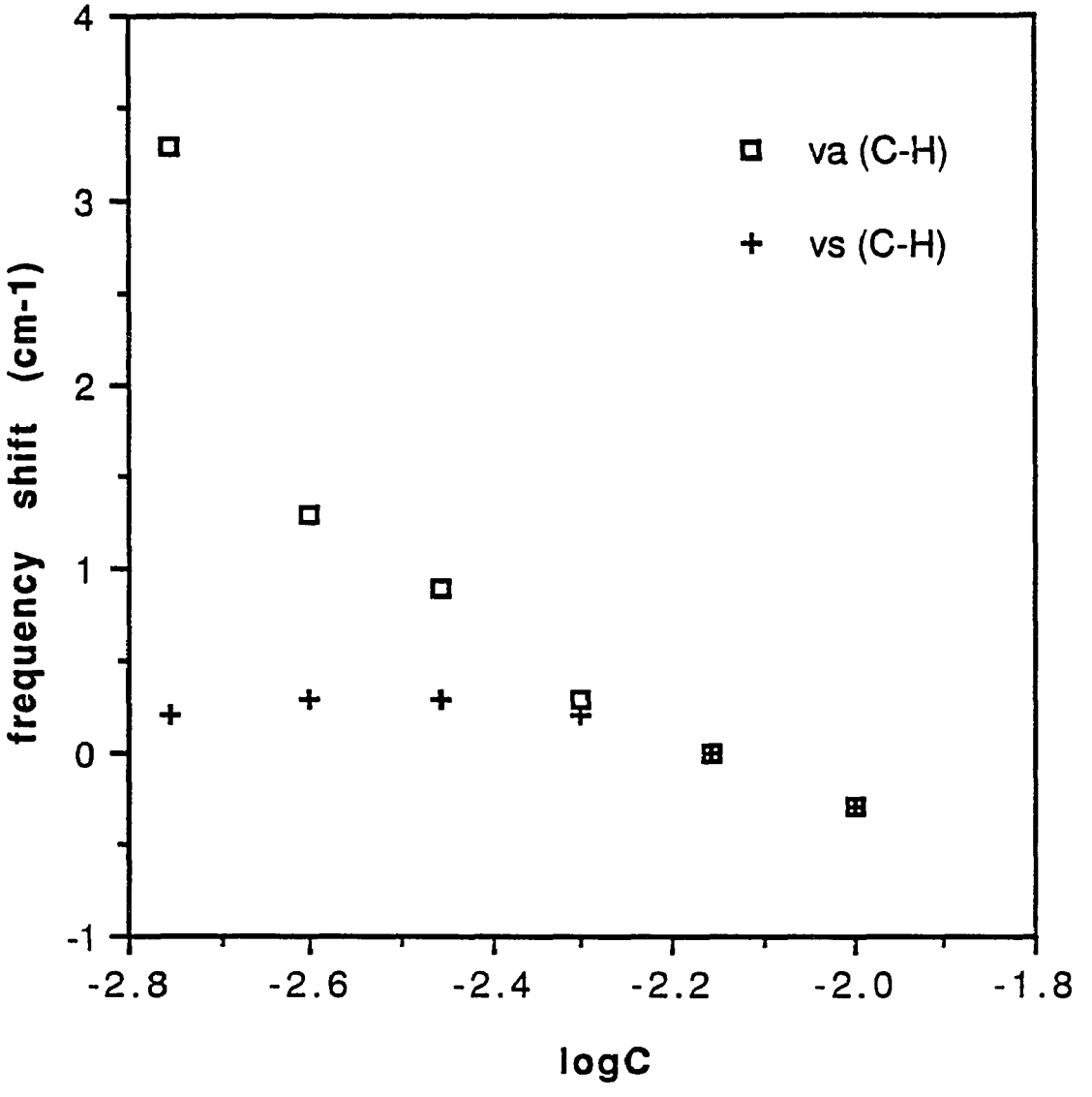


**Fig. 4.3.6. Changes in peak frequency of the adsorbed monolayers of $C_{12}HS$ at the air/water interface with various bulk concentrations in pure water (the C-H stretching region).**

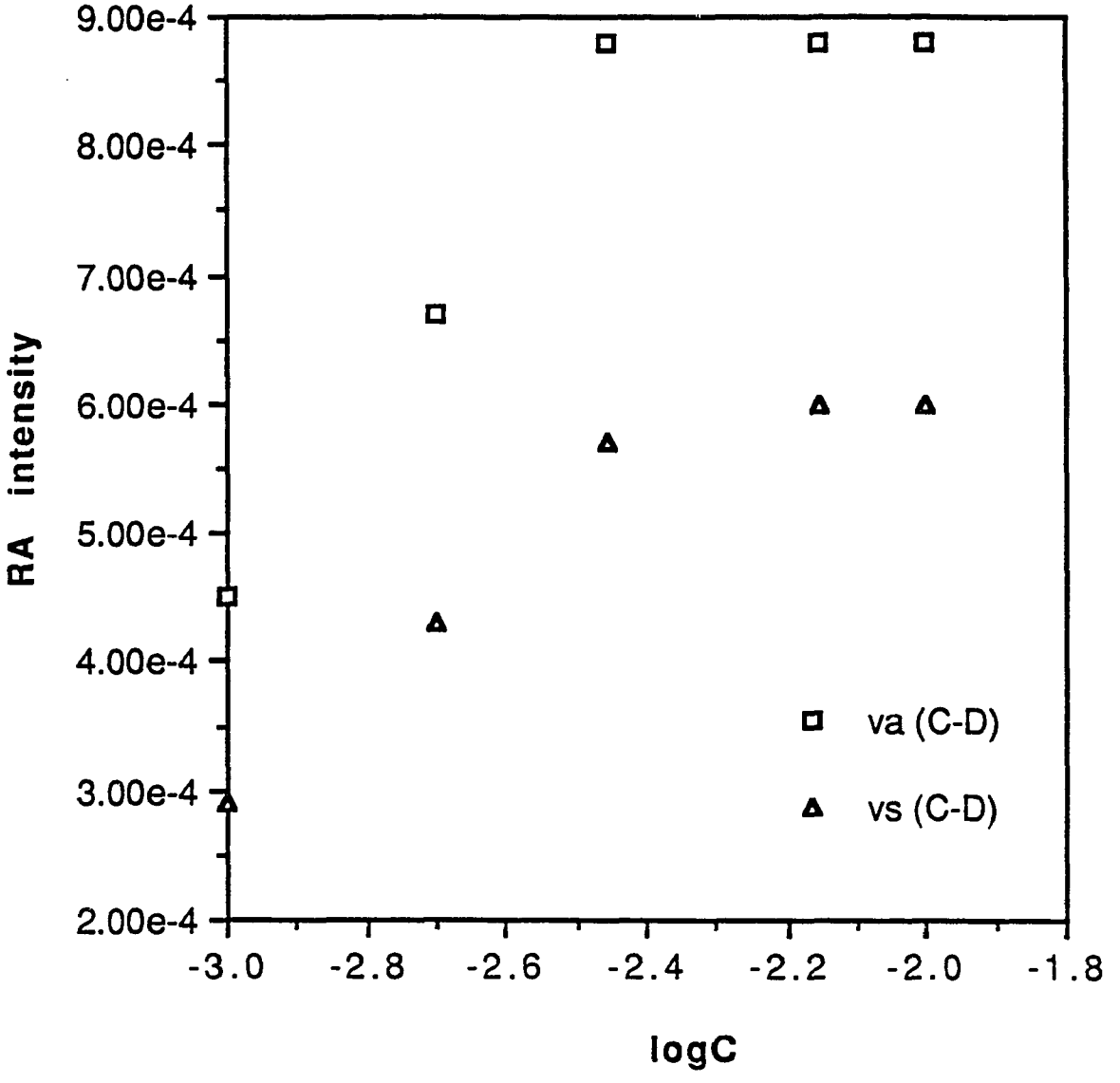


**Fig. 4.3.7. Changes in RA intensity of the adsorbed monolayers of $C_{12}DS$ at the air/water interface with different bulk concentrations in pure $H_2O$ (the C-D stretching region).**

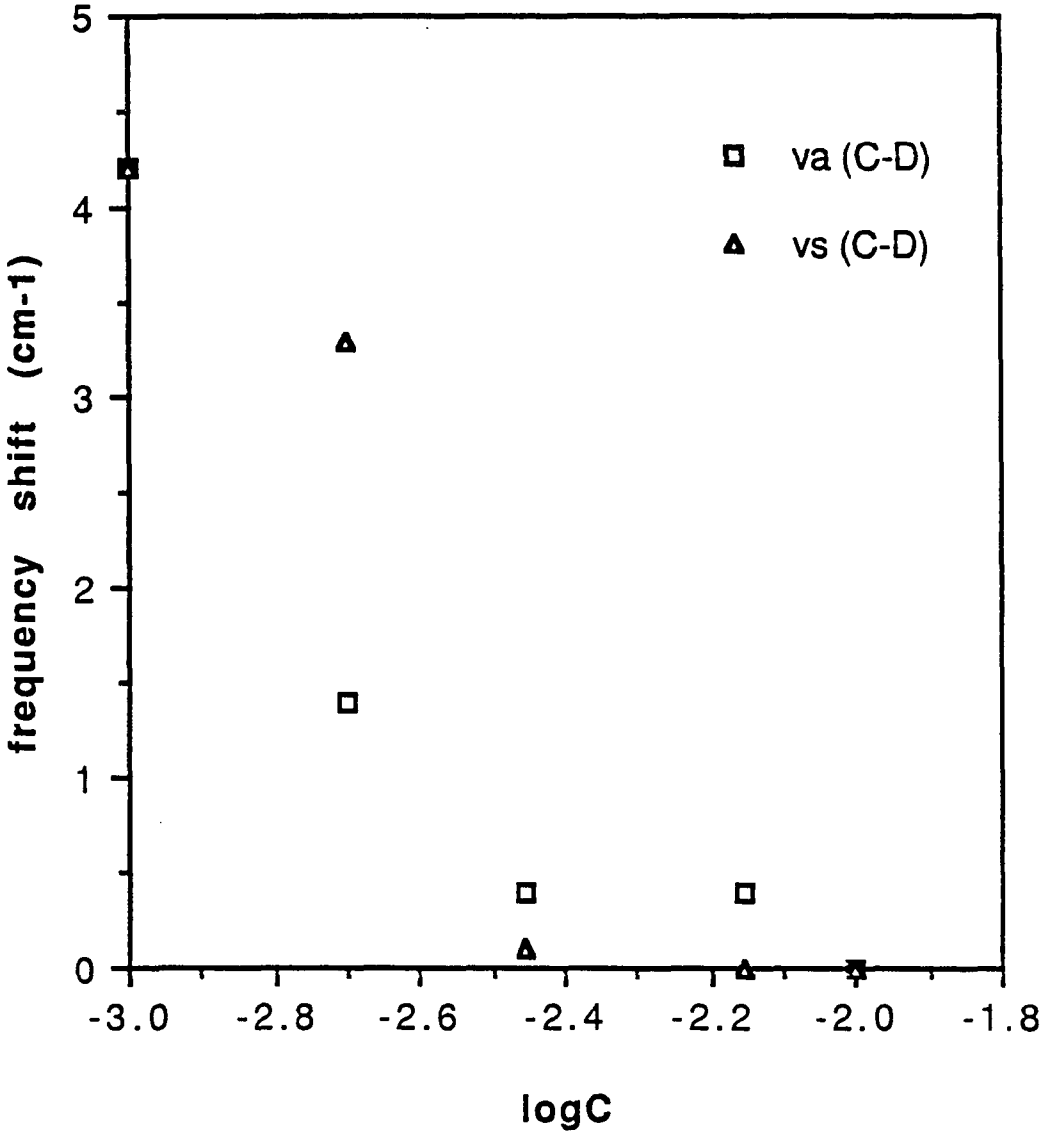


**Fig. 4.3.8. Changes in peak frequency of the adsorbed monolayers of $C_{12}DS$ at the air/water interface with various bulk concentrations in pure water (the C-D stretching region).**

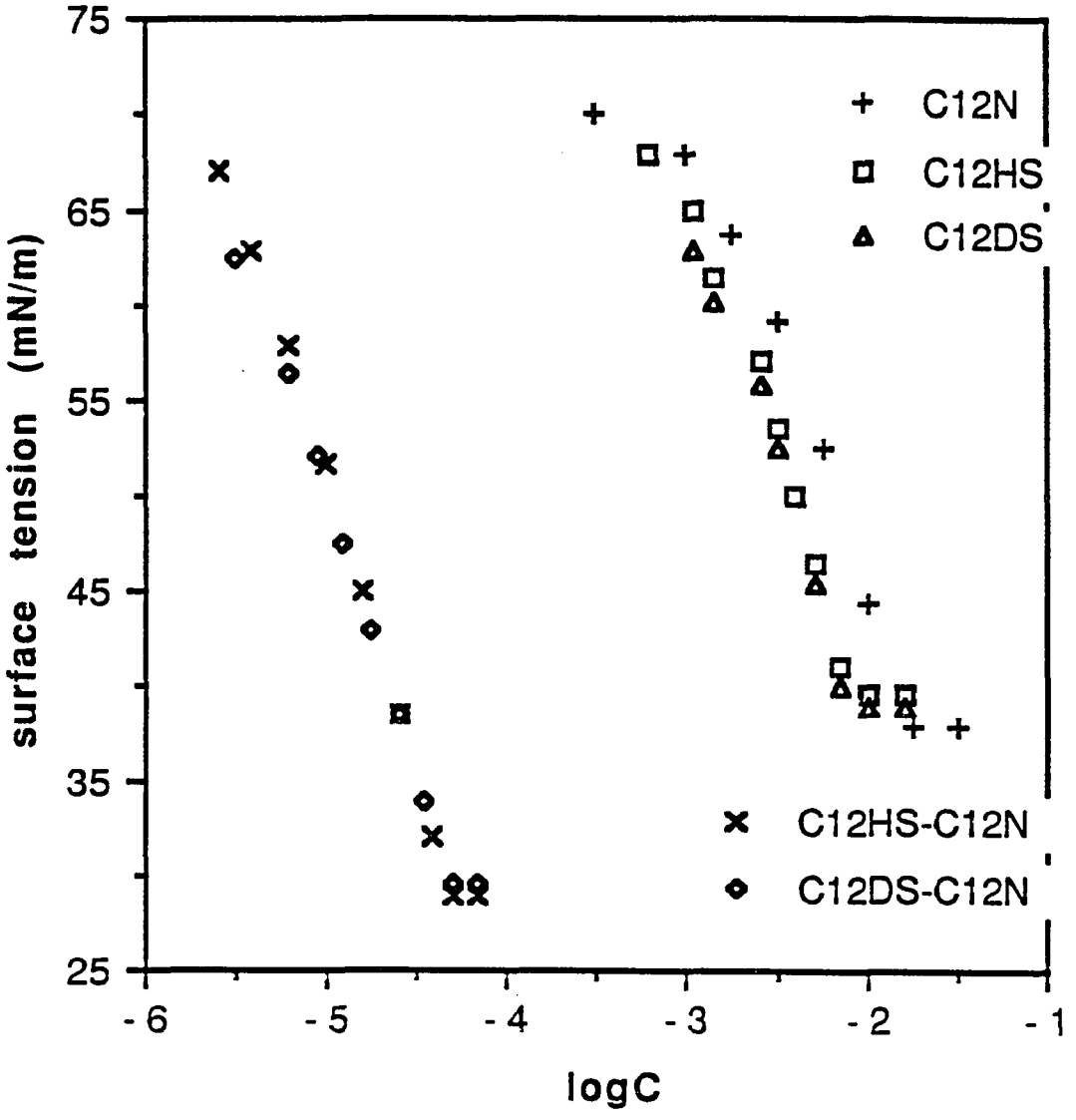


**Fig. 4.4.1(a). Surface tension vs. log of the concentration of $C_{12}HS$, $C_{12}N$, $C_{12}DS$, and equimolar mixtures $C_{12}HS$-$C_{12}N$ and $C_{12}DS$-$C_{12}N$, in water solution at 25.0°C.**

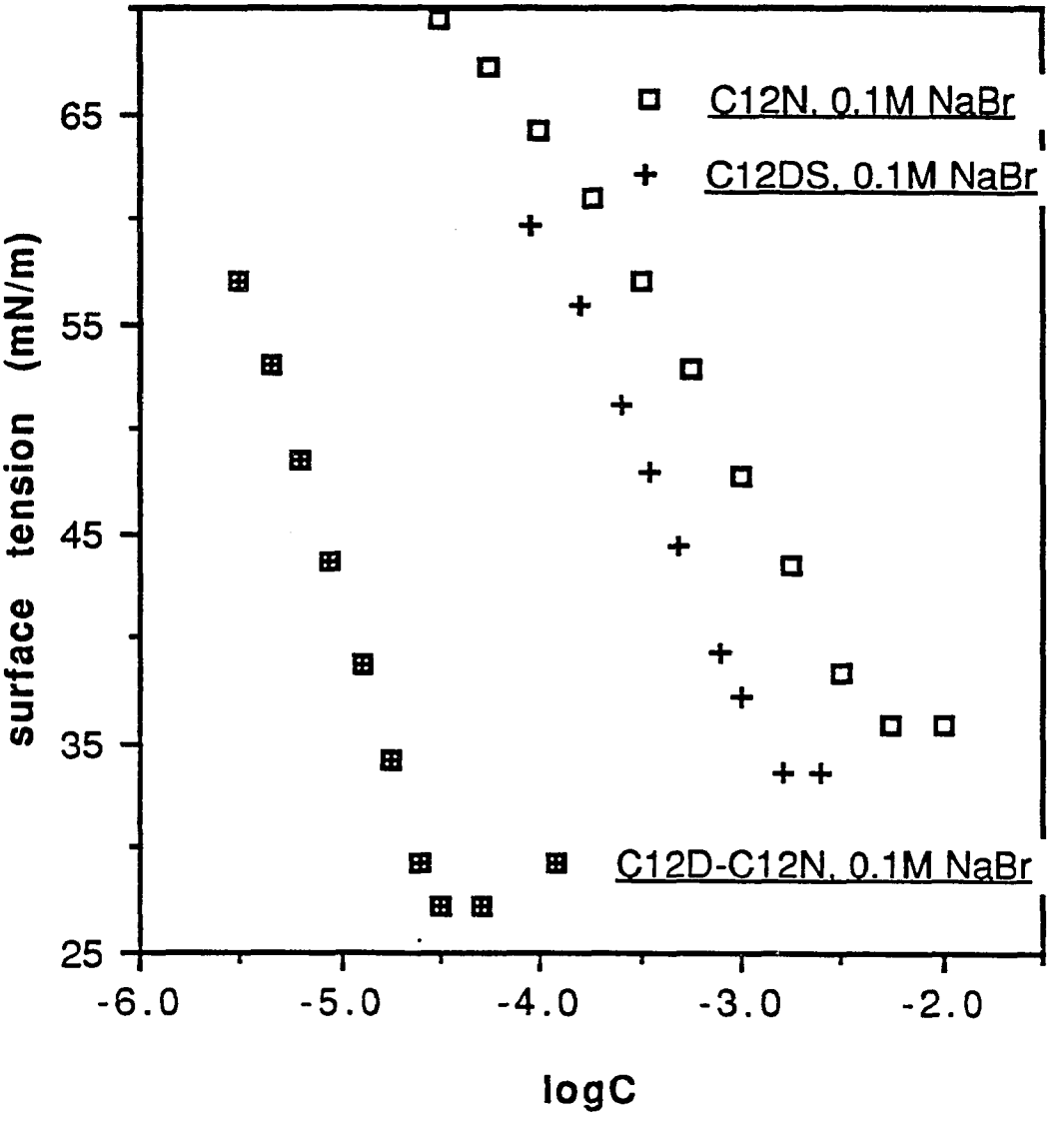


**Fig. 4.4.1(b). Surface tension vs. log of the concentration of $C_{12}N$, $C_{12}DS$, and equimolar mixture $C_{12}DS$-$C_{12}N$ in 0.1M NaBr at 25.0°C.**

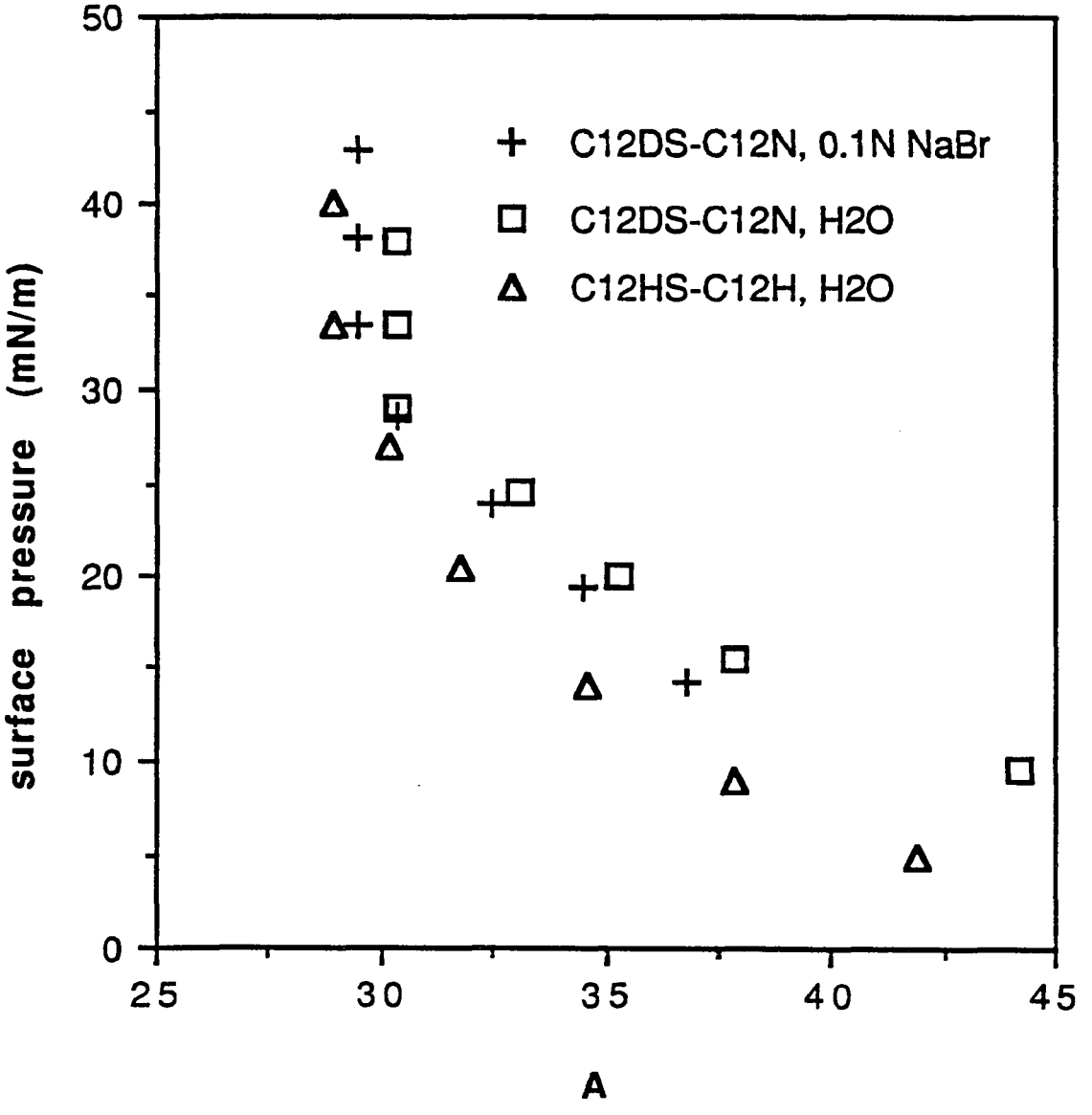


**Fig. 4.4.2. Surface pressure vs. area per molecule (A) of equimolar mixtures $C_{12}HS\text{-}C_{12}N$ and $C_{12}DS\text{-}C_{12}N$ in water and in 0.1M NaBr solution at 25.0°C.**

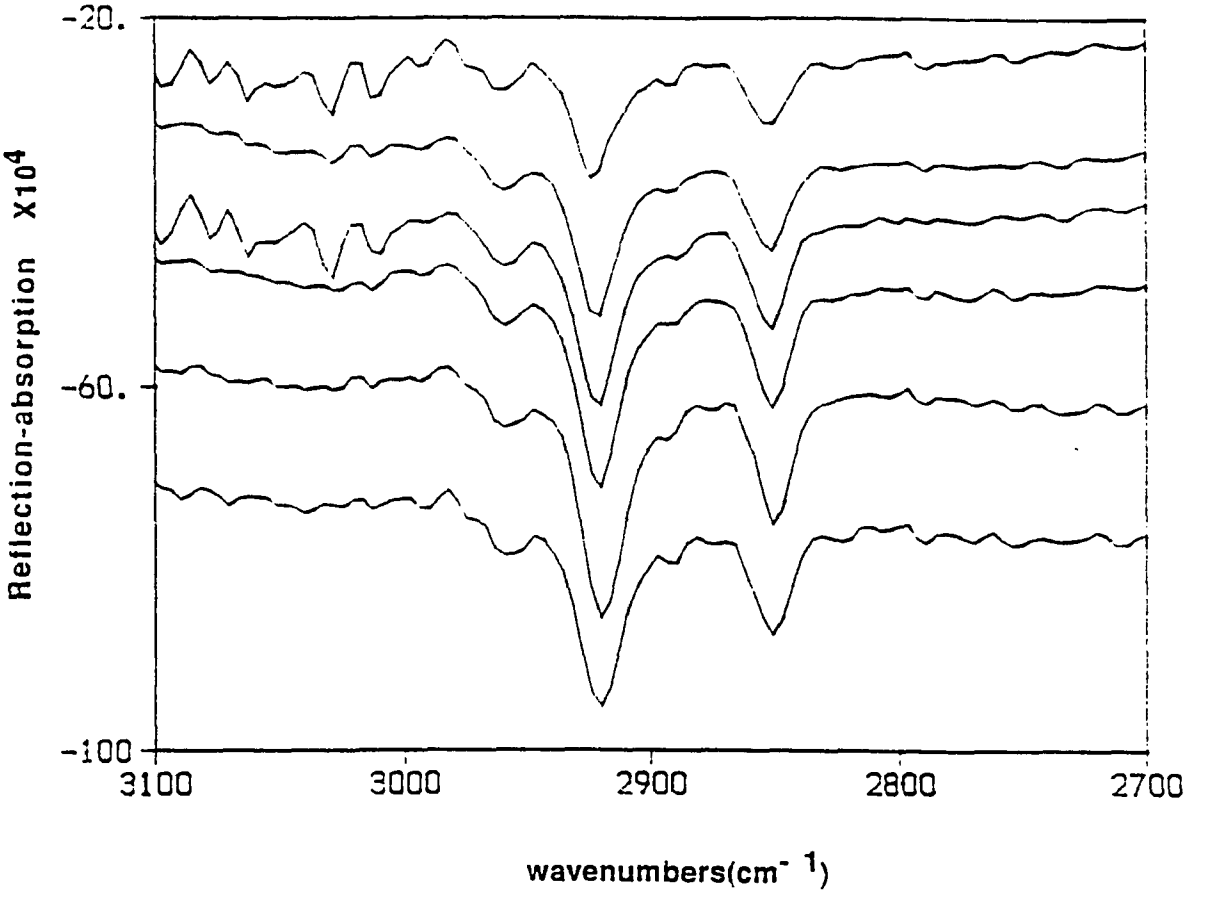


**Fig. 4.4.3. RA spectra of the adsorbed mixed monolayers of equimolar mixture $C_{12}HS$-$C_{12}N$ at the aqueous solution/air interface in pure $H_2O$ at 30° incidence angle and *s*-polarization (the C-H stretching region)**
**From top to bottom:**

| surfactant concentration | logC |
|---|---|
| $2.50X10^{-6}$ M | -5.60 |
| $5.00X10^{-6}$ M | -5.30 |
| $1.00X10^{-5}$ M | -5.00 |
| $2.00X10^{-5}$ M | -4.70 |
| $4.00X10^{-5}$ M | -4.40 |
| $5.00X10^{-5}$ M | -4.30 |

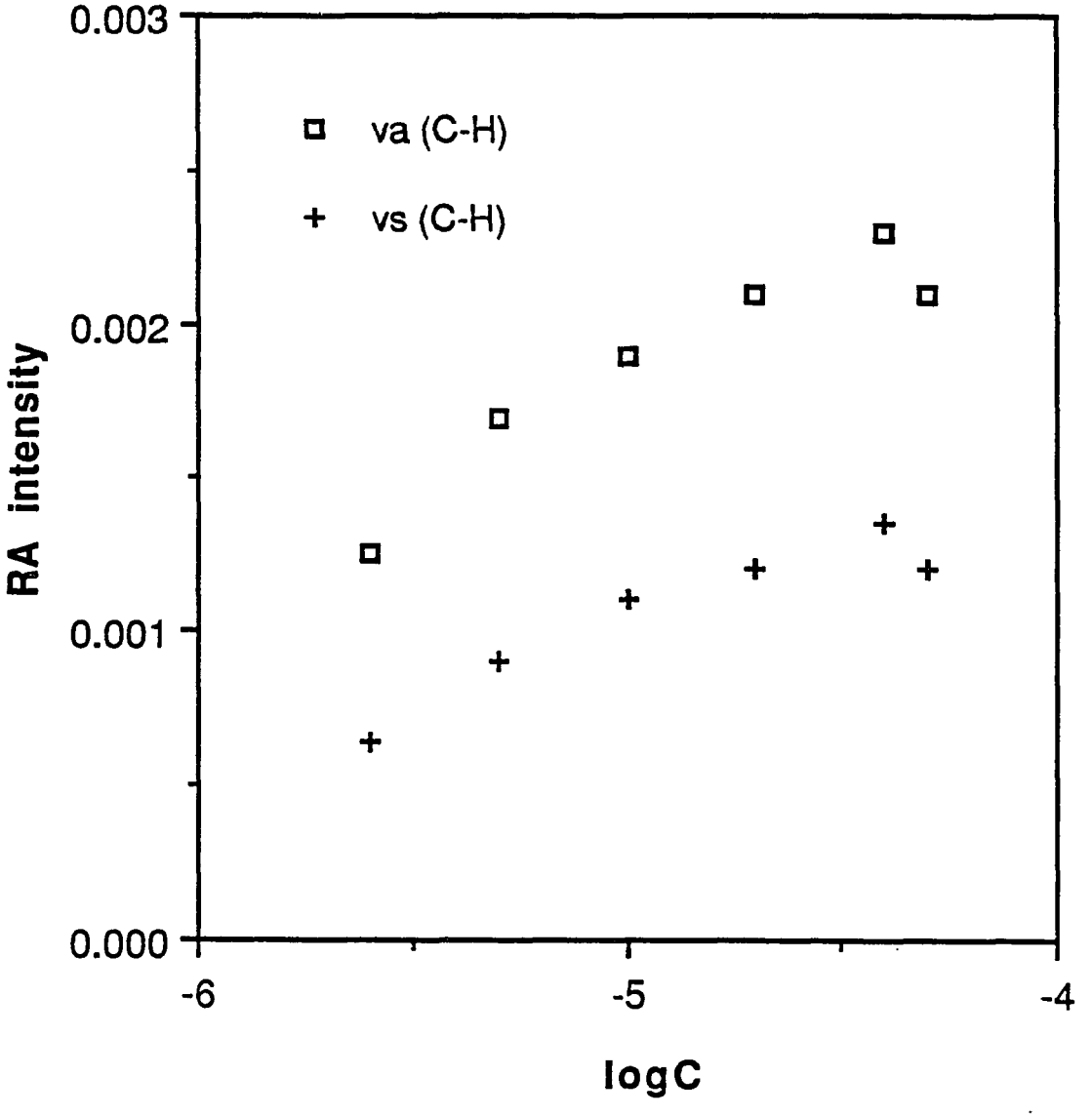


**Fig. 4.4.4. Changes in RA intensity of the adsorbed mixed monolayers of equimolar mixture $C_{12}HS$-$C_{12}N$ at the air/water interface with different bulk concentrations in pure $H_2O$ (the C-H stretching region).**

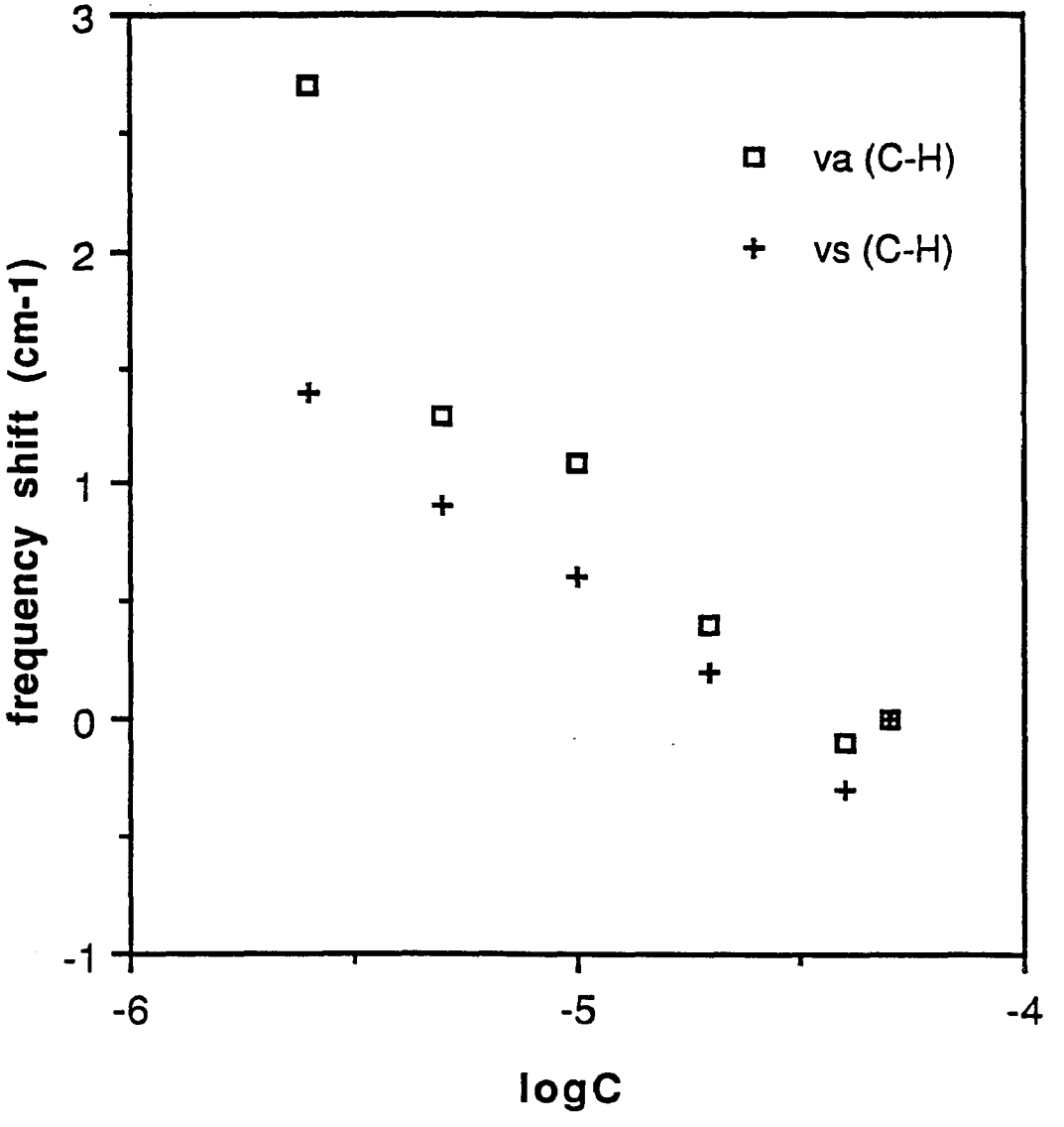


**Fig. 4.4.5. Changes in peak frequency of the C-H stretching modes in the adsorbed mixed monolayers of equimolar mixture $C_{12}HS$-$C_{12}N$ at the aqueous solution/air interface with various bulk concentrations in water.**

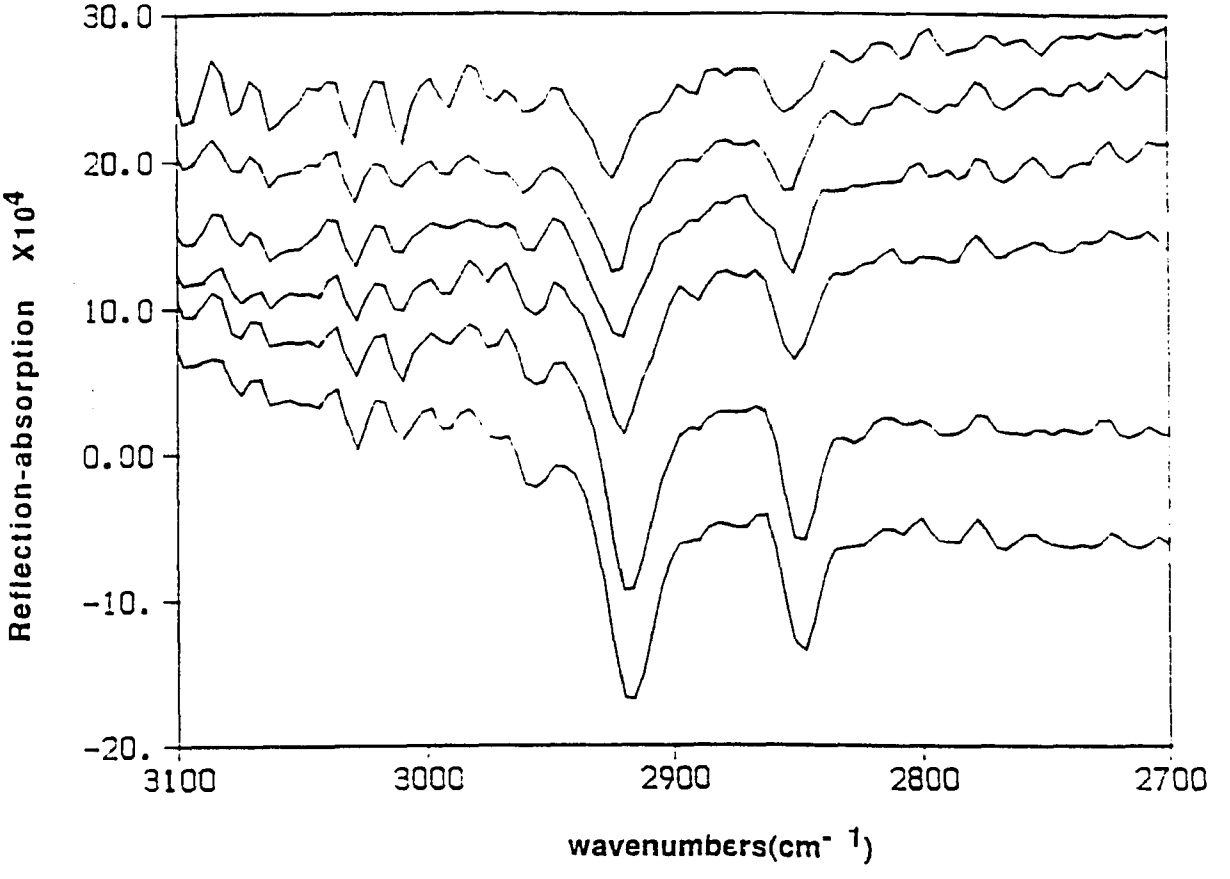


**Fig. 4.4.6(a). RA spectra of the adsorbed mixed monolayers of equimolar mixture $C_{12}DS$-$C_{12}N$ at the aqueous solution/air interface in pure $H_2O$ at 30° incidence angle and *s*-polarization (the C-H stretching bands)**
**From top to bottom:**

| surfactant concentration | logC |
|---|---|
| 2.50X10-$^{6}$ M | -5.60 |
| 5.00X10$^{-6}$ M | -5.30 |
| 1.00X10$^{-5}$ M | -5.00 |
| 2.00X10$^{-5}$ M | -4.70 |
| 4.00X10$^{-5}$ M | -4.40 |
| 5.00X10$^{-5}$ M | -4.30 |

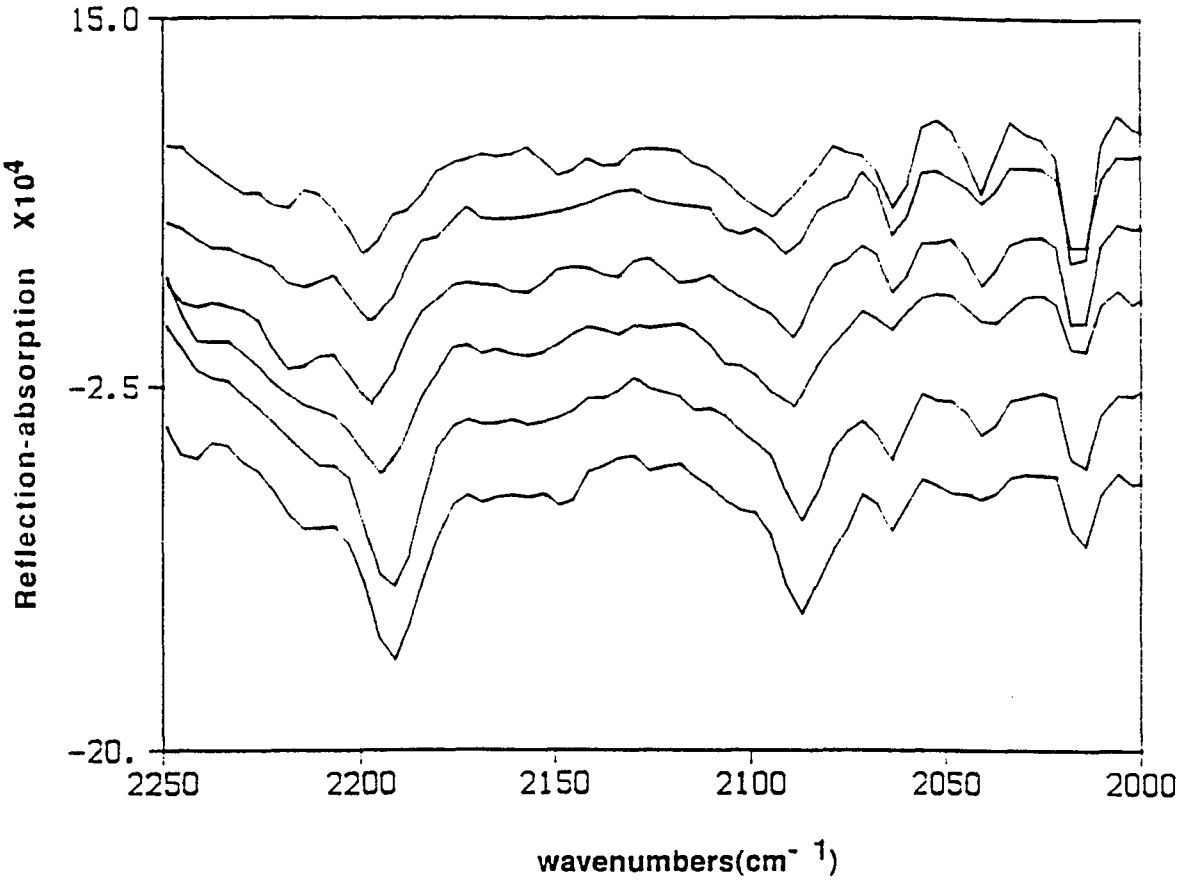


**Fig. 4.4.6(b). RA spectra of the adsorbed mixed monolayers of equimolar mixture $C_{12}DS$-$C_{12}N$ at the aqueous solution/air interface in pure $H_2O$ at 30° incidence angle and *s*-polarization (the C-D stretching bands)**
**From top to bottom:**

| surfactant concentration | logC |
|---|---|
| $2.50X10^{-6}$ M | -5.60 |
| $5.00X10^{-6}$ M | -5.30 |
| $1.00X10^{-5}$ M | -5.00 |
| $2.00X10^{-5}$ M | -4.70 |
| $4.00X10^{-5}$ M | -4.40 |
| $5.00X10^{-5}$ M | -4.30 |

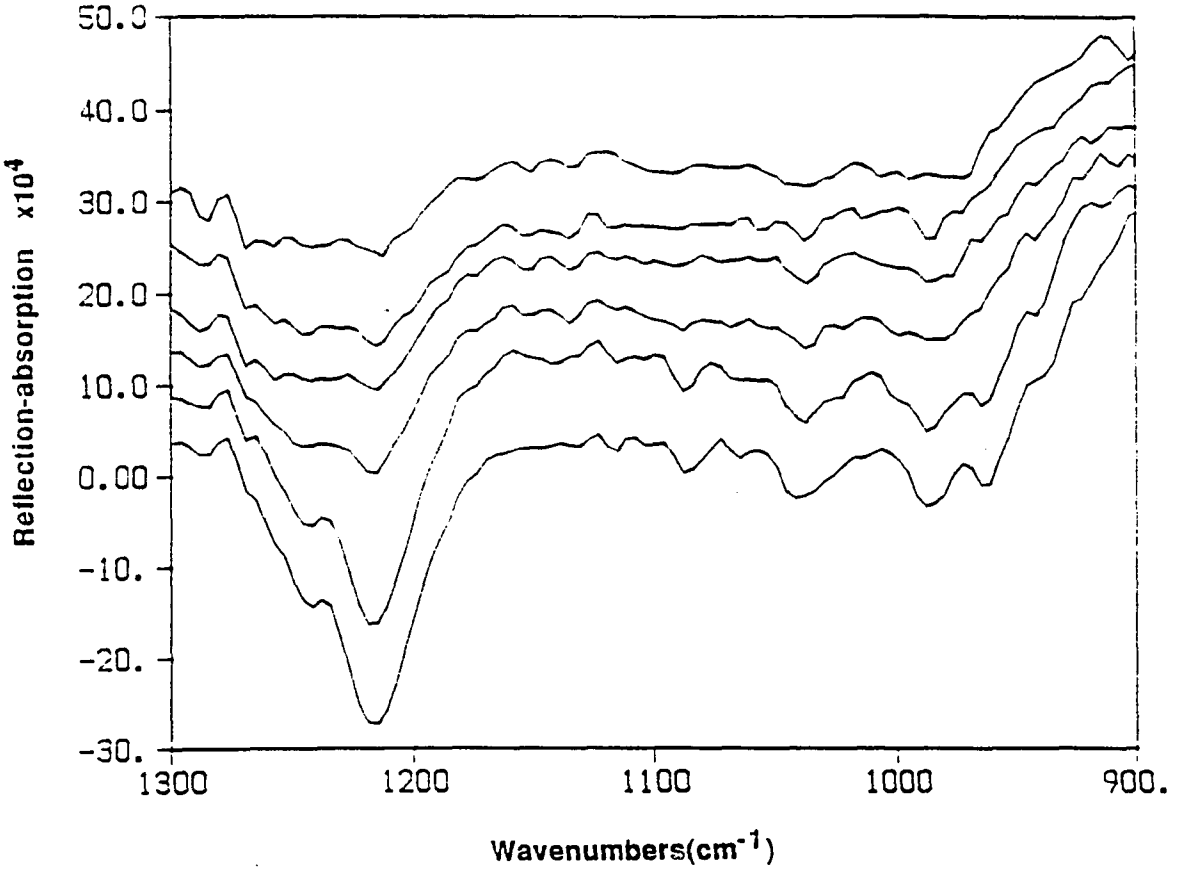


**Fig. 4.4.6(c). RA spectra of the adsorbed mixed monolayers of equimolar mixture $C_{12}DS$-$C_{12}N$ at the aqueous solution/air interface in pure $H_2O$ at 30° incidence angle and *s*-polarization (the S-O stretching bands)**
**From top to bottom:**

| surfactant concentration | logC |
|---|---|
| 2.50X10-$^6$ M | -5.60 |
| 5.00X10$^{-6}$ M | -5.30 |
| 1.00X10$^{-5}$ M | -5.00 |
| 2.00X10$^{-5}$ M | -4.70 |
| 4.00X10$^{-5}$ M | -4.40 |
| 5.00X10$^{-5}$ M | -4.30 |

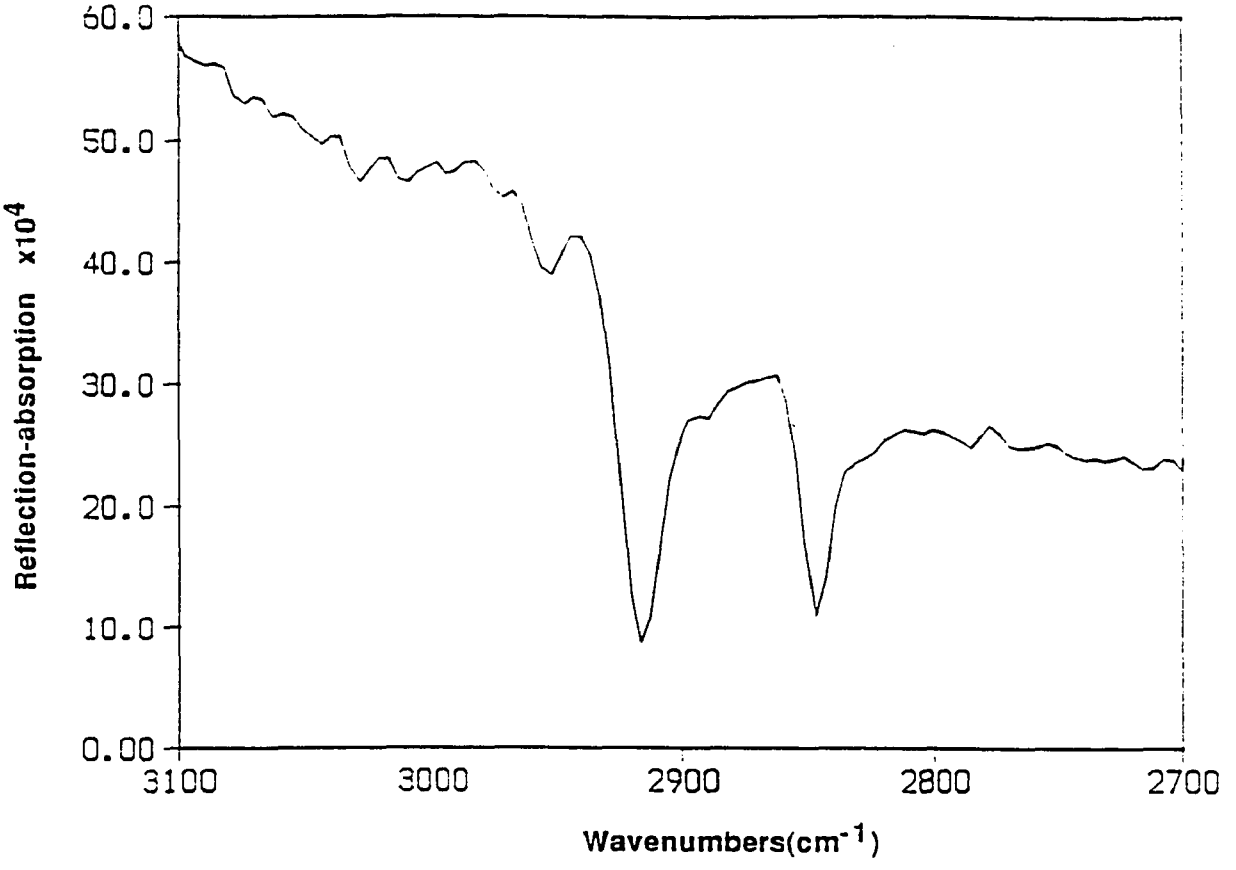


**Fig. 4.4.7(a). RA spectrum of the mixed multilayers (precipitates) of equimolar mixture $C_{12}DS$-$C_{12}N$ (bulk concentration, C = $6.0X10^{-5}$M) at the aqueous solution/air interface in pure $H_2O$ at 30° incidence angle and *s*-polarization (the C-H stretching bands).**

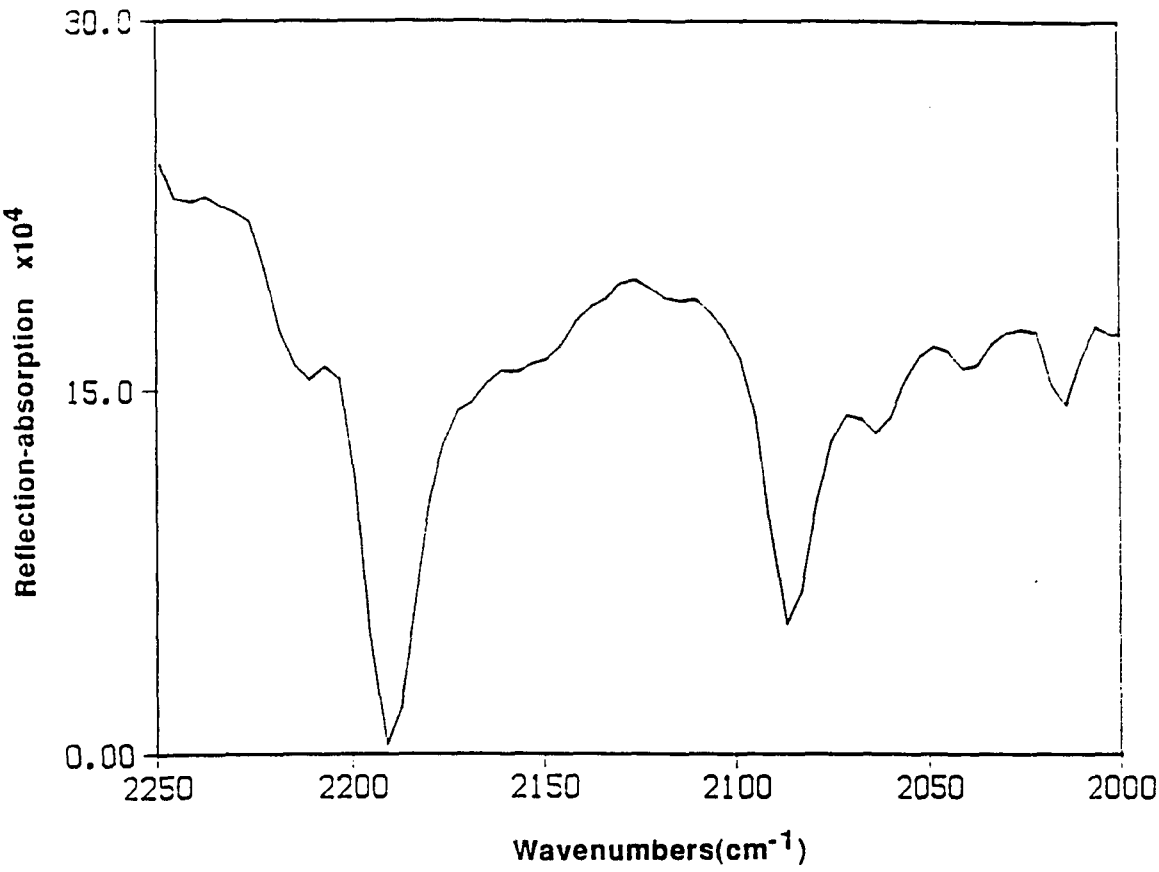


**Fig. 4.4.7(b). RA spectrum of the mixed multilayers (precipitates) of equimolar mixture $C_{12}DS$-$C_{12}N$ (bulk concentration, C = $6.0X10^{-5}$M) at the aqueous solution/air interface in pure $H_2O$ at 30° incidence angle and *s*-polarization (the C-D stretching bands).**

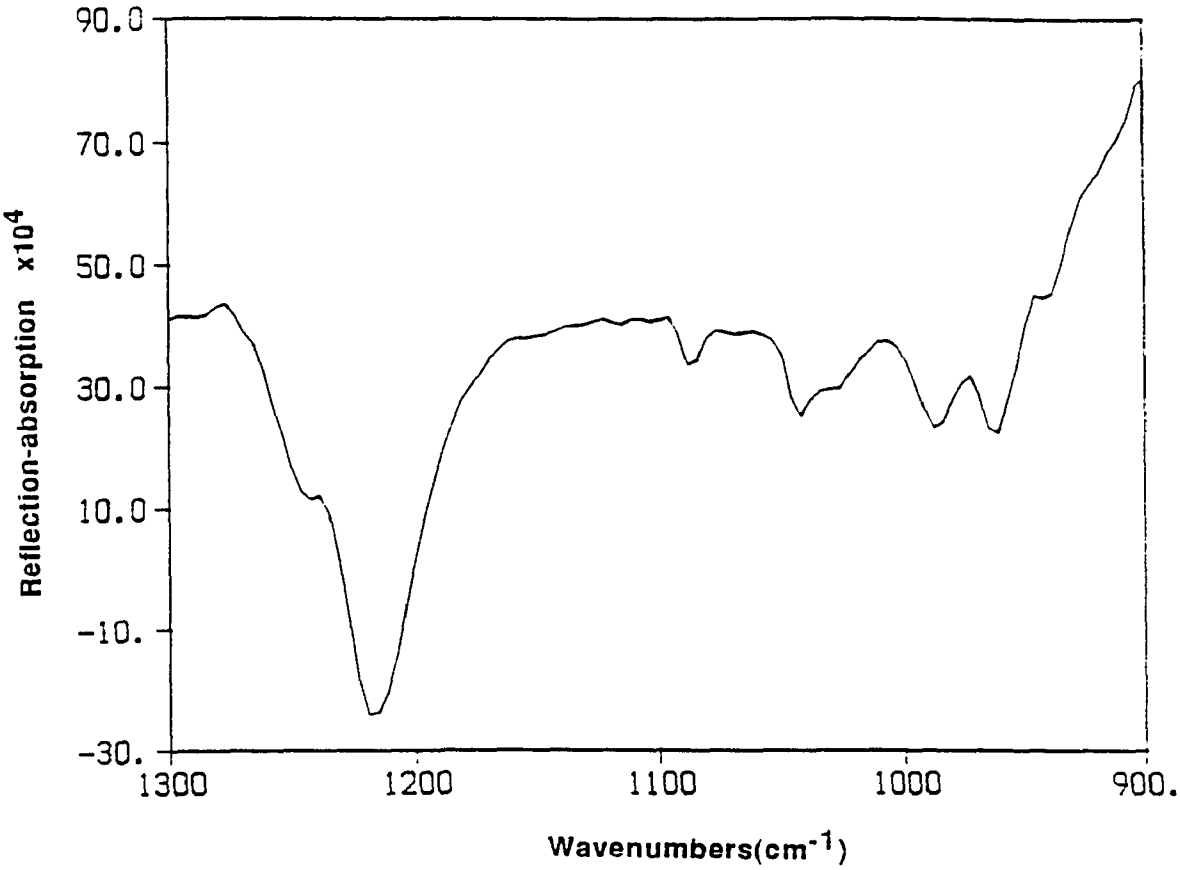


**Fig. 4.4.7(c). RA spectrum of the mixed multilayers (precipitates) of equimolar mixture $C_{12}DS$-$C_{12}N$ (bulk concentration, C = $6.0X10^{-5}$M) at the aqueous solution/air interface in pure $H_2O$ at 30° incidence angle and *s*-polarization (the S-O stretching bands).**

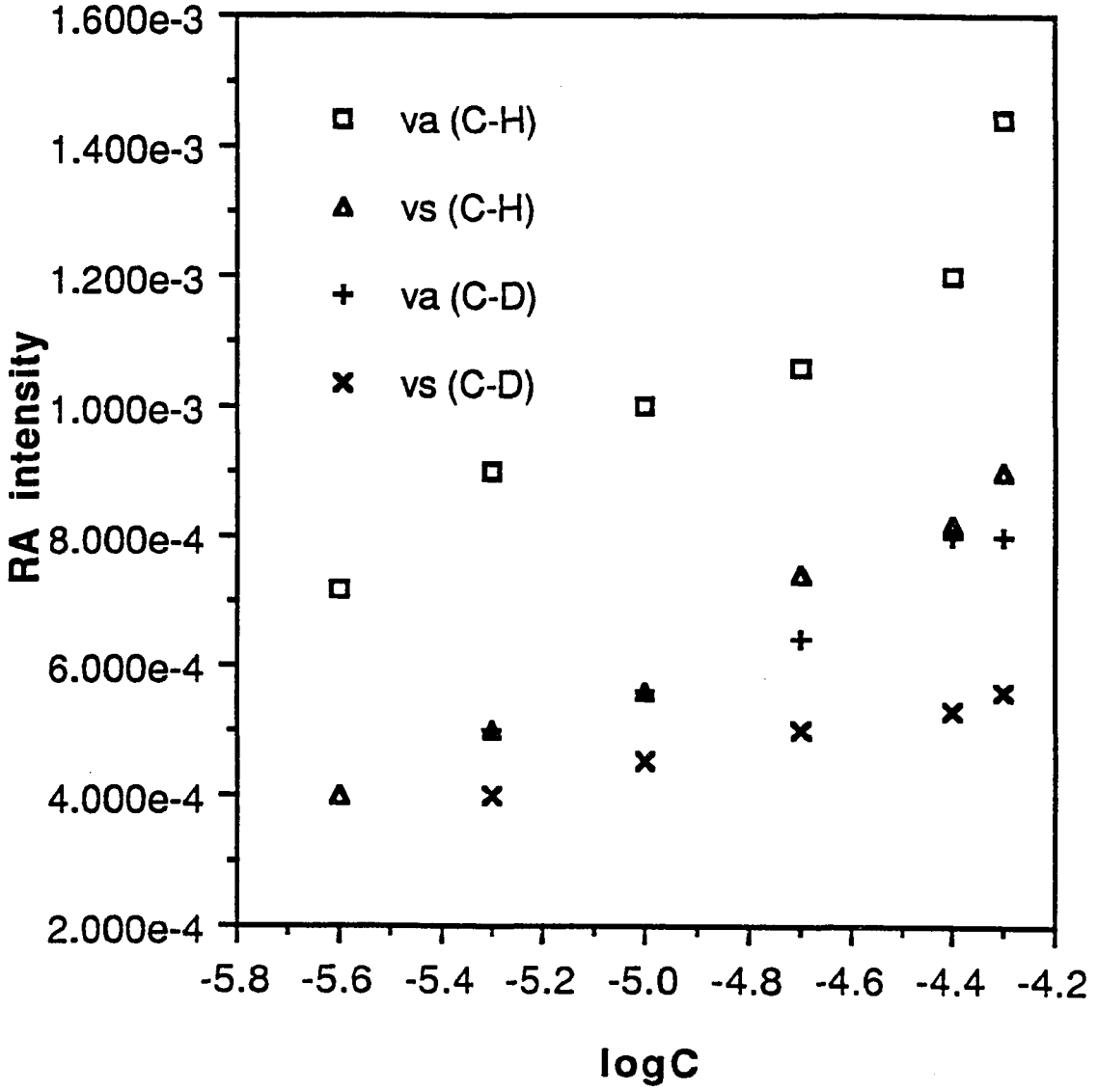


**Fig. 4.4.8. Changes in RA intensity of the adsorbed mixed monolayers of equimolar mixture $C_{12}DS$-$C_{12}N$ at the air/water interface with different bulk concentrations in pure $H_2O$ solution (the C-H and C-D stretching regions).**

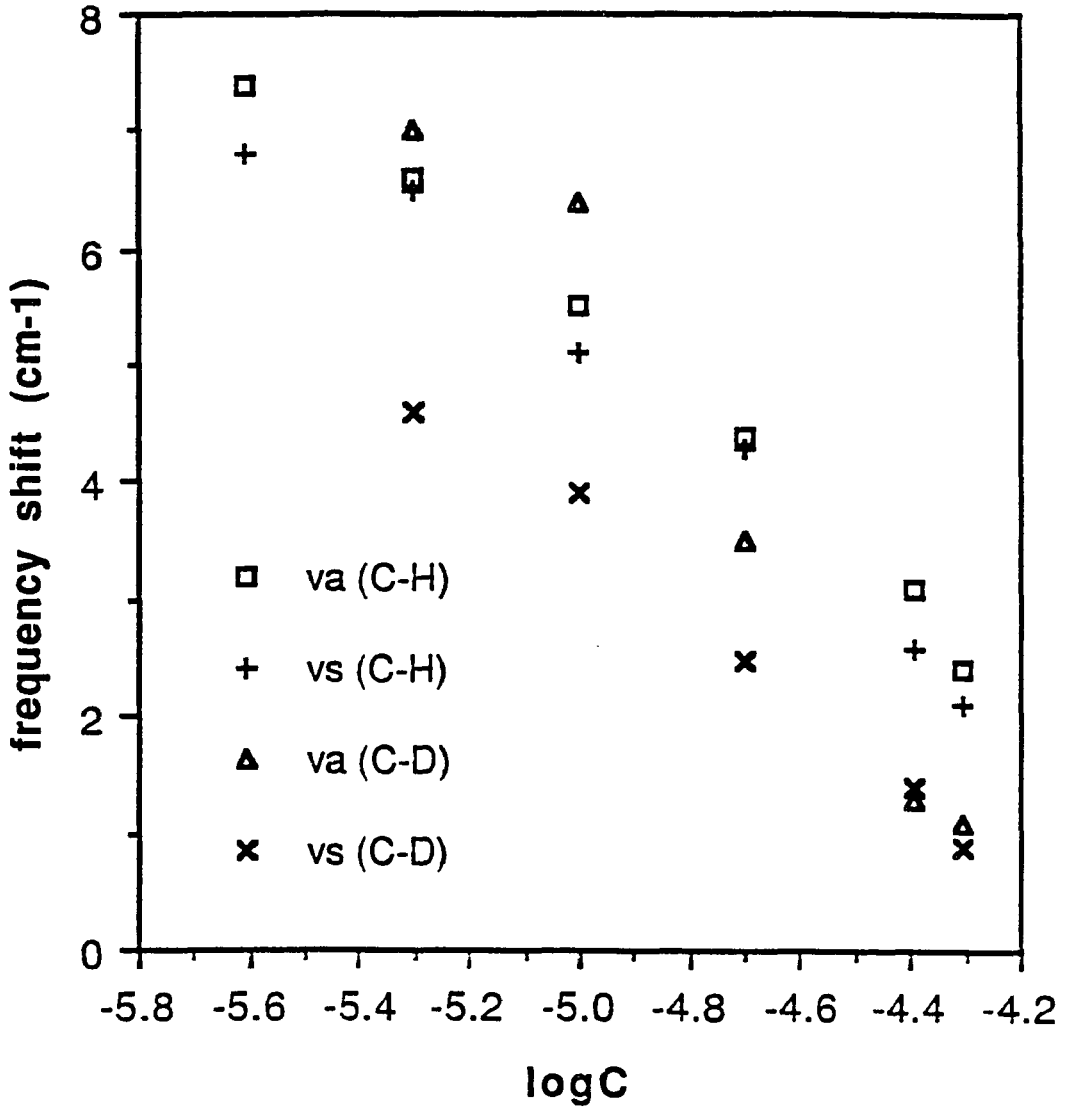


**Fig. 4.4.9. Changes in peak frequency of the adsorbed mixed monolayers of equimolar mixture $C_{12}DS$-$C_{12}N$ at the air/water interface with different bulk concentrations in pure $H_2O$ solution (the C-H and C-D stretching regions).**

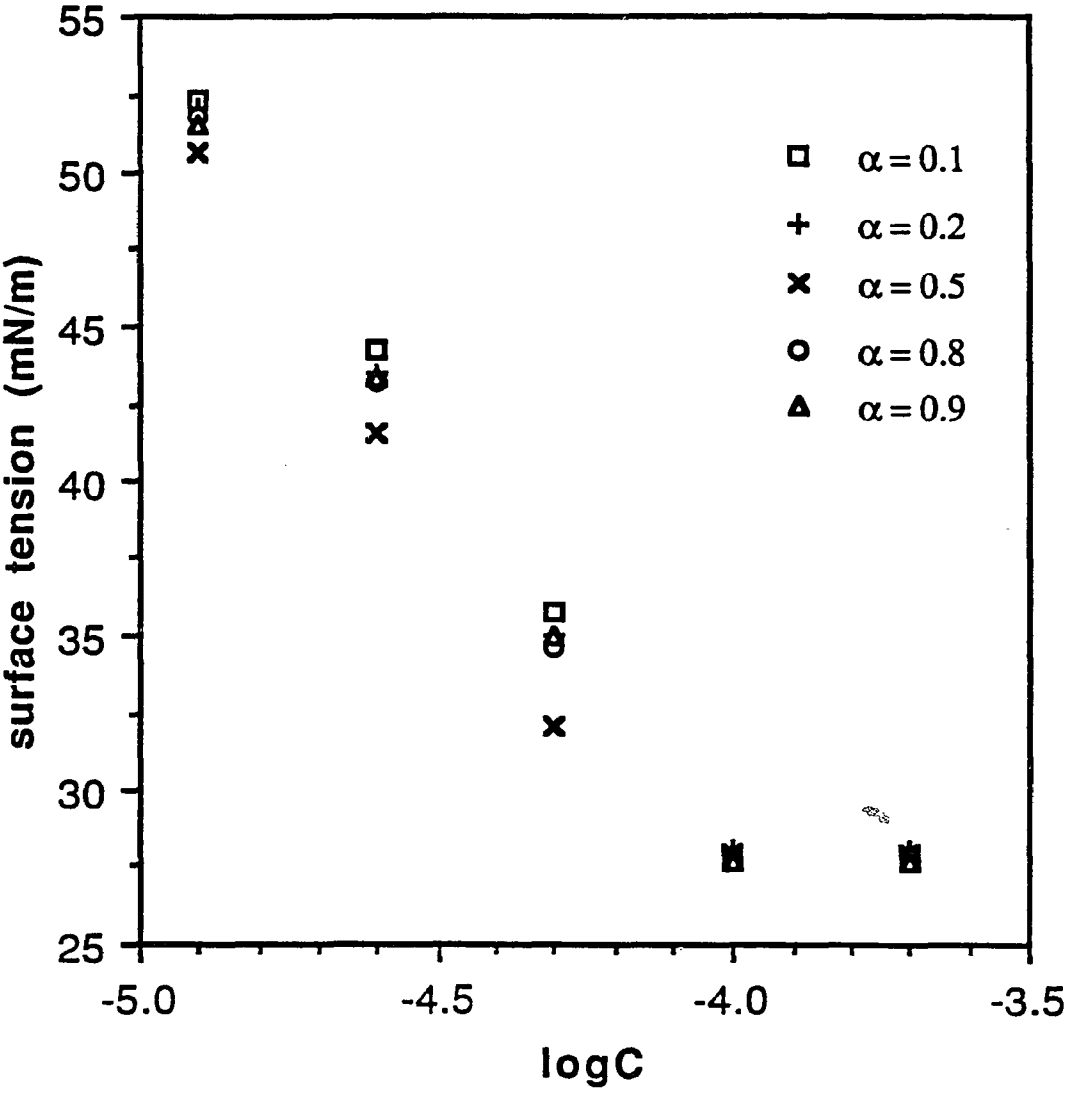


**Fig. 4.4.10. Surface tension vs. log of the total bulk concentration of $C_{12}DS$-$C_{12}N$ in water solution from different α values at 25.0°C.**

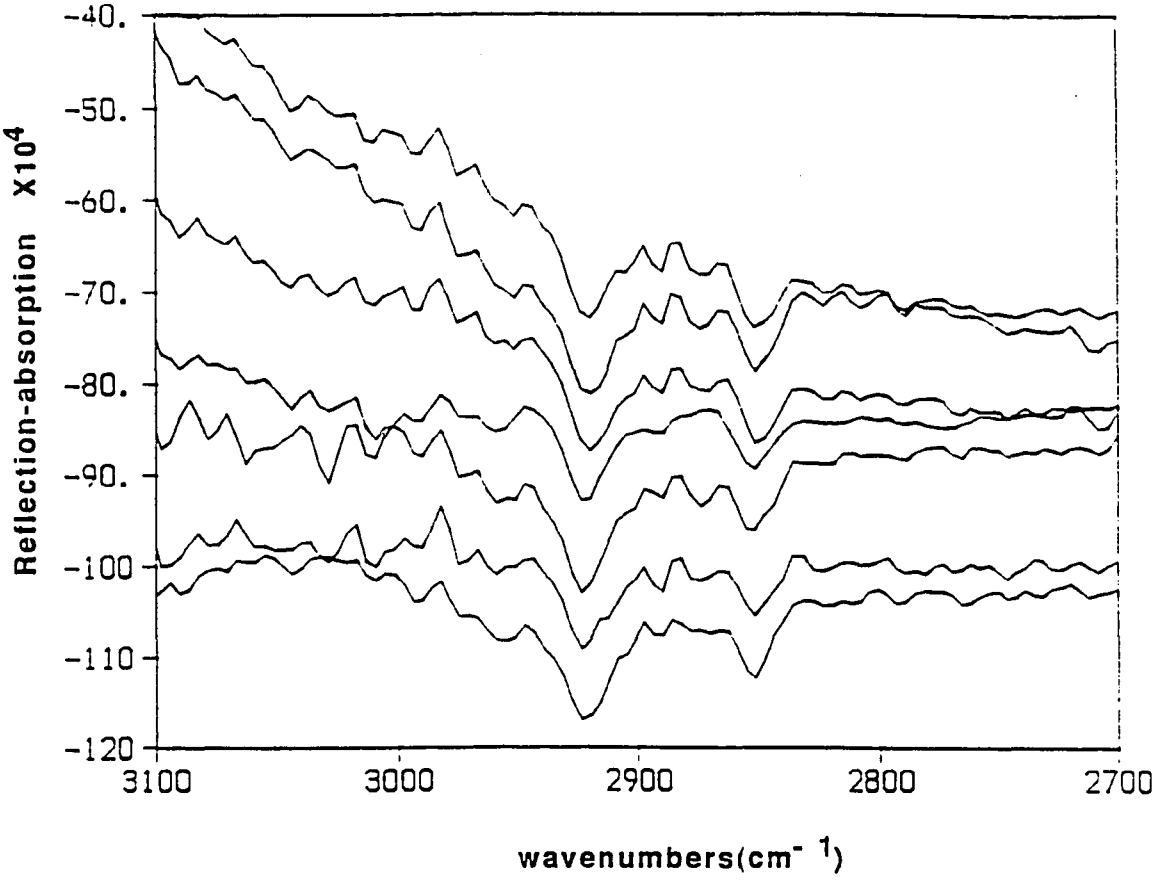


**Fig. 4.4.11(a). RA spectra of the adsorbed mixed monolayers of $C_{12}DS$-$C_{12}N$ ($C_T$ = 8.0X10$^{-5}$M) at the aqueous solution/air interface in pure $H_2O$ at 30° incidence angle and *s*-polarization with various $\alpha$ values (in the C-H stretching region). From top to bottom, $\alpha$ = 0.9, 0.8, 0.6, 0.5, 0.4, 0.2, and 0.1.**

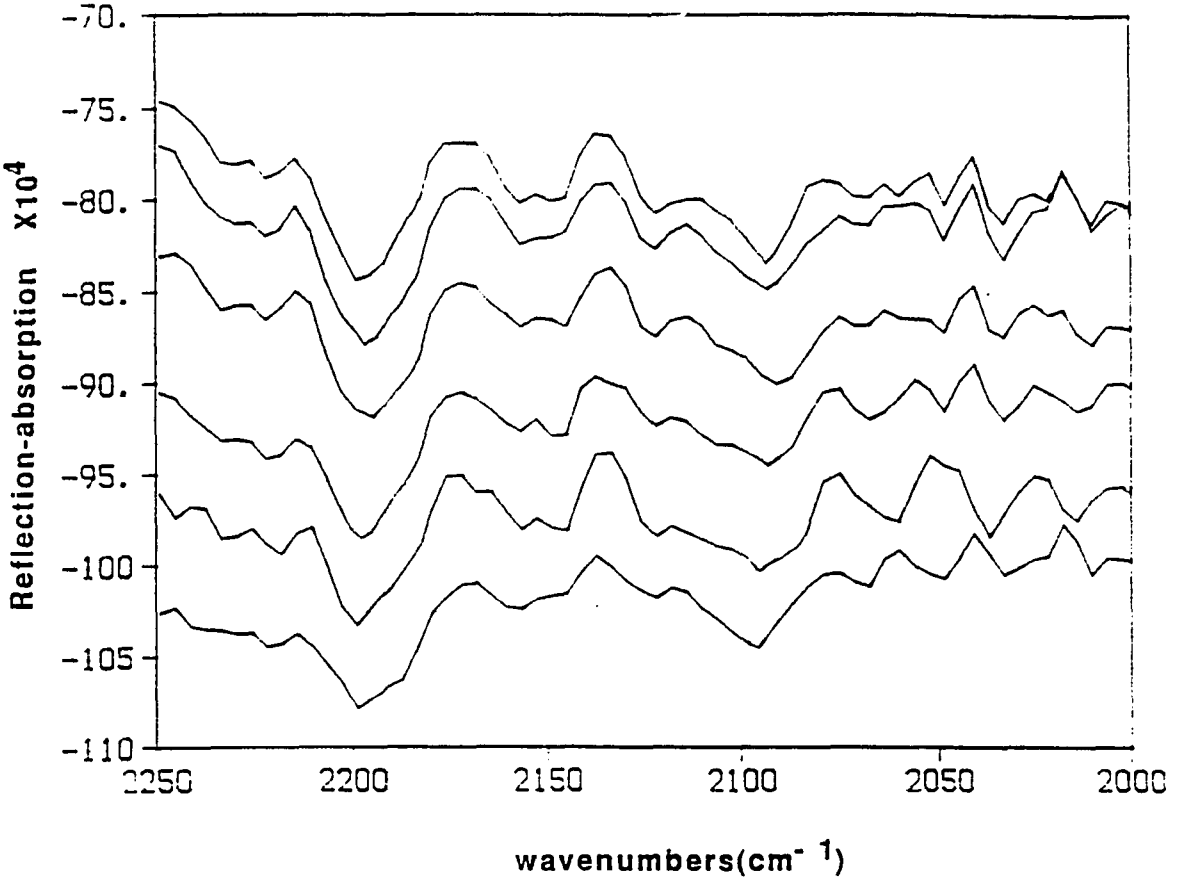


**Fig. 4.4.11(b). RA spectra of the adsorbed mixed monolayers of $C_{12}DS$-$C_{12}N$ ($C_T$ = 8.0X10$^{-5}$M) at the aqueous solution/air interface in pure $H_2O$ at 30° incidence angle and *s*-polarization with various $\alpha$ values (the C-D stretching region). From top to bottom, $\alpha$ = 0.9, 0.8, 0.6, 0.4, 0.2, and 0.1.**

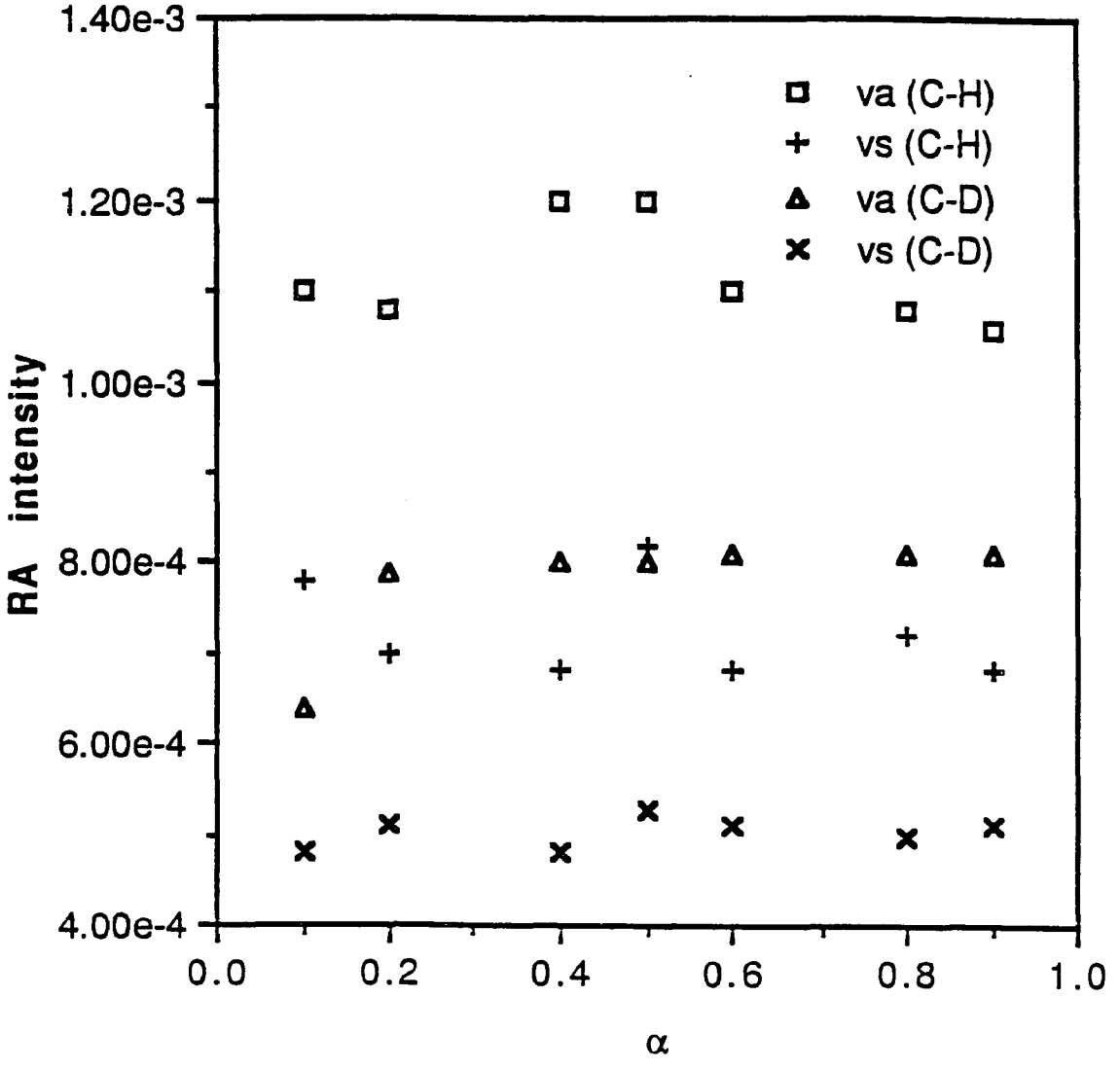


**Fig. 4.4.12. Changes in RA intensity of the adsorbed mixed monolayers of $C_{12}DS$-$C_{12}N$ at the air/water interface with different $\alpha$ values in pure $H_2O$ solution (the C-H and C-D stretching bands).**

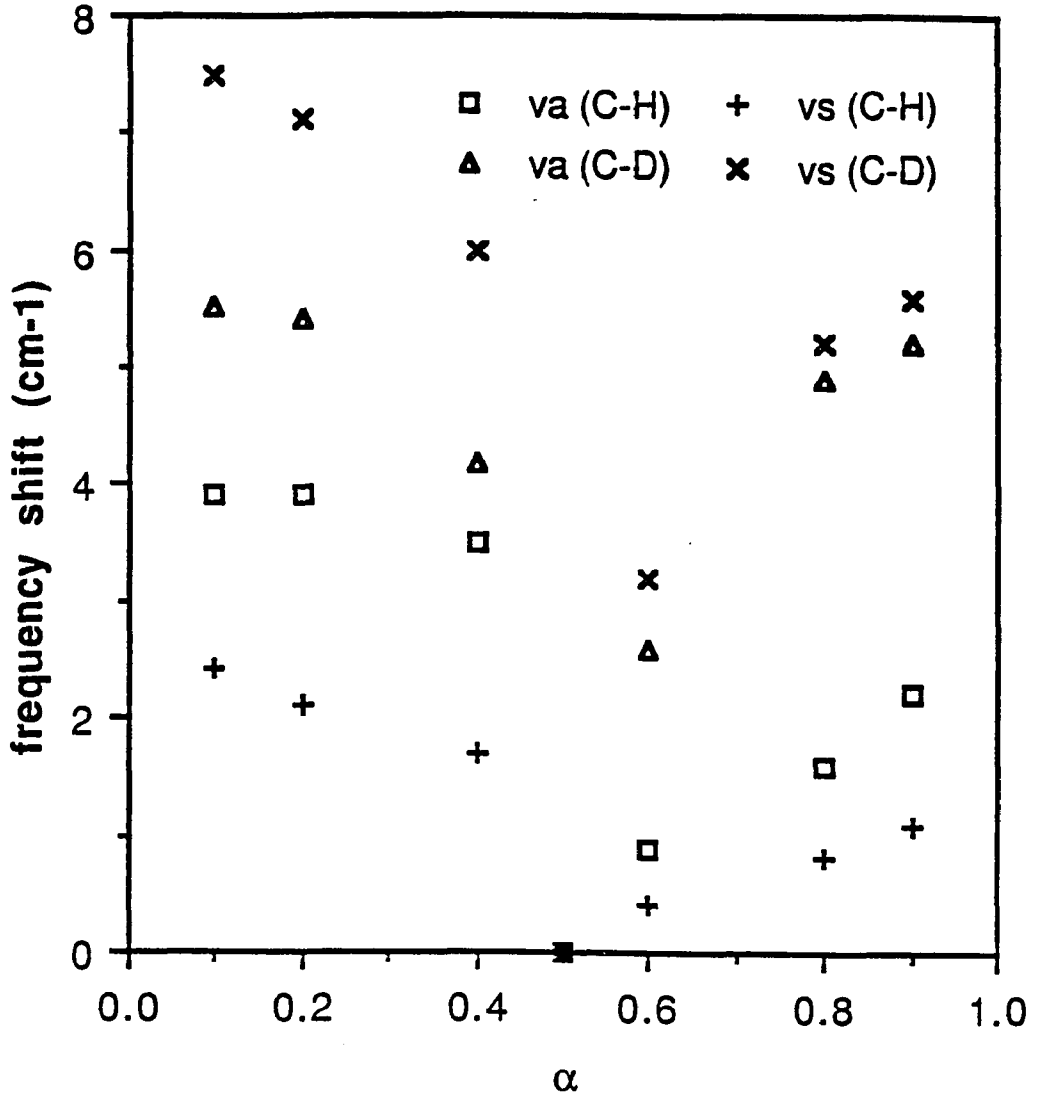


**Fig. 4.4.13 Changes in peak frequencies of the C-H and C-D stretching modes in the adsorbed mixed monolayers of $C_{12}DS$-$C_{12}N$ at the air/water interface with different α values in pure $H_2O$ solution**

**References:**


1. Langmuir, I., *J. Am. Chem. Soc.*, 1917, 39, 1948.
2. Devaux, H., *J. Phys. Radium*, 1912, 2, 891.
3. Meader, A.L. and Criddle, D.W., *J. Coll. Sci.*, 1953, 8, 170.
4. Ter Minassian - Saraga, L., *J. Chim. Phys.*, 1955, 52, 80.
5. Ter Minassian - Saraga, L., *J. Chim. Phys.*, 1955, 52, 99.
6. Ter Minassian - Saraga, L., *J. Coll. Sci.*, 1956, 11, 398.
7. Lange, H., *Koll. Z.*, 1962, 182, 123.
8. Lange, H., *Koll. Z. Z. Polymere*, 1965, 201, 131.
9. Kretzschmar, G. and Vollhardt, D., *Ber. Bunsenges*, 1967, 71, 410.
10. Langmuir, I., *J. Chem. Phys.*, 1933, 1, 756.
11. Vold, M. J., *J. Colloid Sci.*, 1952, 7, 196.
12. Motomura, K. et. al., *J. Colloid Interface Sci.*, 1981, 80, 32.
13. Mokoto, A. et. al., *J. Colloid Interface Sci.*, 1984, 98, 33.
14. Gaines, G.L.Jr., *Insoluble Monolayers at Liquid-Gas Interface*, Interscience, New York, 1966.
15. Gibbs, J.W., *The Collected Works of J.W. Gibbs*, Longmans, Green, London, 1928, Vol. 1, 119.
16. Mcbain, J.W. and Hamphreys, C.W., *J. Phys. Chem.*, 1932, 36, 300.
17. Tajima, K., Muramatsu, M., and Sakasi, T., *Bull. Chem. Soc. Japan*, 1970, 43, 1991.
18. Rubingh, D.N., in *Solution Chemistry of Surfactants*, Mittal, K.L. Ed., Plenum Press, New York, 1979.
19. Hua, X.Y. and Rosen, M.J., *J. Colloid Interface Sci.*, 1982, 86, 164.
20. Murphy, D.S., Ph. D. thesis.
21. Rosen, M. J. and Gu, B., *Colloids Surf.*, 1987, 23, 119.

22. Rosen, M. J., in *Surfactant and Interfacial Phenomena*, Second Ed., John Wiley & Son, 1989, Chapter 11..

23. Rosen, M. J., in *Surfactant and Interfacial Phenomena*, Second Ed., John Wiley & Son, 1989, Chapter 2.

24. Dahanayake, M., Cohen, A.W., and Rosen, M. J., *J. Phys. Chem.*, 1986, 90, 2413.

25. Kjaer, K. and Als-Nielsen, J., *Phys. Rev. Letters*, 1987, 58(21), 2224.

26. Kjaer, K., Als-Nielsen, J., Helm, C. A., Tippman-Krayer, P., and Mohwald, H., *J. Phys. Chem.*, 1989, 93, 3200.

27. Rasing, T., Sheh, Y .R., Kim, M. W., and Grabb, S., *Phys. Rev. Letter*, 1985, 55(2), 2903.

28. Rasing, T., Sheh, Y .R., Kim, M. W., Valint, P. Jr., and Bock, J., *J., Phys. Rev.*, 1985, A31, 537.

29. Lee, E. M., Thomas, R. K., Penfold, J., and Word, R.C., *J. Phys. Chem.*, 1989, 93, 381.

30.Simister, E. A., Lee, E. M., Thomas, R. K., and Penfold, J., *J. Phys. Chem.*, 1992, 96, 1373.

31.Simister, E. A., Lee, E. M., Thomas, R. K., and Penfold, J., *J. Phys. Chem.*, 1992, 96, 1383.

32. Takenaka, T. and Fukuzaki, H., *J. Raman Spectrosc.*, 1979, 8, 151.

33. Dluhy, R. A. and Cornell, D. G., *J. Phys. Chem.*, 1985, 89, 3195.

34. Dluhy, R. A., *J Phys. Chem.*, 1986, 90, 1373.

35. Dluhy, R. A. and Wright, N. A., *Appl. Spectrosc.*, 1988, 42, 138.

36. Fina, L. J. and Tung, Y. S., *Appl. Spectrosc.*, 1991, 45(6), 986.

37. Israelachivili, J.N., Mitchell, D.J., and Ninhan, B.W., *J. Chem. Soc. Faraday Trans. 2*, 1976, 72, 1525.

38. Hansen, W. N. In *Progress in Nuclear Chemistry*, series IX, Vol. 11, Elion, H. A., Stewart, D. C., Ed., Pergamon Press; New York, 1972, Chpter 1.

39. Hansen, W. N. In *Advances in Electrchemistry and Electrochemical Engineering*, Vol. 9, Muller, R. H., Ed., Willey-Interscience: New York, 1973; Chapter 1.

40. Born, M. and Wolf, E., *Principles of Optics*, Pergamon Press: New York, 1970; 4-th ed., Chapter 1.

41. Heavens, O. S. *Optical Properties of ThinSolid Films*, Dover Publications: New York, 1965; Chapter 4.

42. Mcintyre, J. D. E. In Advances in *Electrchemistry and Electrochemical Engineeri* Willey-Interscience: New York, 1973; Chapter 2.

43. Mcintyre, J. D. E. In *Optical Properties of Solids, New Developments*, Seraphin, B. O., Ed.; American Elsevier: New York, 1976; Chapter 11.

44. Schopper, H. *Z. Phys.*, 1952, 132, 146.

45. Fraser, R.D.B. and MacRae,T.P. , *Conformation in Fibrous Proteins and Related Synthetic Polypeptides* (Academic Press, New York, 1973) chap. 4.

46.Downing, H.D. and Williams, D., *J. Geophys. Res.*, 1975, 80, 1656.

47. Snyder, R.G., Hsu, S. L., and Krimm, S., *Spectrochim. Acta*, 1978, 34A, 395.

48. Weers, J.G. and Scheuing, D.R., *J. Coll. Interface Sci.*, 1991, 145, 563.

49. Pastrana, B. A.,Mautone, J., and Mendelsohn, R., *Biochem*, 1991, 30, 10058.

50. Graf, R.T., Koenig, J. L., and Ishida, H., *Polym. Prepr.*, 1984, 25, 188.

51. Kwan, c.c. and Rosen, M.J., *Phys. Chem.*, 1980, 84, 547.

52. Rosen, M.J., *J. Colloid Interface Sci.*, 1981, 79, 587 and 1982, 86, 587.

53. Reid, V.W., Longmem, G.F., and Heinerth, E., *Tenside*, 1967, 4, 292.

54. Li, Z.P. and Rosen, M.J., *Anal. Chem.*, 1981, 53, 1516.

55. Hua, X.Y. and Rosen, M.J., *J. Colloid Interface Sci.*, 1988, 124, 652.

56. Ward, A. F. H. and Tordai, L., *J. Chem. Phys.*, 1946, 14, 453.

57. Hansen, R. S., *J. Phys. Chem.*, 1960, 64, 637.

58. Lingafelter, E.C., *Acta Cryst.*, 1950, 3, 257.

59. Umemura, J., Cameron, D. G., and Mantsch, H. H., *Biochim. Biophys. Acta*, 1980, 602, 32.

60. Okamura, E., Umemura, J., and Takenaka, T., *Biochim. Biophys. Acta*, 1985.

61. Umemura, J., Mantsch, H. H., and Cameron, D. G.,*J. Colloid Interface Sci.*, 1981, 83, 558.

62. Yang, P. W. and Mantsch, H. H., *J. Colloid Interface Sci.*, 1986, 113, 218.

63. Mantsch, H. H.,Kartha, V. B., and Cameron, D. G., In *Surfactans in Solutions*, Lindman, B. , Mittal, K., Eds., Plemum Press, New York, 1984, Vol. 1, 673.

64. Wong,.P. T. T. and Mantsch, H. H., *National Research Council of Canada*, publication 28744.

65. Wong,.P. T. T., Simibovitch, D. J., and Mantsch, H. H.,*Biochim. Biophys. Acta*, 1988, 947, 139.

66. Bell, G. M., Combs, L. L., and Dunne, L. J., *Chem Rev.*, 1981, 81, 15.

67. Penfold, J., Lee, E. M., and Thoms, R. K., *Mol. Phys.*, 1989, 68, 33.

68. Nersasiam, A. and Tohason, P.R., *J. Appl. Poly.Sci.*, 1965, 9, 1653.

69. Umemura, J., Cameron, D.G., and Mantsch, H.H., *J. Phys. Chem.*, 1980, 84, 2272

70. Umemura, J., Mantsch, H.H., and Cameron, D.G., *J. Colloid Interface Sci.*, 1981, 83, 558.

71. Weers, J.G. and Scheuing, D.R., in "*FTIR in Colloid and Interface Science*", Ed. by Scheuing, D.R., ACS Symposium Series 447, p.87.

72. Tanaka, A. and Ikeda,S., *Colloids and Surfaces*, 1991, 56, 217.

73. Colthup, N.B., Daly, L.H., and Wiberley, S.E., in "*introduction to Infrared and Raman Spectroscopy*", 3id Ed., Academic Press, Inc., San Diego, 1990.

74. Szulzewsky, K., Schulz, B., and Vollhardt, D., *Crystal Res. Technol.*, 1983, 18(8), 1003.

75. Bursh, T., Larsson, K., and Lundquist, M., *Chem. Phys. Lipids*, 1968, 2, 102.

76. Lee, E.M., Thomas, R.K., Penforld, J., and Ward, R.C., *J. Phys. Chem.*,1989, 93(1), 381

77. Scheuing, D.R. and Weers, J.G., *Colloids and Surfaces*, 1991, 55, 41.

78. Gotoh, R. and Takenaka, T., *Nippon kagaku Zasshi*, 1963, 84, 392.

79. Sundell, S., *Acta Chemi. Scand.*, 1977, A31, 799.

80. Lucassen-Reynders, E.H., *J. Colloid Interface Sci.*, 1981, 81, 150.

81. Gu, B. and Rosen, M.J., *J. Colloid Interface Sci.*, 1989, 129, 537.

82. Scheuing, D.R. and Weers, J.G., *Langmuir*, 1990, 6, 665.

83. Holler, F. and Callis, J.B., *J. Phys. Chem.*, 1989, 93, 2053.